
This item was submitted to [Loughborough's Research Repository](#) by the author.
Items in Figshare are protected by copyright, with all rights reserved, unless otherwise indicated.

A study of the air-jet type bulked filament yarn process

PLEASE CITE THE PUBLISHED VERSION

PUBLISHER

© Huseyin Sen

PUBLISHER STATEMENT

This work is made available according to the conditions of the Creative Commons Attribution-NonCommercial-NoDerivatives 4.0 International (CC BY-NC-ND 4.0) licence. Full details of this licence are available at:
<https://creativecommons.org/licenses/by-nc-nd/4.0/>

LICENCE

CC BY-NC-ND 4.0

REPOSITORY RECORD

Sen, Huseyin. 2019. "A Study of the Air-jet Type Bulked Filament Yarn Process". figshare.
<https://hdl.handle.net/2134/25582>.

BLDSC no: DX78161

LOUGHBOROUGH
UNIVERSITY OF TECHNOLOGY
LIBRARY

AUTHOR


SEN, H

COPY NO.

016575/02

VOL NO.

CLASS MARK

 Due for return - 7 SEP 1974 LOAN 1 MTH + 2 UNLESS RECALLED 28 JUL 1975	LOAN COPY Due for Return:	22 NOV 1993
	6 JUL 1979	14 NOV 1994
	LOAN 1 MTH + 2 UNLESS RECALLED	12 JUN 1998
	date due: -	2 OCT 1998
	22 NOV 1981	
	LOAN 1 MTH + 2 UNLESS RECALLED	

001 6575 02



A STUDY OF THE AIR-JET TYPE
BULKED FILAMENT YARN PROCESS

A Thesis Submitted

to,

LOUGHBOROUGH UNIVERSITY OF TECHNOLOGY

for

the degree of

DOCTOR OF PHILOSOPHY

by

HÜSEYİN ŞEN
B.Sc. (Manchester)

SUPERVISOR: G. R. Wray, Ph.D., M.Sc. Tech., C. Eng., M.I. Mech. E., F.T.I.

Mechanical Engineering Department

January, 1970.

Loughborough University Of Technology	
Date	Mar. 70
Class	
Acc. No.	016575/02

A C K N O W L E D G E M E N T S

The author wishes to express his sincere thanks to Dr. G. R. Wray, M.Sc.Tech., C.Eng., M.I.Mech.E., F.T.I. for all his valuable help, and for the sustained encouragement he has given throughout the work.

Grateful acknowledgement is also due to the various members of the technical staff of the Mechanical Engineering Department for their help in making the apparatus and for their continued assistance during the course of the work; the author is also grateful to Mr. G. Boyden for his help with the high speed photography and to Miss M. E. Tivey for typing the thesis.

Thanks are also due to the various organisations mentioned in the text for their kindness in supplying the basic yarns and in preparing them for processing, and for allowing the author to use their testing facilities.

A B S T R A C T

Two completely different approaches have been used to study the mechanism of the air-jet method of bulking filament yarns.

Part A is an aerodynamic study of the nature of the air flow and of its characteristics, and of the yarn's behaviour during the bulking process. The experimentation involves the use of scaled-up models of the du Pont type 9 commercial Taslan air-jet and of a typically used parent yarn. The study is extended to include a modification of the jet suggested by earlier workers. The results of these investigations provide new evidence regarding the mechanism of the process and the construction of bulked yarns of this type. It is also concluded that the commercially used air-jet on which the model study has been based, is not ideally designed from the stand-point of efficiency, stability and ease of operation.

In Part B, a suggested mechanism of the air-jet bulking action is simulated by a purely mechanical means. The simulation of the process has been so effective that yarns of the air-jet bulked type are produced by a method not requiring any compressed air. The preliminary work leading to the design of an experimental apparatus is briefly reported. Theoretical and experimental investigations of the process are made, and the bulked yarn properties for various parent yarn particulars and processing conditions are measured and assessed. An economic evaluation of the process has been attempted, based on a comparison with the limited cost figures available for Taslan processing.

The individual nature of each of the two main investigations has necessitated that the results should be separately discussed in the ultimate Chapter of each Part of the thesis. Suggestions for further work are also made for each of the two techniques.

C O N T E N T S

	<u>PAGE</u>
ACKNOWLEDGEMENTS	
ABSTRACT	
<u>CHAPTER 1</u>	<u>INTRODUCTION</u>
1.1 The Objects of Filament Yarn Bulking	1
1.2 Different Methods of Bulking Continuous Filament Yarns	1
1.3 Air-Jet Bulking Methods	2
1.3.1 Previous Publications on Air-Jet Bulking	4
1.4 Some Limitations of the Air-Jet Bulking Process	5
1.5 Objects of the Present Work	5
 <u>P A R T A</u>	 <u>INVESTIGATION OF THE BULKING ACTION OF AN AIR-JET BY USING AN ENLARGED MODEL</u>
<u>CHAPTER 2</u>	<u>SCALING-UP TECHNIQUES</u>
2.1 Introduction	6
2.2 Dynamic Similarity	6
2.2.1 Requirements of Dynamic Similarity	8
2.3 Application of Dynamic Similarity	8
2.4 Measurement of Prototype Air-Jet	9
2.5 Design of Model	9
2.5.1 Design of Model Yarn and Air-Jet	10
2.5.2 Advantages and Disadvantages of using a Lower Scale-up Ratio	13
2.6 Modification and Use of the Mechanical Bulking Apparatus for the Model Study	14
2.6.1 Supply of Compressed Air	16

CHAPTER 3EXPERIMENTAL INVESTIGATION OF THE
FLOW NATURE AND ITS CHARACTERISTICS

3.1	Theoretical Investigation of the Air-Jet Operation without Considering the Feed-Needle	17
3.1.1	Effect of Pressure Ratio on Air-Jet Operation	22
3.2	Theoretical Investigation of the Actual Air-Jet Operation	25
3.3	Application of Dynamic Similarity to the Model Air-Jet to Simulate the Prototype Bulking Jet Action	29
3.4	Operational Settings of the Air-Jet which affect Yarn Bulking	30
3.5	High-Speed Cine Filming of the Process	32
3.6	An Attempt to Investigate the Rotational Nature of the Yarn in the Air-Jet	33
3.7	Visualization of the Flow	35
3.8	Measurement of Air Flow through the Model Jet	40
3.8.1	Calculation of Flow Rate and Reynolds Number	40
3.8.2	Variation of the Flow Rate with Varying Angle of Tilt and Inlet Pressure	42
3.8.3	Variation of the Flow Rate with Varying Longitudinal Feed-Needle Setting and Inlet Pressure	57
3.9	Measurement of Flow Characteristics	57
3.9.1	Constant Temperature Anemometer	59
3.9.2	Probes and their Characteristics	60
3.9.3	Calibration of the Probe	63
3.9.4	Calculation of Flow Velocities	65
3.9.5	Measurement of Mean Flow Velocity	68
3.9.6	Measurement of Turbulence	69
3.9.7	Mean Flow Velocity and Percentage Turbulence Results	71

CHAPTER 4DISCUSSION OF PART (A) AND CONCLUSIONS

4.1	Summary of the Scaled-up Model Taslan Process	132
4.1.1	Application of Geometric Similarity	132
4.1.2	Application of Dynamic Similarity	134

	<u>PAGE</u>
4.2 Summary of the Experimental Investigations	135
4.2.1 Visualization of the Air-Jet Bulking Process	136
4.2.2 Visualization of the Flow in the Air-Jet	137
4.2.3 Measurement of Flow Rate and Calculation of Reynolds Number	138
4.2.4 Measurement of Mean Flow Velocities	139
4.2.5 Measurement of Turbulence	142
4.3 The Flow Natures and Bulking Mechanisms of the Normal and Modified Air-Jets	144
4.4 Production and Costs of a Typical Taslan Mill	147
4.5 Suggestions for Further Work	149

P A R T B

THE MECHANICAL SIMULATION OF AIR-JET BULKING

CHAPTER 5

THE MANUFACTURE OF YARNS OF THE AIR-JET BULKED TYPE WITHOUT THE USE OF AIR

5.1 Preliminary Work	152
5.2 Multi-Purpose Bulking Apparatus	158
5.2.1 Yarn Feed-in Mechanism	158
5.2.2 Yarn Take-up and Winding Mechanism	159
5.2.3 False-Twist Mechanism	159
5.3 The Operation of the Apparatus	160
5.4 Variables likely to affect the Process	161
5.4.1 Initial Twist in the Parent Yarn	161
5.4.2 Total Yarn Denier and Denier per Filament	162
5.4.3 Total Number of Filaments in the Yarn	162
5.4.4 Percentage Overfeeding	163
5.4.5 False-twist Spindle Speed	163
5.4.6 Yarn Tension during Bulking	163
5.4.7 Bulking Speed	164
5.5 Hypothesis of the Bulking Mechanism as Applied to the Mechanical Bulking Method	166
5.6 Experimental Observations	167
5.6.1 The Necessity for extra Untwisting of the Yarn	168
5.6.2 Periodic Bulking	168
5.7 High-Speed Cine-Photography of the Process	173
5.8 Mathematical Analysis of the Ballooning Phenomenon	175

5.9	Improvements to the Design of the False-Twist Unit	178
5.9.1	False-Twist Tube	178
5.9.2	Addition of Localised Turbulent Region to the Bulking Zone	180
5.10	The Adaptation of the Mechanical Bulking Process to the Production of Novelty Effect Yarns	181
5.10.1	Method of Introducing the Fibres into the Core Yarn Structure	181

CHAPTER 6

YARN TESTS AND RESULTS

6.1	Preliminary Testing	183
6.2	Preparation of Parent Yarns	183
6.3	Processing the Parent Yarns	185
6.4	Percentage Denier Increase	186
6.4.1	Results	186
6.5	Physical Bulk Test Based on Package Density Method	192
6.5.1	Results	193
6.6	Water Absorption Test	200
6.6.1	Results	200
6.7	Tensile Testing	208
6.7.1	Results	208
6.8	Instability Test	217
6.8.1	Results	218

CHAPTER 7

DISCUSSION OF PART (B) AND CONCLUSIONS

7.1	Summary of the Experimental Results	225
7.1.1	Percentage Denier Increase	225
7.1.2	Percentage Physical Bulk	226
7.1.3	Water Absorption Test	227
7.1.4	Tensile Tests	228
7.1.5	Instability Test	229
7.1.6	Conclusion	230

7.2	The Possibility of Commercial Exploitation of the Technique	231
7.2.1	Patents	231
7.2.2	Bulking Speed	231
7.2.3	Cost Estimates	232
7.3	Suggestions for Future Work	234

REFERENCES

CHAPTER 1

I N T R O D U C T I O N

1.1. The Objects of Filament Yarn Bulking

The differences between the characteristics of yarns composed of continuous filaments and those made from staple fibres have prevented the former from competing effectively with staple yarns in the past. These differences arise principally from differences in the yarn structure. The virtually parallel filaments are compactly packed in the normal types of man-made filament yarns, whereas spun yarns, e.g. yarns made from natural fibres or man-made staples, have a more open structure with a greater bulkiness resulting from a more random fibre arrangement. Hence, by comparison, synthetic filament yarns have a hardness of handle, less covering power in fabric construction, a lower moisture absorption capacity, poorer thermal insulation, and greater lustre and transparency. Although in certain cases some of these properties are advantageous, they are usually regarded as defects which cause discomfort to the wearer of garments made from such yarns; it is, therefore, desirable that bulking methods should be found for changing the characteristics of filament yarn structures so that such modified filament (bulked yarns) could simulate the properties of spun staple yarns and thus be used in end-uses previously considered unsuitable.

1.2 Different Methods of Bulking Continuous Filament Yarns

There are various methods of bulking continuous filament yarns. These methods have been devised to produce the desired extra characteristics and some have, in turn, produced properties (e.g. high extensibility at low loads) not to be found in yarns made from natural fibres and man-made staples. Most of the methods of bulking are licensed and information about them is not readily available to non-licensees. However, the methods for producing the most common yarn types are well known, e.g. false-twist methods, edge-crimping methods, stuffer-box methods, knit-deknit methods, and

air-jet bulking methods. These methods, with the exception of air-jet bulking, will not be discussed here as information about them could easily be found elsewhere. (1,2,3,4)

1.3. Air-Jet Bulking Methods

The process for producing air-jet bulked yarns consists of feeding a usually pre-twisted yarn through the turbulent region of an air-jet at a faster rate than it is drawn off. The most essential elements of the du Pont type 9 jet, as usually employed for manufacturing this type of bulked yarns, are illustrated in Fig. 1.1. The feed needle A is partially cut away at its end so as to form a semi-cylindrical channel at the place where the overfed yarn enters the air-jet throat. The needle may be rotated (i.e. tilted about its longitudinal axis), but the open channel must ~~face~~ the exit end of the jet so that the yarn can be conveniently fed into the action of the air-stream, i.e. into the turbulent wake caused by the presence of the needle itself. In Fig. 1.1.(b) 'draughtsman's licence' has been applied since the feed-needle angle of tilt α has been drawn in the plane of the paper; in practice the feed-needle is also inclined at a fixed injection angle of 45° to the air-jet axis, but the angle α represents an inclination of the stepped feed needle about its own longitudinal axis.

Unlike the other bulking methods mentioned in section 1.2. the air jet bulked yarn process does not depend on either the thermoplastic or the chemical setting properties of fibres. The process offers some other advantages over the other bulked yarn types. It offers the possibility of blending different filament yarns and fibres, and, by blending yarns of two or more colours, many varieties of colour combinations can be created. By intermittently varying the over-feeding rate fancy yarns can be produced for speciality purposes.

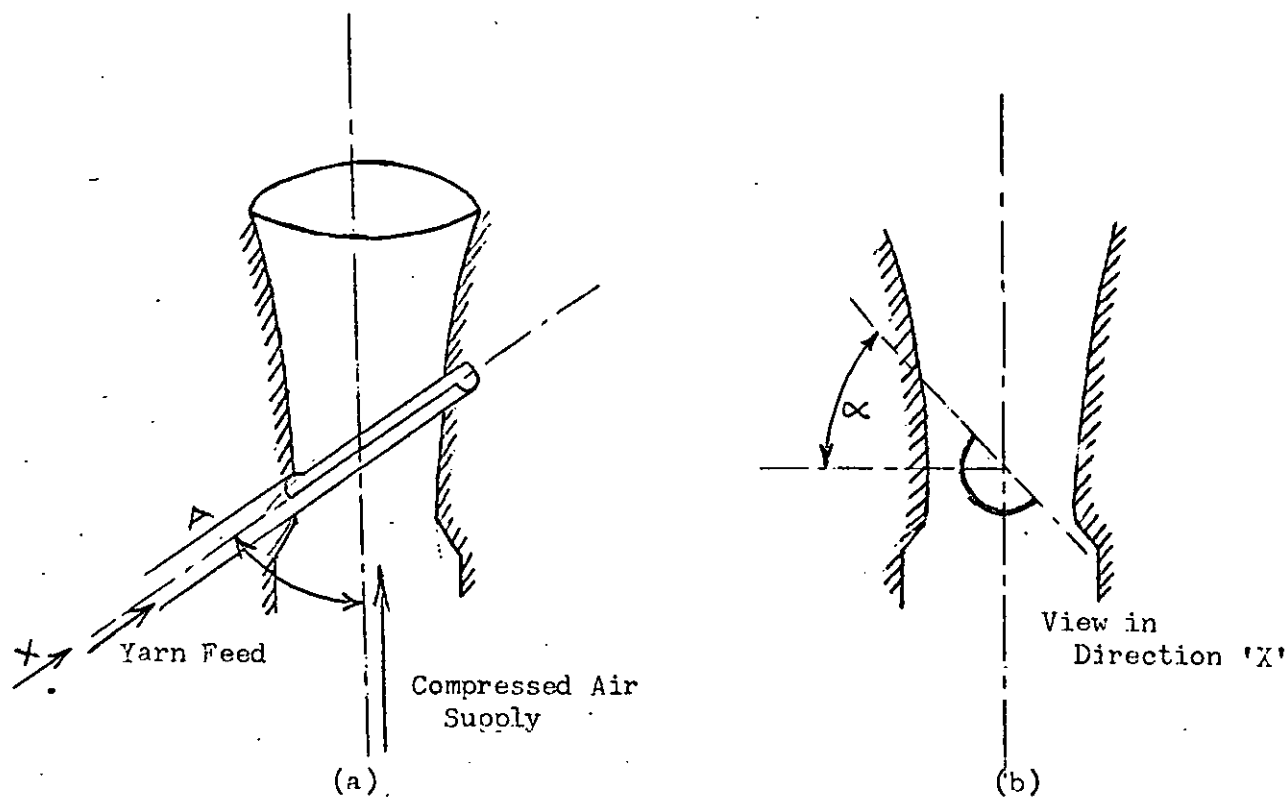


Fig. 1.1 Normal Taslan Air-Jet

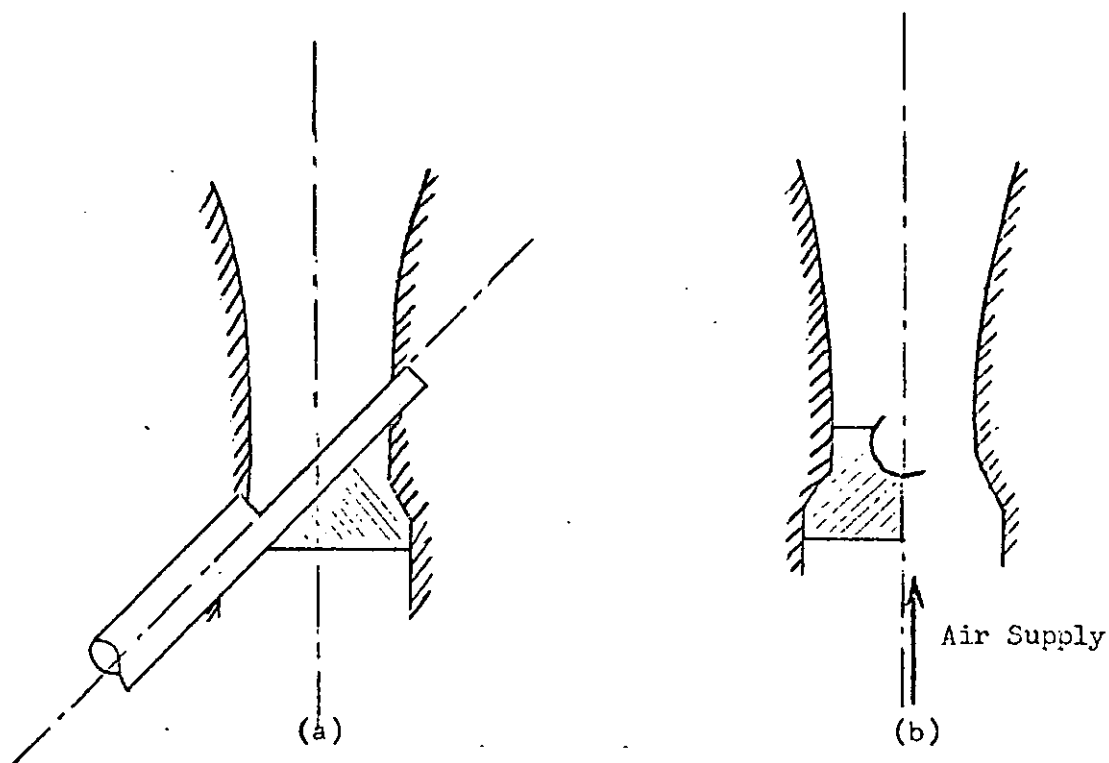


Fig. 1.2 Modified Air-Jet

The process produces yarns of high bulk, i.e. of increased specific volume, and this is achieved with relatively very little increase in weight. For instance, if the supply yarn is over fed by 15 to 20%, the denier would increase in the same proportion but the total bulk of the yarn would increase by 150 to 200%. Although this is not as great a bulk increase as that obtained in stretch yarns made by false-twisting, stuffer-box crimping, etc., the resultant bulked yarn is generally more stable to applied loads. The air-jet process provides yarns with greater opacity, higher thermal insulation and greater moisture retention than normal unbulked filament yarns. An added advantage offered by the process is that it enables the bulked filament yarns to be used in non-slippery threads and fabrics due to their peculiar surface characteristics.

1.3.1 Previous Publications on Air-Jet Bulking

As the air-jet bulked yarns designated by the trade mark "Taslan" are made by a licensed process, very little technical literature dealing with the subject is published. Only the patents^(5,6,7,8), with very general information⁽⁹⁾ on the process and the characteristics and uses of such yarns, are available to non-licensees of the Taslan process. However, from these, it would appear that little fundamental research has been undertaken on the process. Y. E. Chandhari⁽¹⁰⁾ and, more recently, G. R. Wray⁽¹¹⁾ have carried out investigations on the subject. An explanation has been suggested^(12,13) for the bulking mechanism for the type of air-jet typically used in the Taslan process. Briefly stated, the argument is that the twisted bundle of yarn is temporarily false-untwisted in the air-jet by the turbulent air stream created behind the semi-cylindrical feed needle. The filaments are allowed to form into loops owing partially to the deflection of individual filaments by the air-forces and partially to the snarling

of the twist-lively filaments under the slackening effect of the overfeed. The yarn is removed at right angles to the air flow on leaving the air-jet, and here the twist in the yarn bundle redistributes itself to lock these loops in place. Wray's research was continued by Wray and Entwistle⁽¹⁴⁾, the main outcome being a modification of the air-jet by blocking half of it off by a plug on the upstream side of the feed needle (see Fig. 1.2.). This modification enables reduced quantities of compressed air to be used. Wray⁽¹⁵⁾ has also given an account of the properties of air-textured filament yarns.

1.4 Some Limitations of the Air-Jet Bulking Process

Although the air-jet bulking method has some advantages over other well-known methods of bulking (see section 1.3.), the reasons for this method not being more widely used are that its bulking speed is low, and that the process is expensive mainly because of the high costs of initial yarn twist and compressed air, and partly because the licence fees are said to be unusually high.

1.5 Objects of the Present Work

This research is designed to use two different approaches to study the air-jet bulking mechanisms of the normal and modified jets in more detail than previously^(13,14).

(i) It is intended to investigate the mechanism of the air-jet by using a scaled-up model air-jet and a model yarn which are geometrically and dynamically similar to the actual air-jet and to a 70 denier/34 filament Nylon 6.6 respectively. It is hoped that this study could eventually lead to designs of more advanced air-jets and to a reduction of the cost of producing this type of yarn.

(ii) By simulating the air-jet action on the yarn by a mechanical means, it is intended to verify the suggested bulking mechanism. If the simulation was to prove successful this could also be an alternative way of producing air-jet type bulked yarns at reduced cost, and thus if the yarns so produced were acceptable, their use could be greatly increased.

P A R T A

INVESTIGATION OF THE BULKING ACTION OF
AN AIR-JET BY USING AN ENLARGED MODEL

CHAPTER 2

SCALING-UP TECHNIQUES

2.1 Introduction

In problems such as the air-jet bulking process, where air is flowing through a small system in a complex turbulent fashion, it is difficult to visualise the flow characteristics by using normal instrumentation because the system is not sufficiently large. It is, therefore, desirable to find an alternative means, and one possibility is to use the principle of similarity to design an enlarged model. Information can then be obtained from the experiments made on the model, provided that a correct relationship between the results obtained from the model and from the prototype (i.e. full size) air-jet can be established. This relationship will be simple only if the conditions in the model are such that the fluid is geometrically and dynamically similar to that in the prototype air-jet. Two systems are geometrically similar when the ratio of corresponding lengths in the two systems is constant so that one is a scale model of the other. The conditions for dynamic similarity are discussed below.

2.2 Dynamic Similarity

Two systems are dynamically similar when the several forces acting on corresponding fluid elements have the same ratio to one another in both systems, so that the paths followed by the corresponding elements in the two systems will be geometrically the same. When a fluid particle is set in motion its behaviour will depend on its inertia which carries it at a certain velocity along a path, and upon the action of the forces resisting the motion. If the ratio of inertia to resisting force is the same in the two systems the two motions will be dynamically similar.

Let l be a characteristic length in the system under consideration, and let t be a time. Then the mass of an element of fluid is proportional to ρl^3 and its acceleration to $\frac{l}{t^2}$ (where ρ is the density of the fluid).

Inertia force is proportional to $\left[(\text{mass}) \cdot (\text{acceleration}) \right]$,
and thus it is proportional to

$$\left[\rho \cdot l^3 \cdot \frac{l}{t^2} \right]$$

$$\left[= \rho \cdot l^2 \cdot \left(\frac{l}{t} \right)^2 = \rho \cdot l^2 \cdot v^2 \right]$$

(where v is the velocity).

Now if the fluid motion is controlled by viscous resistance,
the flow in the two systems will be dynamically similar if the
ratio of $\frac{\text{inertia force}}{\text{viscous force}}$ is the same.

Viscous force is proportional to $\left[(\text{viscous shear stress}) \cdot (\text{area}) \right]$,
and thus it is proportional to $\left[\eta \cdot (\text{velocity gradient}) \cdot l^2 \right]$,
(where η is the dynamic viscosity).

Since velocity gradient is proportional to $\frac{v}{l}$ then,
viscous force is proportional to $(\eta \cdot v \cdot l)$.

Therefore, $\frac{\text{inertia force}}{\text{viscous force}}$ is proportional to

$$\left[\frac{\rho \cdot v^2 \cdot l^2}{\eta \cdot v \cdot l} \right]$$

$$\left[= \frac{\rho \cdot v \cdot l}{\eta} \right]$$

which is the Reynolds number, R .

Thus, for viscous resistance, the requirement for dynamic
similarity in the two systems is equality of R .

For elastic compression of a fluid the elastic force depends
on the bulk modulus E of the fluid. Then, elastic force is
proportional to $(E \cdot l^2)$. Thus, $\frac{\text{inertia force}}{\text{elastic force}}$ is proportional to

$$\left[\frac{\rho \cdot v^2 \cdot l^2}{E \cdot l^2} \right]$$

$$\left[= \frac{v}{\sqrt{E/\rho}} \right] = \left[\frac{v}{a} \right]$$

which is the Mach number M .

(a is the local velocity of sound).

For compressibility effects, dynamic similarity is obtained when M is the same in both systems.

Similarly, if the resisting force is due to gravity or surface tension, then for dynamical similarity, Froude number or Weber number should be the same.

2.2.1 Requirements of Dynamic Similarity

Ideally it is desirable that both the model and the prototype systems should meet the requirements of complete geometrical and dynamical similarity. However, this is not entirely necessary and indeed it is not always possible. Therefore, a close study of the flow process is essential to discover the forces mainly involved in the flow so that the closest simulation of actual conditions can be made.

As it is the case in this work (see Section 3.1) the high speed flow of air is through a convergent-divergent nozzle, then the resistance to the motion F of a body moving through a compressible fluid of density ρ dynamic viscosity η and bulk modulus E is given by

$$F = \rho \cdot v^2 \cdot l^2 \cdot \phi \left[\frac{\rho \cdot v \cdot l}{\eta} \cdot \frac{v}{\sqrt{E/\rho}} \right] \text{ -----(2-1)}$$

Therefore, for dynamic similarity, both R and M must have same values respectively in both the model and the prototype air-jets.

2.3 Application of Dynamic Similarity

In order to satisfy the dynamical similarity requirements, the use of fluids other than air for the model is not practical or applicable to this particular problem. Indicating quantities in the model by suffix m and the prototype air-jet by suffix p and considering the use of air, with the static pressure in the model being maintained the same as in the full size jet, then $\rho_m = \rho_p$ and $\eta_m = \eta_p$.

Thus, for equality of R:-

$$\frac{\rho_m \cdot V_m \cdot l_m}{\eta_m} = \frac{\rho_p \cdot V_p \cdot l_p}{\eta_p} \quad \text{-----} \quad (2-2)$$

and for equality of M:-

$$\frac{V_m}{a_m} = \frac{V_p}{a_p} \quad \text{-----} \quad (2-3)$$

These two equations are incompatible: this difficulty can be overcome by using different pressures, thus making density ρ_m smaller than ρ_p while leaving η_m substantially unchanged when compared with η_p . Thus, if the linear scale $\frac{l_p}{l_m} = n$, and the pressure in the model is reduced to n^{th} of the pressure in the prototype air-jet, then $\rho_m = n \cdot \rho_p$. Now, for equality of R, $V_m = V_p$. As ρ varies directly with P and since $E = \gamma \cdot P$ (where γ is the ratio of specific heats) and $a = \sqrt{\frac{E}{\rho}}$, the value of a is unchanged and equality of M can be maintained.

2.4 Measurement of Prototype Air-Jet

A variety of air-jets are used for conventional air-jet bulking, but the one believed to be most typically used by Taslan licencees is the type 9 B.S. jet. One of these had been obtained from the du Pont Company. Since no scale drawing was available, it was first necessary that an accurate measurement of the jet dimensions should be made. In order to do this a plastic moulding of the inside of the air-jet was taken, and from the measurements obtained a full size drawing was made, (see Section 2.5.1).

2.5 Design of Model

Initially, it was decided from the fluid mechanics viewpoint that a scale-up ratio $\left(n = \frac{l_p}{l_m}\right)$ of $\frac{1}{10}$ would be satisfactory, so the original drawing of the prototype air-jet was enlarged 10 times and a full size model jet was manufactured from a block of perspex. This decision was influenced by the choice of a suitable model yarn for complete geometrical similarity, and a

200 denier monofilament Nylon 6.6 had been judged necessary for the individual filaments in the construction of the scaled-up model yarn, since yarns comprising 2 denier filaments were used in the previous work⁽¹¹⁾. However, when required, such a monofilament was no longer available commercially. Therefore, 210 denier/34 filaments multi-filament yarn had to be substituted for the 200 denier monofilament. It was realised that this was a poor approximation to geometrical similarity as there might well be "filamentation" within the individual filaments during operations on the model air-jet. Therefore, it was decided that the air-jet dimensions should be made to conform with those of a suitable model yarn made from the largest available monofilament nylon, i.e. 30 denier Nylon 6. A new scaled-up model of the prototype air-jet should then be made to suit the model yarn.

2.5.1 Design of Model Yarn and Air-Jet

For the scaled-up model, a complete geometrical similarity under the working conditions should be satisfied in order that the high speed camera technique could be used to record the paths of movement of the yarn and the formation of the loops. It was decided that the model yarn should be a scaled-up version of the 70 denier/34 filaments nylon 6.6 (15 turns/in) parent yarn used by Wray⁽¹¹⁾ in his investigation. For complete geometrical similarity, the model yarn should also have 34 filaments in its construction. Therefore, the total model yarn denier, made from 30 denier monofilaments, is:-

$$34 \times 30 = 1020 \text{ denier}$$

Now, if d and D are the full size and model yarn diameters respectively, then

$$\left(\frac{d}{D}\right)^2 = \frac{70}{1020} = \frac{1}{14.57}$$

$$\frac{d}{D} = \frac{1}{3.81}$$

STOR-A-FILE IMAGING LTD

DOCUMENTS OF POOR ORIGINAL HARD COPY

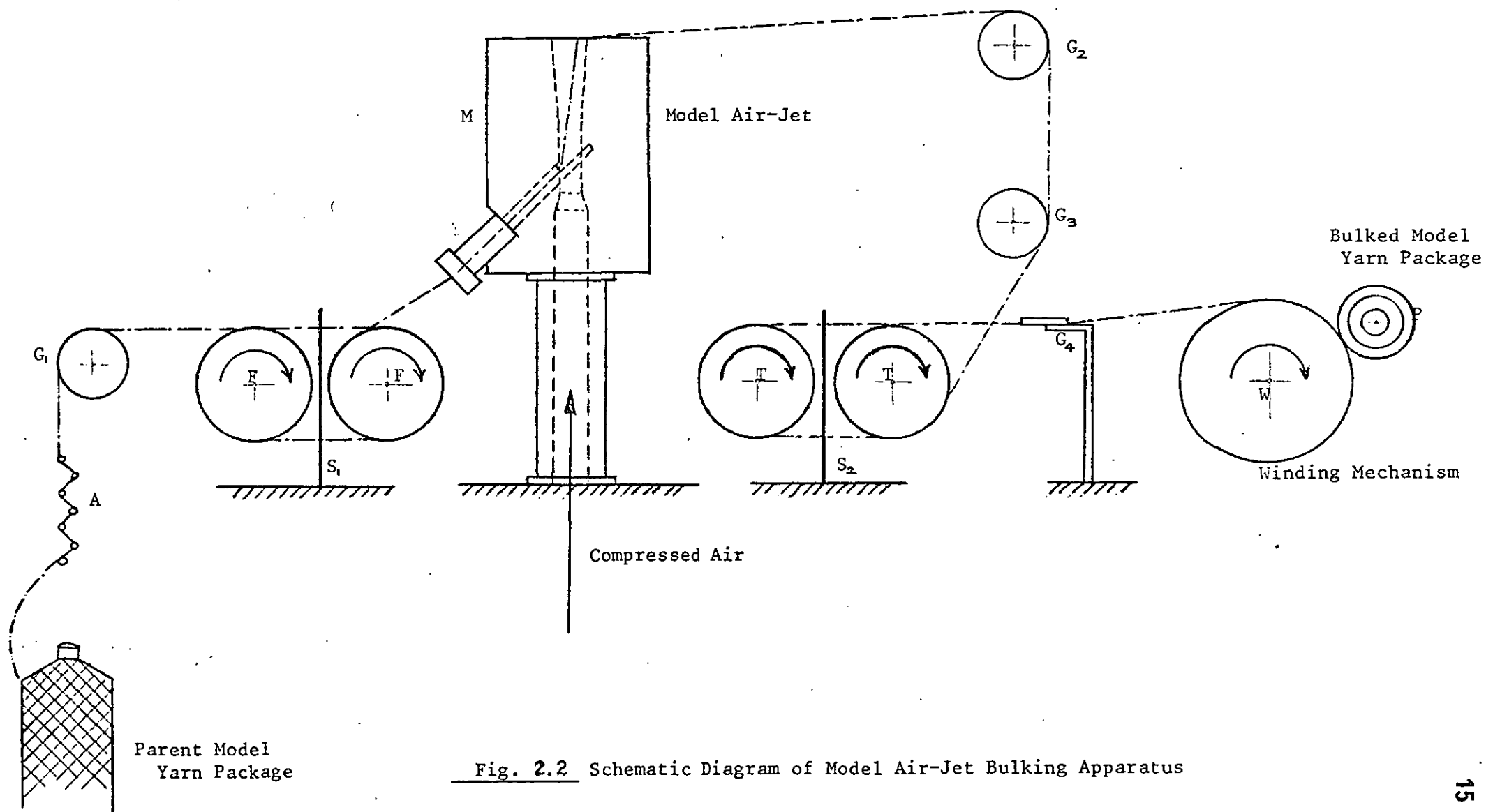


Fig. 2.2 Schematic Diagram of Model Air-Jet Bulking Apparatus

several times around a pair of feeding rollers F F and fed into the model air-jet M. When the bulked yarn leaves the jet it passes over direction guide rollers G_2 and G_3 and then it is taken up by take-up rollers T T and finally the bulked yarn wound on to a package P. The take-up roller diameters are less than feeding rollers so that a constant yarn over feed is maintained. Separators, S_1 and S_2 separate the model yarn during the feeding and take-up operations.

2.6.1 Supply of Compressed Air

A Broomwade two-stage air compressor was used to pump air into a tank of capacity 15 ft^3 , the maximum permissible pressure in the tank being 200 lbf/in^2 (gauge). When the compressed air leaves the tank it passes through a water trap followed by a pressure reducer. Then it flows along a long straight pipe before it enters an orifice plate (see Section 3.8). From the orifice it passes through a series of 6 fine filters and then it is connected to the inlet section of model air-jet, which is attached to the modified mechanical bulking apparatus as described above.

CHAPTER 3

EXPERIMENTAL INVESTIGATION OF THE FLOW NATURE AND ITS CHARACTERISTICS

3.1 Theoretical Investigation of the Air-Jet Operation without Considering the Feed-Needle

For preliminary investigation, if it is assumed that the feed-needle (a semi-cylindrical rod) is not present, then it can be considered that the flow through the jet is similar to an isentropic flow of a perfect gas through a convergent-divergent nozzle. The equations governing such flows are well known^(16,17,18,19).

The velocity at any section can be obtained from the isentropic energy equation:

$$\frac{\gamma R}{\gamma - 1} dT + V \cdot dV = 0 \quad \text{--- (3-1)}$$

(where γ is the ratio of specific heats, R is the gas constant, T is the absolute temperature ($^{\circ}\text{F}$), and V is the velocity).

By integrating equation (3-1) and incorporating (a), the perfect gas equation,

$$\frac{P}{\rho} = R \cdot T \quad \text{--- (3-2)}$$

(where P is the pressure, and ρ is the density),
and (b) the continuity equation,

$$G = A \cdot V \cdot \rho = \text{Constant} \quad \text{--- (3-3)}$$

(where G is the mass rate of flow, and A is the area),
and (c) the isentropic relationship for the perfect gas,

$$\frac{P}{\rho^{\gamma}} = \text{Constant} \quad \text{--- (3-4)}$$

then, the velocity at any section is given by:

$$V = \frac{1}{\sqrt{1 - \left(\frac{A}{A_i}\right)^2 \left(\frac{P}{P_i}\right)^{2/\gamma}}} \cdot \sqrt{\frac{2\gamma}{\gamma - 1} \cdot \frac{P_i}{\rho_i} \left[1 - \left(\frac{P}{P_i}\right)^{\frac{\gamma-1}{\gamma}}\right]} \quad \text{--- (3-5)}$$

(where the suffix i indicates the inlet condition).

Hence, the mass rate of flow can be obtained:

$$G = \frac{A \cdot P_i}{\sqrt{1 - \left(\frac{A}{A_i}\right)^2 \left(\frac{P}{P_i}\right)^{2/\gamma}}} \cdot \sqrt{\frac{2\gamma R}{\gamma - 1} \cdot T_i \left[\left(\frac{P}{P_i}\right)^{2/\gamma} - \left(\frac{P}{P_i}\right)^{\frac{\gamma+1}{\gamma}}\right]} \quad \text{--- (3-6)}$$

Because the mass rate is constant and A is variable for a given P_i , the ratio $\frac{G}{A}$ must have a maximum. Assuming $\frac{A}{A_i} \ll 1$, and differentiating the equation (3-6) with respect to $\frac{P}{P_i}$ and equating to zero, then solving for $\frac{P}{P_i}$ gives the critical pressure ratio:

$$\frac{P_c}{P_i} = \left(\frac{2}{\gamma+1} \right)^{\frac{\gamma}{\gamma-1}} \quad \text{-----} (3-7)$$

Because $\frac{G}{A}$ is maximum at the throat of the nozzle, it follows that the critical pressure P_c exists at the throat. Hence the velocity at the throat is given by:

$$V_t = \sqrt{\frac{2\gamma R T_i}{\gamma+1}} = \sqrt{\frac{2}{\gamma+1} \cdot a^2} \quad \text{-----} (3-8)$$

(where a is the speed of sound).

Therefore, the velocity at the throat is equal to that of sound in the flowing medium - i.e. the Mach number $M = 1$.

When $\frac{A}{A_i} \ll 1$

$$V = a \sqrt{\frac{2}{\gamma-1} \left[\left(\frac{P_i}{P} \right)^{\frac{\gamma-1}{\gamma}} - 1 \right]}$$

or

$$M = \sqrt{\frac{2}{\gamma-1} \left[\left(\frac{P_i}{P} \right)^{\frac{\gamma-1}{\gamma}} - 1 \right]} \quad \text{-----} (3-9)$$

Now, considering the continuity equation (3-3) in its differential form,

$$\frac{d\rho}{\rho} + \frac{dV}{V} + \frac{dA}{A} = 0 \quad \text{-----} (3-10)$$

and Euler's equation for one dimensional steady flow in the absence of losses,

$$\frac{dP}{\rho} + V \cdot dV = 0 \quad \text{-----} (3-11)$$

and substituting $a^2 = \frac{dP}{d\rho}$ and $M^2 = \frac{V^2}{a^2}$,
then:

$$\frac{dA}{A} = \frac{dV}{V} (M^2 - 1) \quad \text{-----} (3-12)$$

TABLE 3.1 Gas Tables Calculated from the Measurement of the
Full Size Air-Jet (Assuming $P_i = 240 \text{ lbf/in}^2$)

Distance from Air-Jet entrance (in)	$\frac{A(\text{local})}{A(\text{throat})}$	$M(\text{local})$	$\frac{P(\text{local})}{P(\text{inlet})}$
0.000	2.550	0.2345	0.9615
0.010	2.280	0.2647	0.9520
0.020	2.025	0.3020	0.9380
0.030	1.790	0.3470	0.9200
0.040	1.570	0.4070	0.8915
0.050	1.360	0.4900	0.8480
0.060	1.170	0.6180	0.7725
0.070	1.000	0.9800	0.5400
0.325	1.000	1.0200	0.5150
0.385	1.015	1.1400	0.4450
0.455	1.175	1.5000	0.2720
0.520	1.315	1.6800	0.2085
0.587	1.625	1.7600	0.1850
0.640	1.790	2.0700	0.1145
0.6775	2.230	2.3200	0.0775
0.7050	2.550	2.4700	0.0613
0.7550 (Exit)	2.550	2.4700	0.0613

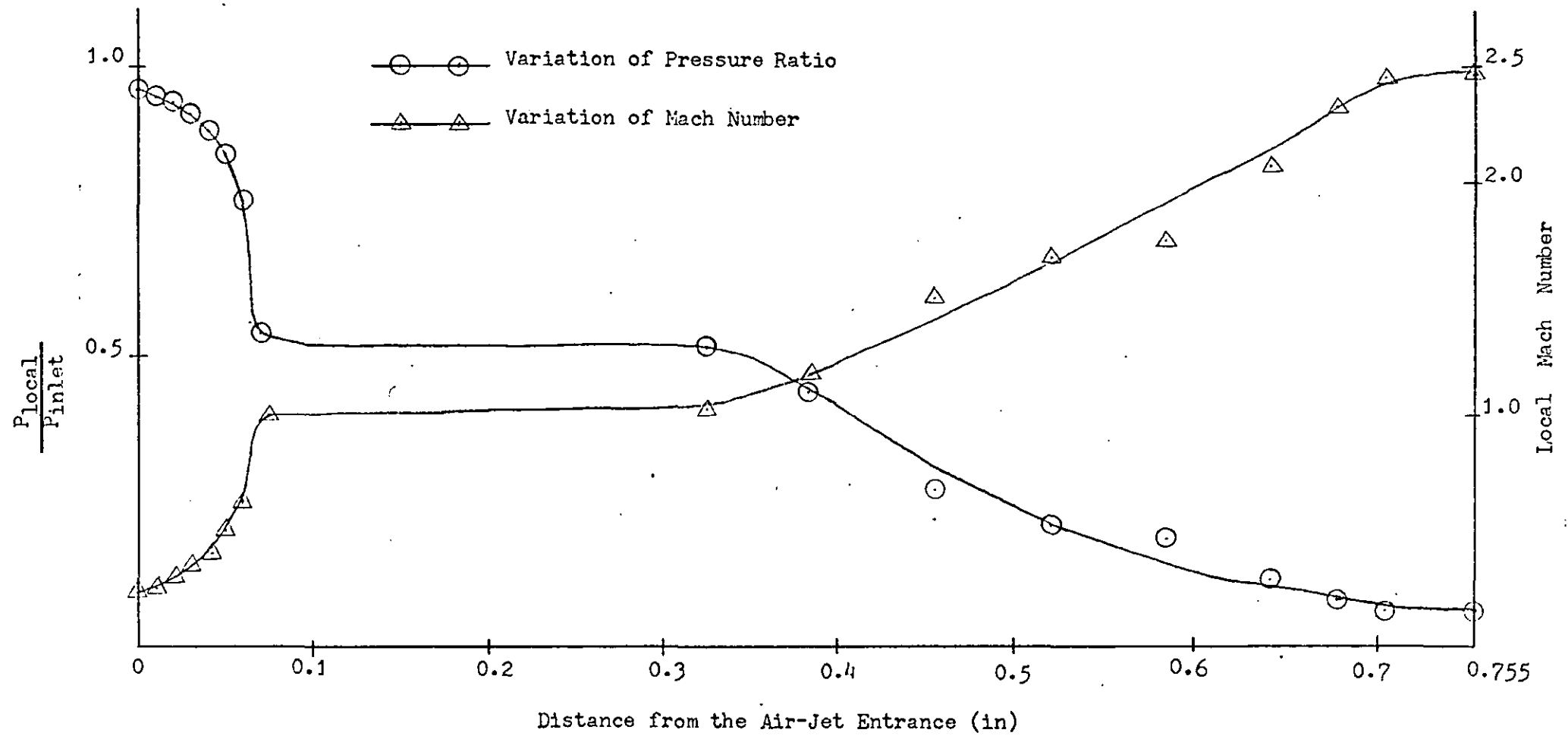


Fig. 3.1 Variation of Pressure Ratio and Mach Number at a Distance along the Air-Jet
 (Assuming, $P_i = 240 \text{ lbf/in}^2, \text{abs.}$ and No Feed Needle Present)

By definition, $M = \frac{v}{a}$

Therefore:
$$\frac{dM}{M} = \frac{dv}{v} - \frac{da}{a} \quad \text{--- (3-13)}$$

For isentropic transformation,

$$\frac{da}{a} = \frac{1}{2} \left(\frac{dP}{P} - \frac{d\rho}{\rho} \right) = \frac{1}{2} \frac{dP}{P} \left(1 - \frac{1}{\gamma} \right) \quad \text{--- (3-14)}$$

therefore, from equations (3-12), (3-13) and (3-14),

$$\frac{dA}{A} = \frac{M^2 - 1}{1 + \frac{\gamma - 1}{2} M^2} \cdot \frac{dM}{M},$$

or in finite form:

$$\frac{A_1}{A_2} = \frac{M_2}{M_1} \left[\frac{M_1^2 + \frac{2}{\gamma - 1}}{M_2^2 + \frac{2}{\gamma - 1}} \right]^{\frac{\gamma + 1}{2(\gamma - 1)}} \quad \text{--- (3-15)}$$

If A_t is the air-jet throat where $M = 1$ is reached, then,

$$\frac{A}{A_t} = \frac{1}{M} \left[\frac{\frac{\gamma - 1}{2} M^2 + 1}{\frac{\gamma + 1}{2}} \right]^{\frac{\gamma + 1}{2(\gamma - 1)}} \quad \text{--- (3-16)}$$

From the measurements of the prototype air-jet (see

Section 2.4 and Fig. 2.1), the values of $\frac{A}{A_t}$ along the air-jet axis are calculated. Then, using the equations (3-16) and (3-9) the values of M and $\frac{P}{P_1}$ are found. These are tabulated in Table 3.1 and are shown graphically in Fig. 3.1.

From equation (3-12) the following conditions can be stated:

(i) for a convergent section:

$$M^2 > 1, \text{ the velocity decreases,}$$

$$M^2 < 1, \text{ the velocity increases,}$$

(ii) for a divergent section:

$$M^2 > 1, \text{ the velocity increases,}$$

$$M^2 < 1, \text{ the velocity decreases,}$$

(iii) for $A = \text{constant}$:

$$\text{the velocity is constant, or } M^2 = 1.$$

Finally, it must be remembered that the flow is influenced not only by the passage contour but also by the entrance Mach number. However, during the above theoretical analysis, it is assumed that the flow entrance velocity is very small.

3.1.1 Effect of Pressure Ratio on Air-Jet Operation

With reference to Fig. 3.2, if $P_i = P_a$ there is no flow through the jet. Now, if P_i is increased but $\frac{P_i}{P_a}$ is less than the critical pressure, then the flow in the jet is subsonic and $P_e = P_a$ (curve a). When the critical pressure is reached the velocity at the throat becomes sonic. If no losses occur, in order to obtain $M = 1$ at the throat then $\frac{P_i}{P_a} = 1.8886$ (curve b). Now, if P_i is further increased (i.e. $P_i > 1.8886 P_a$) M is still unity at the throat and $\frac{P_i}{P_t} = 1.8886$ and $P_t > P_a$. Therefore, the flow undergoes an expansion from the throat, and supersonic flow exists in the part of the divergent section. If P_i is sufficiently high so that at the exit the flow is supersonic, then the flow in the jet is independent of P_a , and P_e is a function of the geometry of the air-jet.

For the flow to be supersonic at the exit,

$$\frac{P_a}{P_i} = 0.0613 \quad (\text{see Fig. 3.1}),$$

$$\text{and, therefore, } P_i = \frac{14.72}{0.0613} = 240 \text{ lbf/in}^2 \text{ (absolute).}$$

If $P_e > P_a$ - i.e. $P_i > 240 \text{ lbf/in}^2$ (abs.) an expansion occurs in the flow at the exit, and if $P_e < P_a$ - i.e. $P_i < 240 \text{ lbf/in}^2$ (abs.) a compression occurs.

If P_e is just slightly less than P_a , compression occurs at the exit and shock waves are present there. The intensity of the shock is a function of M in front of the shock, and depends on the variation of P_e to P_a . Fig. 3.3(a) shows diagrammatically the formation of shock and expansion waves corresponding to this condition. The characteristics and formation of these waves are fully explained by Ferri⁽²⁰⁾ and Carafoli⁽²¹⁾. If the value of P_e decreases with respect to P_a (i.e. P_i decreasing) then reflection of the shock CD cannot occur, and thus a pattern similar to Fig. 3.3(b) is obtained. A further decrease in P_e increases the distance between D and D' and, if P_i continues to decrease, a point could be reached where the

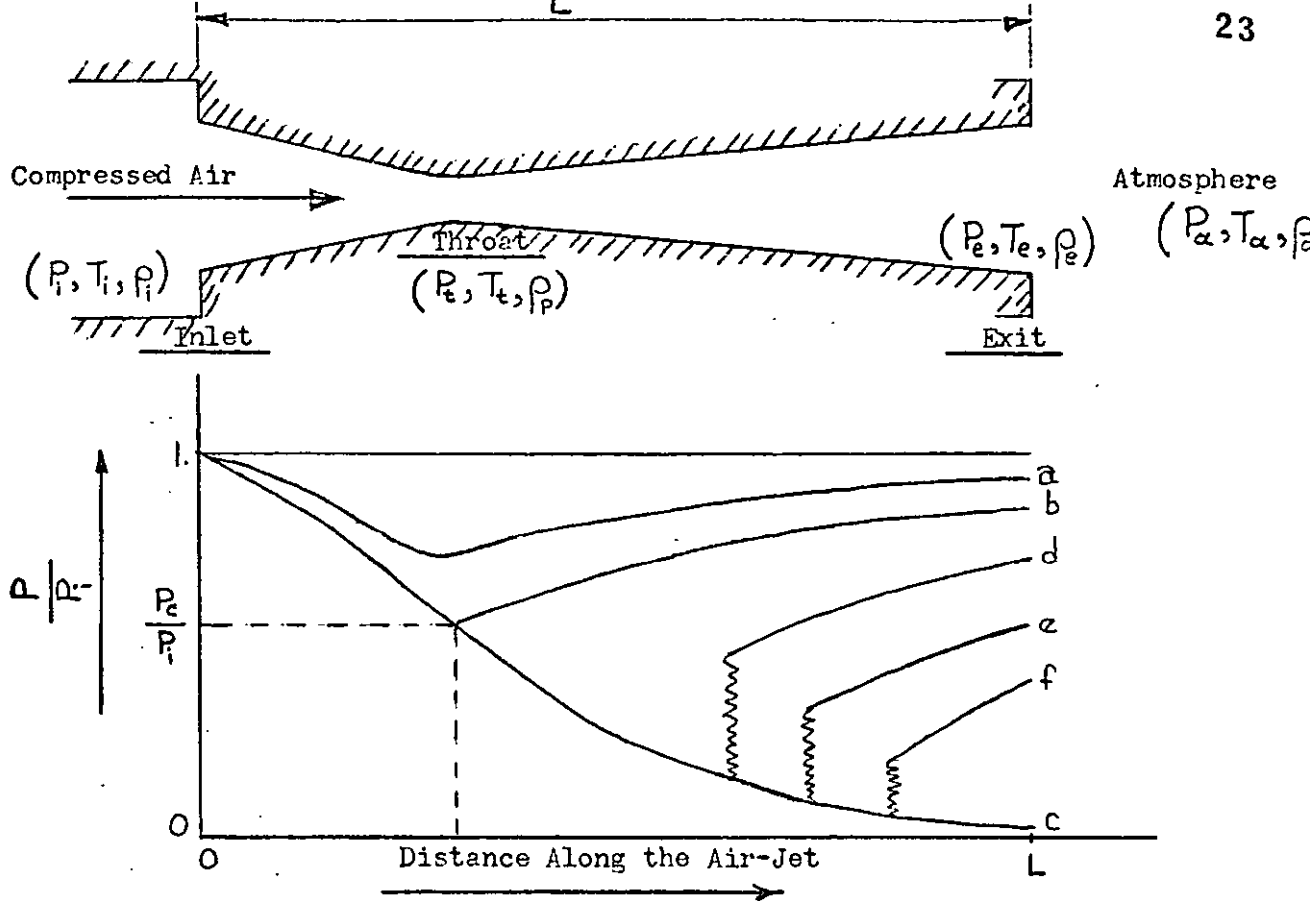


Fig. 3.2 Pressure Distribution in Convergent-Divergent Air-Jet

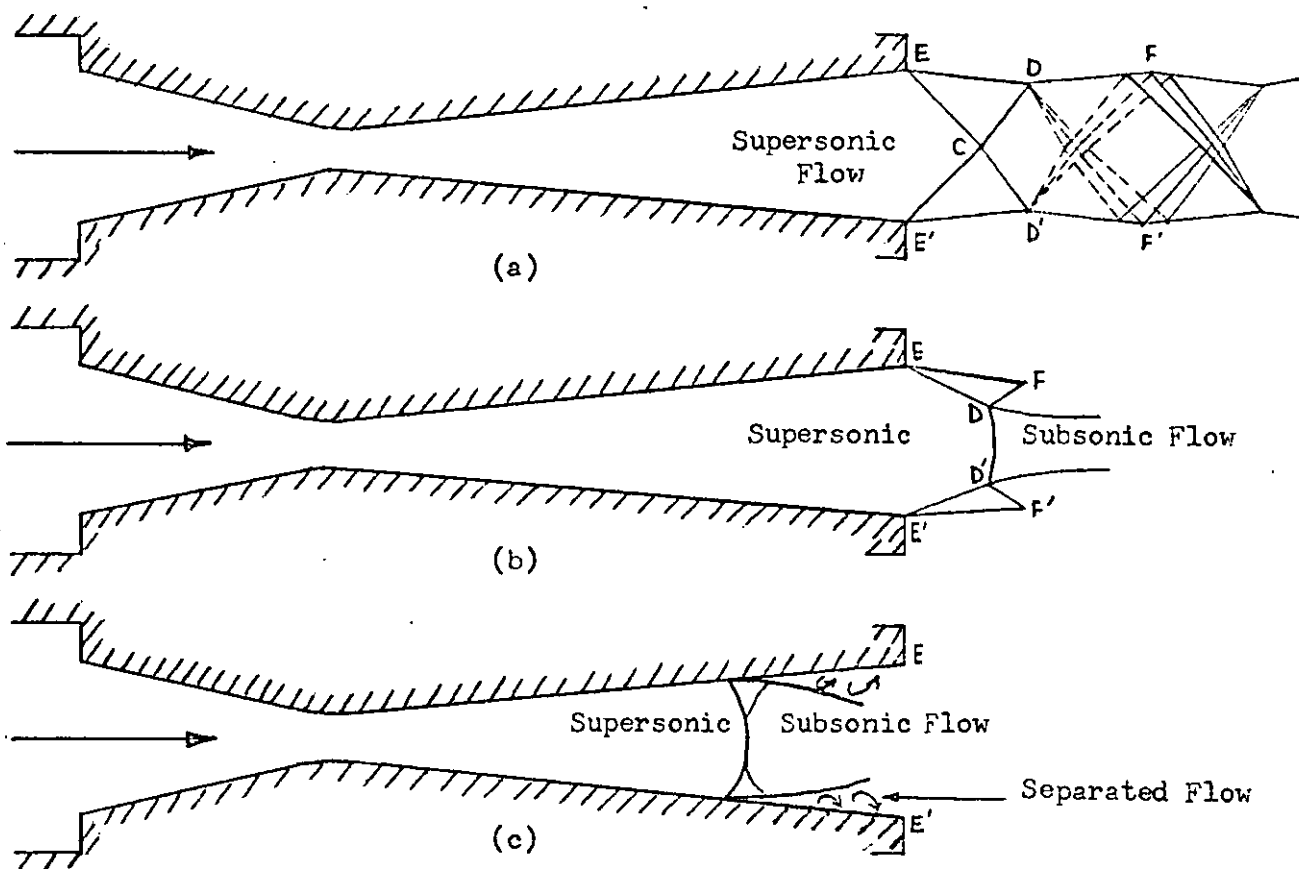


Fig. 3.3 The Shock Waves Pattern at the Discharge of the Supersonic Air-Jet

waves disappear and a strong normal shock occurs across the exit.

If P_i decreases further with respect to the value for which a normal shock occurs at EE' an isentropic flow in the air-jet is no longer possible and the strong shock moves inside as shown in Fig. 3.3(c).

It was found by Wray^(11,12) that the supply of compressed air to the Taslan type 9 air-jet should be maintained at $P_i = 50 \text{ lbf/in}^2$ (gauge) for satisfactory bulking of the yarn, and thus

$$\frac{P_a}{P_i} = \frac{14.72}{(50 + 14.72)} = 0.2275$$

$$\text{but } \frac{P_a}{P_c} = 0.52828$$

Therefore, at the normal working conditions of the jet, $P_i > P_c$, and $M = 1$ at the throat, and, since $P_i < 240 \text{ lbf/in}^2$ (abs.), the flow in the divergent part is partly supersonic, and shock waves will be present as shown in Figs. 3.2, curves (d) and (e).

In the above consideration, it was assumed that no boundary layer exists on the walls of the air-jet and that separation of the flow from the walls cannot occur. However, in practice the boundary layer exists; moreover it plays an important part in the flow equilibrium and this becomes even more significant when the difference between P_a and P_e increases. The boundary layer modifies the formation of the shock waves that occur at the exit of the jet by separating the flow from the walls. However, the boundary layer can undergo compression without separation and such separation occurs only when the pressure increase is large.

3.2 Theoretical Investigation of the Actual Air-Jet Operation (i.e. considering the feed needle)

The fact that the feed needle (a semi-cylindrical body) crosses the air-jet throat (at an angle of 45° to the jet axis) makes the actual flow in the bulking jet more complicated than was explained in section 3.1.

As an aid to understanding the flow behind the feed needle, one can consider a cylindrical rod placed in a flow region perpendicular to the main flow direction. It is a well known fact that at a very low Reynolds number R the flow is completely laminar; with increasing values of R a laminar separation starts and, with further increases, the separation point moves downstream from the back surface of the cylinder. In the region from $R = 100$ to $R = 100,000$ the separated flow assumes a periodicity of frequency n . A dimensionless quantity known as the Strouhal number S relates this with the cylinder diameter D and the velocity V , by the expression $S = \frac{n \cdot D}{V}$. The flow pattern in the wake of the cylinder is fairly regular and vortices move alternately clockwise and counter clockwise. This phenomenon extends for a considerable distance downstream before decomposing itself. At higher values of R the flow becomes fully turbulent, having lost all traces of regularity.

The boundary layer separation on the cylinder is related to the pressure distribution in the boundary layer. The separation occurs at a region with an adverse pressure gradient. Fig. 3.4 shows diagrammatically the boundary layer growth. Due to the reversal of the flow there is a considerable thickening of the boundary layer. At the point of separation one stream-line intersects the cylinder wall at a certain angle, and the point of separation itself is determined by the condition that the velocity gradient normal to the wall vanishes there.

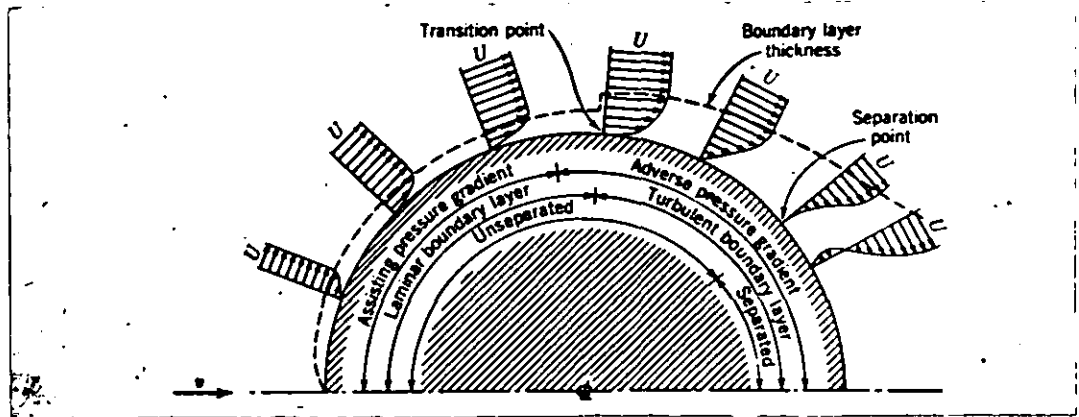


Fig. 3.4 Diagrammatic Representation of Boundary Layer Growth on a Cylinder for a High Reynolds Number. (The Boundary Layer Thickness is Exaggerated for Clarity)

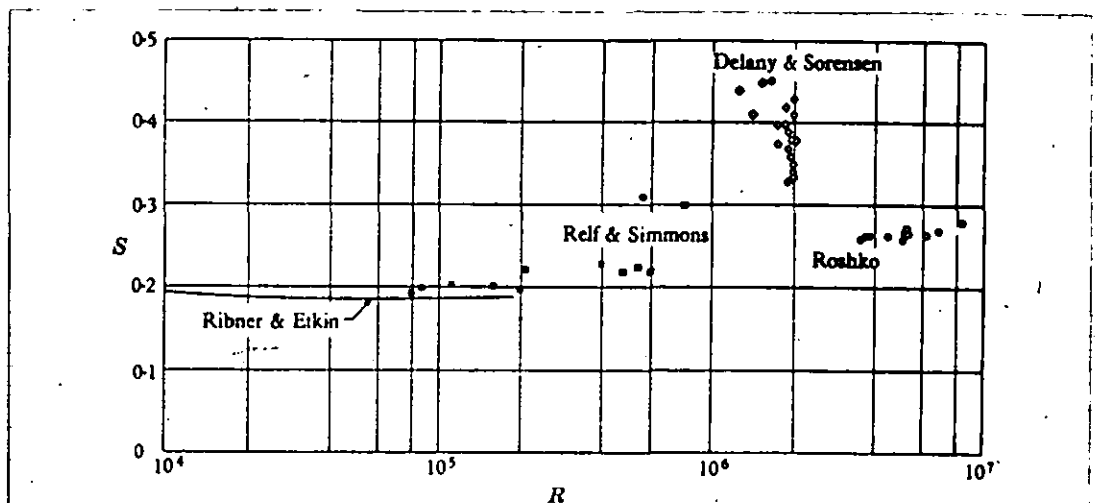
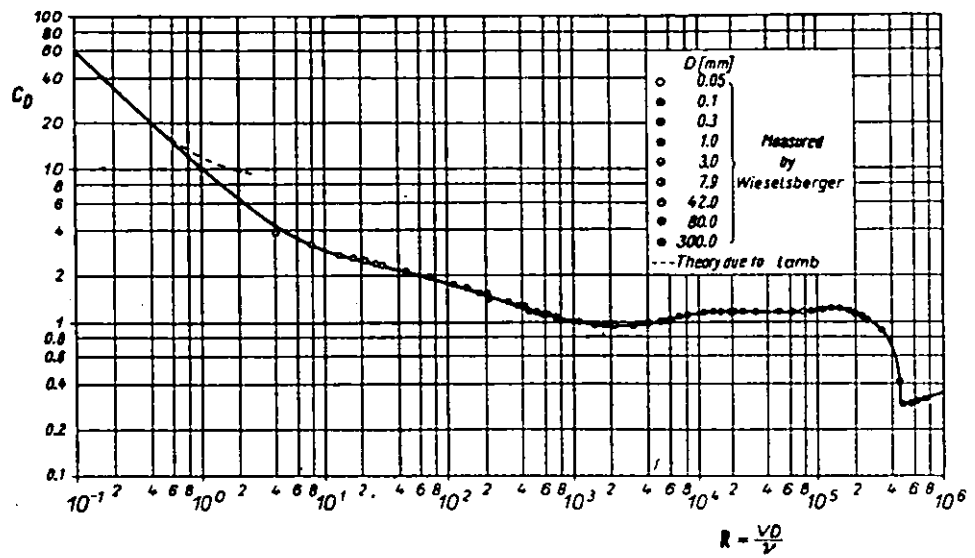
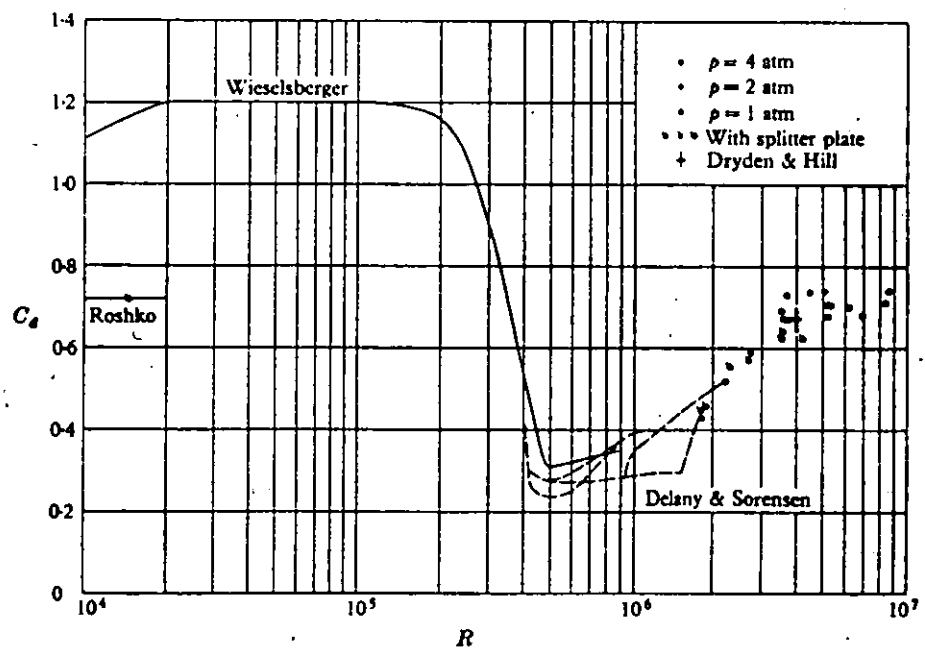


Fig. 3.5 The Variation of Strouhal Number S at High Reynolds Number R (after Roshko)



a



b

Fig. 3.6 Drag Coefficient for Cylinders as a Function of R
(after Schlichting)

Roshko⁽²²⁾ and many other investigators made extensive investigations of the wake behind a circular cylinder. Koveinsznay⁽²³⁾ and Bloor⁽²⁴⁾ made their investigations at low and high values of R respectively and they both used the hot-wire anemometry technique. Figs. 3.5 and 3.6 show respectively the variation of Strouhal number and drag coefficient measurements for circular cylinders, obtained by various investigators at high values of R . The experimental results reported exhibit a good agreement at subcritical values of R , but in the super critical range there is little agreement; the value of R at which the drag coefficient C_d suddenly decreases is called the critical R .

This lack of agreement in the results of the various investigators could be due to the difficulty of accurate measurement in such a highly complex situation, or it could be that the flow in the wake of the cylinder is extremely sensitive to slight differences in the imposed experimental conditions.

In the above discussion, it was assumed that the fluid was incompressible (i.e. $M < 0.3$) and that C_d was only dependant on R , but, when compressibility has to be taken into account, then C_d is a function of both R and M , and the influence of compressibility increases with the increase in M .

The actual flow in the divergent part of the Taslan air-jet approximates to the above-mentioned analogies only in the fact that a cylindrical tube (feed needle) lies across the throat of a convergent-divergent nozzle (air-jet). However, the flow is extremely complicated by the facts that, the feed needle is hollow and semi-cylindrical in cross-section, its axis lies at 45° to main flow direction, and it can be rotated about its own axis. Under the normal working conditions of the Taslan jet, R is high. The jet is small in size, the ratio of the feed needle diameter to the jet

throat diameter is large, and the operating pressure ratio $\frac{P_i}{P_a}$ is high. Therefore, a local region of supersonic velocity is formed in the very small gap between the jet wall and the feed needle. The transition from supersonic to subsonic flow will take place through a shock wave. On crossing this shock wave, the pressure, density and temperature of the air all change at very high rates.

Many research workers^(25,26,27,28) have investigated the changes which occur in the circumferential pressure distribution, the drag coefficient C_d , and the flow characteristics in the wake of circular cylinder subjected to high speed flow. However, they have mainly conducted their experiments in a wind tunnel with a large cross-sectional working area and a low level of turbulence, and moreover, they investigated the influences of one condition at a time. There is no published work known to the author dealing with any experimental set-up similar to the actual Taslan air-jet, with its several conditions each of which could influence the flow. In this investigation, a mathematical analysis of the flow in the wake of the feed needle is not attempted because of its complexity, but in the region where turbulence develops and the transition of the parent yarn to the bulked yarn state occurs this is investigated experimentally by using hot-film anemometry technique (see Section 3.9).

3.3 Application of Dynamic Similarity to the Model Air-Jet to Simulate the Prototype Bulking Jet Action

For complete dynamic similarity between the model and prototype air-jets equality of R and M should be maintained in both systems (see Section 2.3). Therefore, the pressure in the model should be $(1/3.81)$ times the pressure in the prototype jet. Assuming an inlet pressure of 50 lbf/in^2 (gauge) for the normal operation of the prototype jet, then the exit of the model jet should be kept in vacuum during its operation. To satisfy this operating requirement of an exit vacuum

condition, would be difficult while the model yarn is running through the jet, and it would present further difficulties to the carrying out of detailed experimentation. Moreover, if the effect of prototype inlet pressures below 56 lbf/in^2 (absolute) had to be investigated, then, both inlet and exit sections would have to be kept in vacuum.

Therefore, in order to overcome the above-mentioned difficulties, a working compromise was made in that it was decided that initially only the equality of M should be maintained. The effect of M in similarity is more significant when $M > 0.3$, because it was shown in Section 3.1.1 that at the normal operating conditions of the Taslan jet, the operating pressure ratio $\frac{P_a}{P_i}$ is above the critical, and a region of supersonic flow is formed. Hence, equating M_p to M_m (where the suffices p and m refer to the prototype and model jets respectively) is closer to the requirements of dynamic similarity than equating R_p to R_m .

Operating the model jet at the conditions set by $M_p = M_m$ with the scaled-up yarn produced a bulked model yarn similar in appearance to the normal Taslan type bulked yarn. Therefore, it is reasonable to assume that equating M alone is justified, since it creates a very near approximation to dynamic similarity. Hence, it can be taken that the requirement of equating both M and R is not absolutely necessary for dynamic similarity in this particular problem, since the effect of R is negligible.

3.4 Operational Settings of the Air-Jet which affect Yarn Bulking

The inlet pressure P_i , the angular feed-needle setting α , and the longitudinal needle setting L along the axis of its mating bore are three important factors affecting the flow in the jet and therefore affecting the bulking. Wray⁽¹¹⁾ has observed the importance

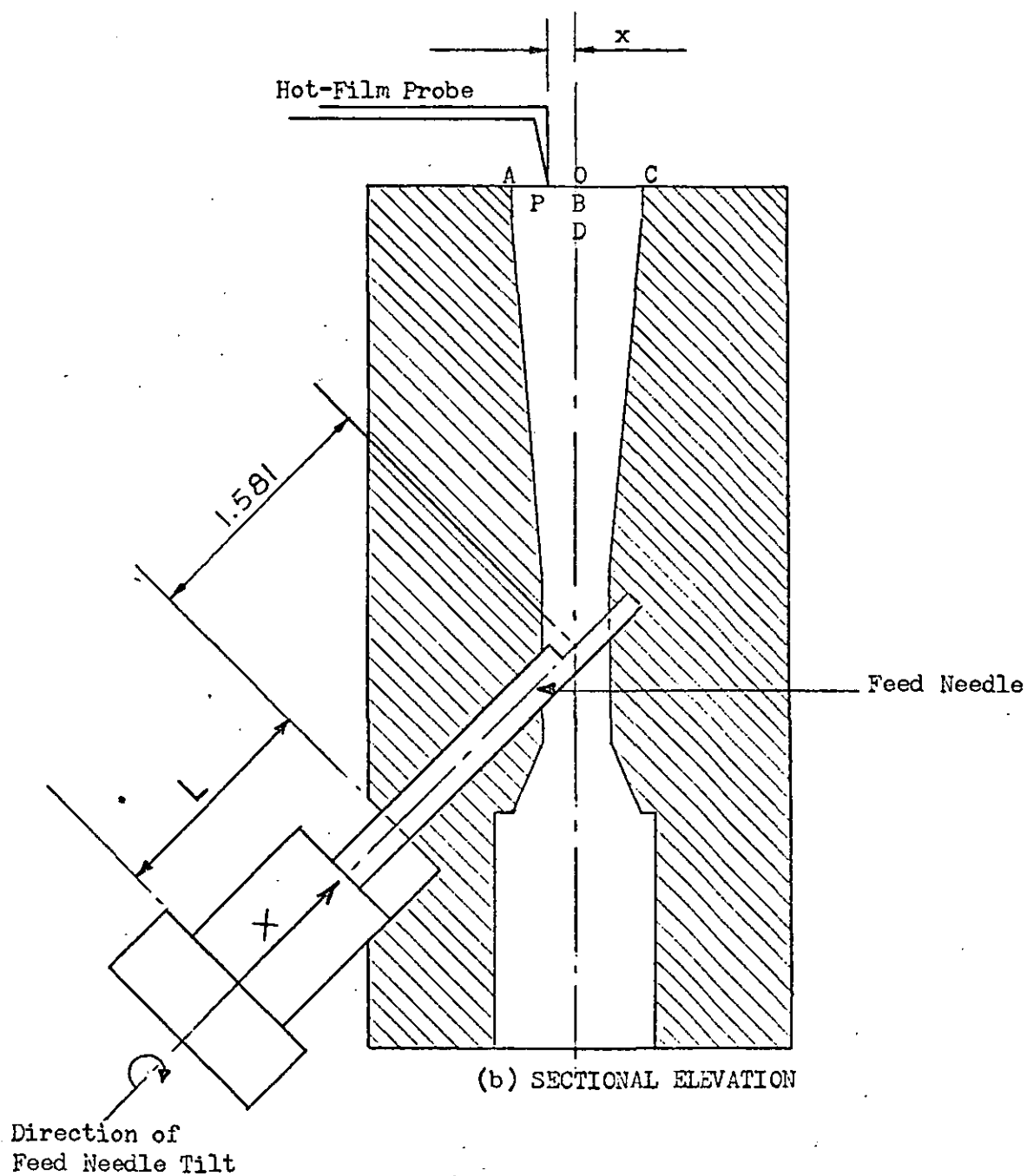
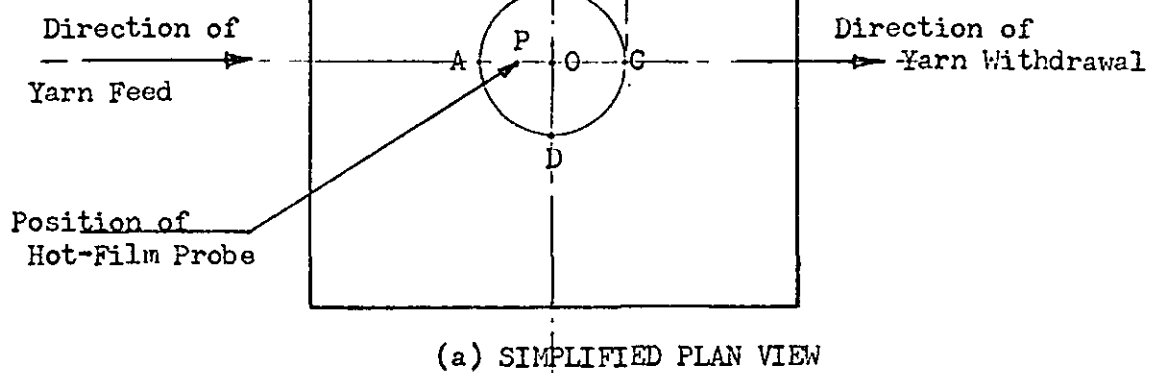


Fig.3.7 Setting of the Model Air-Jet for the Experimental Investigations

of these settings on bulking by studying the properties of the bulked yarn produced with varying processing conditions. He also reported that every jet behaves differently as regards the needle settings, and that optimum settings for satisfactory yarn bulking for a particular needle could only be obtained by a trial and error method. However, he was only able to offer a partial explanation for the phenomena observed⁽¹²⁾.

In the following Sections it is intended to study the flow characteristics of the large scale model jet with varying inlet pressures and feed-needle settings in order that, as a result of this study, a better understanding may be obtained of the factors involved.

During the investigations, the feed needle was always tilted towards the right-hand side of the jet when viewed in the direction of arrow X in Fig. 3.7. The modification of the jet (where used) was such as to block the left-hand channel as shown in Fig. 1.2.

3.5 High-Speed Cine Filming of the Process

In order to investigate the model yarn bulking phenomenon during operation, various regions of the bulking model jet were filmed. These films are available in the Department of Mechanical Engineering for inspection purposes. The model parent yarn was 1020 total denier, having 34 filaments and possessed 4 turns/in. (Z) twist (see Section 2.5.1). During the filming, the process variables were maintained as follows:-

Bulking speed = 150 ft/min.

Overfeed = 10%

Inlet pressure P_1 = 50 lbf/in² (gauge).

Feed needle angle of tilt α = 45° and the longitudinal setting L = 1.050 in.

A Fastax high speed cine camera was used, and the film speed was approximately 6000 frames/sec. at the end of filming, the camera being accelerated from rest.

A close examination of these films shows that the part of the pre-twisted model yarn, contained instantaneously within the air-jet, is completely open, and the actual bulking action takes place immediately as the yarn exits from the jet. A false untwisting of the yarn appears to occur in the region where the yarn leaves the jet at a right angle to its axis. The twist-free filament bundle inside the jet balloons out and, due to overfeeding, the extra available length of filaments snarl into a looped and entangled configuration. After the yarn leaves the air-jet, the twist reasserts itself and locks the already formed filament loops into position.

3.6 An Attempt to Investigate the Rotational Nature of the Yarn in the Air-Jet

The rotational nature of the yarn inside the jet was first observed by Wray^(11, 13) who also made a qualitative assessment of the twists inserted in the parent yarn prior to its entry into the jet. However, his experiments were carried out while the yarn was stationary because of the inherent difficulties of dynamic measurement of the phenomenon. Here, an attempt was made to measure the yarn rotation accurately while the bulking process was occurring. Fig. 3.8 shows a device, designed for this purpose. A straight beam of light, provided from a laser, crosses the air-jet perpendicular to its axis. The light beam falls on to a photo-cell on the other side of the jet. The concept was that each time the rotating yarn crosses the light path a shadow should be formed on the photo-cell. If the pulses generated are then amplified and fed into a digital counter, the number of shadows formed could be counted and therefore the amount

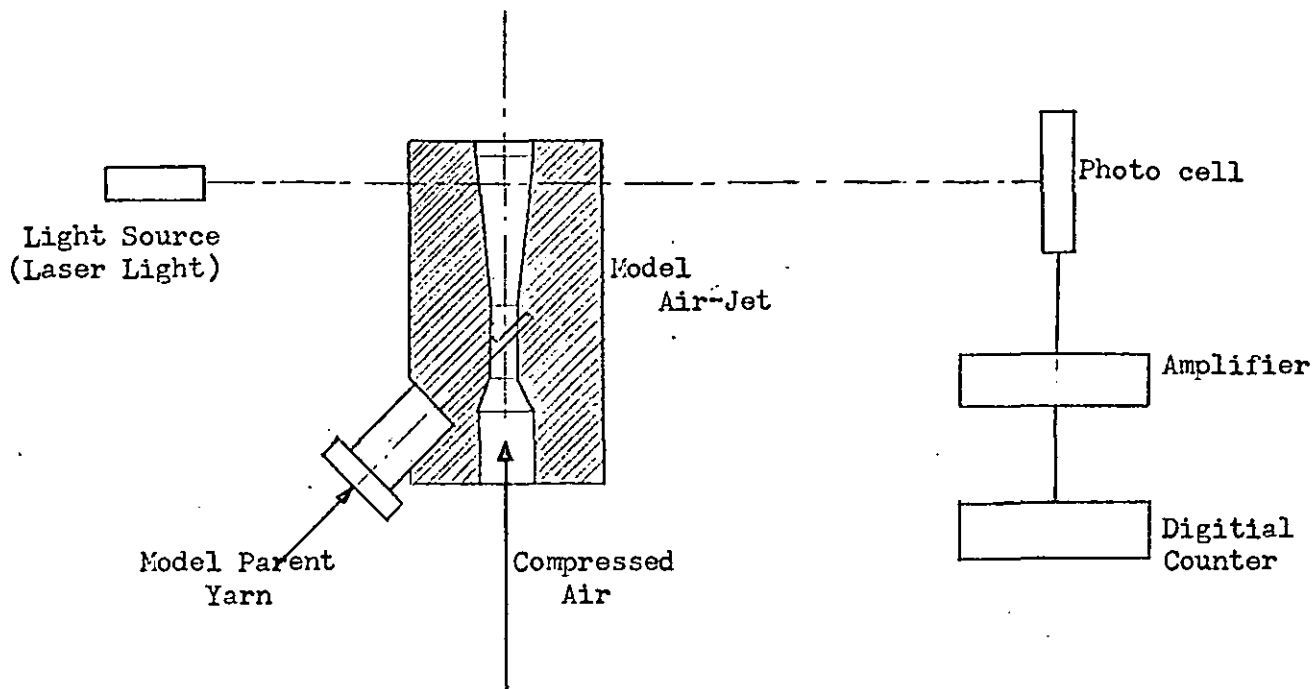


Fig. 3.8 Method of Measuring Yarn Rotation

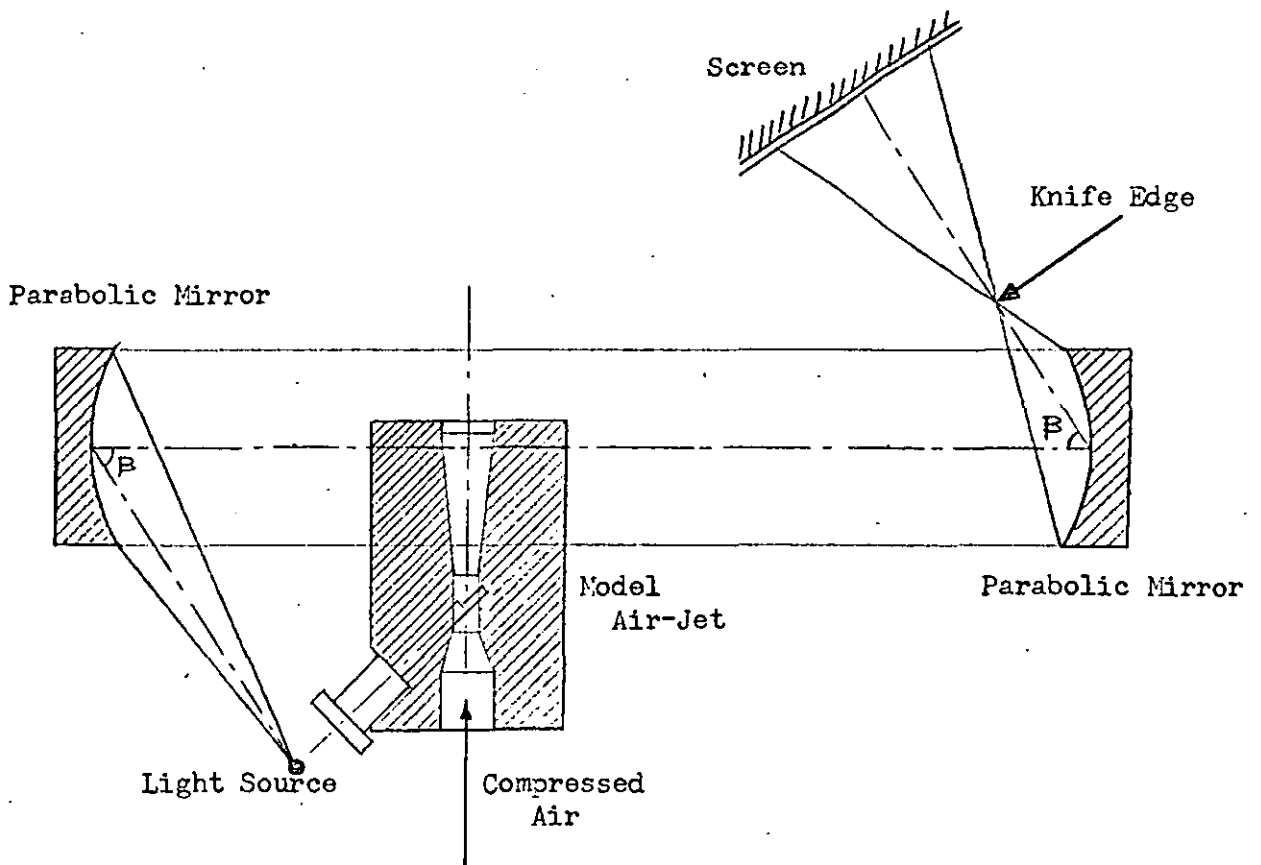


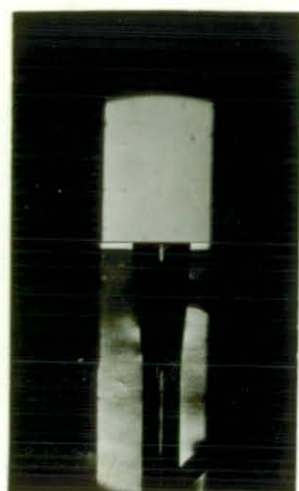
Fig. 3.9 Toepler-Schlieren Arrangement with Mirrors

of rotation could be known. However, this technique was devised before the high-speed photography (Section 3.5) was undertaken which revealed the inconsistency of the technique because the bundle of yarn inside the air-jet was shown to be completely open during the bulking operation, whereas it had been previously assumed that the yarn bundle would rotate as a whole at some section of the jet. Thus, filaments could cross the light beam either in groups or individually, and therefore the technique was susceptible to error and the attempt to measure yarn rotation inside the jet was abandoned as a failure.

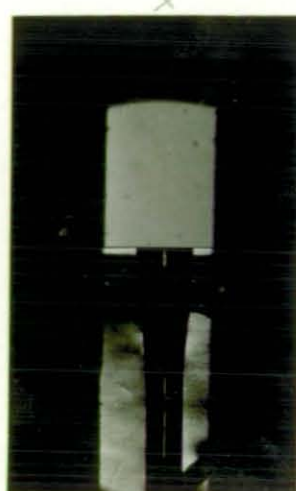
3.7 Visualization of the Flow

In order to obtain the flow nature in the jet the Schlieren method of investigation was employed. This method takes advantage of the change in density that accompanies changes in static pressure along the jet axis. Fig. 3.9 shows a schematic diagram of the arrangement.

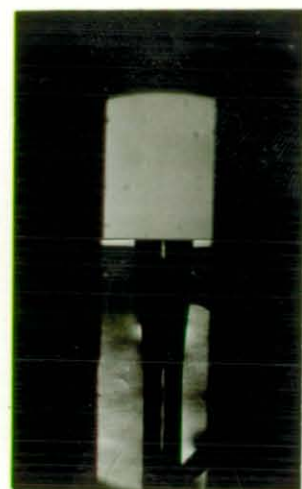
Rays from a mercury lamp light source pass through a pair of full-silvered parabolic mirrors and are caught on a screen. A knife edge is placed at the focal point of the second mirror and, as a result of this, part of the light beam is cut out and, therefore, the illumination of the screen is uniformly reduced. The model air-jet is positioned between the two mirrors. If, during its operation, a density gradient at some point along the flow direction is produced then this will give a downward or upward deflection of the light beams and these beams are either blocked or allowed to pass through by the knife-edge. Hence, a local increase or decrease in the light intensities falling on the screen will be produced and these can be photographed. In conventional wind tunnel practice, the Schlieren technique gives good results if the flow is contained in a rectangular cross-sectional channel and the observation windows through



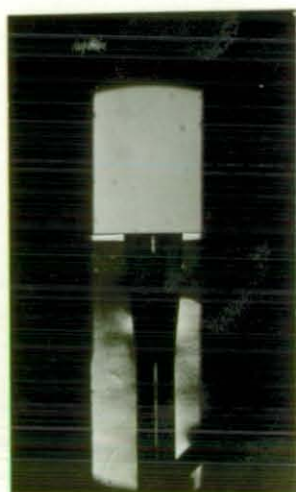
(a)

 $P_1 = 0 \text{ lbf/in}^2(\text{gauge})$ 

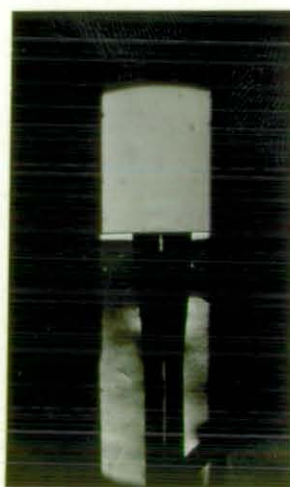
(b)

 $P_1 = 10 \text{ lbf/in}^2(\text{gauge})$ 

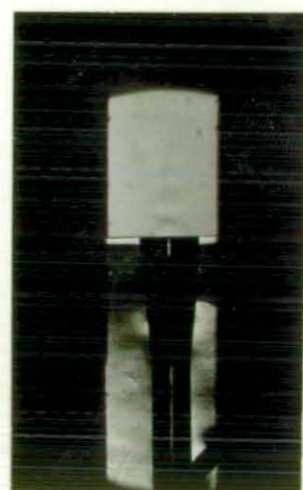
(c)

 $P_1 = 15 \text{ lbf/in}^2(\text{gauge})$ 

(d)

 $P_1 = 20 \text{ lbf/in}^2(\text{gauge})$ 

(e)

 $P_1 = 25 \text{ lbf/in}^2(\text{gauge})$ 

(f)

 $P_1 = 30 \text{ lbf/in}^2(\text{gauge})$

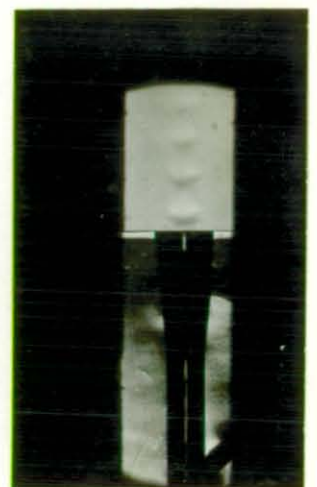
Fig. 3.10 Schlieren Photographs of the Flow through the Air-Jet without the Feed Needle, Showing the Development of Shock Waves at the Exit for a Varying Inlet Pressure P_1 . The Flow is from Bottom to Top



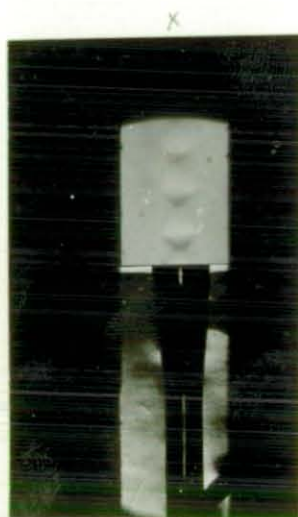
(g)

 $P_i = 35 \text{ lbf/in}^2 (\text{gauge})$ 

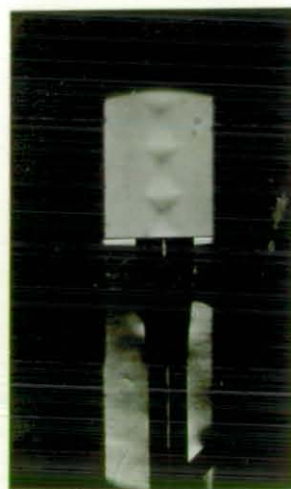
(h)

 $P_i = 40 \text{ lbf/in}^2 (\text{gauge})$ 

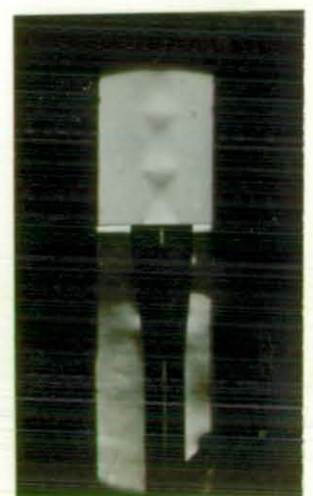
(j)

 $P_i = 45 \text{ lbf/in}^2 (\text{gauge})$ 

(k)

 $P_i = 50 \text{ lbf/in}^2 (\text{gauge})$ 

(l)

 $P_i = 55 \text{ lbf/in}^2 (\text{gauge})$ 

(m)

 $P_i = 60 \text{ lbf/in}^2 (\text{gauge})$

Fig. 3.10
(Cont.)

Schlieren Photographs of the Flow through the Air-Jet without the Feed Needle, Showing the Development of Shock Waves at the Exit for a Varying Inlet Pressure P_i . The Flow is from Bottom to Top

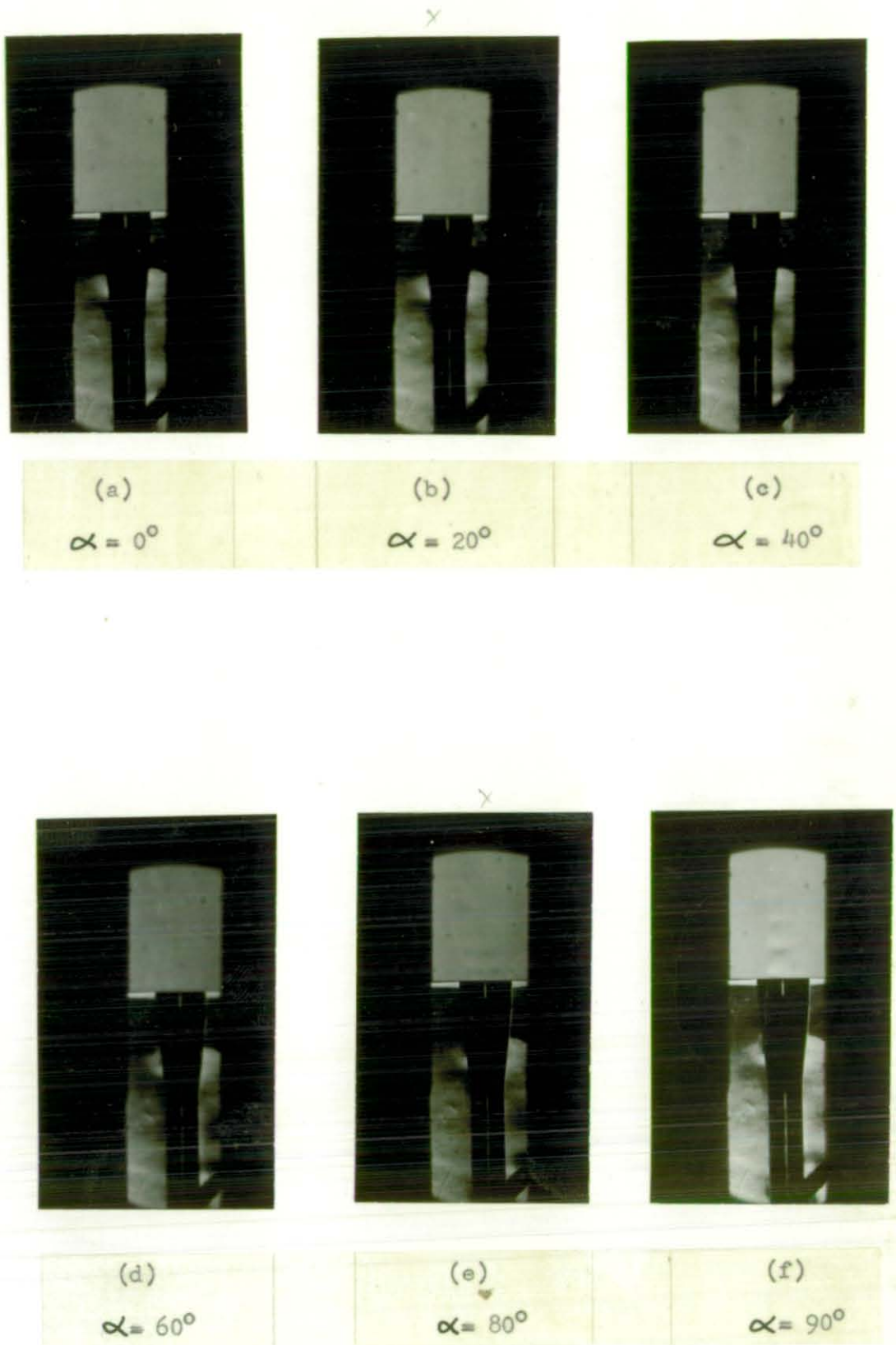


Fig. 3.11 Schlieren Photographs of the Flow through the Air-Jet with the Feed Needle Present, Showing the Development of Shock Waves at the Exit for a Varying Angle of Tilt α of the Feed Needle and Inlet Pressure $P_1 = 60 \text{ lbf/in}^2$ (gauge). The Flow is from Bottom to Top

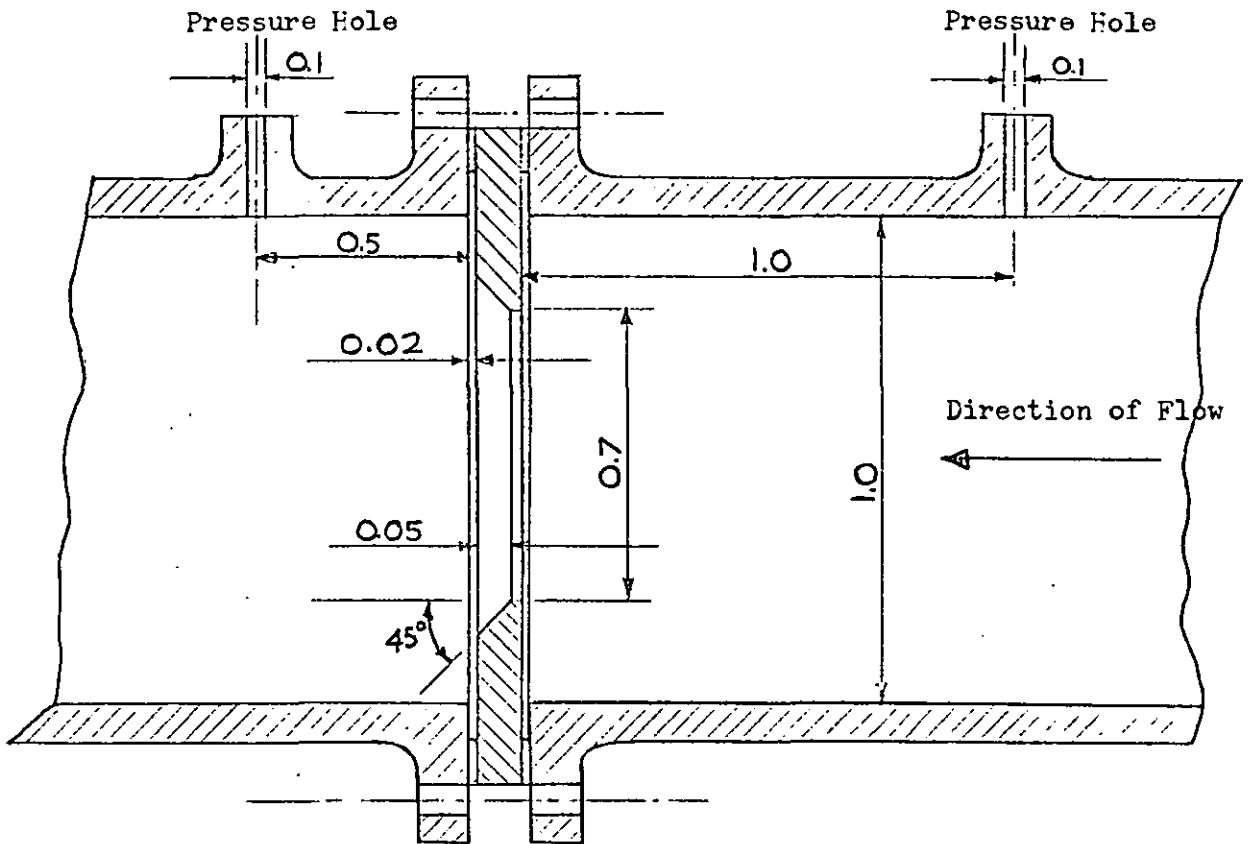


Fig. 3.12 Orifice Plate with D and D/2 Tappings

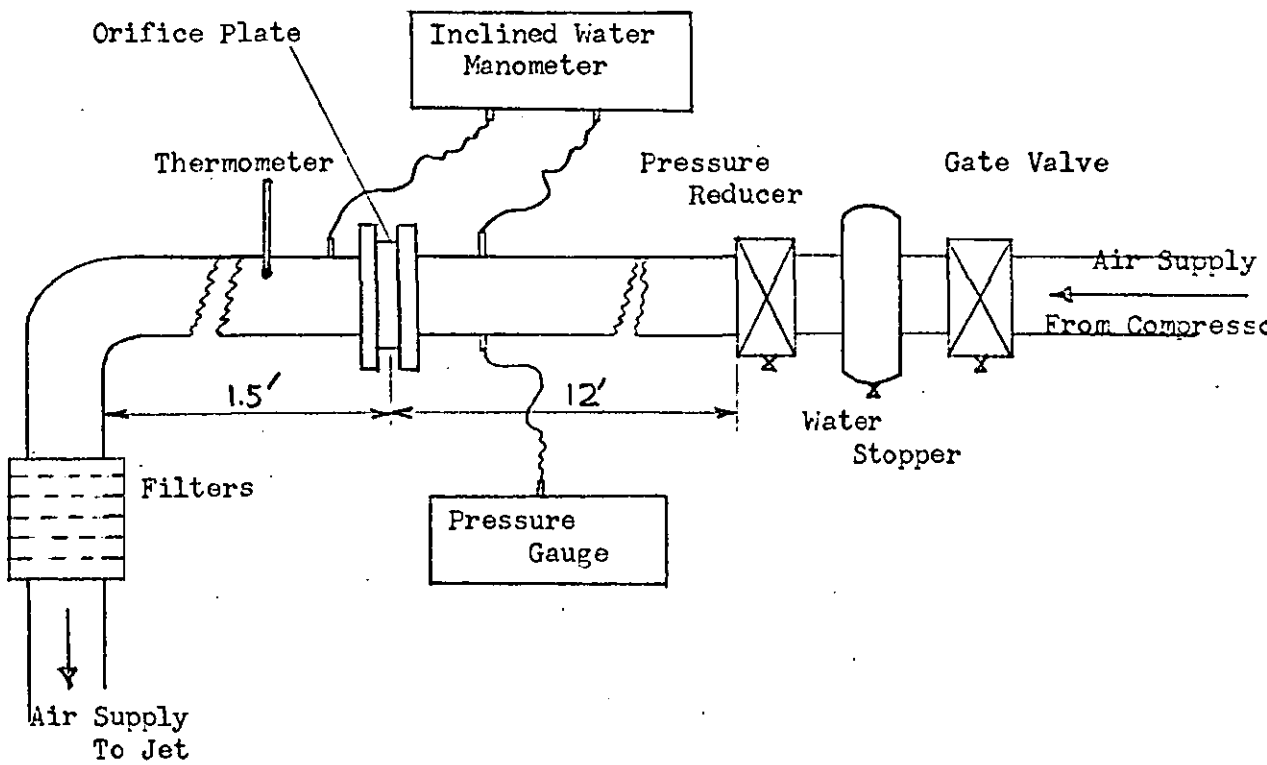


Fig. 3.13 Schematic Diagram of Air Supply Arrangement

which the light passes are made of plane surfaced high quality glass. However, in this case, the air-jet was made from perspex and the actual flow channel is of circular cross section with varying area along its axis and, therefore, a uniform illumination of the test section is not possible. Although the flow pattern at the exit of the jet is very clear on the photographs, it is not possible to obtain a satisfactory quality of definition for the inside of the jet. Figs. 3.10 and 3.11 respectively show the developments of shock waves at the exit of the air-jet for varying values of operating pressure ratio and feed needle angle while the longitudinal feed needle setting was fixed at $L = 1.050$ in.

3.8 Measurement of Air Flow through the Model Jet

The flow rate through the air-jet varies with the inlet pressure P_i , the angle of tilt α , and longitudinal setting of feed needle L and therefore, each of these was systematically varied. A square-edged orifice plate was employed to measure the flow rate. The design of this orifice plate was made to satisfy the requirements of B.S.I. ⁽²⁹⁾ (see Fig. 3.12). D and $D/2$ pressure tapings were used to measure the pressure differences. A schematic diagram of experimental arrangement is shown in Fig. 3.13. An inclined U-tube manometer was made to withstand high pressures and to record the pressure differences. A thermometer was inserted in the downstream section of the pipe to record the air temperature, the upstream static pressure being recorded by means of a pressure gauge.

3.8.1 Calculation of Flow Rate and Reynolds Number

The equations for flow rate through an orifice plate are given in Ref. (29). The mass rate of flow, $W = 359.2 C.Z.E.d\sqrt{h_p}$ (lb/hr.). The Reynolds number, $R = \frac{W}{15.8 \times \eta d}$ (based on the orifice diameter).

Method of Calculation: Assuming the air is dry, the following measurements are made initially:

- (a) Orifice or throat diameter, d (in).
- (b) Internal diameter of upstream pipe, D (in).
- (c) Pressure difference, h (in. H_2O).
- (d) Density of fluid at upstream tapping, ρ (lb/ft^3),
(the formula, $\rho = \frac{2.7 \times P}{T}$ (lb/ft^3) is used).
- (e) Viscosity of fluid at upstream tapping, η (poise).
- (f) Absolute temperature of fluid at upstream tapping, T ($^{\circ}F$).
(note: actual measured temperature was T_0 , $^{\circ}C$).
- (g) Absolute pressure at upstream tapping, P_0 (lb/in^2 , gauge).
- (h) Specific heat ratio, γ .

Then, the following calculations are to be made from the above measurements:

- (j) Diameter ratio, d/D .
- (k) Area ratio, $m (= \frac{d^2}{D^2})$.
- (l) Pressure difference ratio, $\frac{h}{P}$ (in $H_2O/lbf/in^2$).
- (m) Velocity of approach factor, $E (= \frac{1}{\sqrt{1 - m^2}})$.

The values of the basic coefficient C corresponding to the area ratio m , and the value of the expansibility factor ϵ corresponding to the pressure difference ratio $\frac{h}{P}$, are obtained from the graphs in Ref. (29). A provisional value of the flow rate W is calculated by taking the correction factor Z equal to unity. This value is used to calculate the Reynolds number. Finally, the value of Z corresponding to the R , pipe diameter D , and the area ratio m , is obtained from the graphs in Ref. (29) and the corrected rate of flow is found by multiplying the provisional value by the correction factor Z .

The volume rate of flow, Q (ft³/hr), at a reference condition of 60°F and 30 in.Hg. is found by dividing the mass rate of flow by the density at this reference condition.

The Reynolds number based on the air-jet throat diameter is calculated assuming the temperature at the throat is equal to the orifice upstream pressure tapping. If the Reynolds number based on the feed needle diameter is required, then the R based on the throat diameter is multiplied by $\left[\frac{\text{needle diameter}}{\text{throat diameter}} = \frac{a}{b} \right]$ and finally, this must be corrected for wall interference effects. The formula given by Allen and Vincenti⁽³⁰⁾ could be used.

$$R_{\text{(corrected)}} = R_{\text{(calculated)}} \left[1 + \frac{1}{4} C_d \left(\frac{a}{b} \right) + 0.82 \left(\frac{a^2}{b^2} \right) \right]$$

(where C_d is the drag coefficient)

3.8.2 Variation of the Flow Rate with Varying Angle of Tilt and Inlet Pressure

During this experimental investigation, the longitudinal setting of the feed needle L i.e. the distance between the feed needle shoulder and the air-jet block (see Fig. 3.7), was kept constant at $L = 1.050$ in.

At the time that the measurements were made, the atmospheric temperature was 20°C (527°F, abs.) and the atmospheric pressure was 760 mm Hg (14.696 lbf/in², abs.).

Neglecting the pressure losses between the orifice inlet pressure tapping and the inlet to the air-jet, then P_i can be taken as equal to P_o .

Table 3.2 gives the flow rates and Reynolds numbers (based on air-jet throat diameter) for variations of feed needle angle of tilt α and inlet pressure P_o for the normal model jet. Table 3.3 gives the corresponding results for the modified model jet, i.e. with a plug inserted to block off the left-hand half of the

TABLE 3.2. Flow Rate and Reynolds No. for Normal Model Air-Jet

When $L = 1.050$ in.

(Varying Angle of Tilt and Inlet Pressure)

α (degree)	h (in.H ₂ O)	T ₀ (°C)	W (lb/hr.)	Q (ft ³ /hr.)	R $\times (10^5)$
0	2.21	20.0	84.570	1107.607	0.9880
10	2.27	18.5	86.012	1126.493	1.0104
20	2.28	18.0	86.111	1127.786	1.0144
30	2.28	17.0	86.254	1129.652	1.0189
40	2.44	23.0	88.317	1156.682	1.0318
50	2.74	17.0	94.463	1237.163	1.1159
60	2.95	18.0	97.825	1281.201	1.1523
70	3.25	18.0	102.619	1343.980	1.2089
80	3.42	24.0	104.203	1364.734	1.1977
90	3.58	20.0	107.364	1406.129	1.2544
(a) $P_0 = 10$ lbf/in ² (gauge)					

0	3.23	19.0	120.395	1583.871	1.4129
10	3.30	18.5	122.565	1605.212	1.4398
20	3.36	18.0	123.544	1618.038	1.4554
30	3.43	17.0	125.019	1637.349	1.4769
40	3.63	23.0	127.311	1667.370	1.4874
50	4.02	17.0	135.278	1771.720	1.5981
60	4.33	18.0	140.138	1835.362	1.6509
70	4.92	18.0	149.307	1955.453	1.7590
80	5.06	24.0	149.900	1963.211	1.7229
90	5.42	20.0	156.233	2046.158	1.8253
(b) $P_0 = 20$ lbf/in ² (gauge)					

0	4.29	19.0	157.911	2068.136	1.8449
10	4.33	18.5	159.069	2083.304	1.8687
20	4.41	18.0	160.363	2100.248	1.8891
30	4.53	17.0	162.783	2131.945	1.9230
40	4.80	23.0	165.853	2172.145	1.9377
50	5.30	17.0	175.954	2304.441	2.0786
60	5.70	18.0	182.118	2385.170	2.1454
70	6.25	18.0	190.627	2496.611	2.2457
80	6.53	24.0	192.879	2526.106	2.2169
90	7.00	20.0	201.087	2633.595	2.3494
(c) $P_0 = 30$ lbf/in ² (gauge)					

TABLE 3.2
(Cont.)

Flow Rate and Reynolds No. for Normal Model Air-Jet

When $L = 1.050$ in.

(Varying Angle of Tilt and Inlet Pressure)

α (degree)	h (in.H ₂ O)	T ₀ (°C)	W (lb/hr.)	Q (ft ³ /hr.)	R ×(10 ⁵)
0	5.37	19.0	195.097	2555.150	2.2794
10	5.35	18.5	195.253	2557.193	2.2938
20	5.55	18.0	198.640	2601.553	2.3400
30	5.71	17.0	201.797	2642.895	2.3839
40	6.02	23.0	209.299	2741.155	2.4453
50	6.57	17.0	216.333	2833.269	2.5555
60	7.12	18.0	224.767	2943.738	2.6479
70	7.87	18.0	236.216	3093.678	2.7827
80	8.07	24.0	236.779	3101.047	2.7215
90	8.60	20.0	246.152	3223.804	2.8759
(d) $P_0 = 40 \text{ lbf/in}^2$ (gauge)					

0	6.40	19.0	231.299	3029.285	2.7024
10	6.45	18.5	232.821	3049.209	2.7352
20	6.57	18.0	234.729	3074.208	2.7652
30	6.80	17.0	239.151	3132.113	2.8251
40	7.20	23.0	248.599	3255.855	2.9045
50	7.87	17.0	257.127	3367.547	3.0375
60	8.50	18.0	266.674	3492.578	3.1415
70	9.25	18.0	278.081	3641.969	3.2759
80	9.65	24.0	281.184	3682.609	3.2319
90	10.15	20.0	290.378	3803.028	3.3926
(e) $P_0 = 50 \text{ lbf/in}^2$ (gauge)					

0	7.52	19.0	269.033	3523.472	3.1432
10	7.56	18.5	270.467	3542.257	3.1774
20	7.68	18.0	272.318	3566.504	3.2080
30	7.95	17.0	277.468	3633.947	3.2778
40	8.43	23.0	288.613	3779.914	3.3720
50	9.14	17.0	297.305	3893.744	3.5121
60	9.92	18.0	309.097	4048.184	3.6413
70	10.85	18.0	323.070	4231.180	3.8060
80	11.40	24.0	327.839	4293.646	3.7682
90	12.20	20.0	341.434	4471.692	3.9891
(f) $P_0 = 60 \text{ lbf/in}^2$ (gauge)					

TABLE 3.3. Flow Rate and Reynolds No. for Modified Model Air-Jet

When $L = 1.050$ in.

(Varying Angle of Tilt and Inlet Pressure)

α (degree)	h (in. H ₂ O)	T_o (°C)	W (lb/hr.)	Q (ft ³ /hr.)	R $\times (10^{-5})$
0	0.55	20.0	42.480	556.360	0.4963
10	0.57	20.0	43.035	563.627	0.5028
20	0.55	21.0	42.146	551.989	0.4910
30	0.60	20.0	44.244	579.458	0.5169
40	0.65	21.0	46.069	603.364	0.5368
50	0.72	21.0	48.298	632.558	0.5627
60	0.87	22.0	53.014	694.317	0.6160
70	0.99	22.0	56.619	741.540	0.6579
80	1.09	22.0	59.333	777.078	0.6894
90	1.14	21.0	60.717	795.198	0.7074
(a) $P_o = 10$ lbf/in ² (gauge)					

0	0.87	20.0	63.234	828.166	0.7388
10	0.94	20.0	65.495	857.786	0.7652
20	0.93	21.0	64.888	849.835	0.7560
30	1.00	20.0	67.756	887.388	0.7916
40	1.30	21.0	76.771	1005.459	0.8945
50	1.20	21.0	73.634	964.375	0.8579
60	1.40	22.0	79.368	1039.478	0.9222
70	1.57	22.0	84.024	1100.456	0.9763
80	1.65	22.0	86.172	1128.588	1.0013
90	1.77	21.5	89.373	1170.507	1.0385
(b) $P_o = 20$ lbf/in ² (gauge)					

0	1.20	20.0	83.893	1098.731	0.9802
10	1.22	20.0	84.485	1106.487	0.9871
20	1.21	21.0	83.826	1097.857	0.9767
30	1.32	20.0	87.841	1150.448	1.0263
40	1.44	21.0	91.396	1197.006	1.0649
50	1.64	21.0	97.720	1279.819	1.1386
60	1.91	22.0	105.100	1376.480	1.2212
70	2.08	22.5	109.442	1433.350	1.2717
80	2.21	22.0	113.031	1480.350	1.3134
90	2.30	21.5	115.270	1509.678	1.3394
(c) $P_o = 30$ lbf/in ² (gauge)					

TABLE 3.3. Flow Rate and Reynolds No. for Modified Model Air-Jet
(Cont.)

When $L = 1.050$ in.

(Varying Angle of Tilt and Inlet Pressure)

α (degree)	h (in. H ₂ O)	T_o (°C)	W (lb/hr.)	Q (ft ³ /hr.)	R $\times (10^5)$
0	1.57	20.0	105.735	1384.791	1.2353
10	1.59	20.0	106.800	1398.745	1.2478
20	1.59	21.0	106.455	1394.220	1.2403
30	1.70	21.0	109.799	1438.015	1.2793
40	1.89	21.0	115.664	1514.831	1.3476
50	2.13	21.0	122.939	1610.113	1.4324
60	2.38	21.5	129.845	1700.562	1.5087
70	2.57	22.5	134.659	1763.605	1.5647
80	2.72	22.0	138.509	1814.027	1.6094
90	2.85	21.5	141.893	1858.345	1.6487
(d) $P_o = 40$ lbf/in ² (gauge)					

0	1.93	20.0	127.629	1671.536	1.4911
10	1.96	20.0	128.551	1683.612	1.5019
20	1.97	21.0	128.463	1682.463	1.4968
30	2.11	21.0	133.038	1742.380	1.5501
40	2.25	21.0	137.367	1799.078	1.6005
50	2.49	21.0	144.335	1890.331	1.6817
60	2.83	21.5	153.897	2015.562	1.7882
70	3.34	22.5	166.826	2184.894	1.9384
80	3.23	22.0	164.084	2148.977	1.9066
90	3.33	21.5	166.733	2183.678	1.9374
(e) $P_o = 50$ lbf/in ² (gauge)					

0	2.26	20.0	148.393	1943.481	1.7337
10	2.27	20.0	148.655	1946.916	1.7368
20	2.34	21.0	150.482	1970.843	1.7533
30	2.49	21.0	155.215	2032.831	1.8085
40	2.68	21.0	160.997	2108.547	1.8758
50	2.97	21.0	169.365	2218.139	1.9733
60	3.26	21.5	177.396	2323.325	2.0613
70	3.55	22.5	184.734	2419.427	2.1465
80	3.75	22.0	190.008	2488.502	2.2078
90	3.87	21.5	193.169	2529.905	2.2445
(f) $P_o = 60$ lbf/in ² (gauge)					

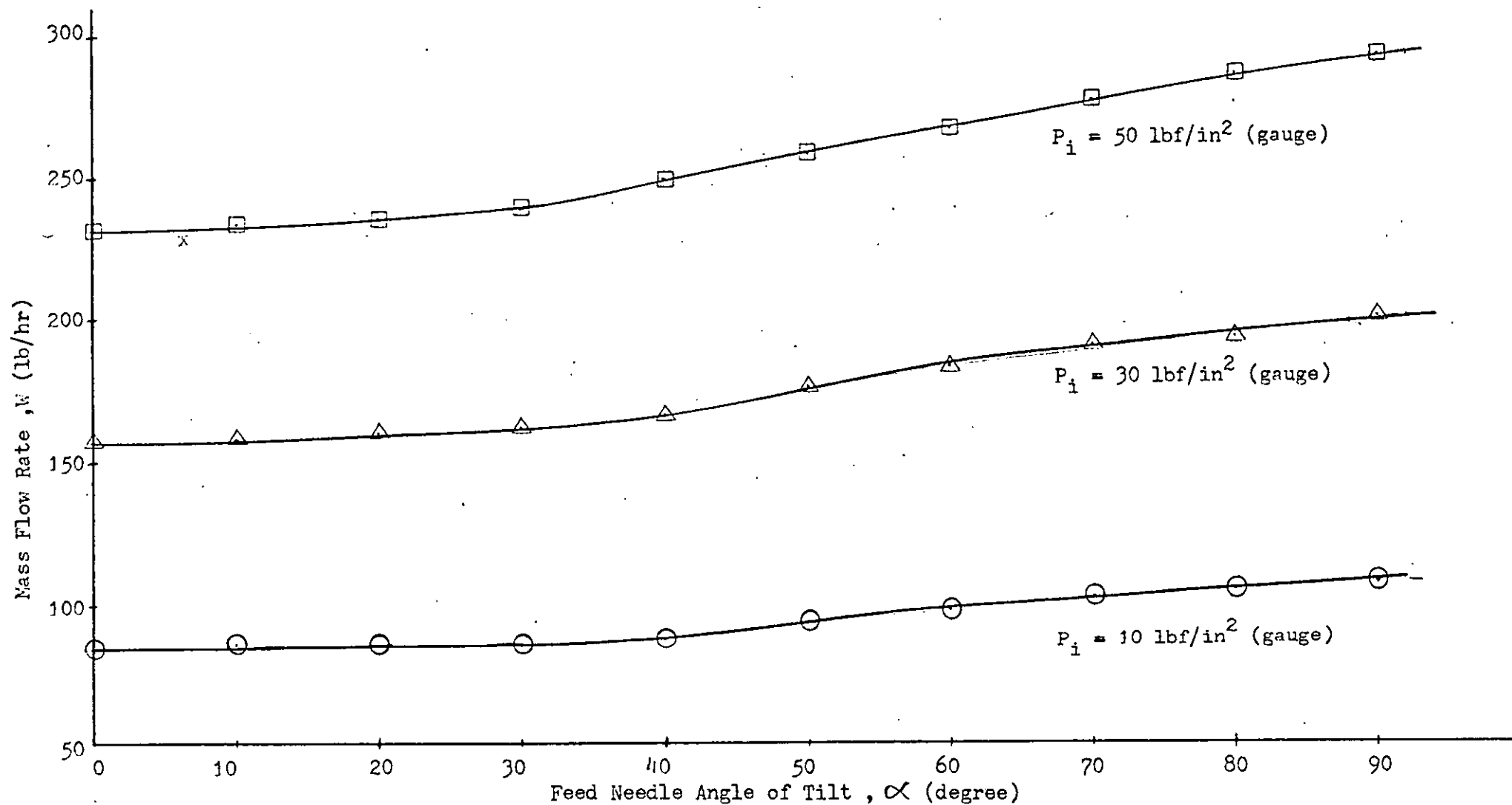


Fig. 3.14 Flow Rate for Normal Model Air-Jet with Varying Feed Needle Angle of Tilt

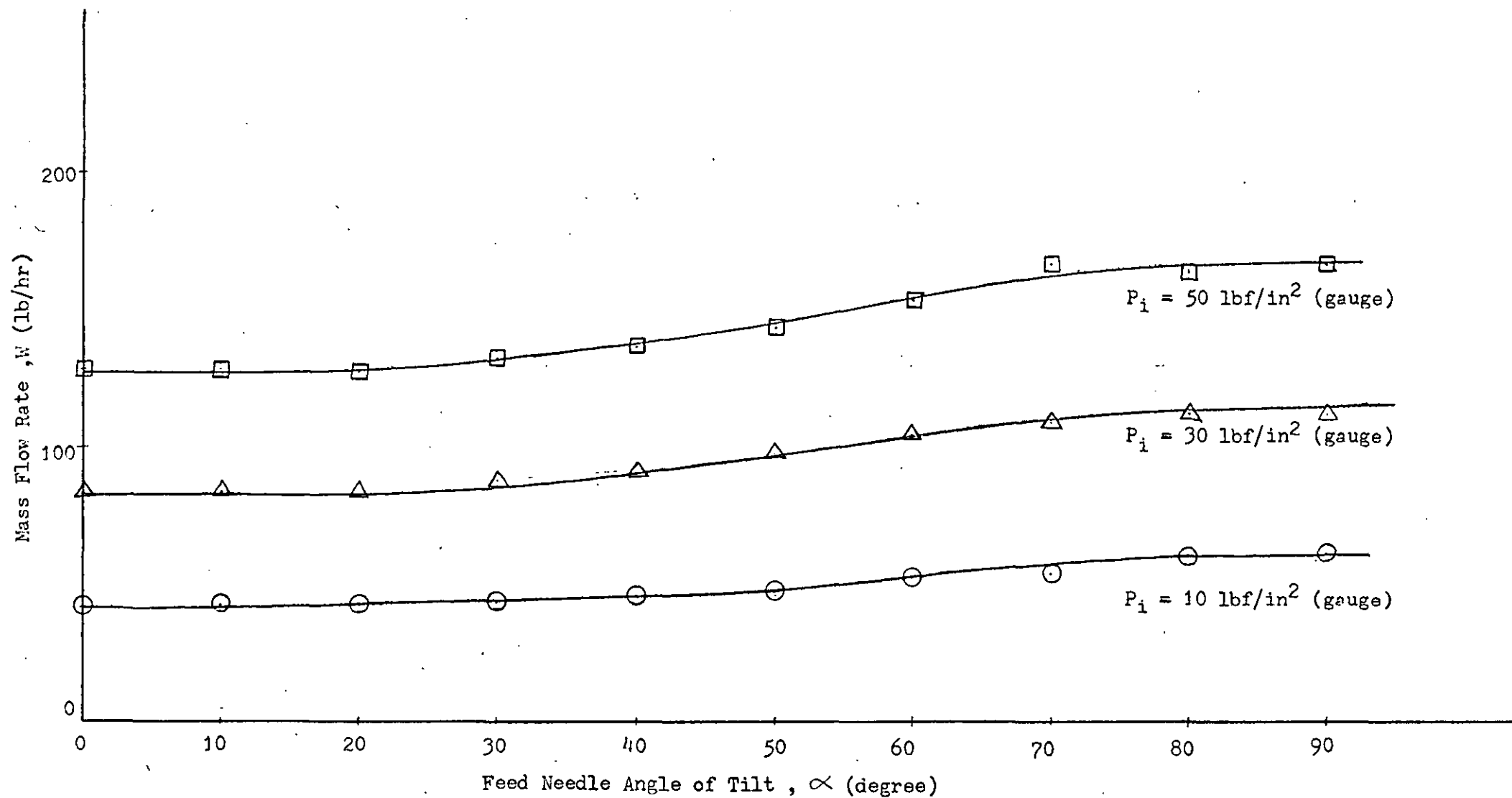


Fig. 3.15 Flow Rate for Modified Model Air-Jet with Varying Feed Needle Angle of Tilt

TABLE 3.4.1

Flow Rate and Reynolds No. for Normal Model Air-Jet
When $\alpha = 40^\circ$
(Varying Longitudinal Setting and Inlet Pressure)

L (in)	h (in.H ₂ O)	T _o (°C)	W (lb/hr.)	Q (ft ³ /hr.)	R ×(10 ⁵)
0.754	2.41	18.5	88.9402	1161.748	1.0449
0.862	2.42	18.0	89.2008	1165.1525	1.0508
0.950	2.36	15.4	88.4628	1155.512	1.0509
1.004	2.49	16.0	90.7614	1185.537	1.0752
1.057	2.73	17.0	94.8243	1238.607	1.1203
1.090	2.81	18.0	96.0260	1254.304	1.1312
(a) P _i = 10 lbf/in ² (gauge)					
0.754	3.50	18.5	126.5316	1652.772	1.4865
0.862	3.44	18.0	125.5620	1640.107	1.4792
0.950	3.50	16.0	127.0687	1659.787	1.5053
1.004	3.68	16.5	130.1698	1700.294	1.5420
1.057	3.98	17.0	135.2288	1766.370	1.5975
1.090	4.15	18.0	137.8446	1800.543	1.6239
(b) P _i = 20 lbf/in ² (gauge)					
0.754	4.62	18.5	164.6419	2150.573	1.9342
0.862	4.53	18.0	163.2019	2131.764	1.9226
0.950	4.53	16.0	163.7385	2138.773	1.9397
1.004	4.82	16.5	168.7193	2203.832	1.9987
1.057	5.24	17.0	175.7130	2295.185	2.0757
1.090	5.41	18.0	178.2279	2328.035	2.0996
(c) P _i = 30 lbf/in ² (gauge)					
0.754	5.72	19.0	202.1067	2639.943	2.3613
0.862	5.65	18.0	201.2245	2628.420	2.3705
0.950	5.65	16.0	201.8856	2637.055	2.3916
1.004	5.99	17.0	207.4724	2710.031	2.4509
1.057	6.51	17.0	216.2478	2824.656	2.5546
1.090	6.73	18.0	219.4863	2866.958	2.5856
(d) P _i = 40 lbf/in ² (gauge)					
0.754	6.81	19.0	239.5026	3128.413	2.7982
0.862	6.74	18.5	238.0708	3109.710	2.7968
0.950	6.77	16.0	240.0099	3135.040	2.8432
1.004	7.16	17.0	246.3520	3217.881	2.9102
1.057	7.75	17.0	256.2253	3346.847	3.0268
1.090	7.97	18.0	259.4072	3388.409	3.0559
(e) P _i = 50 lbf/in ² (gauge)					
0.754	7.89	19.0	276.6588	3613.752	3.2323
0.862	7.83	19.0	275.6046	3599.982	3.2200
0.950	7.87	16.0	277.6828	3627.128	3.2895
1.004	8.37	17.0	285.8175	3733.384	3.3764
1.057	8.98	17.0	295.9617	3865.889	3.4902
1.090	9.31	18.5	300.5365	3925.645	3.5307
(f) P _i = 60 lbf/in ² (gauge)					

TABLE 3.4.2

Flow Rate and Reynolds No. for Normal Model Air-Jet
When $\alpha = 80^\circ$
(Varying Longitudinal Setting and Inlet Pressure)

L (in)	h (in. H ₂ O)	T _o (°C)	W (lb/hr.)	Q (ft ³ /hr.)	R × (10 ⁵)
0.754	2.44	18.5	89.4832	1168.841	1.0512
0.862	2.54	18.0	91.3588	1193.340	1.0762
0.950	2.93	16.0	98.3482	1284.637	1.1650
1.004	3.33	16.5	104.6711	1367.266	1.2399
1.057	3.76	17.5	108.9226	1422.760	1.2867
1.090	4.13	18.0	116.2216	1518.101	1.3691
(a) P _i = 10 lbf/in ² (gauge)					
0.754	3.52	18.5	126.8927	1657.488	1.4907
0.862	3.69	18.0	130.0190	1698.325	1.5317
0.950	4.28	16.0	140.4334	1834.359	1.6636
1.004	4.92	16.5	150.3783	1964.260	1.7814
1.057	5.51	17.5	158.8189	2074.513	1.8762
1.090	6.07	18.0	166.4967	2174.801	1.9614
(b) P _i = 20 lbf/in ² (gauge)					
0.754	4.62	19.0	164.5219	2149.006	1.9222
0.862	4.84	18.5	168.4999	2200.966	1.9795
0.950	5.59	16.5	181.5891	2371.939	2.1511
1.004	6.46	17.0	194.9642	2546.646	2.3031
1.057	7.22	17.5	205.8150	2688.381	2.4313
1.090	7.89	18.0	214.9188	2807.296	2.5318
(c) P _i = 30 lbf/in ² (gauge)					
0.754	5.75	19.0	202.6362	2646.859	2.3675
0.862	6.05	18.5	207.9864	2716.744	2.4434
0.950	6.84	16.5	221.8082	2897.286	2.6276
1.004	8.01	17.0	239.6816	3130.751	2.8314
1.057	8.98	17.5	253.4611	3310.741	2.9942
1.090	9.77	18.5	263.8359	3446.257	3.0995
(d) P _i = 40 lbf/in ² (gauge)					
0.754	6.84	19.0	240.0294	3135.294	2.8043
0.862	7.20	19.0	246.2162	3216.107	2.8766
0.950	8.12	17.0	262.2185	3425.130	3.0976
1.004	9.52	17.0	283.7567	3706.466	3.3521
1.057	10.69	17.5	300.2811	3922.310	3.5473
1.090	11.61	18.5	312.2667	4078.867	3.6685
(e) P _i = 50 lbf/in ² (gauge)					
0.754	7.97	19.0	278.0302	3631.665	3.2483
0.862	8.28	19.0	283.3574	3701.249	3.3106
0.950	9.59	16.0	306.2860	4000.745	3.6283
1.004	11.17	17.0	329.7250	4306.909	3.8951
1.057	12.44	17.5	347.4934	4539.002	4.1050
1.090	13.62	19.0	362.5587	4735.787	4.2359
(f) P _i = 60 lbf/in ² (gauge)					

TABLE 3.5.1 Flow Rate and Reynolds No. for Modified Model Air-Jet
When $\alpha = 40^\circ$
(Varying Longitudinal Setting and Inlet Pressure)

L (in)	h (in.H ₂ O)	T _o (°C)	W (lb/hr.)	Q (ft ³ /hr.)	R ×(10 ⁻⁵)
0.754	0.74	18.0	49.6108	648.023	0.5844
0.862	0.72	19.0	48.8583	638.193	0.5708
0.950	0.84	20.0	52.6907	688.253	0.6139
1.004	0.78	20.0	50.7833	663.338	0.5917
1.057	0.84	20.0	52.6125	687.132	0.6130
1.090	0.95	20.0	56.0074	731.576	0.6526
(a) P _i = 10 lbf/in ² (gauge)					
0.754	1.08	18.0	70.7618	924.300	0.8336
0.862	1.02	19.0	68.6726	897.011	0.8023
0.950	1.26	20.5	75.9912	992.606	0.8830
1.004	1.20	20.0	74.1743	968.874	0.8642
1.057	1.31	20.0	77.5276	1012.675	0.9033
1.090	1.46	20.0	81.7978	1068.453	0.9531
(b) P _i = 20 lbf/in ² (gauge)					
0.754	1.43	18.0	92.0823	1202.790	1.0848
0.862	1.34	19.0	89.0314	1162.939	1.0402
0.950	1.69	21.0	99.4979	1299.654	1.1561
1.004	1.60	20.0	96.8502	1265.069	1.1284
1.057	1.75	20.0	101.2191	1322.136	1.1793
1.090	1.96	20.0	107.0572	1398.395	1.2474
(c) P _i = 30 lbf/in ² (gauge)					
0.754	1.78	18.5	113.2708	1479.558	1.3307
0.862	1.69	19.0	110.2893	1440.613	1.2885
0.950	2.09	21.0	122.1715	1595.819	1.4196
1.004	2.00	20.0	119.5354	1561.386	1.3927
1.057	2.18	20.5	124.7619	1629.656	1.4497
1.090	2.43	20.0	131.7949	1721.522	1.5356
(d) P _i = 40 lbf/in ² (gauge)					
0.754	2.11	18.5	133.9776	1750.032	1.5740
0.862	2.06	19.0	132.2841	1727.912	1.5455
0.950	2.51	21.0	145.4364	1899.708	1.6899
1.004	2.43	20.5	143.1140	1869.373	1.6629
1.057	2.64	20.5	149.2674	1949.750	1.7344
1.090	2.92	20.5	156.9221	2049.736	1.8234
(e) P _i = 50 lbf/in ² (gauge)					
0.754	2.46	18.5	155.2797	2028.283	1.8242
0.862	2.45	19.0	154.8357	2022.483	1.8090
0.950	2.88	21.0	167.2201	2184.250	1.9430
1.004	2.88	20.5	167.2201	2184.250	1.9430
1.057	3.10	20.5	173.5837	2267.372	2.0170
1.090	3.43	20.5	182.5200	2384.099	2.1208
(f) P _i = 60 lbf/in ² (gauge)					

TABLE 3.5.2 Flow Rate and Reynolds No. for Modified Model Air-Jet
When $\alpha = 80^\circ$
(Varying Longitudinal Setting and Inlet Pressure)

L (in)	h (in.H ₂ O)	T _o (°C)	W (lb/hr.)	Q (ft ³ /hr.)	R ×(10 ⁻⁵)
0.754	0.74	18.0	49.6108	648.023	0.5844
0.862	0.78	19.0	50.8385	664.059	0.5940
0.950	1.10	20.0	60.4615	786.754	0.7045
1.004	1.08	20.0	59.6817	779.570	0.6954
1.057	1.27	20.0	64.6748	844.790	0.7535
1.090	1.26	20.0	64.4197	841.458	0.7506
(a) P _i = 10 lbf/in ² (gauge)					
0.754	1.07	18.0	70.4336	920.012	0.8297
0.862	1.14	19.0	72.5573	947.752	0.8477
0.950	1.67	20.5	87.4148	1141.823	1.0157
1.004	1.62	20.0	86.2326	1126.381	1.0047
1.057	1.92	20.0	93.7771	1224.928	1.0926
1.090	1.91	20.0	93.5326	1221.735	1.0898
(b) P _i = 20 lbf/in ² (gauge)					
0.754	1.40	18.0	91.1294	1190.343	1.0735
0.862	1.49	19.0	93.8177	1225.459	1.0961
0.950	2.22	21.0	113.9032	1487.818	1.3235
1.004	2.13	20.0	111.8427	1460.903	1.3031
1.057	2.52	20.0	121.6037	1588.403	1.4168
1.090	2.51	20.0	121.3624	1585.251	1.4140
(c) P _i = 30 lbf/in ² (gauge)					
0.754	1.72	18.5	111.3562	1454.549	1.3082
0.862	1.90	19.0	116.9070	1527.054	1.3659
0.950	2.47	21.0	132.7620	1734.154	1.5426
1.004	2.64	20.0	137.5491	1796.684	1.6026
1.057	3.09	20.0	148.5169	1939.947	1.7257
1.090	3.10	20.0	148.9782	1945.972	1.7358
(d) P _i = 40 lbf/in ² (gauge)					
0.754	2.09	18.5	133.3409	1741.715	1.5665
0.862	2.31	19.0	140.0264	1829.042	1.6360
0.950	2.88	21.0	155.7263	2034.117	1.8095
1.004	3.13	20.5	162.4350	2121.746	1.8874
1.057	3.38	20.5	168.7472	2204.197	1.9608
1.090	3.66	20.5	175.5459	2293.002	2.0398
(e) P _i = 50 lbf/in ² (gauge)					
0.754	2.47	18.5	155.5800	2032.206	1.8277
0.862	2.73	19.0	163.3797	2134.086	1.9088
0.950	3.36	21.0	180.5119	2357.869	2.0975
1.004	3.65	20.5	188.2452	2458.882	2.1873
1.057	3.89	20.5	194.2782	2537.686	2.2574
1.090	4.23	20.5	202.5113	2645.228	2.3531
(f) P _i = 60 lbf/in ² (gauge)					

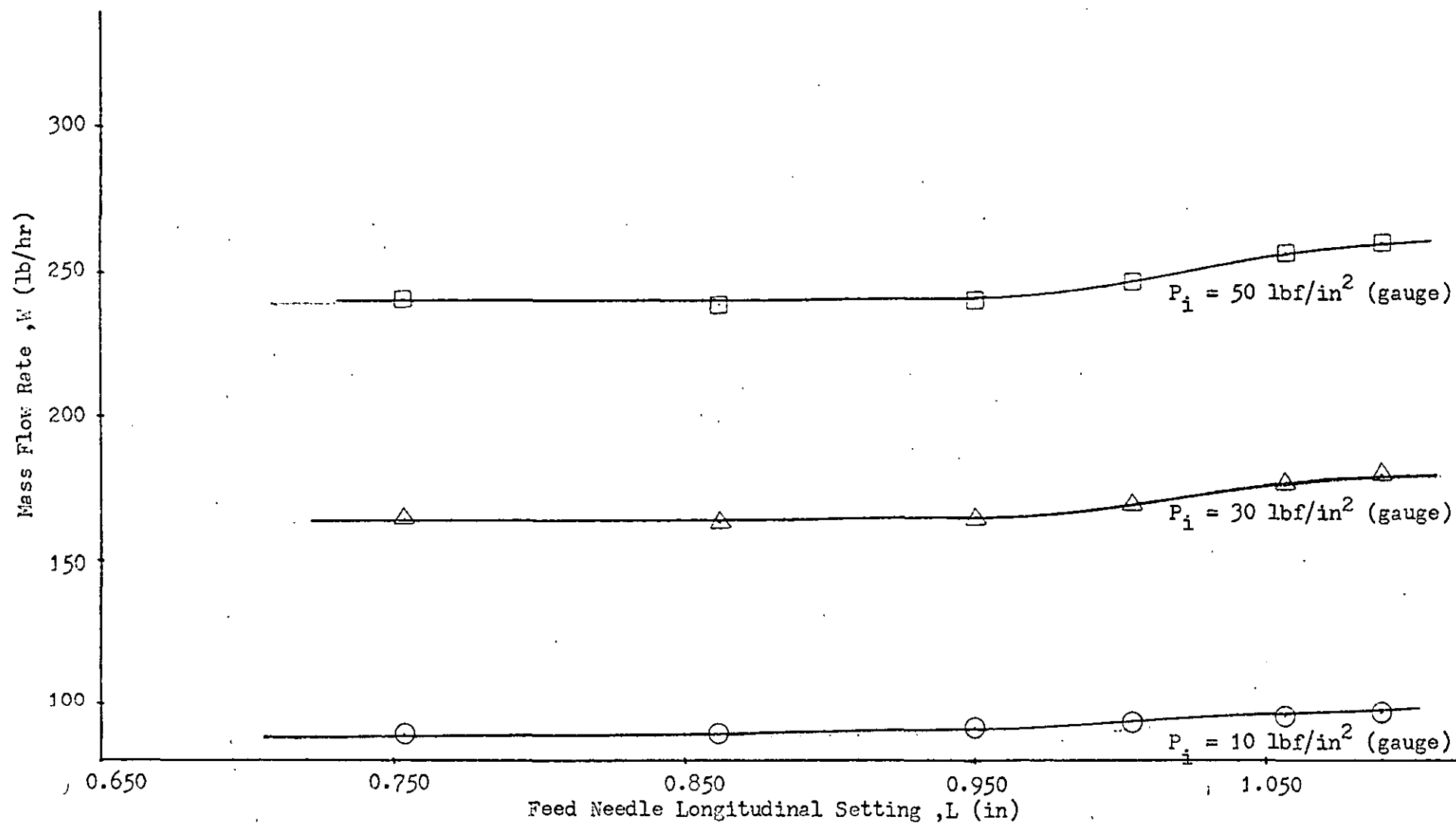


Fig. 3.16.1 Flow Rate for Normal Model Air-Jet with Varying Feed Needle Longitudinal Setting ; When $\alpha = 40^\circ$

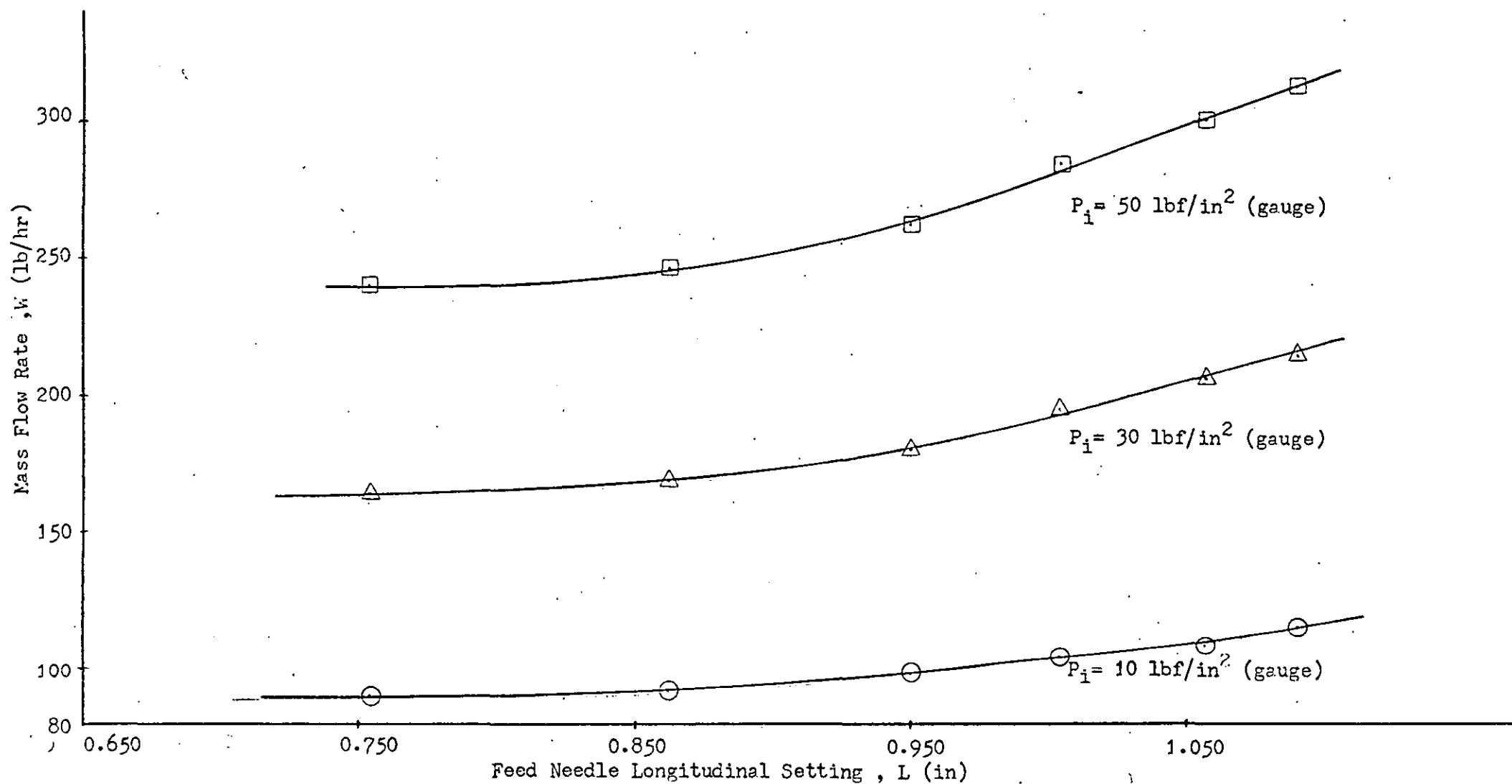


Fig. 3.16.2 Flow Rate for Normal Model Air-Jet with Varying Feed Needle Longitudinal Setting ; When $\alpha = 80^\circ$

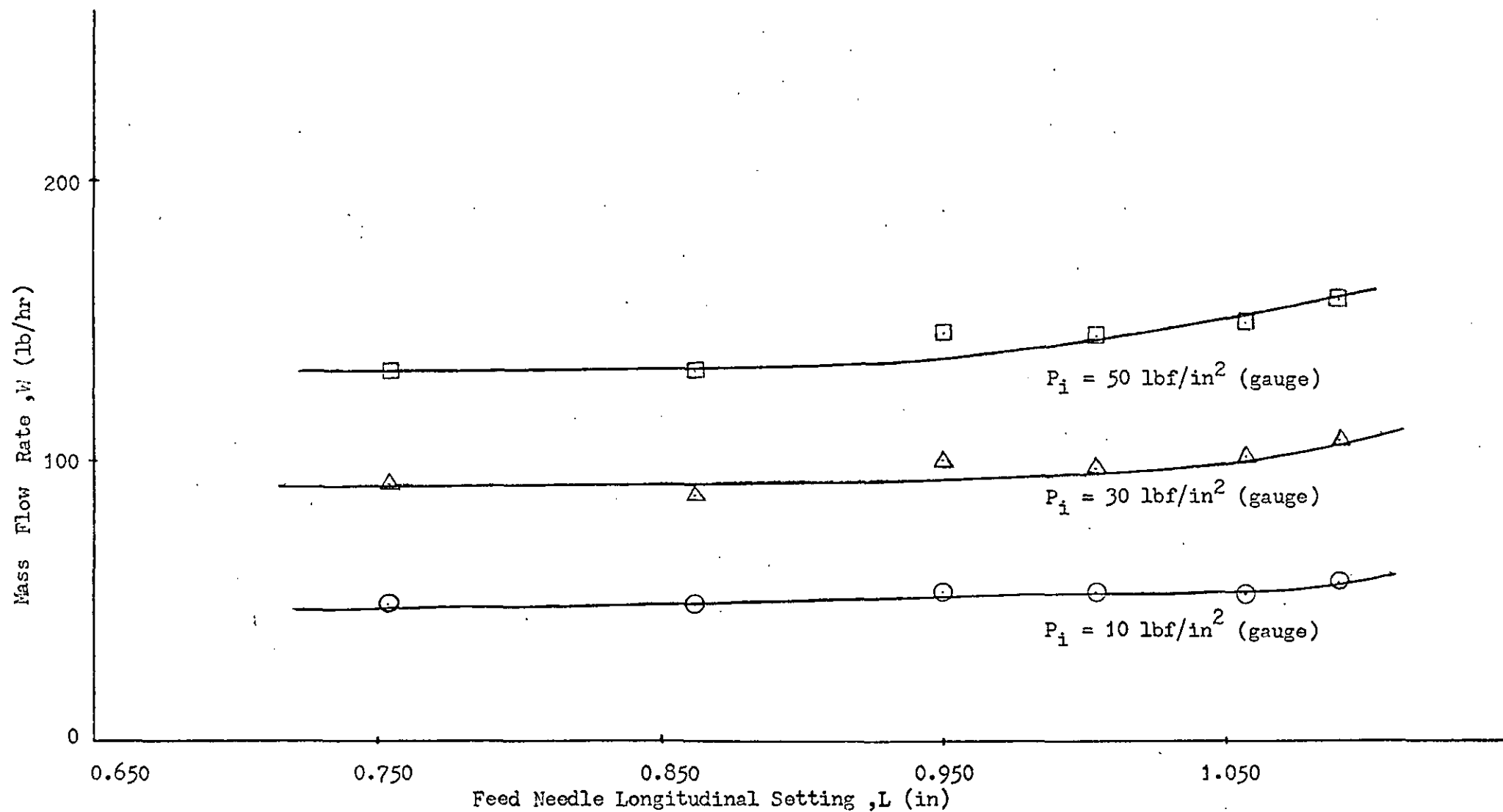


Fig. 3.17.1 Flow Rate for Modified Model Air-Jet with Varying Feed Needle Longitudinal Setting; When $\alpha = 40^\circ$

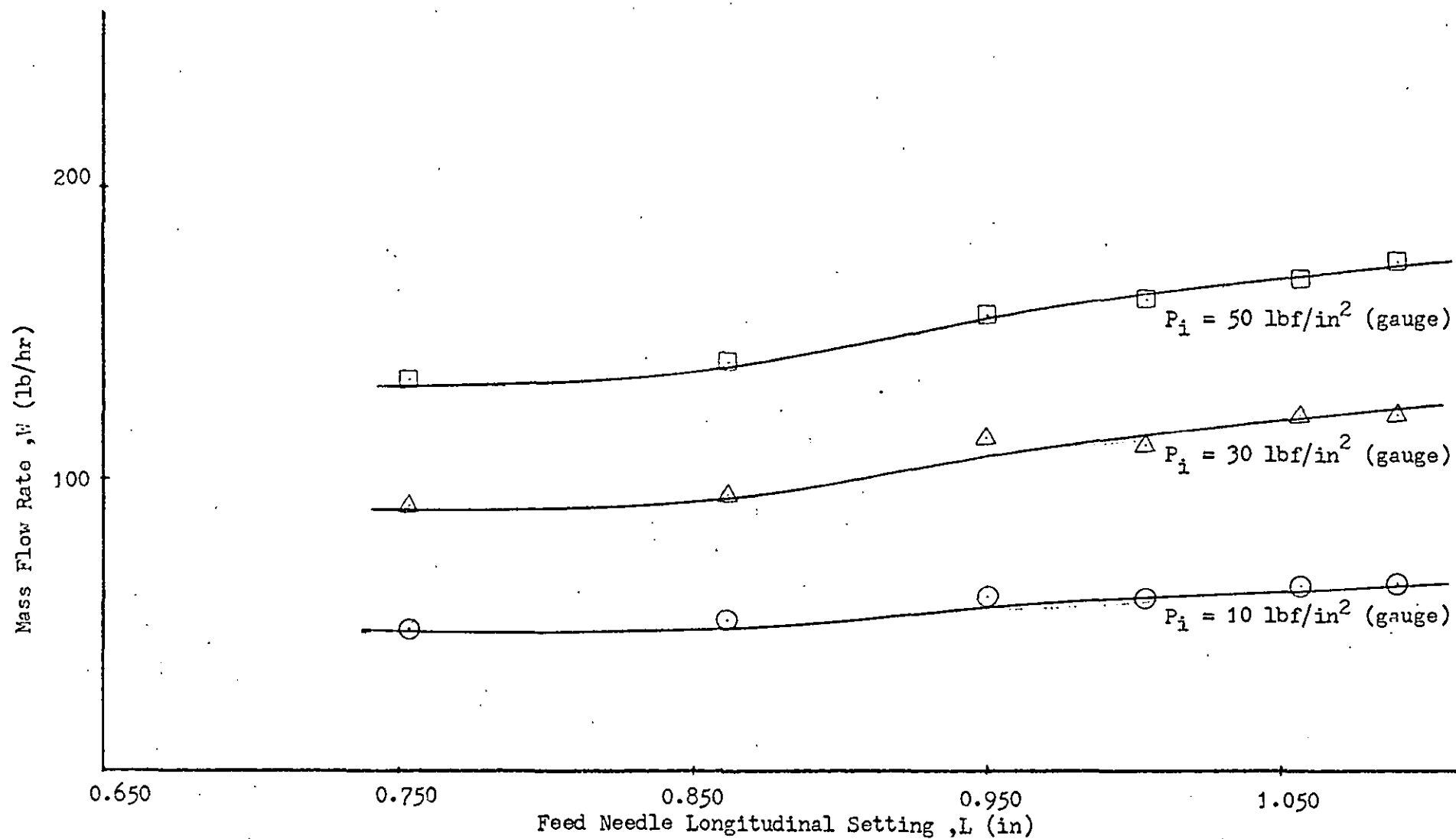


Fig. 3.17.2 Flow Rate for Modified Model Air-Jet with Varying Feed Needle Longitudinal Setting ; When $\alpha = 80^\circ$

jet in the upstream side of the feed needle as described by Wray and Entwistle⁽¹⁴⁾ (see Fig. 1.2).

Figs. 3.14 and 3.15 show typical variations of mass flow rate at selected pressures with varying feed needle angles for the two types of jet.

3.8.3 Variation of the Flow Rate with Varying Longitudinal Feed Needle Setting and Inlet Pressure

During this experimental investigation the feed needle angle of tilt α was kept constant at one of two values, i.e. either $\alpha = 40^\circ$ or $\alpha = 80^\circ$.

At the time that the measurements were made, the atmospheric temperature was 18°C (524°R) and the atmospheric pressure was 768 mm Hg (14.85 lbf/in^2 , abs.).

Table 3.4 gives the flow rates and Reynolds numbers (based on air-jet throat diameter) for variations of the feed needle longitudinal setting L and inlet pressure P_0 for the normal model jet. Table 3.5 gives the corresponding results for the modified model jet. Fig. 3.16 and 3.17 show typical variations of mass flow rate at selected pressures with varying feed needle longitudinal setting for the two types of jet.

3.9 Measurement of Flow Characteristics

As explained in Section 3.5, the high-speed cine-photography revealed that the main action between the turbulent flow and the parent yarn takes place as the yarn leaves the divergent part of the air-jet, and transformation of the parent yarn to the bulked yarn state occurs at this exit region. As the flow in the air-jet has been shown to be greatly dependent on the inlet pressure, and the two positional settings of the feed needle (see Section 3.8), then one would also expect that, at different points of the jet exit region, the action of the air on the yarn would be different for each

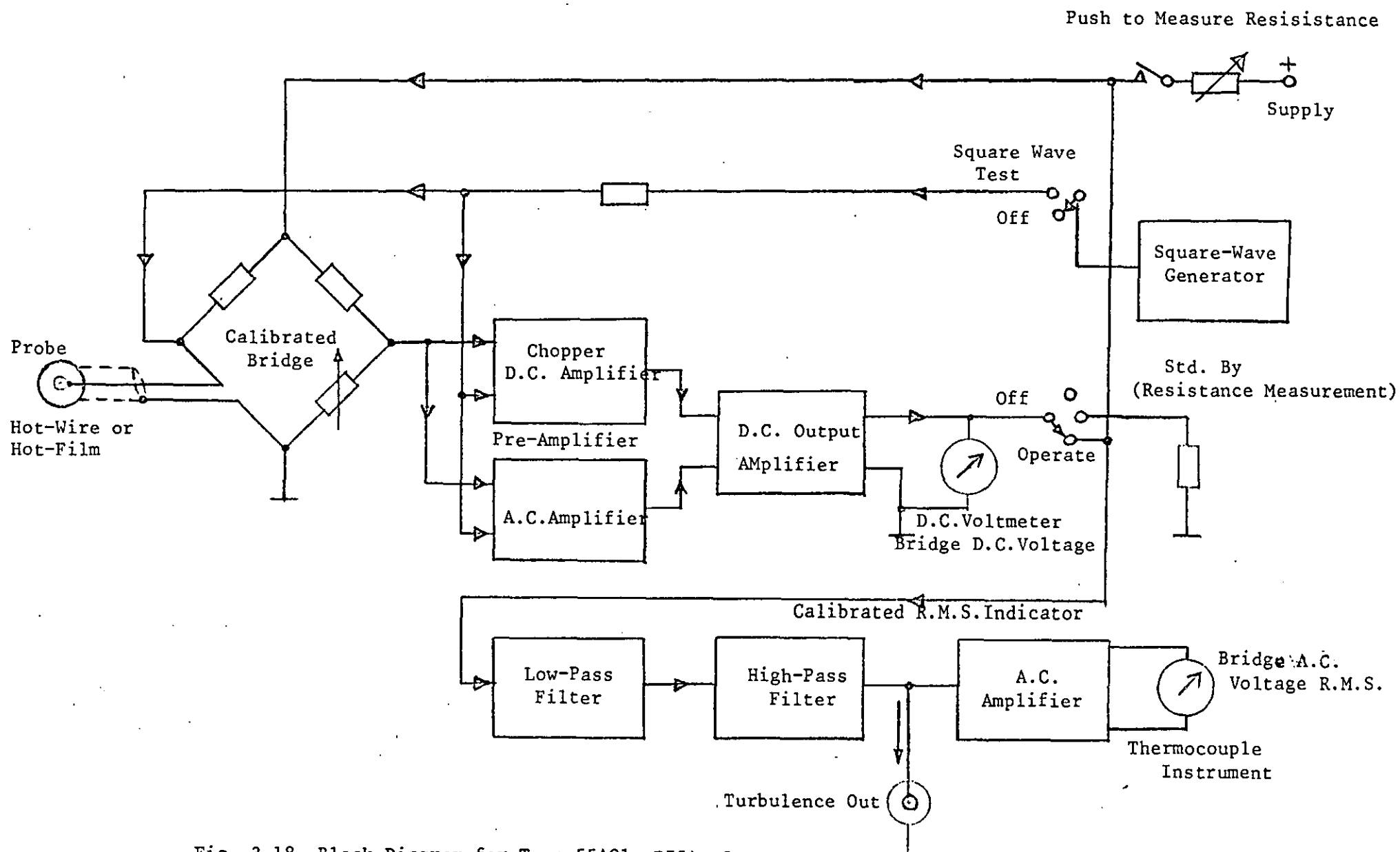


Fig. 3.18 Block Diagram for Type 55A01 DISA Constant Temperature Anemometer

variation of these settings. Although it would have been useful to study the flow characteristics inside the jet, the limitations imposed by the scale-up ratio preclude the use of any instrumentation inside the jet since these cause considerable blockage to the air flow and thus affect its nature. Hence the experimental analysis of the flow characteristics was limited to the exit region only. A constant temperature anemometer⁽³¹⁾ was used to measure the mean flow velocity and its fluctuation, and, from these, the velocity profiles and the percentage turbulences were calculated.

3.9.1 Constant Temperature Anemometer

The principle of this technique is that a transducer (hot-wire or hot-film probe) is placed in a flow region and is heated electrically. The measurement of the velocity of flow relies on laws governing the convective heat transfer from the probe. Fig. 3.18 shows a block diagram of the DISA type 55A01⁽³²⁾ constant temperature anemometer which was used for this work. The transducer probe is one arm of a bridge circuit, the other variable arm consisting of three resistance decades. The bridge is fed by an amplifier whose input voltage is controlled by the bridge unbalance. During the operation of air-flow measurement when the transducer's resistance and the already set adjustable bridge arm are unequal, a voltage will be present across the measuring terminals of the bridge. This voltage undergoes very high amplification and is fed back to the bridge as a supply voltage. The bridge voltage increases when the transducer resistance is low. This will cause the bridge current to increase and so will the current through probe, and, therefore, this will cause heating of probe and its resistance will increase. This in turn reduces the original amount of bridge unbalance.

The instrument has two meters to indicate the mean flow velocity and the r.m.s. value of the velocity fluctuations. The probe D.C. current is a measure of the mean velocity of flow and

this is read on a D.C. voltmeter. There is a calibrated r.m.s. indicator connected across the output terminals of the D.C. output amplifier (via low-pass and high-pass filters) and this instrument indicates the r.m.s. value of A.C. voltage.

3.9.2 Probes and their Characteristics

The hot-wire or hot-film probes are primarily sensitive to the component of flow velocity normal to the sensing element. The signal from the turbulence out terminal (see Fig. 3.18) corresponds to the fluctuating component of this velocity. During the air jet's normal operation high values of velocities and turbulences were reached. Therefore, a suitable probe with a high mechanical strength needed to be selected.

Initially, DISA type 55A25⁽³³⁾ miniature hot-wire probes were used, but frequent breakages of sensing element made it impossible to carry out a satisfactory investigation. Then DISA 55A82⁽³³⁾ type hot film probes were tried. Although this particular probe is mechanically stronger than hot-wire probes, during the experimentation it was observed that its cold resistance increased with usage. This increase in resistance must have been due to small dust particles in the air colliding at high speeds with the sensing element and damaging it. Finally, another type of hot film probe DISA 55A83⁽³³⁾ was tried. The sensing element of this probe consisted of a thin platinum film fixed on the wedge shaped tip of a quartz support, the sensing element being insulated with a thin quartz coating. It was found that this coating gave extra mechanical strength, together with protection to the sensing element, and this made it suitable for use in this investigation.

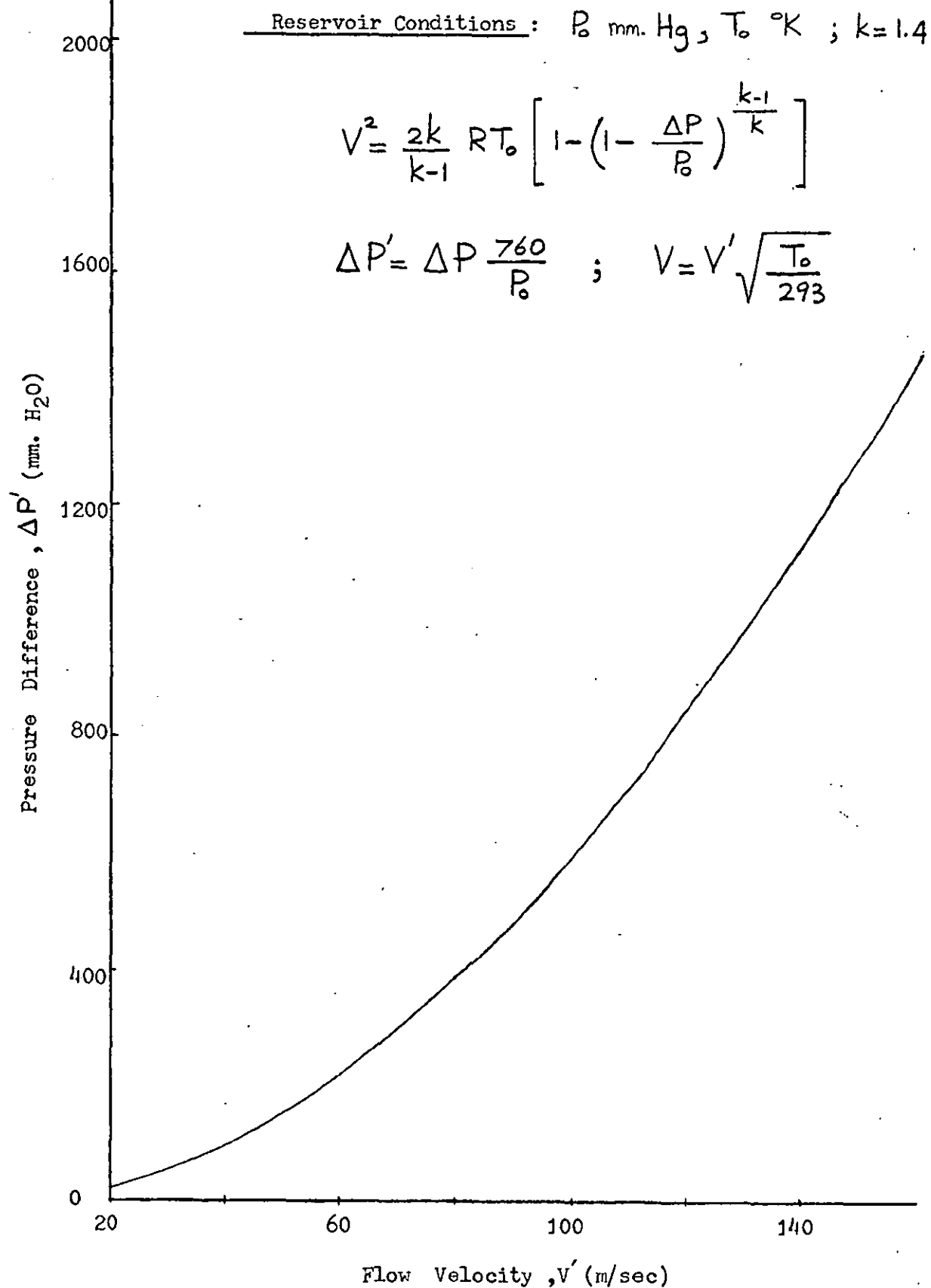


Fig. 3.19 DISA Wind Tunnel Calibration Curve

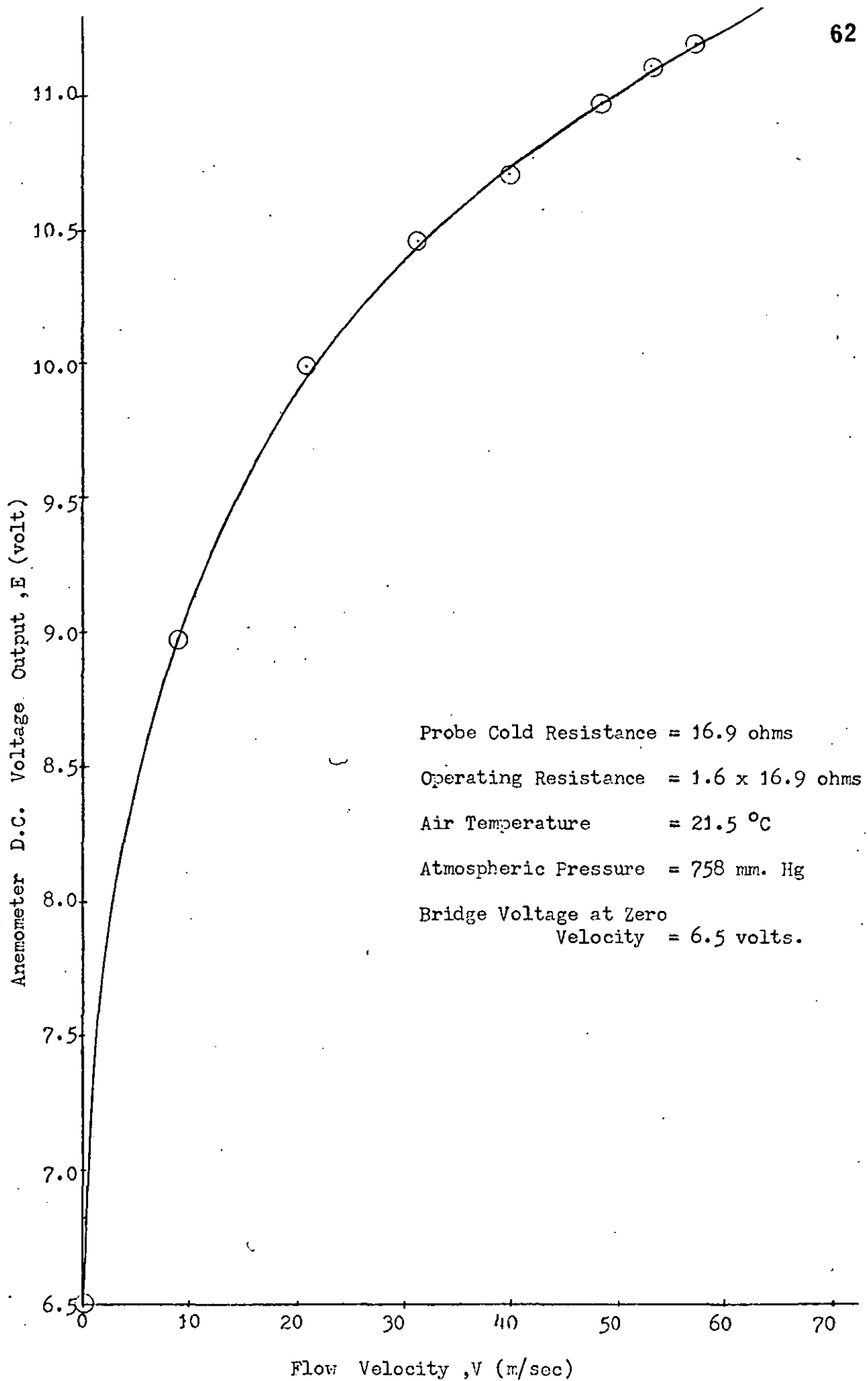


Fig. 3.20

Calibration of Hot-Film Probe for Low Velocities
(Using DISA Calibration Wind Tunnel)

The data for the DISA type 55A83 hot film probe is as follows:

Film length	= 1 mm
Film width	= 0.2 mm
Temperature coefficient resistance	= 2.5% per $^{\circ}\text{C}$
Probe cold resistance (R_0)	= 16.9 ohms
Overheating ratio	= 0.6
Max. velocity in air	= 500 metre/sec.
Min. velocity in air	= 0.1 metre/sec.
Upper frequency limit	= 30 kHz
Frequency limit	= 0.4 Hz
Max. ambient temp.	= 150°C
Max. film temp.	= 300°C

3.9.3 Calibration of the Probe

In order to derive the mean flow velocities from the D.C. voltage output measurements of the anemometer, a calibration of the probe has to be made. For velocities below 150 metres/sec. a DISA calibration wind tunnel⁽³⁴⁾ with a special adapter, suitable for a right-angled probe, was used. Accurate flow velocity measurements are based on the measurement of the static pressure differences between the reservoir and the measuring section of the wind tunnel. Fig. 3.19 shows a calibration curve for the type of tunnel used.

The calibration of the probe consists in reading the bridge D.C. voltage in the anemometer and deriving the flow velocity from the above mentioned pressure differences. Fig. 3.20 shows the calibration curve derived for low speed flows. For higher velocity calibration the probe and a pitot static tube were placed side by side in a flow region, i.e. a rectangular cross-sectioned jet, so made as to have a similar flow region to that at the top of the

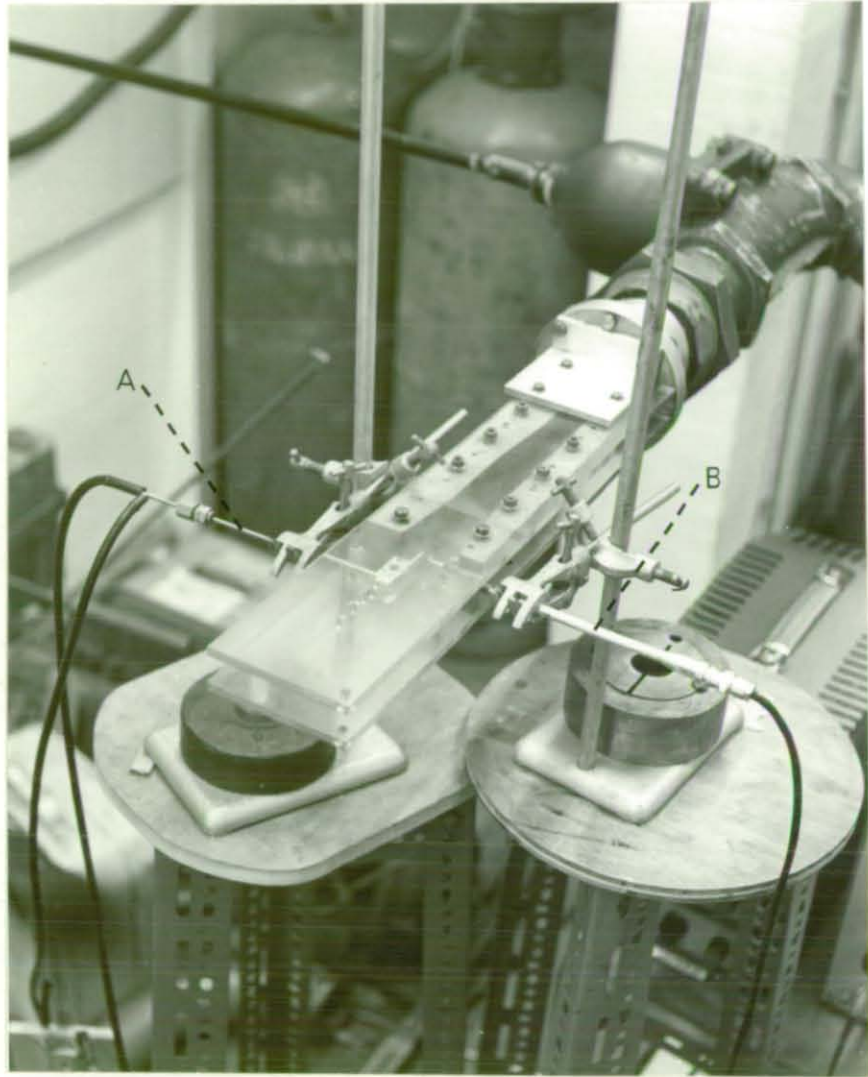


Fig. 3.21 Experimental Set Up for the Calibration of the Probe
for High Velocities

A - Pitot-Static Tube

B - Hot-Film Probe

bulking jet where the measurements would have to be made.

(See Fig. 3.21). The velocities were varied over the required range by means of two compressors. One of these compressors had a variable speed control and the other was coupled in at full speed whenever it was required. In order to get dust free compressed air, a series of fine filter units had to be fitted at the entrance to the calibration jet.

3.9.4 Calculation of Flow Velocities

Bernoulli's general equation for compressible flow is

$$P_o = P \left[1 + \frac{\gamma-1}{2} M^2 \right]^{\gamma/(\gamma-1)} \text{-----} (3-17)$$

where,

P_o = stagnation pressure (total pressure),

P = static pressure,

M = Mach number, and

γ = ratio of specific heats

This equation is true for both subsonic and supersonic flows provided that shock waves are not present. If the above equation is expanded by the binomial theorem, then:

$$P_o = P + \frac{\gamma M^2}{2} P \left[1 + \frac{M^2}{4} + \frac{2-\gamma}{24} M^4 + \dots \right]$$

For air γ is closely equal to 1.4 and therefore:

$$P_o = P \left[1 + \frac{7}{10} M^2 + \frac{7}{40} M^4 + \frac{7}{400} M^6 + \dots \right] \text{---} (3-18)$$

To determine M , the procedure may be summarized as follows:

- (i) The stream static pressure P and the pitot pressure P_o are measured relative to the atmospheric pressure.
- (ii) The atmospheric pressure and temperature are noted.
- (iii) Pressures P and P_o are then expressed in absolute pressure units. Let these be denoted by P' and P'_o respectively.

TABLE 3.6 Results for Calibration of Probe Type DISA 55A83

Probe Cold Resistance = 16.9 ohms
 Operating Resistance = 27 ohms
 Atmospheric Pressure = 764.5 mm. Hg
 Atmospheric Temperature = 25°C.

Anemometer D.C. Voltage (volt)	Static Pressure (P) (cm. Hg)	Pitot Pressure (P ₀) (cm. Hg)	$\frac{P \text{ (abs.)}}{P_0 \text{ (abs.)}}$	Mach Number (M)	Local Velocity (V) (m/sec)
6.50	0.000	0.00	1.00000	0.000	0.00
10.75	-0.056	0.71	0.99007	0.120	41.52
11.10	-0.074	1.14	0.98435	0.150	51.90
11.425	-0.095	1.80	0.97578	0.182	62.97
11.685	-0.113	2.52	0.96665	0.220	76.12
11.95	-0.130	3.46	0.95507	0.255	88.24
12.20	-0.149	4.55	0.94198	0.296	102.42
12.45	-0.186	6.15	0.92329	0.340	117.65
12.65	-0.223	7.75	0.90530	0.380	131.49
12.90	-0.223	10.00	0.88174	0.428	148.10
13.15	-0.335	12.50	0.85570	0.477	165.06
13.30	-0.372	16.75	0.81628	0.546	188.93
13.5	-0.447	21.50	0.77593	0.613	212.12
13.66	-0.372	26.70	0.73754	0.674	233.23
14.05	-0.894	34.40	0.68160	0.760	262.99
14.375	-0.447	44.70	0.62734	0.844	292.05
14.575	-0.223	55.10	0.57945	0.928	321.12
14.775	0.000	64.30	0.54316	0.976	337.73
15.00	0.447	71.70	0.51904	1.015	351.23
15.20	-2.230	81.50	0.46989	1.097	380.12

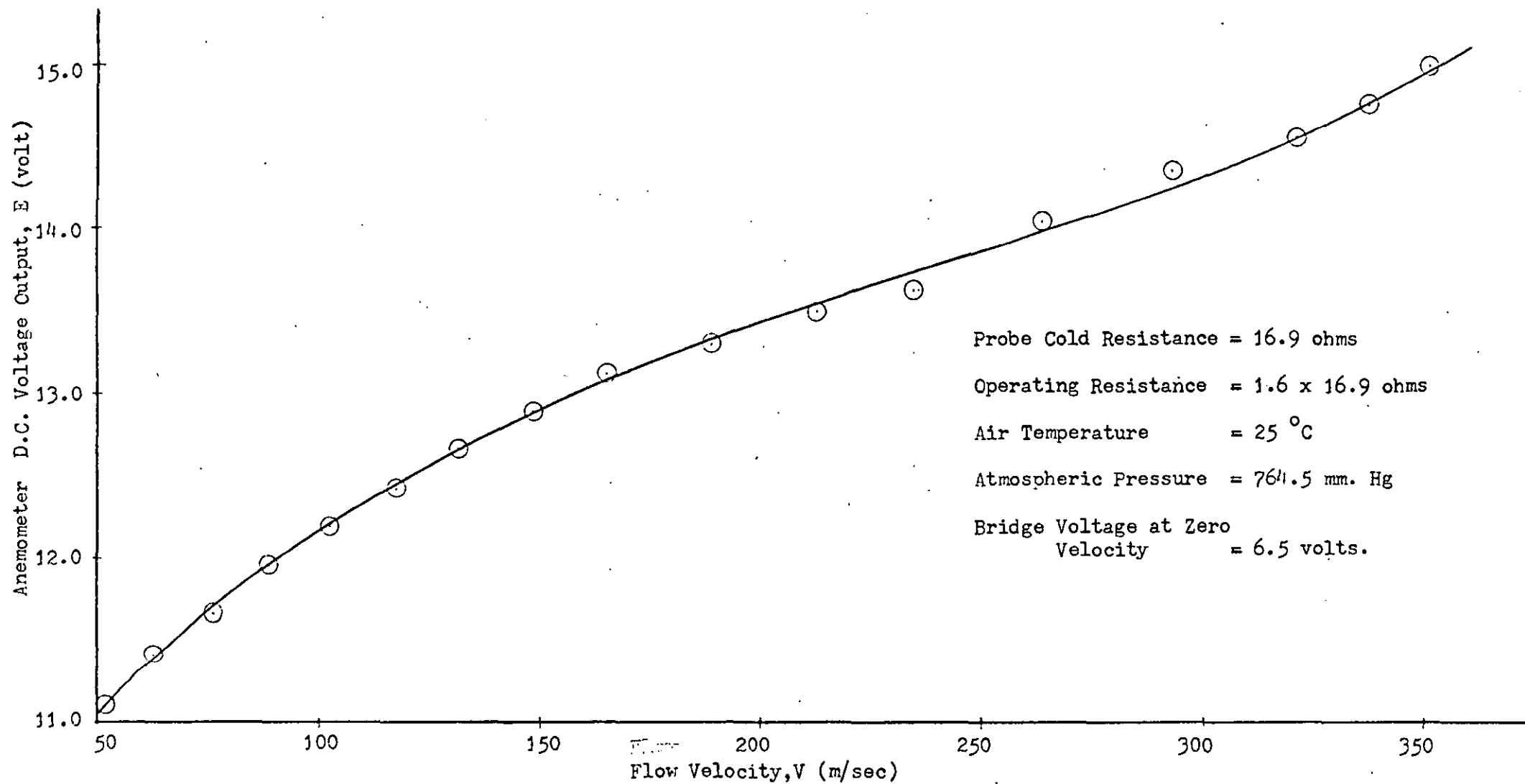


Fig. 3.22 DISA Type 55A83 Hot-Film Probe Calibration Curve for High Speed Flow (Using Pitot-static Tube)

(iv) If $\frac{P}{P_0} < 0.528$, the flow is subsonic and therefore no shock waves are present. Hence, the measured total pressure, P_0 , is the undisturbed stream pressure. Then M of the undisturbed flow can be calculated using the formula (3-18).

If $\frac{P}{P_0} > 0.528$, the flow is supersonic and M should be calculated accordingly. However this is not required for the present work since the flow at the exit remains subsonic throughout the investigation.

In order to derive the flow velocity from the calculated M , the speed of sound needs to be known. This requires measurement of the temperature, and here it is assumed that the static temperature of the air at the exit is equal to the atmospheric temperature. Hence, the local velocity of flow is derived from the formula

$$V = M \cdot a = M \sqrt{\gamma R T} \text{ --- (3-19)}$$

Fig. 3.22 shows the calibration curve obtained for the DISA type 55A83 hot film probe, based on the readings given in Table 3.6.

3.9.5 Measurement of Mean Flow Velocity

Generally, the probe will respond to any change of heat flux, whether caused by a change in temperature, pressure, or velocity. Here, the only interest is in measuring the mean flow velocities and the flow fluctuations.

The nonlinear relation between the velocity V , and the output voltage E is represented by the equation $E^2 = C + DV^n$ (where C , D and n are constants). The hot-film probe is mounted in the flow region - i.e. at the exit of the air-jet. The bridge D.C. voltage is read, and the actual flow velocity is then obtained from the calibration curves, (see Figs. 3.20 and 3.22). The probe, firmly connected to its mount to eliminate any vibration, is placed

with its hot film sensing element perpendicular to the main flow direction. Although the air passes through a series of six fine filters before it enters into the jet, there is still the possibility that small dust particles could accumulate on the probe sensing element. Therefore, to eliminate any possible malfunctioning, the probe tip is regularly and carefully cleaned with carbon tetrachloride during its operation.

3.9.6 Measurement of Turbulence

Turbulence measurements are based upon the slope of the curve of the anemometer bridge D.C. voltage versus the flow velocity. The r.m.s. voltage for one per cent turbulence is then given by the expression:

$$E_{1\%} = \frac{\text{Mean Flow Velocity}}{100} \cdot A \text{ (volts)} \quad \text{---(3-20)}$$

(where A is the slope),

$$\text{and thus, percentage turbulence} = \frac{E_{r.m.s.}}{E_{1\%}} = \frac{E_{r.m.s.} \times 100}{A \cdot \text{Mean Flow Velocity}}$$

King's law states that,

$$\frac{E^2}{R_{op}} = c + d\sqrt{V} = \frac{E_o}{R_{op}} + d\sqrt{V} \quad \text{---(3-21)}$$

(where E is bridge voltage, V is the mean flow velocity,

R_{op} is the probe operating resistance, c, and d are two constants, and E_o is the bridge voltage at zero velocity).

$$\text{By the definition given above, } A = \frac{dE}{dV},$$

but, from equation (3-21)

$$\frac{2E}{R_{op}} \cdot \frac{dE}{dV} = d \cdot \frac{1}{2\sqrt{V}}$$

$$\text{Therefore, } A \cdot V = \frac{d \cdot R_{op} \sqrt{V}}{4E}$$

but,

$$d\sqrt{V} = \frac{E^2 - E_o^2}{R_{op}}$$

Therefore,

$$A \cdot V = \frac{E^2 - E_o^2}{4E} \quad \text{---(3-22)}$$

$$\text{and percentage turbulence} = \frac{4E \cdot E_{r.m.s.}}{E^2 - E_o^2} \times 100 \quad \text{---(3-23)}$$

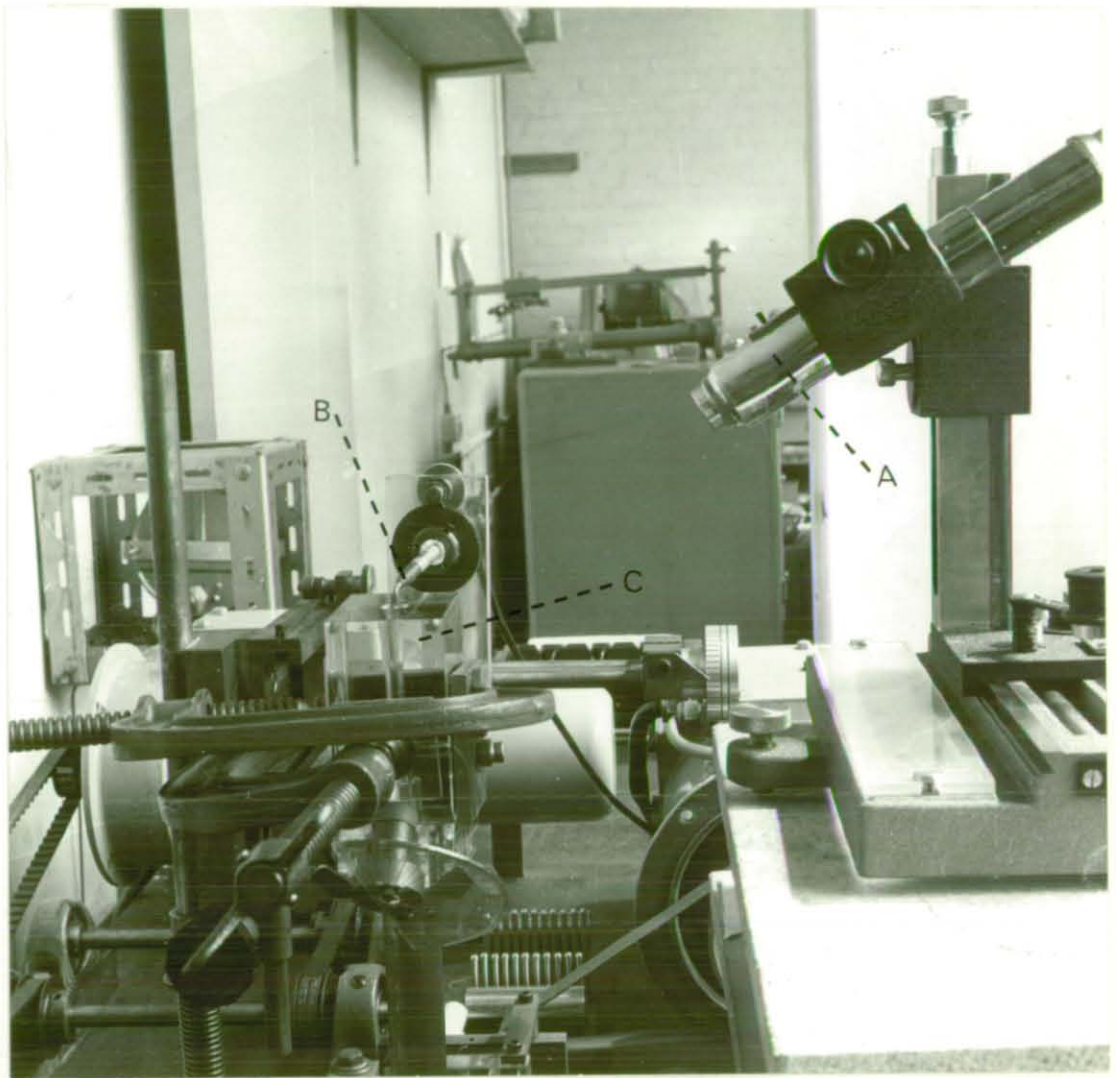


Fig. 3.23 General View of Experimental Set Up

A - Travelling Microscope

B - Hot-Film Probe

C - Air-Jet

Thus, it will be observed that the turbulence measurement does not actually require a plotting of the anemometer bridge voltage with respect to the flow velocity.

3.9.7 Mean Flow Velocity and Percentage Turbulence Results

In Section 3.4, it was pointed out that three important factors affect the flow in the jet (i.e. the inlet pressure P_i , the feed-needle angle of tilt setting α , and the longitudinal needle setting L along its mating bore. However, in order to reduce the amount of experimentation involved during the mean flow velocity and percentage turbulence measurements, the longitudinal needle setting was maintained constant while both the feed-needle angle of tilt and the inlet pressure were varied.

Fig. 3.23 shows a general view of the experimental set-up. The positioning of the hot-film probe at a distance X along a radius r is varied as shown in Fig. 3.7. The position of the sensing element of the probe is denoted by P and this can be moved along the four radii OA, OB, OC and OD. Tables 3.7, 3.8, 3.9 and 3.10 show the values for flow velocity and percentage turbulence for each of these radii respectively, when the angle of tilt of the feed-needle α and the inlet pressure P_i are systematically varied. Selected values from these tables are also shown graphically in Figs. 3.24 to 3.27 and Figs. 3.28 to 3.31 for the velocity and percentage turbulence distributions respectively.

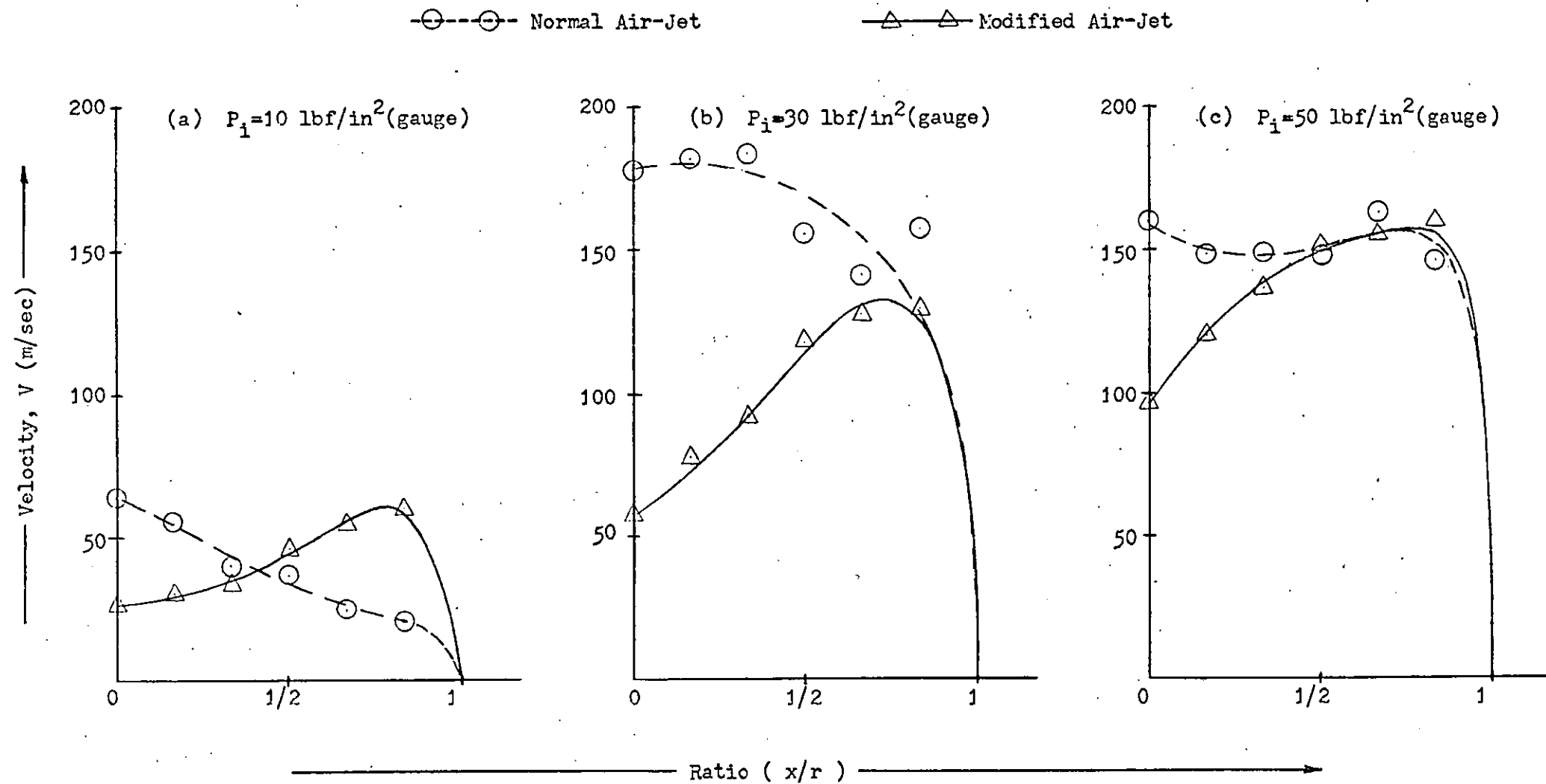


Fig. 3.24.1 Velocity Distribution Along OA When $\alpha = 0^\circ$

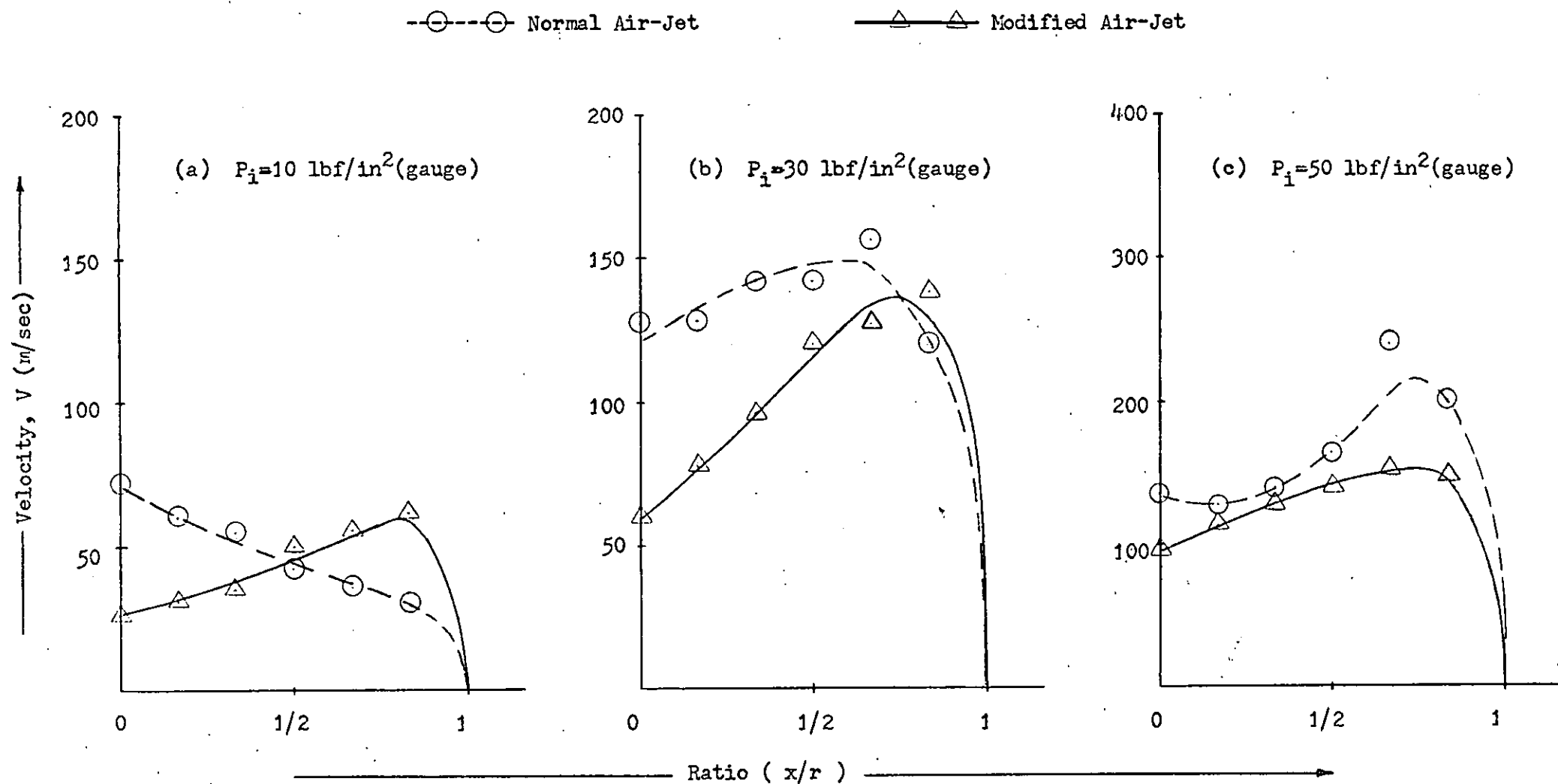


Fig. 3.24.2 Velocity Distribution Along OA When $\alpha = 20^\circ$

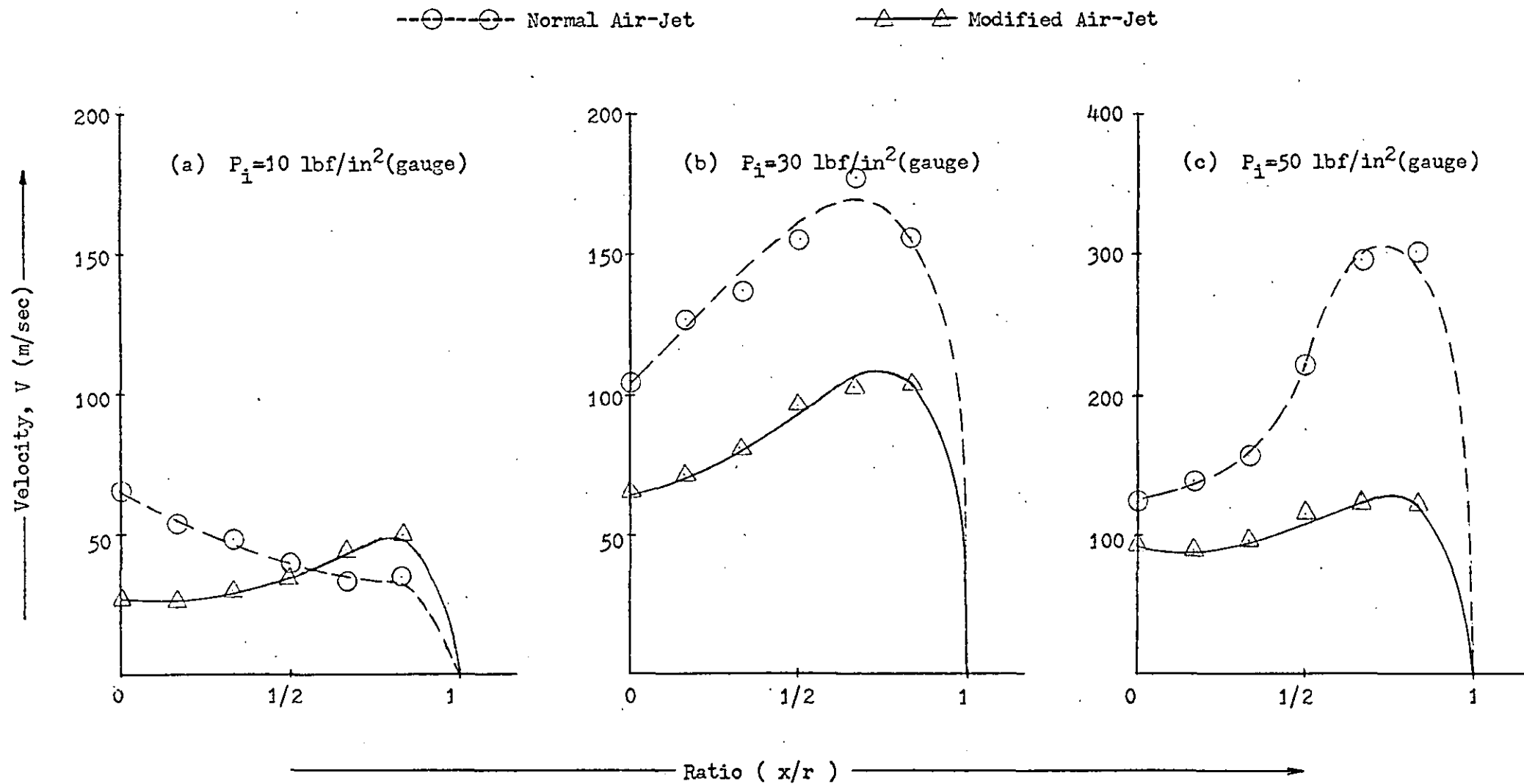


Fig. 3.24.3 Velocity Distribution Along OA When $\alpha = 40^\circ$

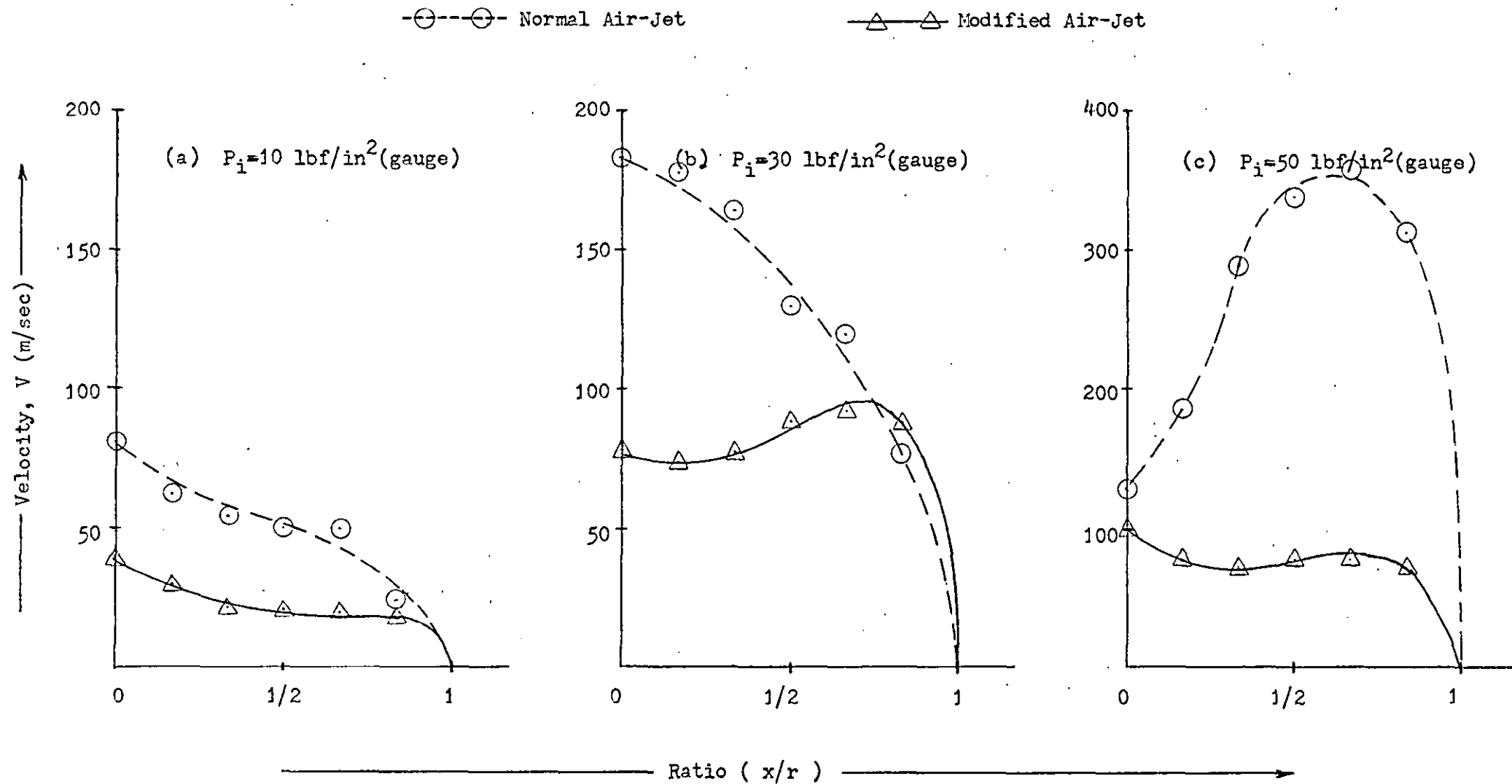


Fig. 3.24.4 Velocity Distribution Along OA When $\alpha = 60^\circ$

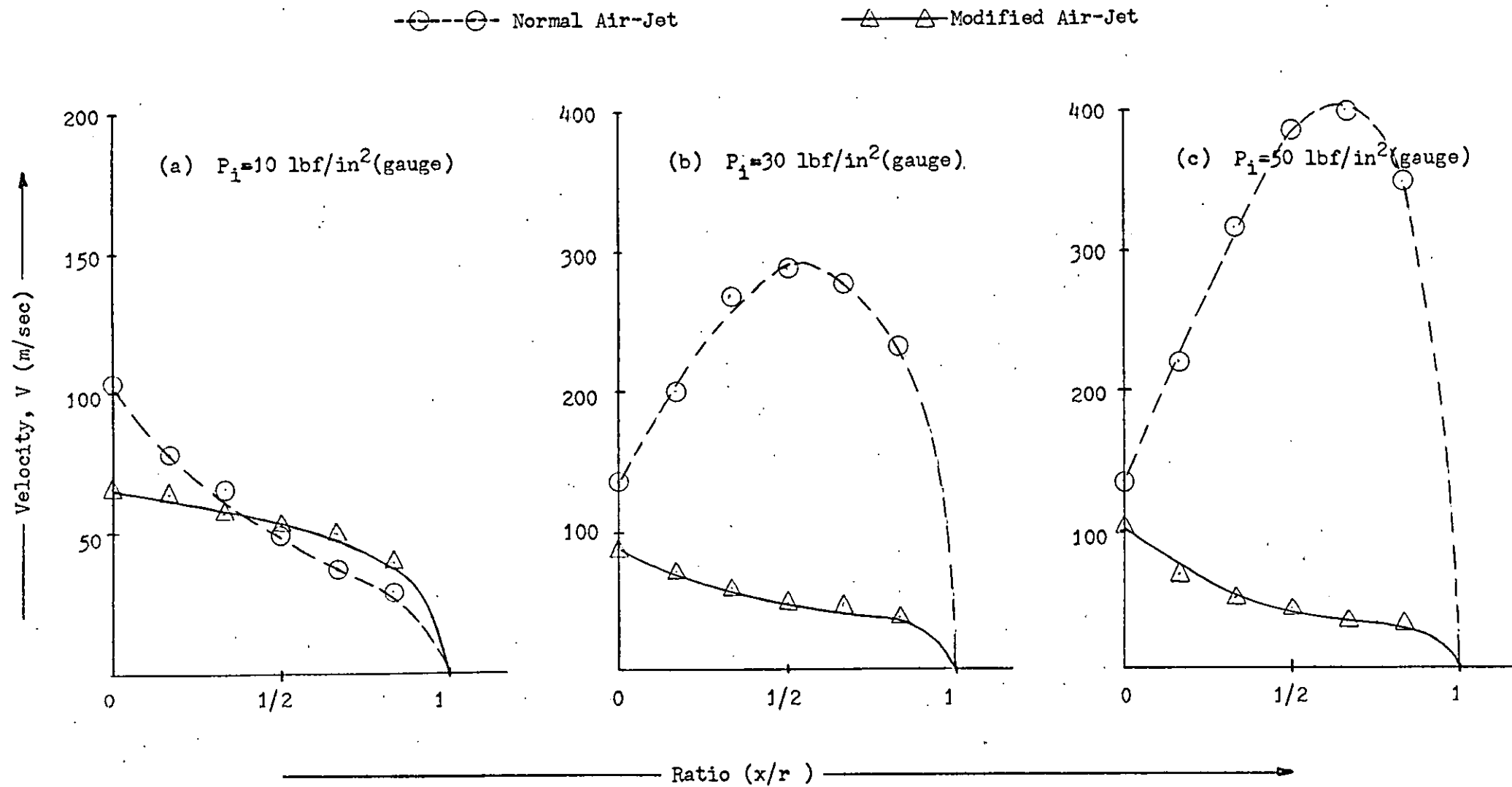


Fig. 3.24.5 Velocity Distribution Along OA When $\alpha = 80^\circ$

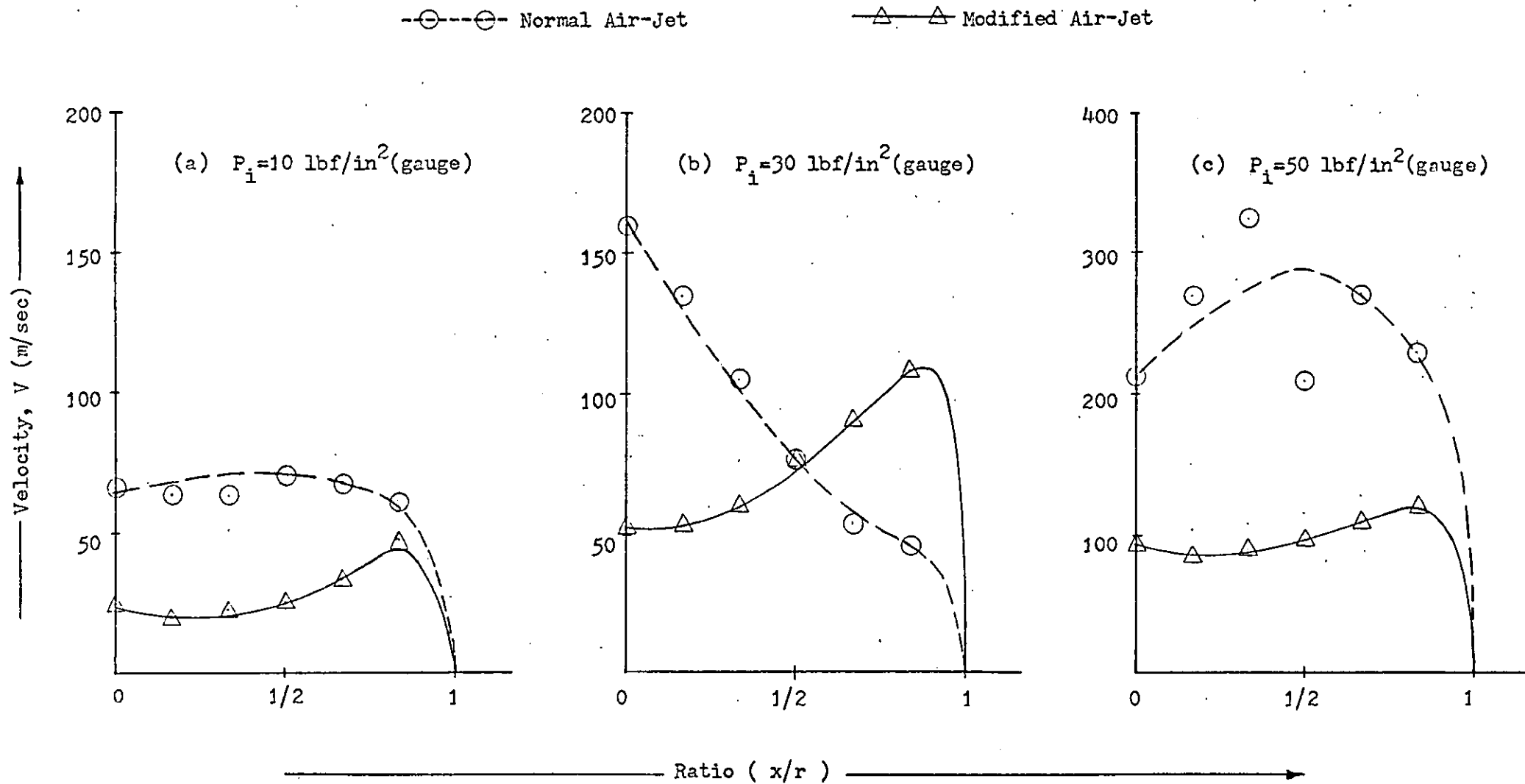


Fig. 3.25.1 Velocity Distribution Along OR When $\alpha = 0^\circ$

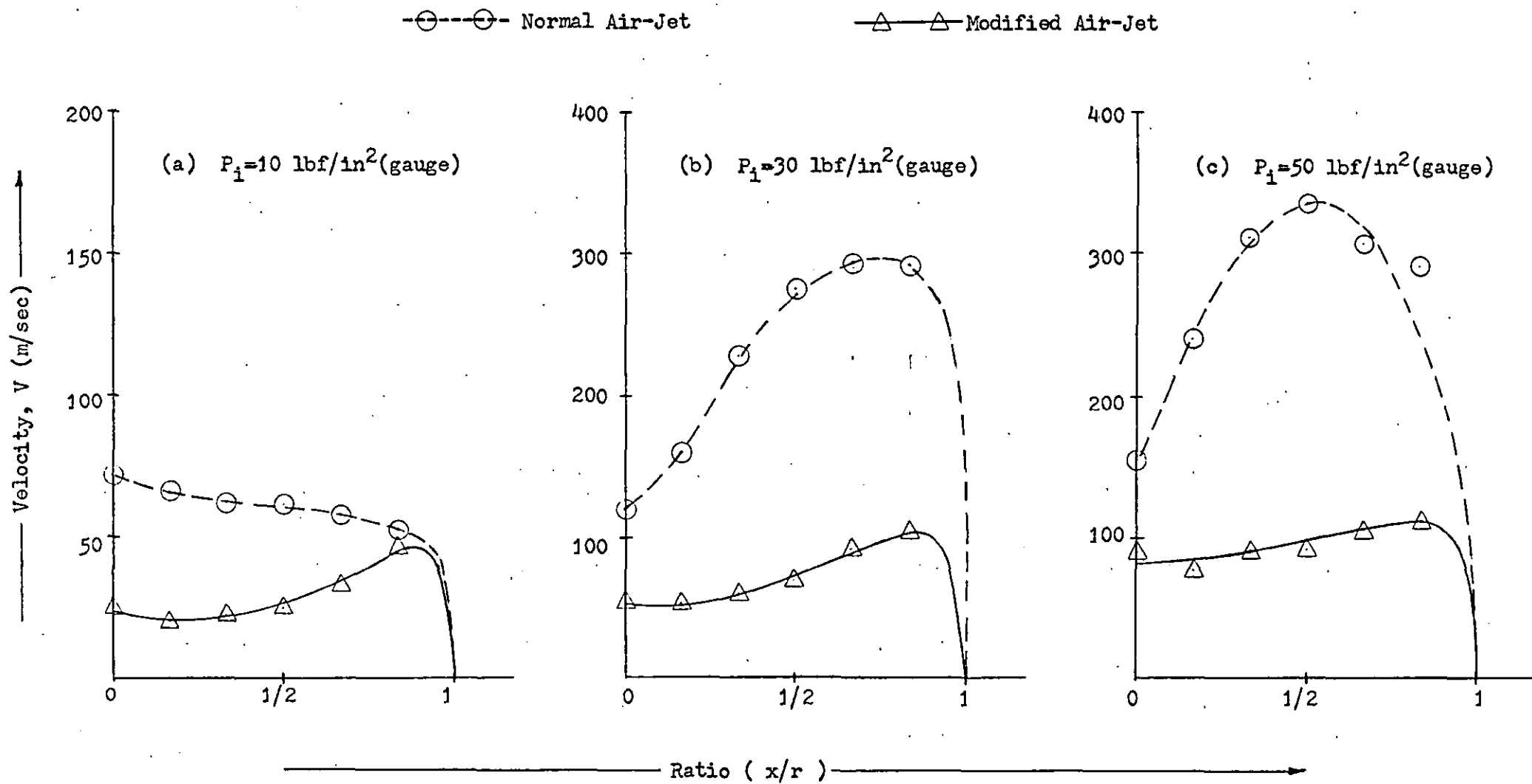


Fig. 3.25.2 Velocity Distribution Along OB When $\alpha = 20^\circ$

○---○ Normal Air-Jet

△---△ Modified Air-Jet

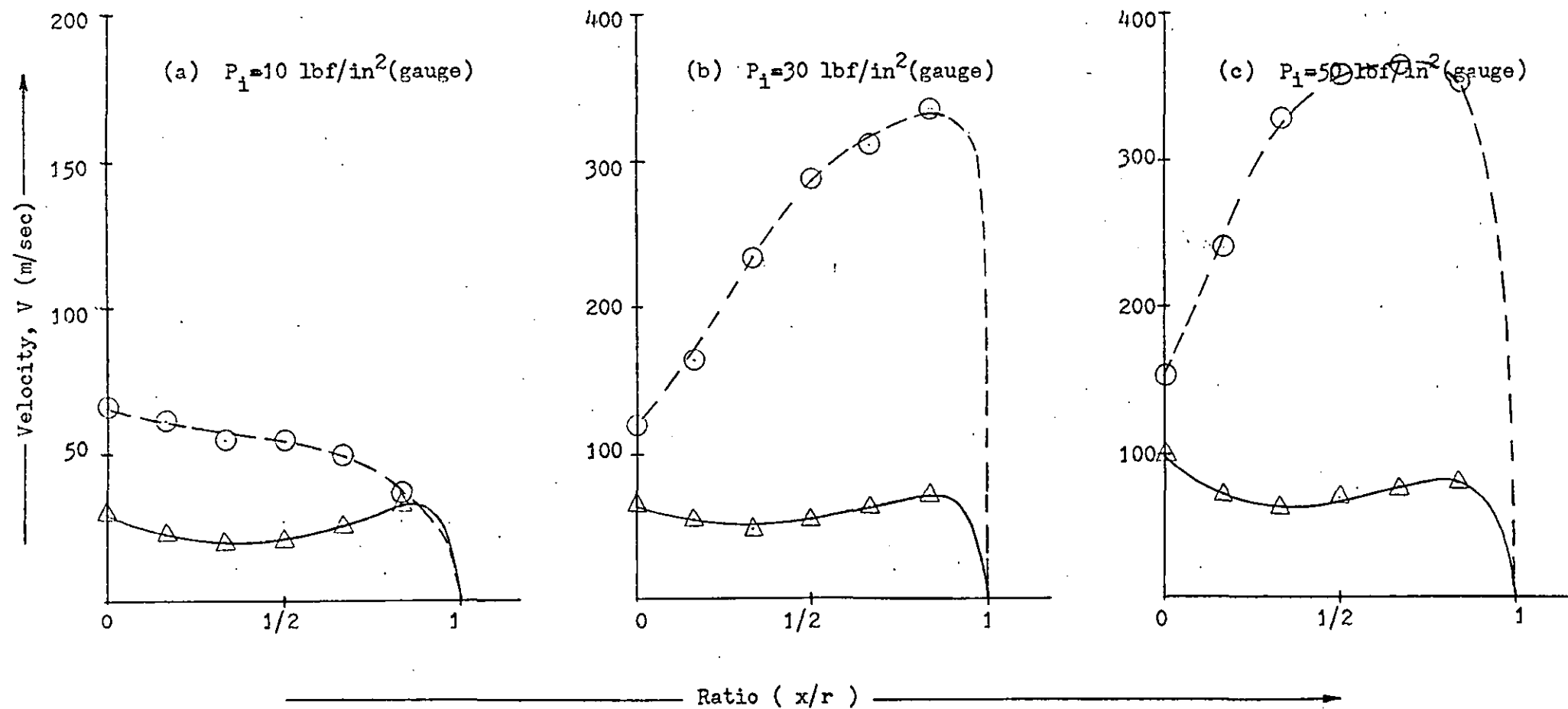


Fig. 3.25.3 Velocity Distribution Along OB When $\alpha = 40^\circ$

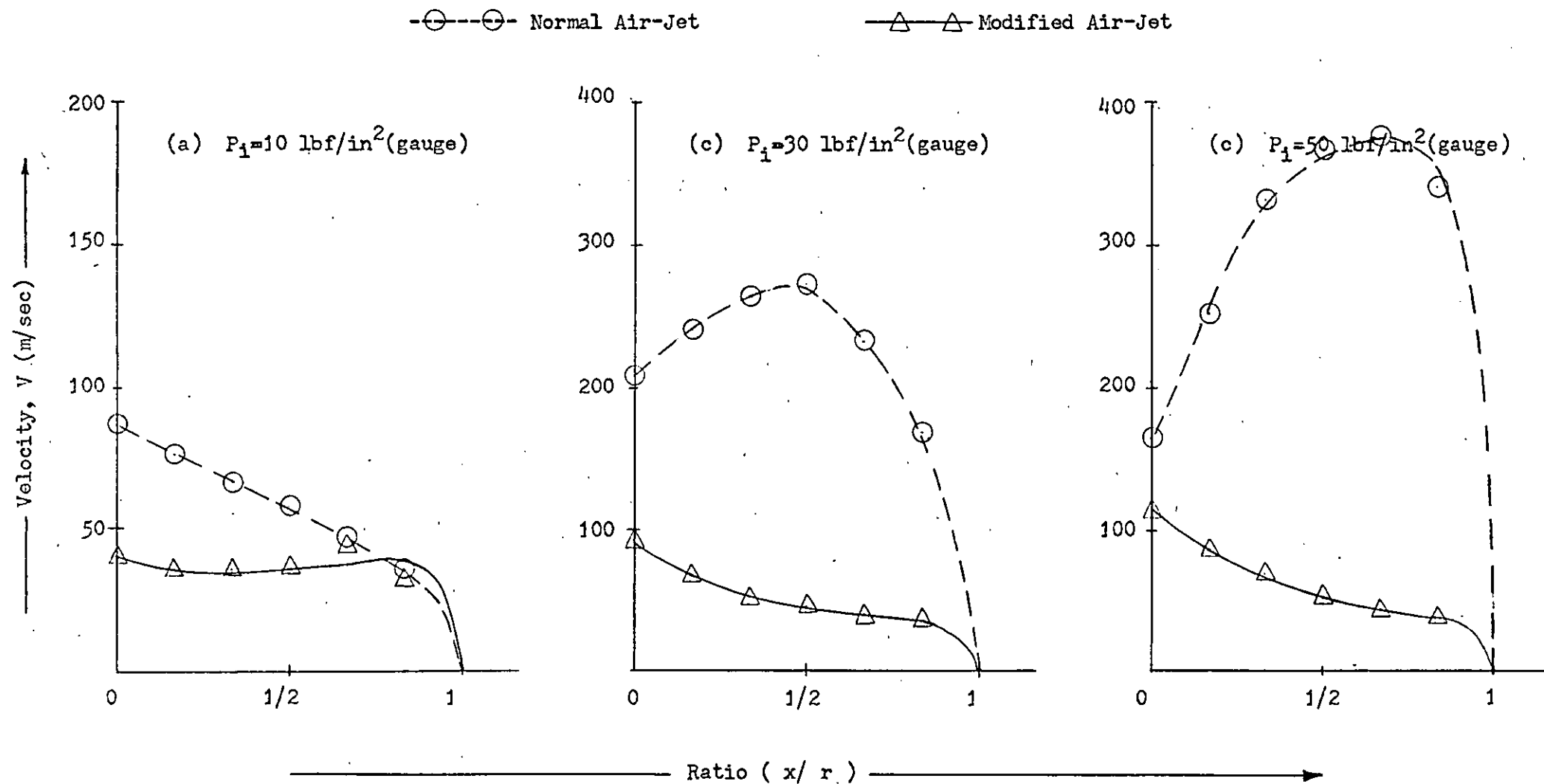


Fig. 3.25.4 Velocity Distribution Along OB When $\alpha = 60^\circ$

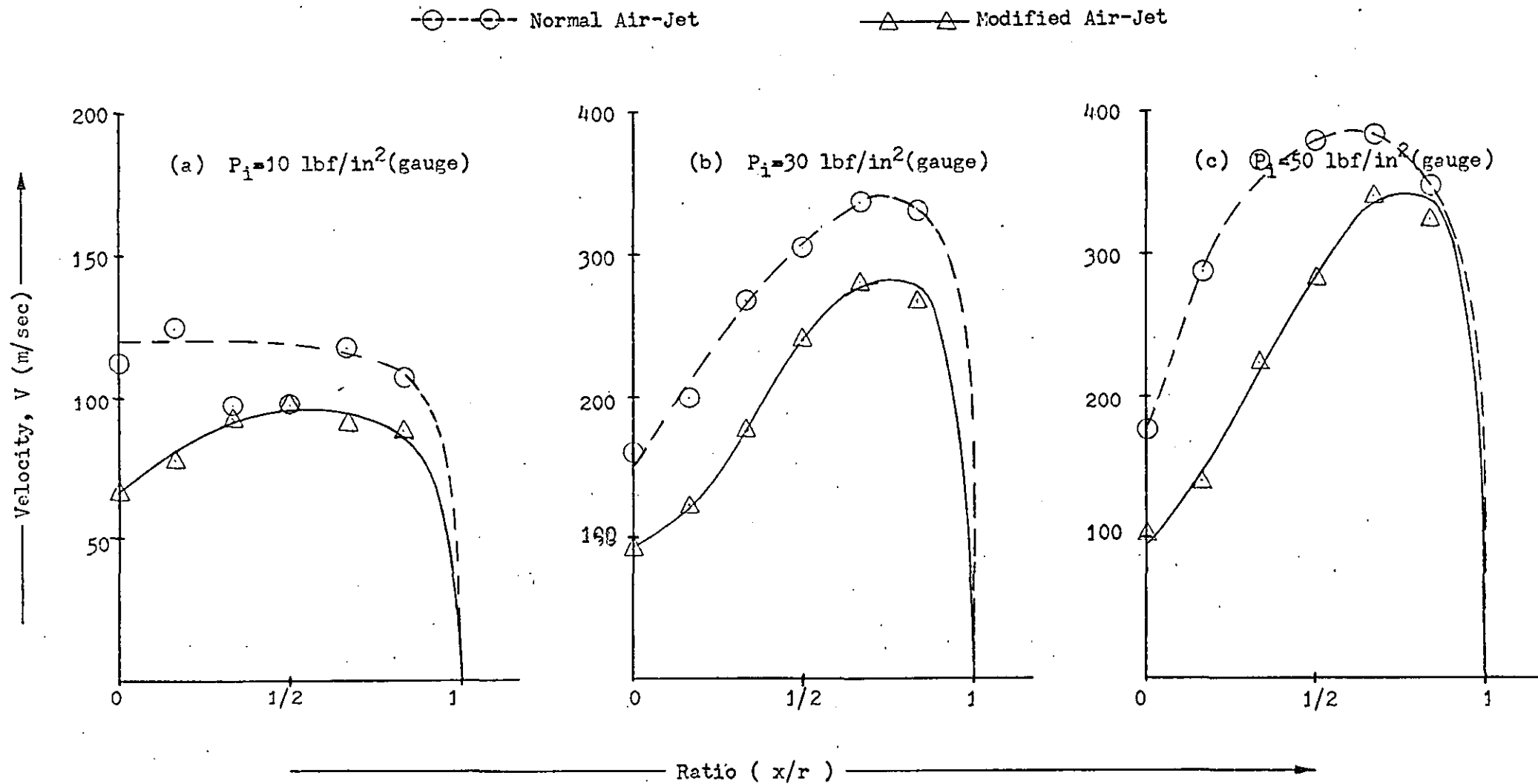


Fig. 3.25.5 Velocity Distribution Along OB When $\alpha = 80^\circ$

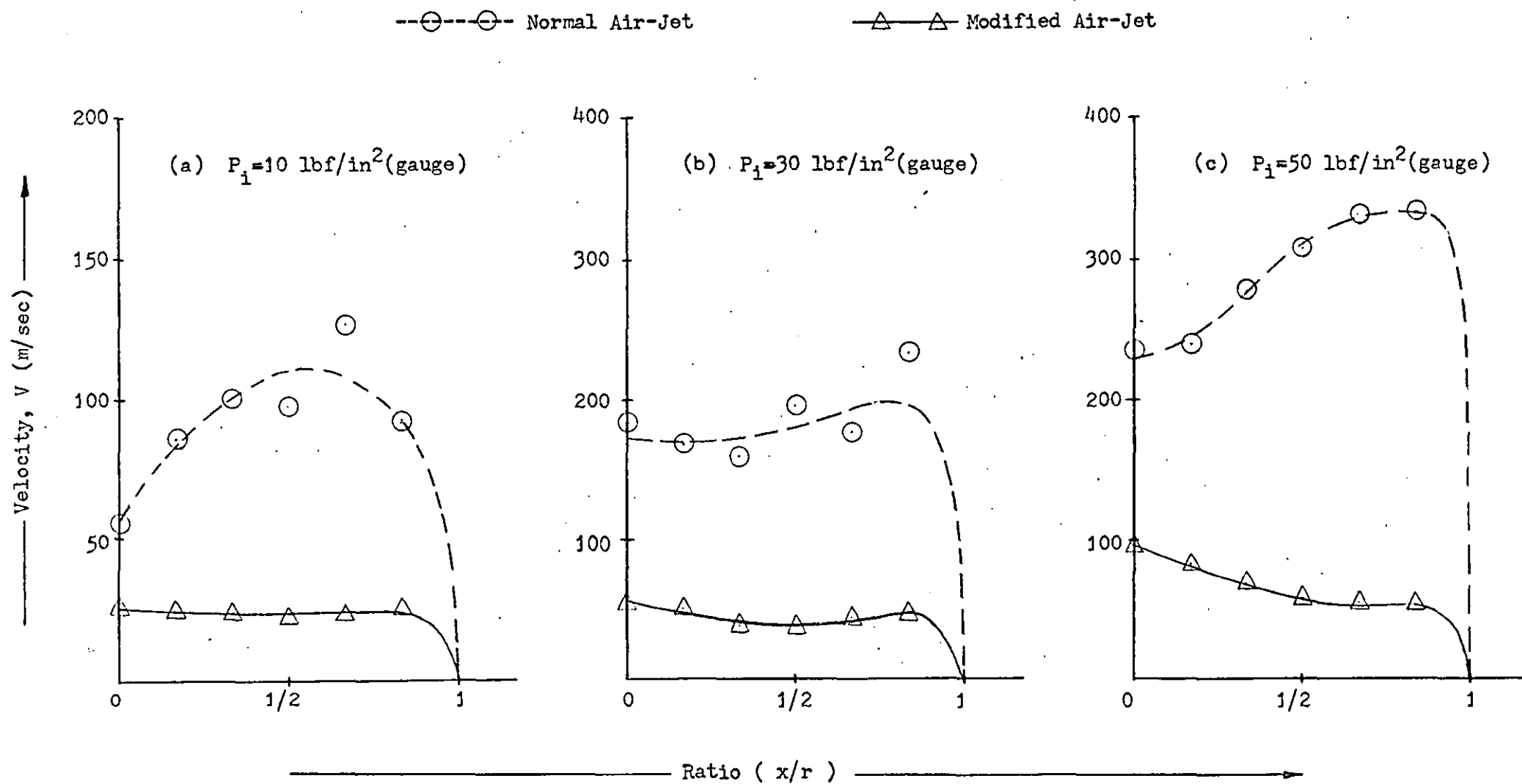


Fig. 3.26.1 Velocity Distribution Along OC When $\alpha = 0^\circ$

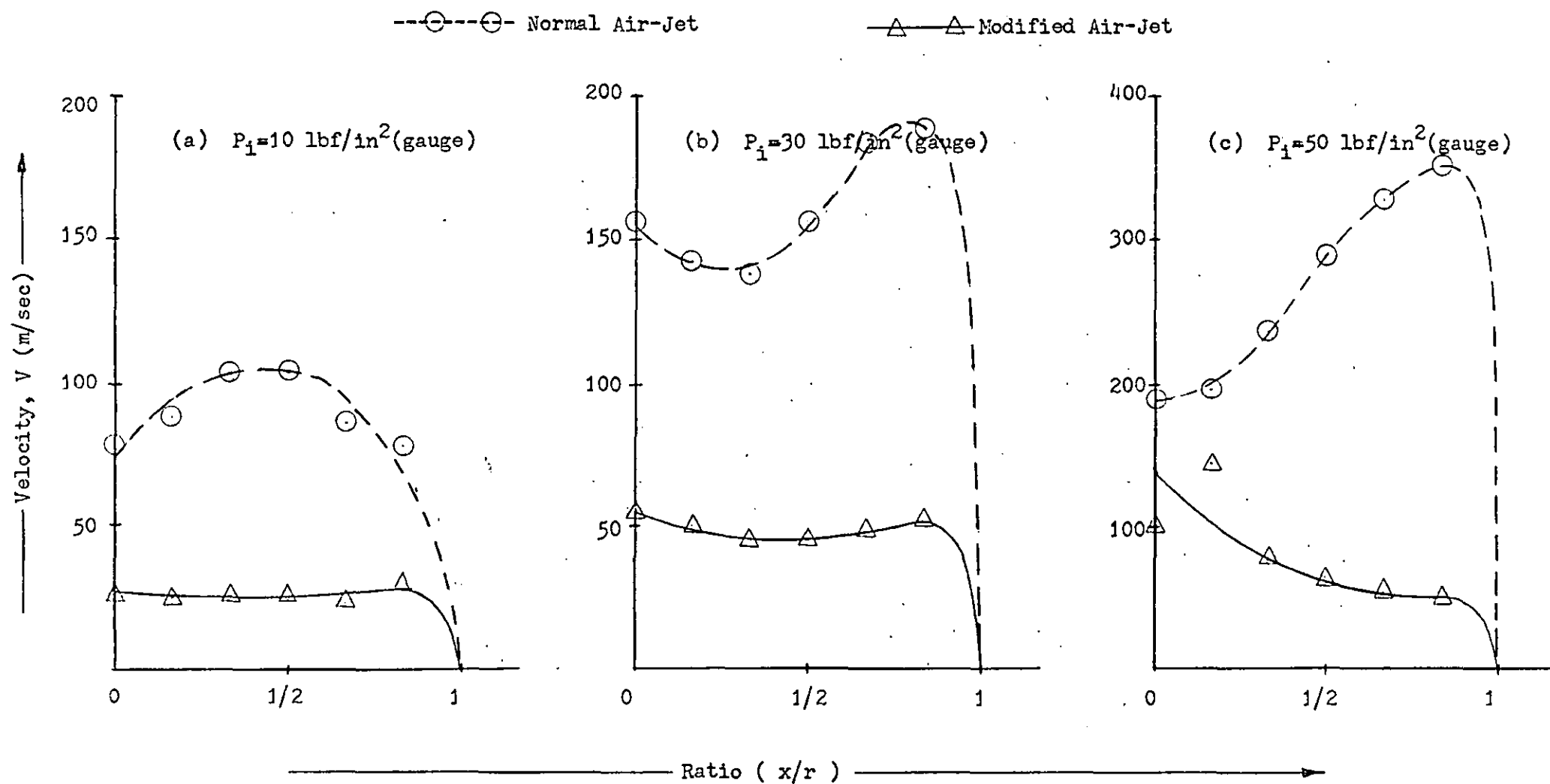


Fig. 3.26.2 Velocity Distribution Along OC When $\alpha = 20^\circ$

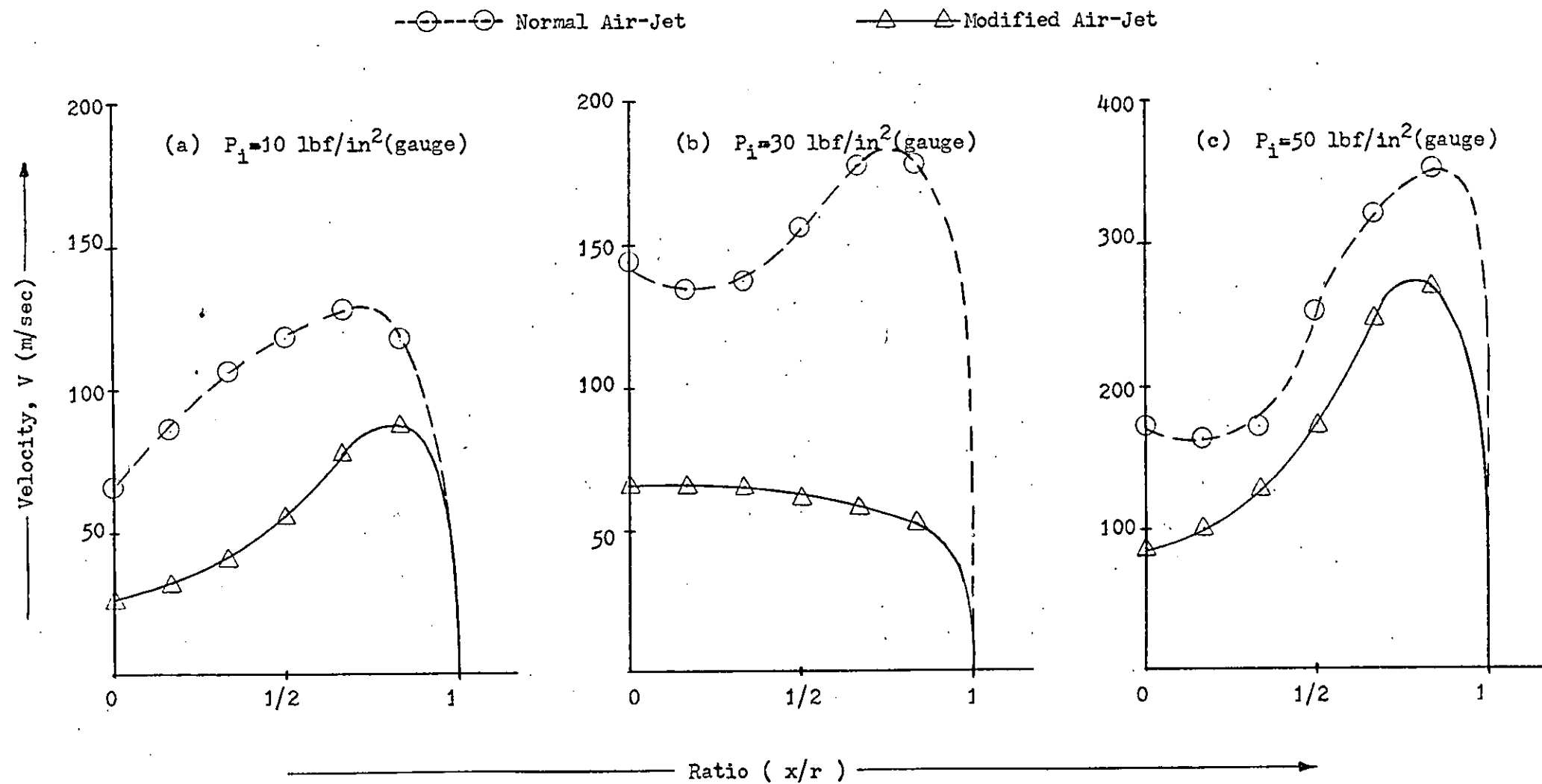


Fig. 3.26.3 Velocity Distribution Along OC When $\alpha = 40^\circ$

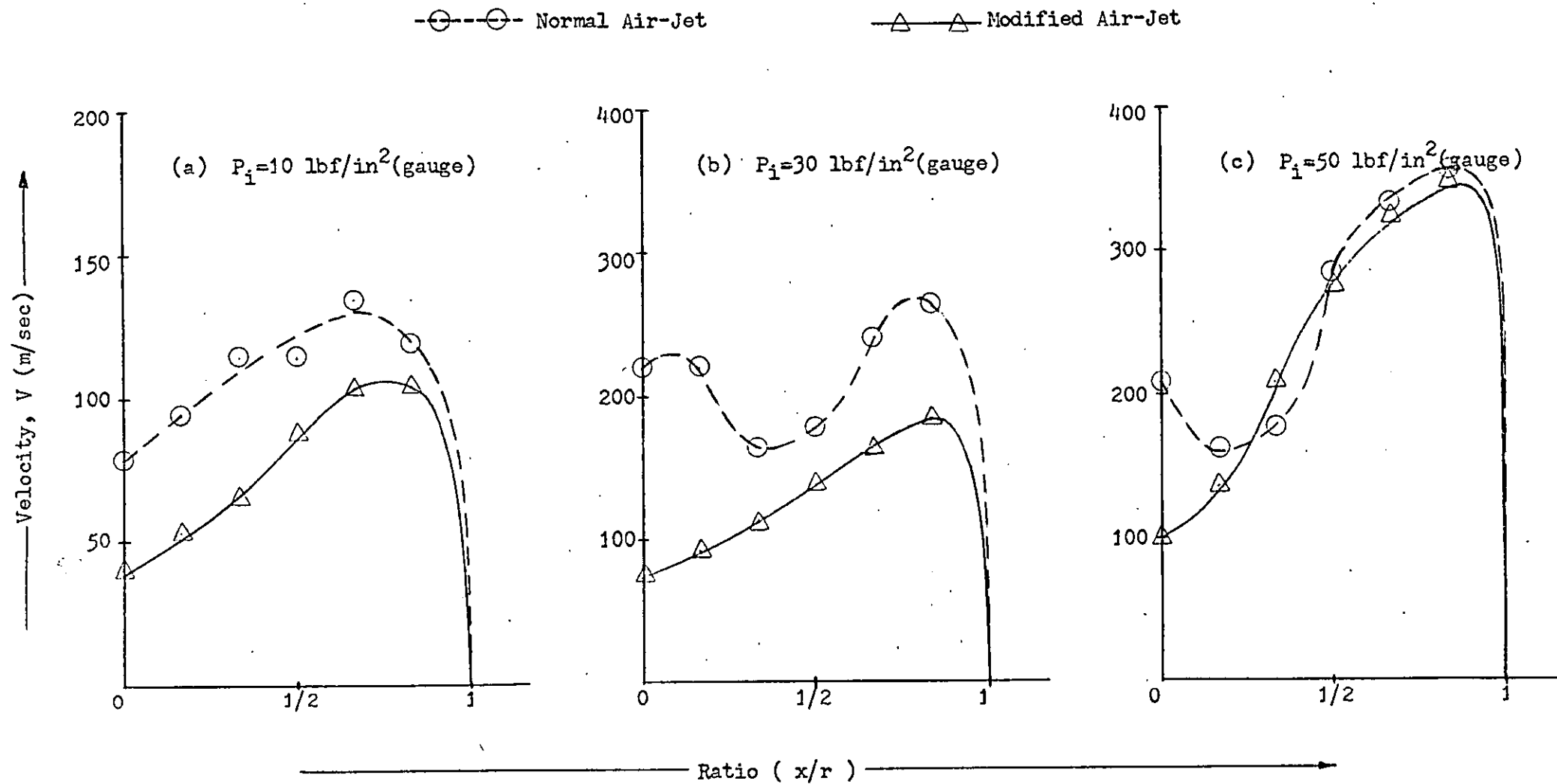


Fig. 3.26.4 Velocity Distribution Along OC When $\alpha = 60^\circ$

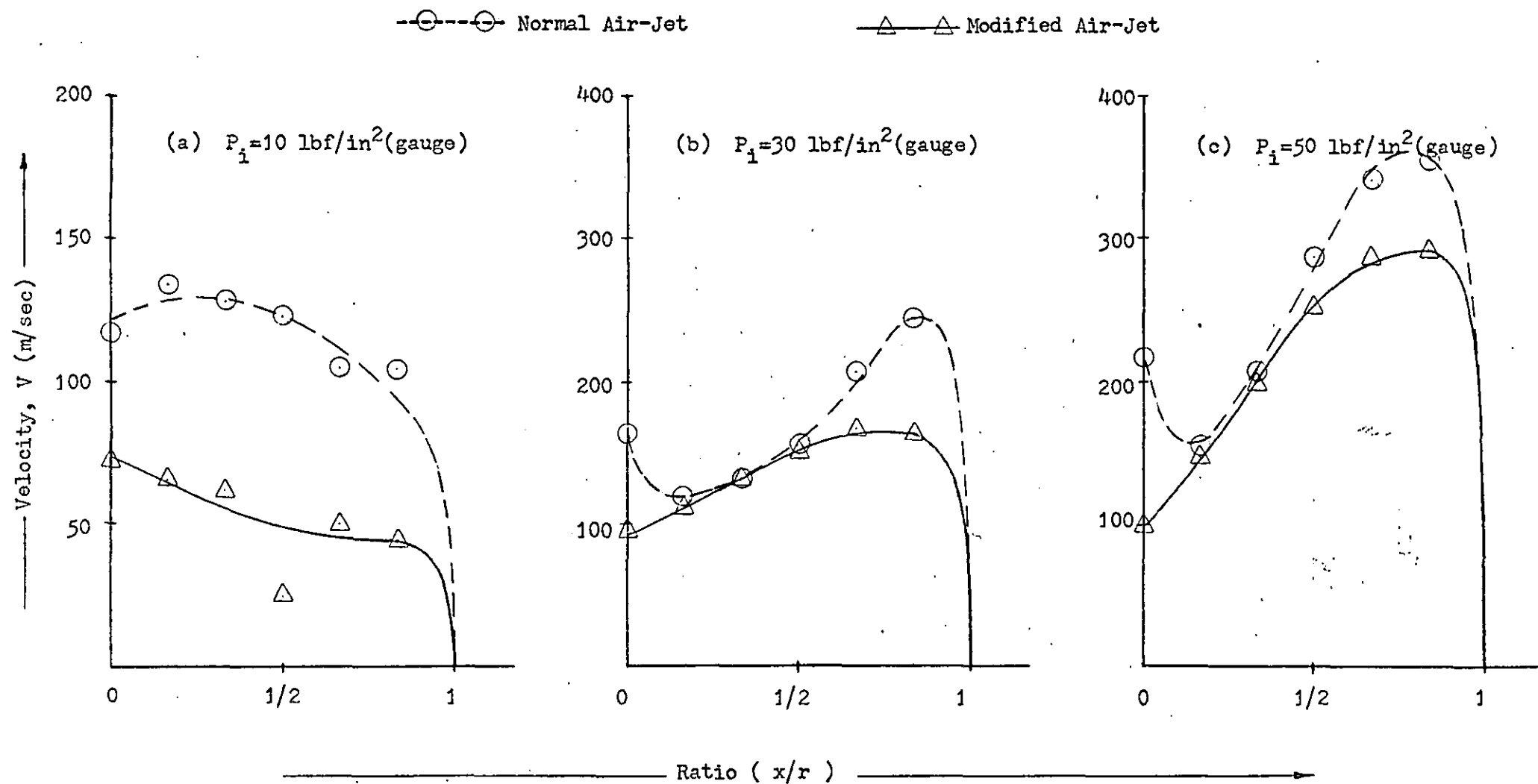


Fig. 3.26.5 Velocity Distribution Along OC When $\alpha = 80^\circ$

○---○ Normal Air-Jet

△---△ Modified Air-Jet

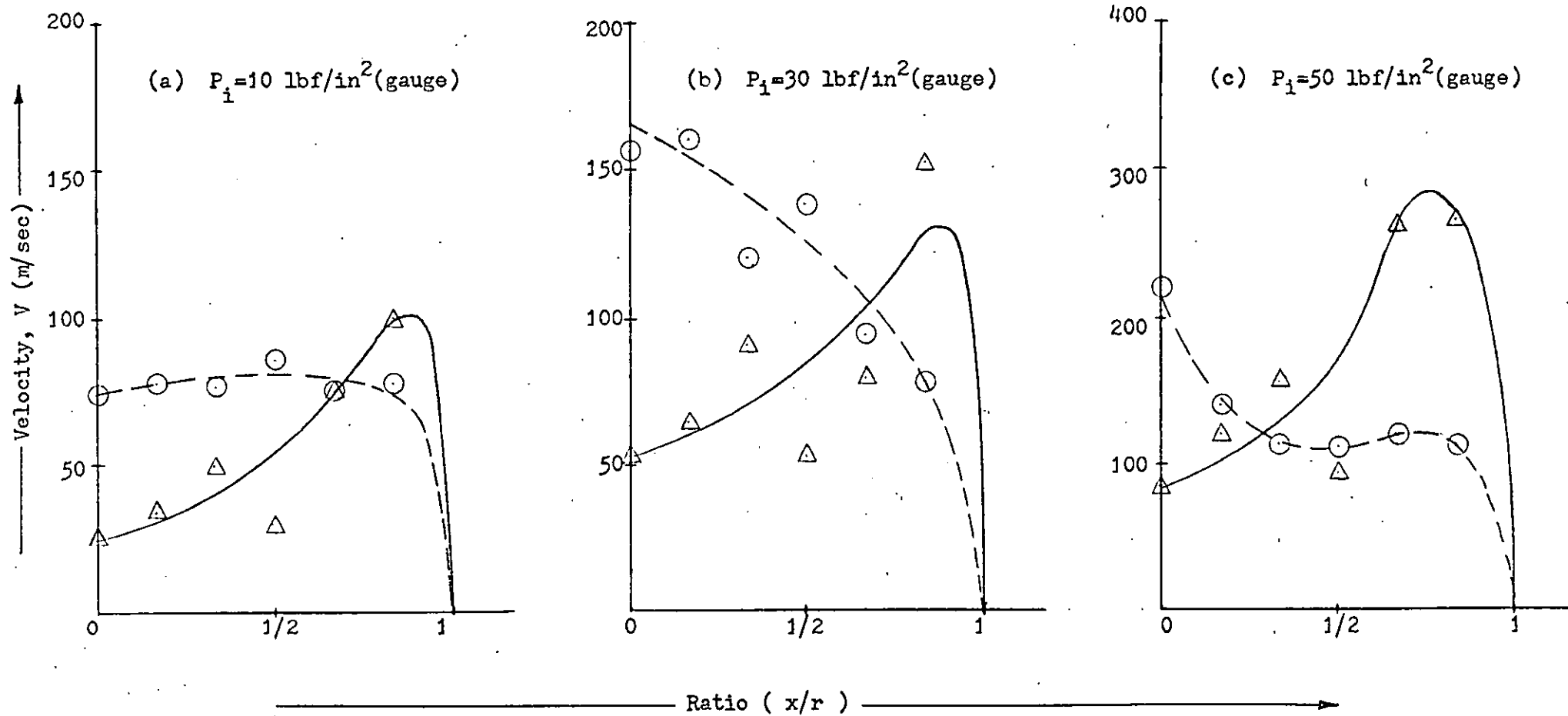


Fig. 3.27.1 Velocity Distribution Along OD When $\alpha = 0^\circ$

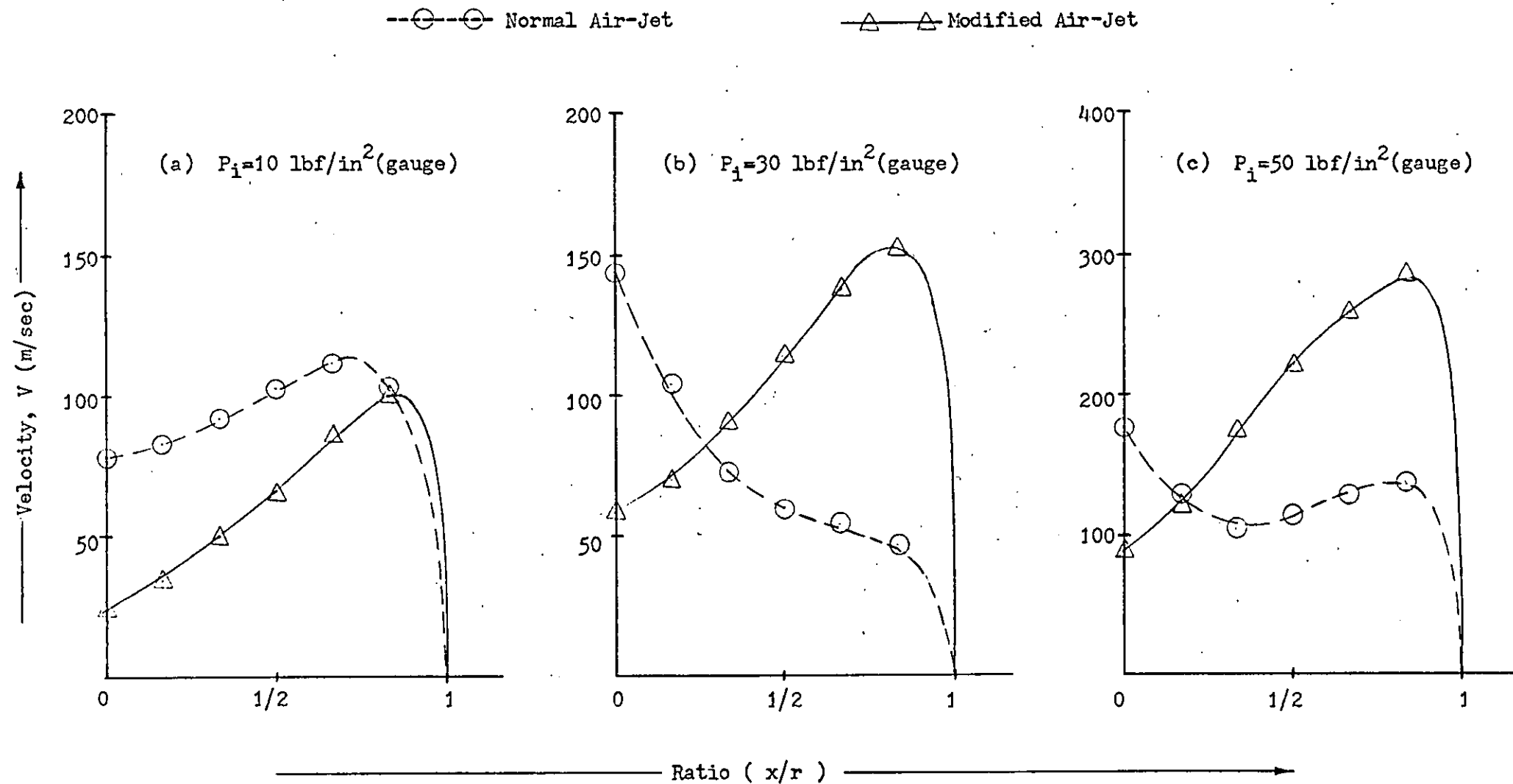


Fig. 3.27.2 Velocity Distribution Along OD When $\alpha = 20^\circ$

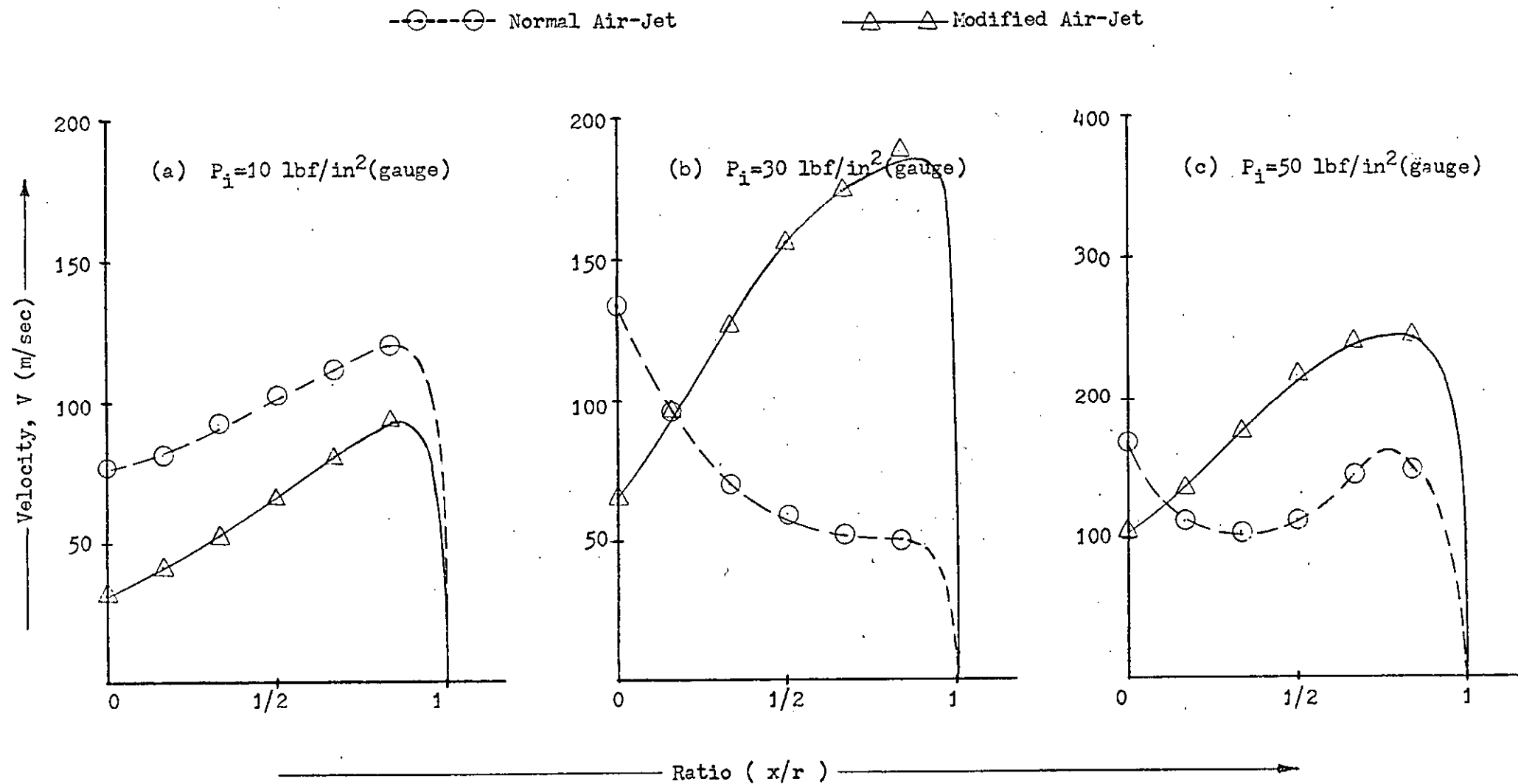


Fig. 3.27.3 Velocity Distribution Along OD When $\alpha = 40^\circ$

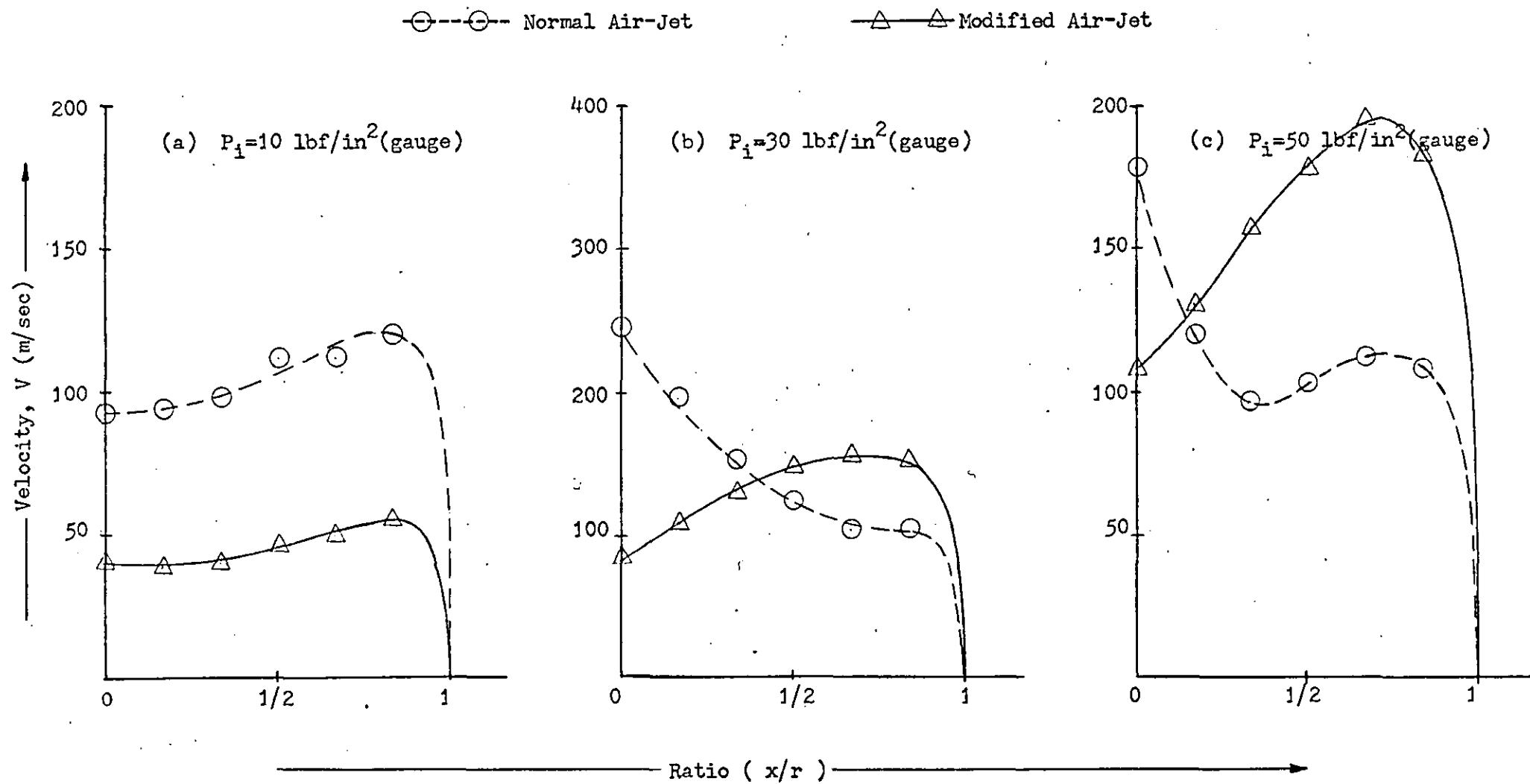


Fig. 3.27.4 Velocity Distribution Along OD When $\alpha = 60^\circ$

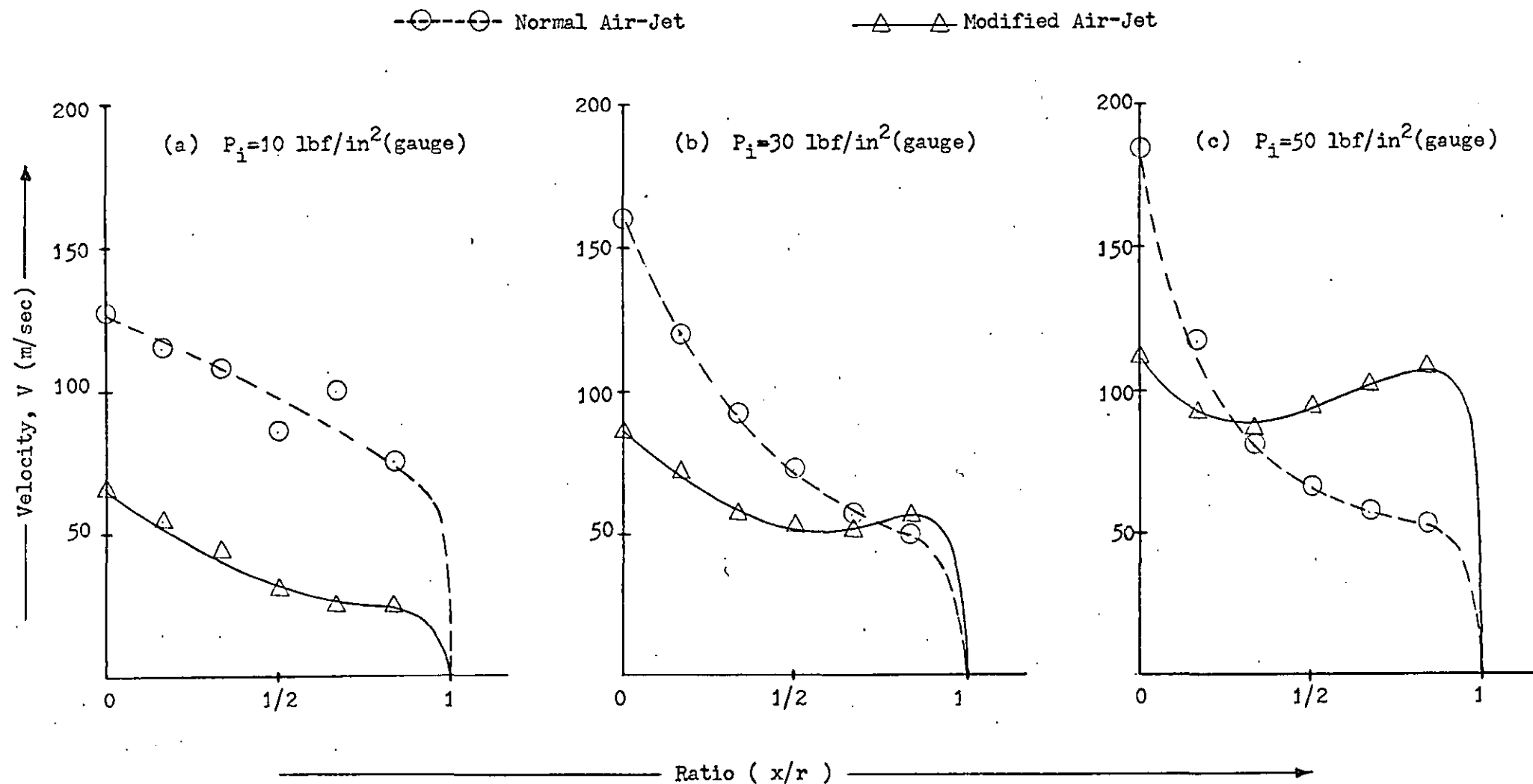


Fig. 3.27.5 Velocity Distribution Along OD When $\alpha = 80^\circ$

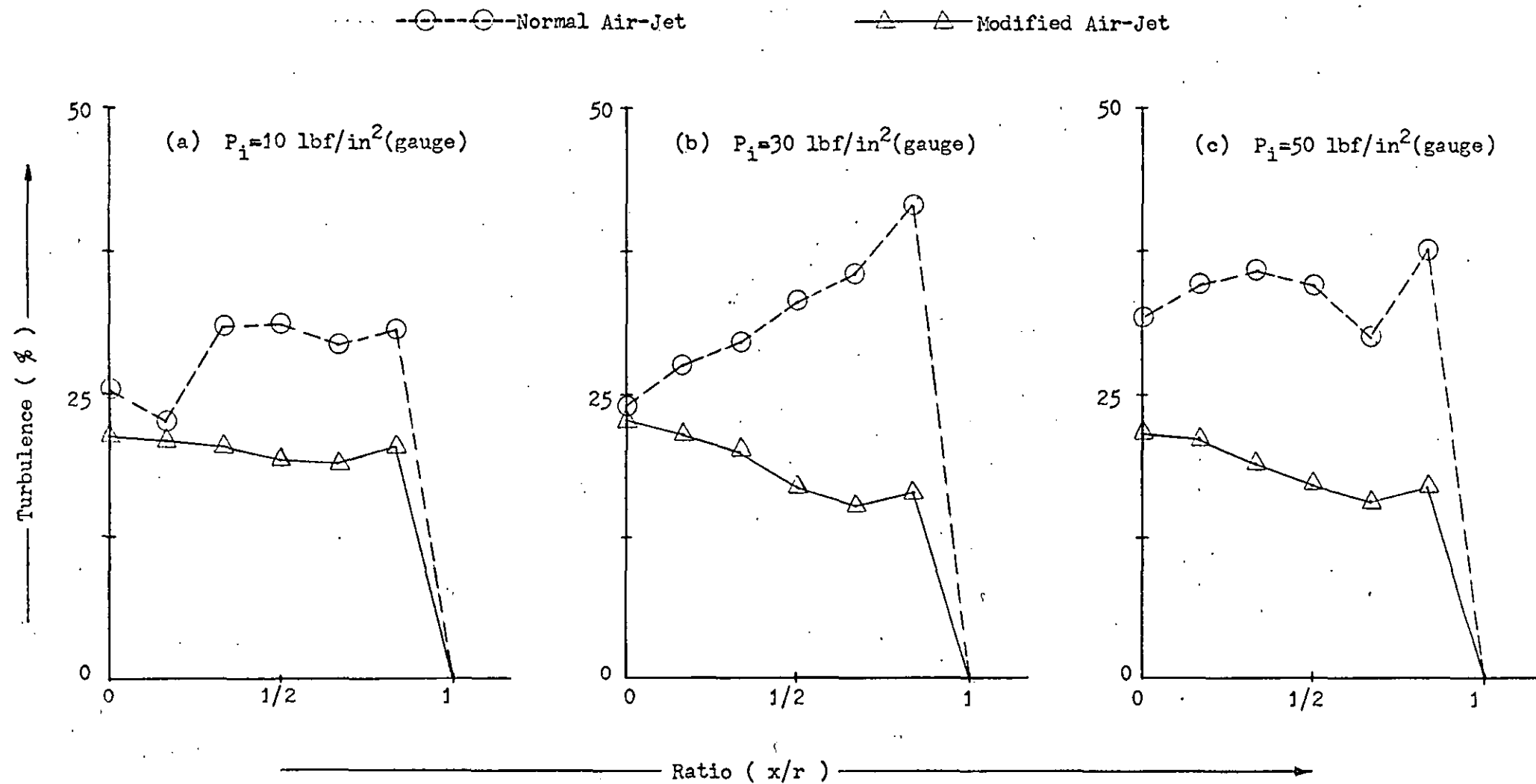


Fig. 3.28.1 Percentage Turbulence Distribution Along OA When $\alpha = 0^\circ$

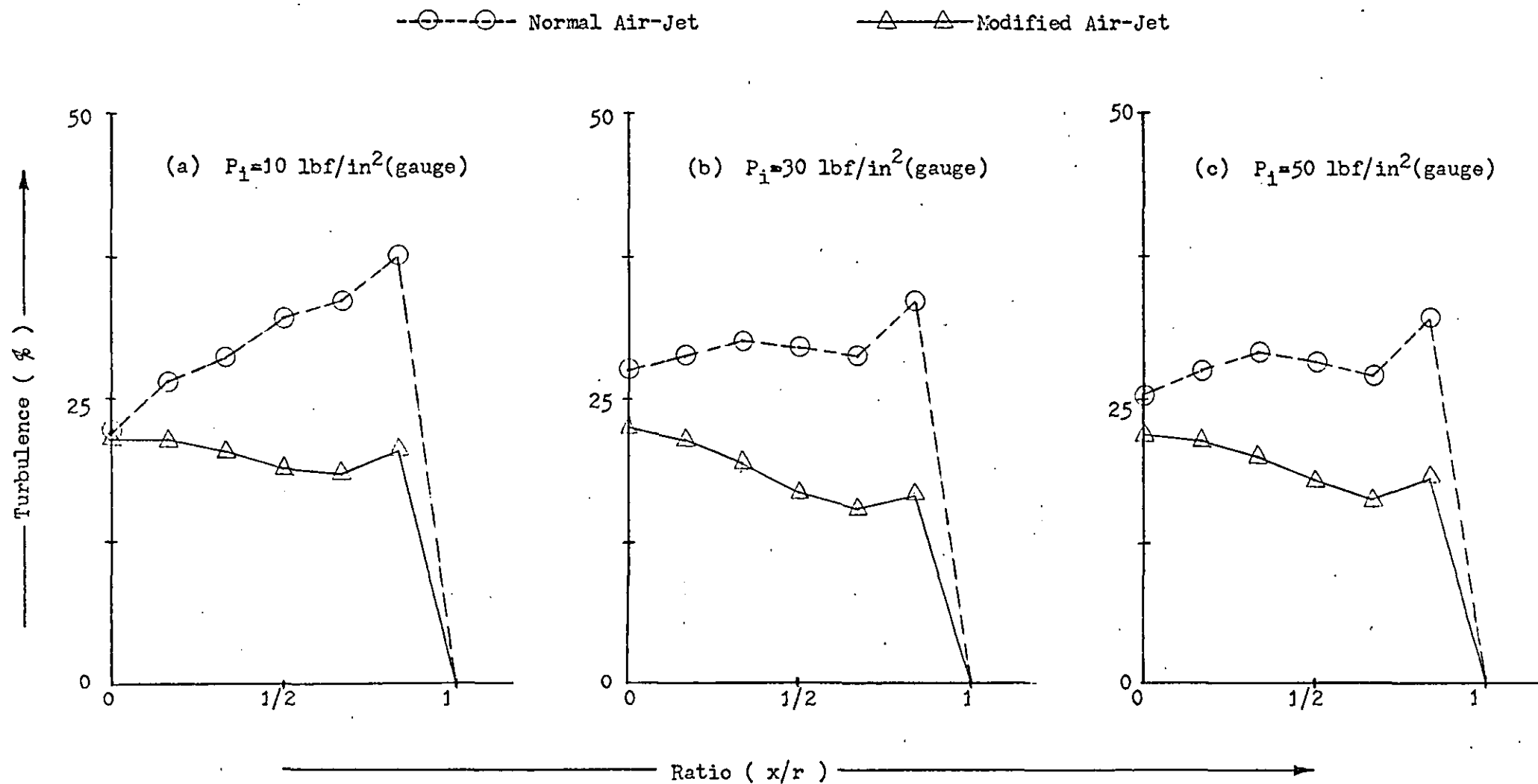


Fig. 3.28.2 Percentage Turbulence Distribution Along OA When $\alpha = 20^\circ$

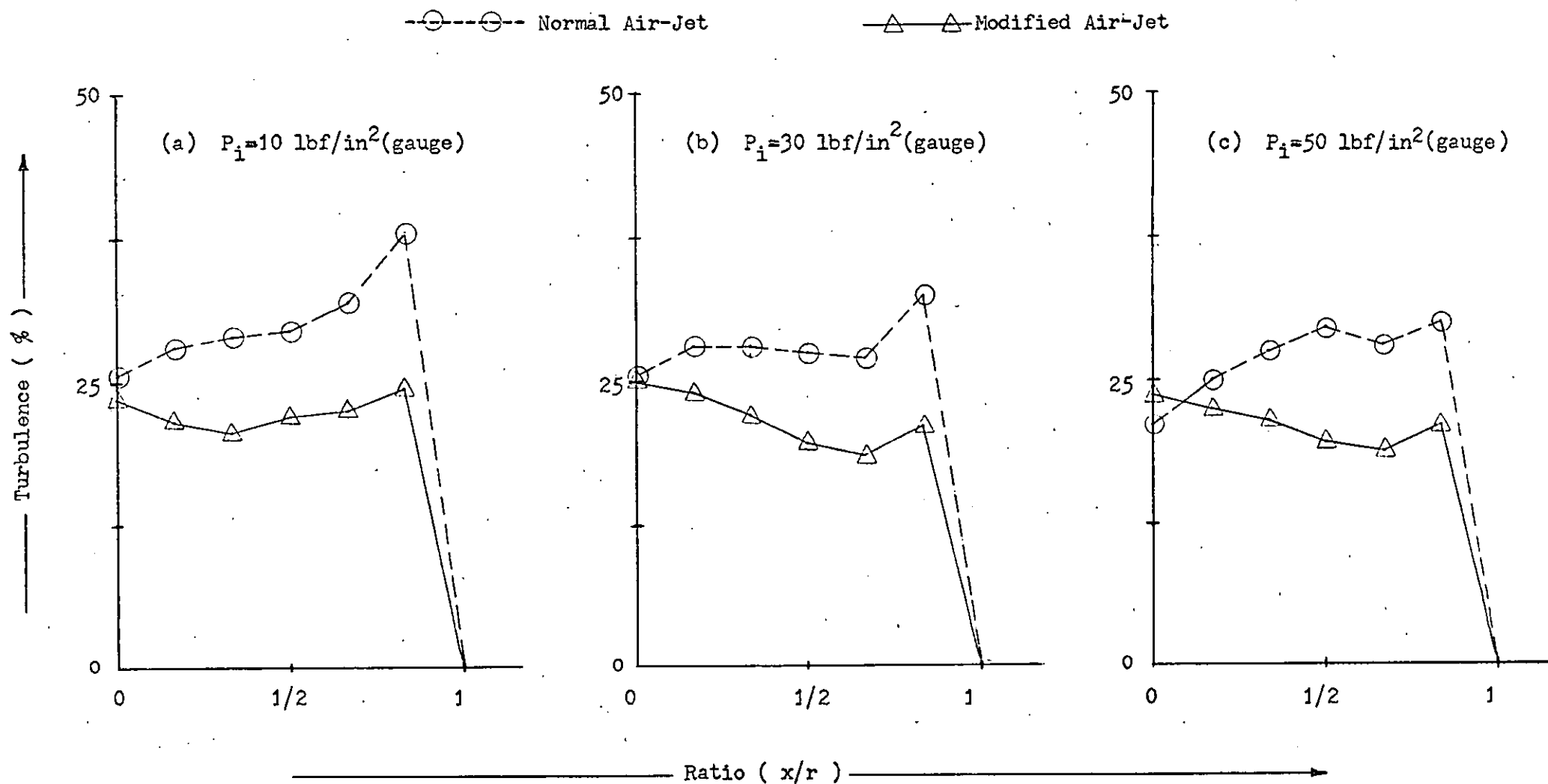


Fig. 3.28.3 Percentage Turbulence Distribution Along OA When $\alpha = 40^\circ$

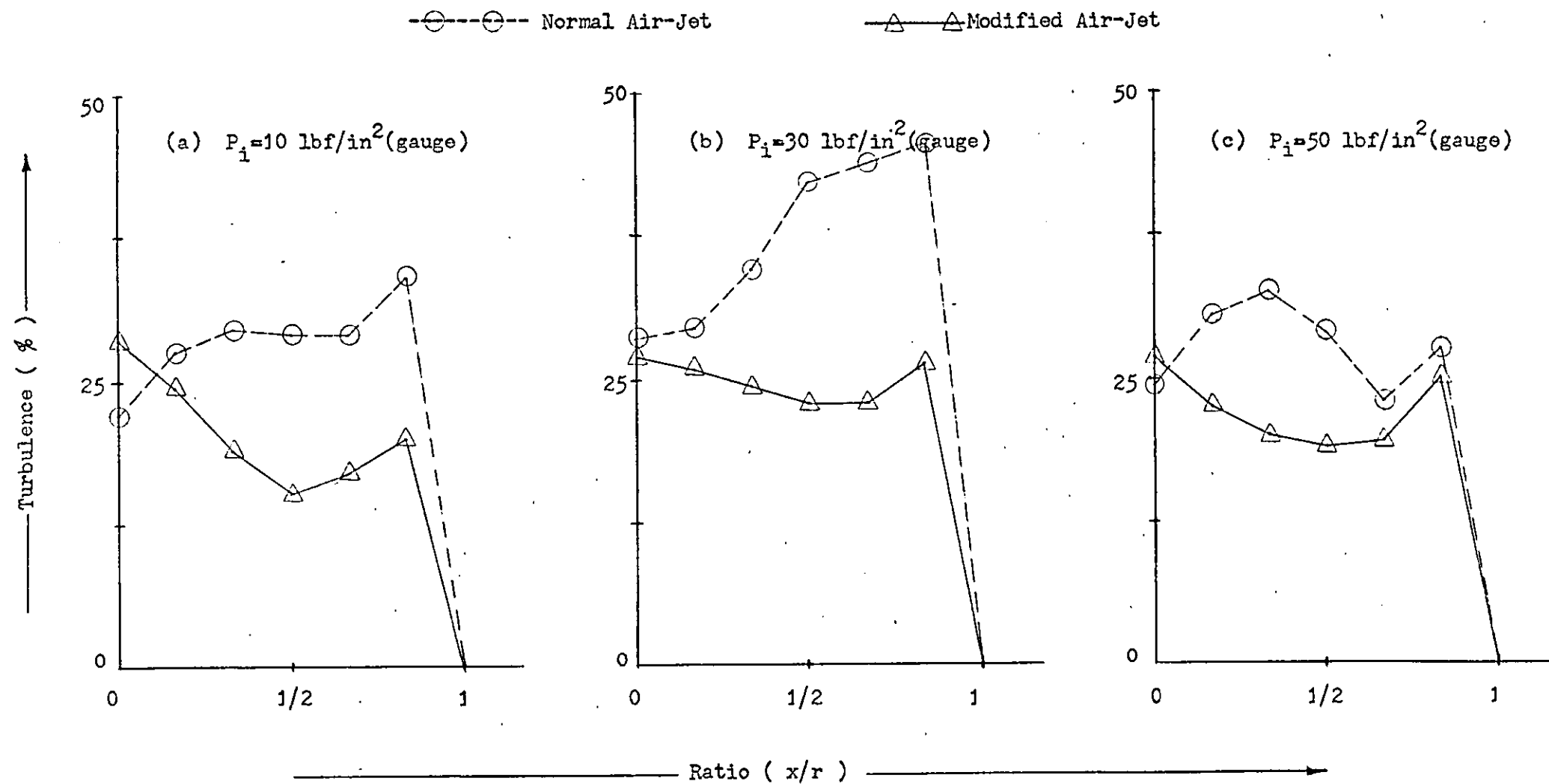


Fig. 3.28.4 Percentage Turbulence Distribution Along OA When $\alpha = 60^\circ$

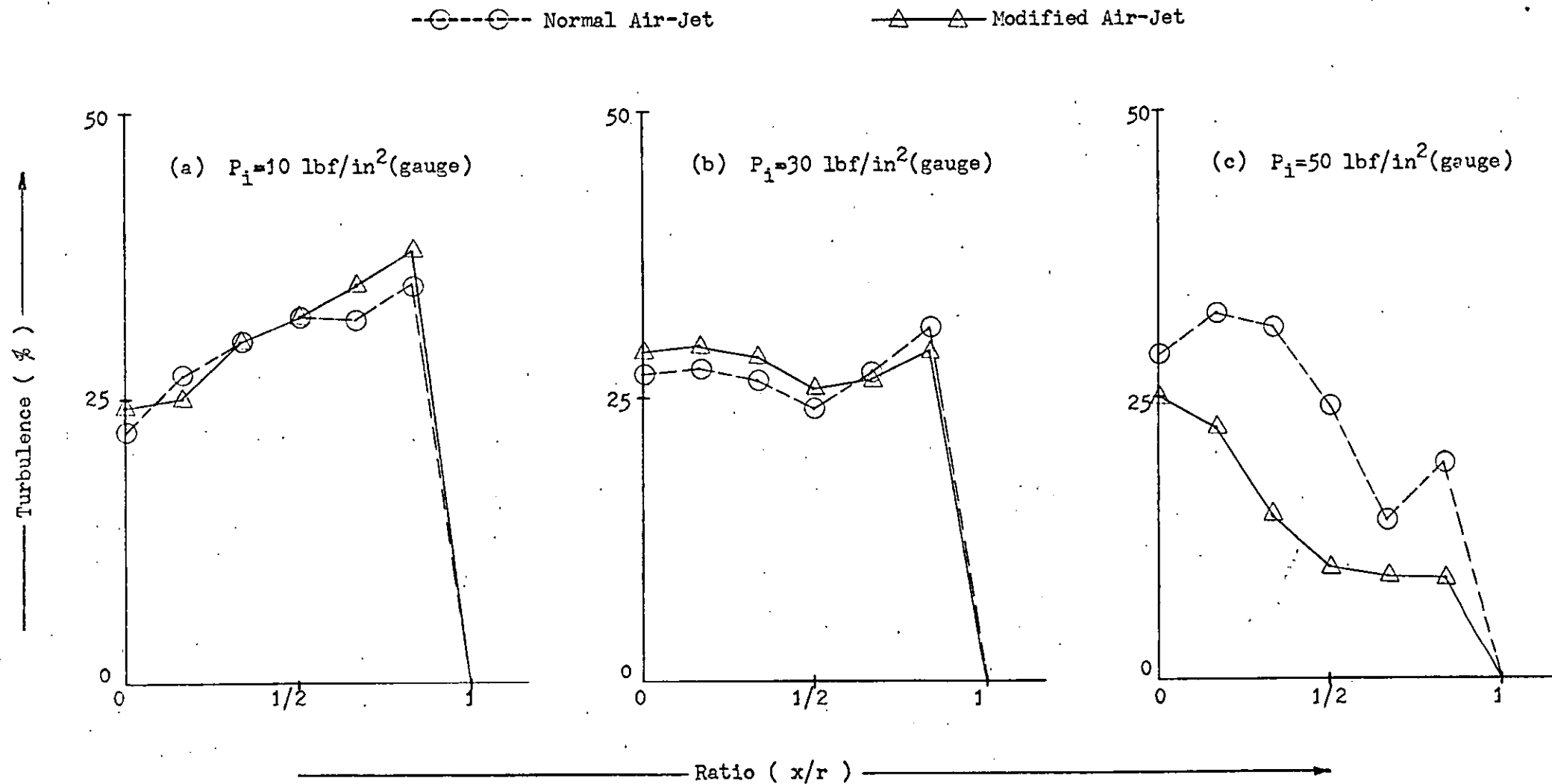


Fig. 3.28.5 Percentage Turbulence Distribution Along OA When $\alpha = 80^\circ$

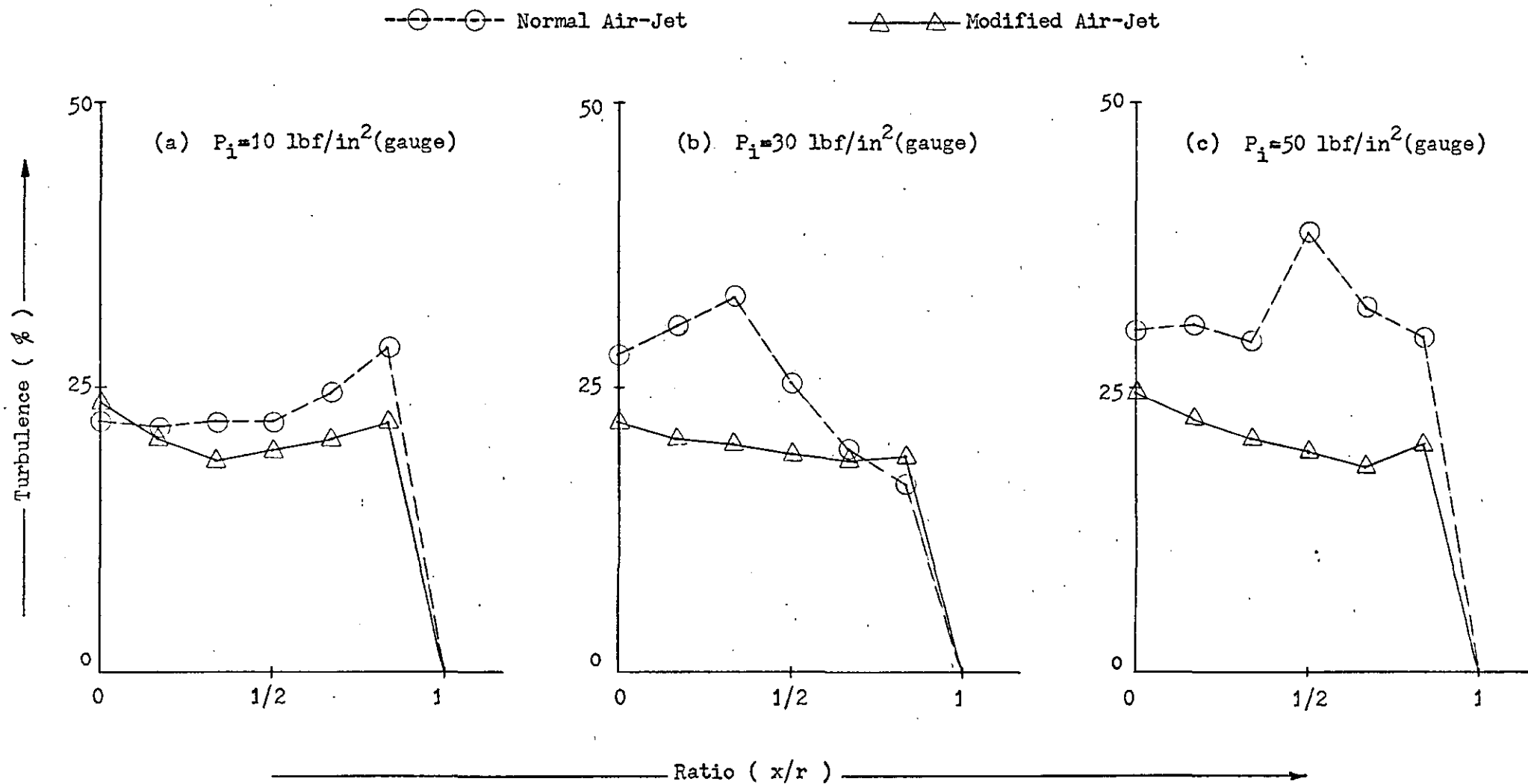


Fig. 3.29.1 Percentage Turbulence Distribution Along OB When $\alpha = 0^\circ$

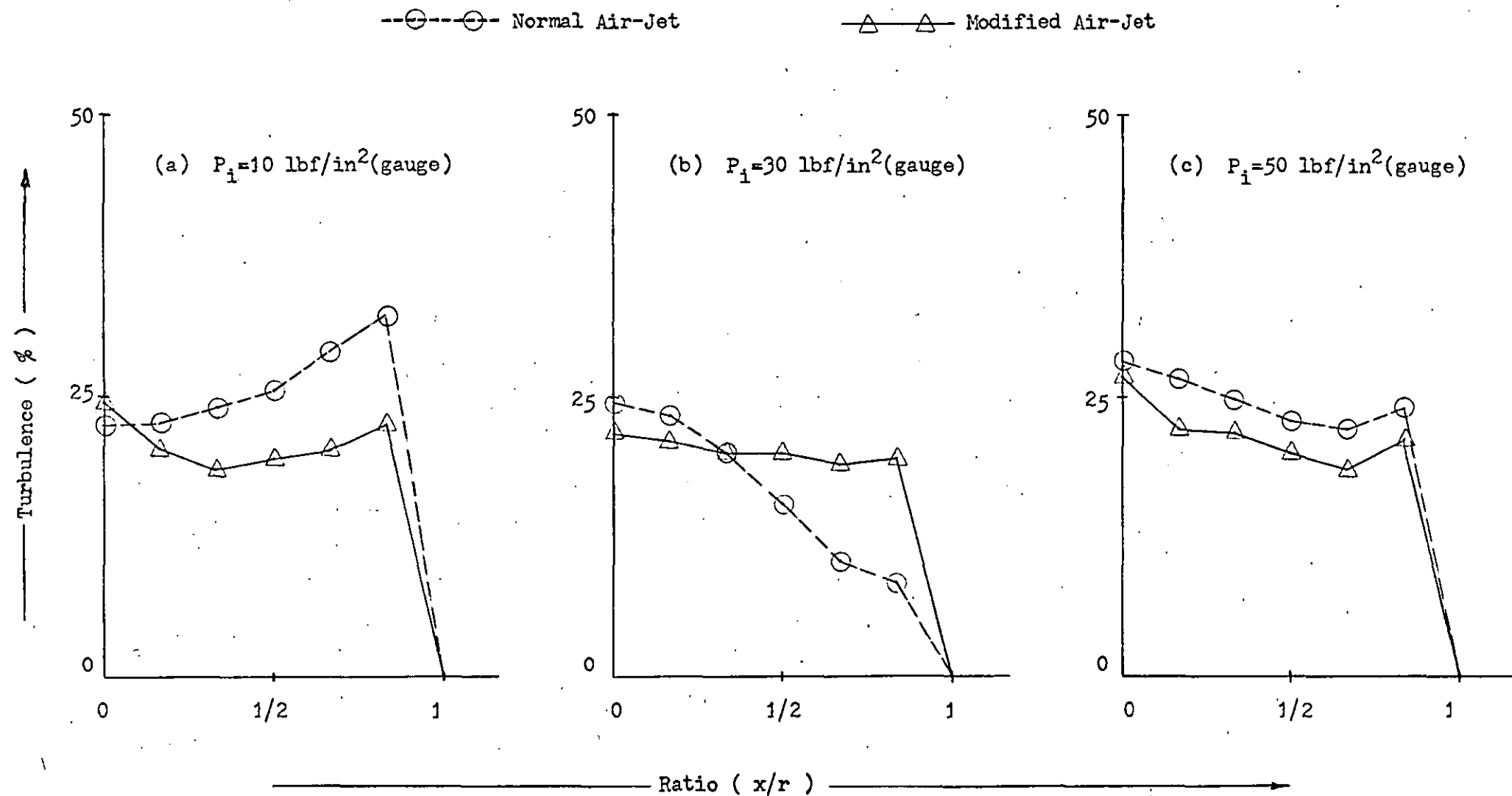


Fig. 3.29.2 Percentage Turbulence Distribution Along OB When $\alpha = 20^\circ$

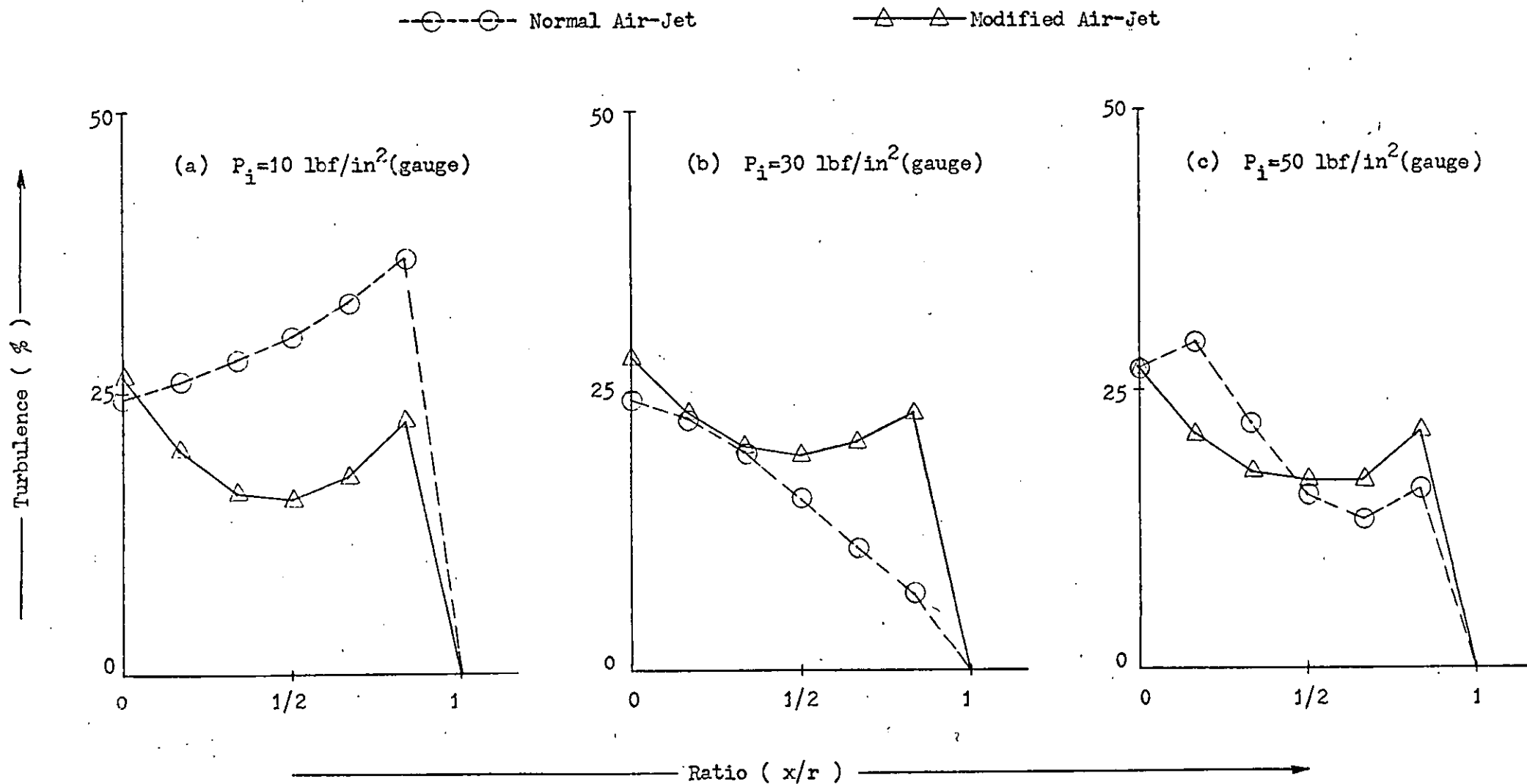


Fig. 3.29.3 Percentage Turbulence Distribution Along OB When $\alpha = 40^\circ$

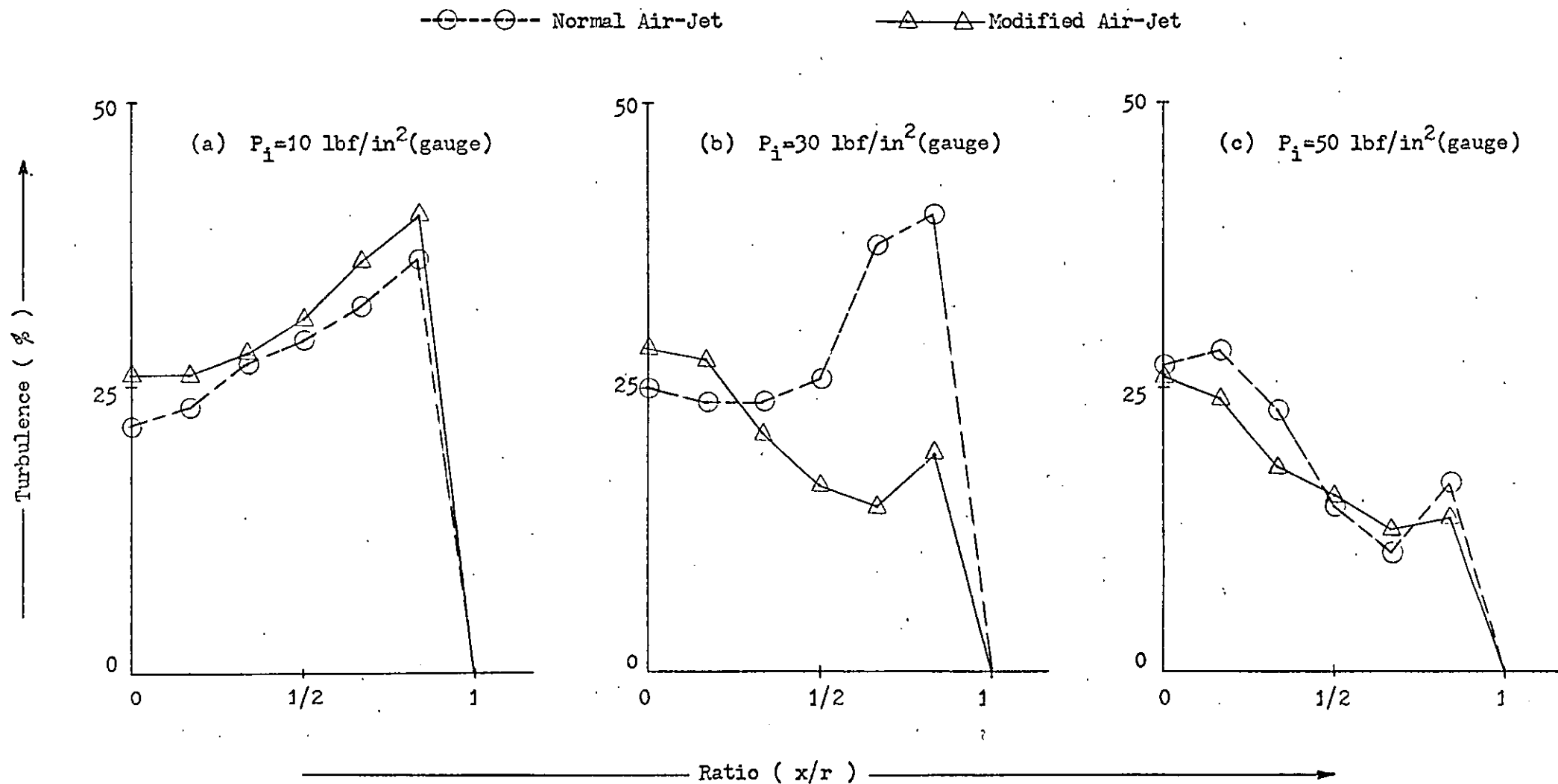


Fig. 3.29.4 Percentage Turbulence Distribution Along OB When $\alpha = 60^\circ$

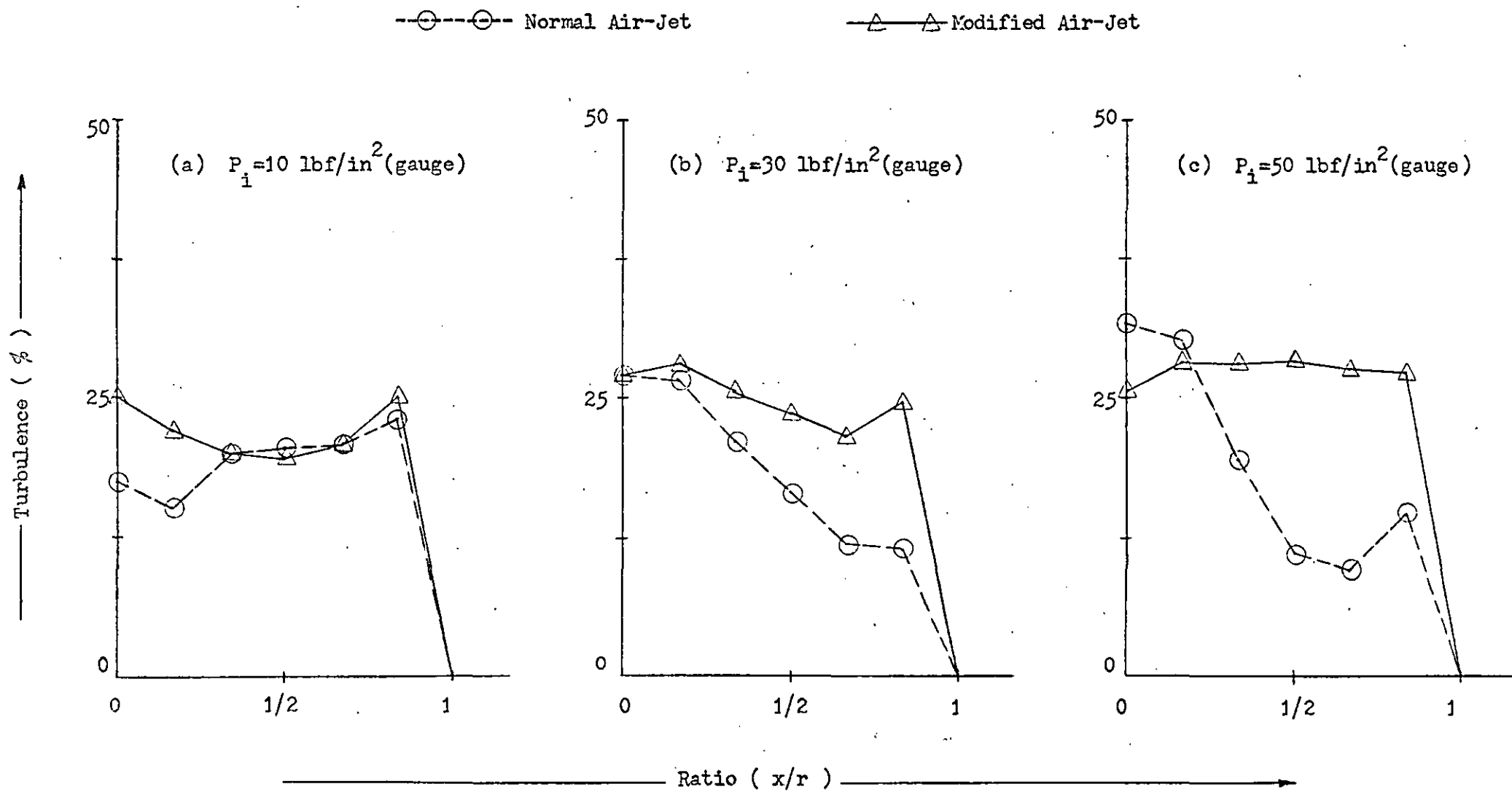


Fig. 3.29.5 Percentage Turbulence Distribution Along OB When $\alpha = 80^\circ$

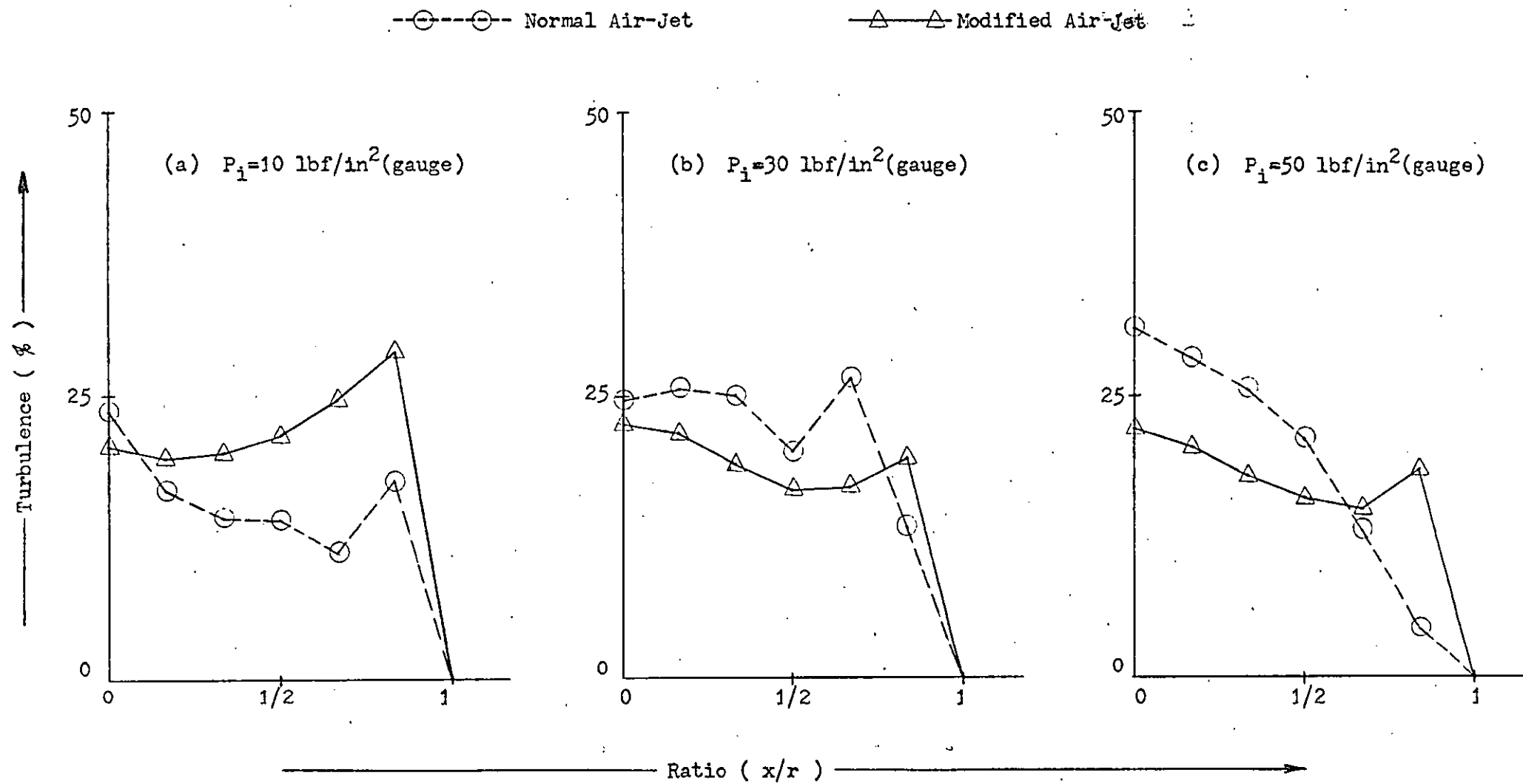


Fig. 3.30.1 Percentage Turbulence Distribution Along OC When $\alpha = 0^\circ$

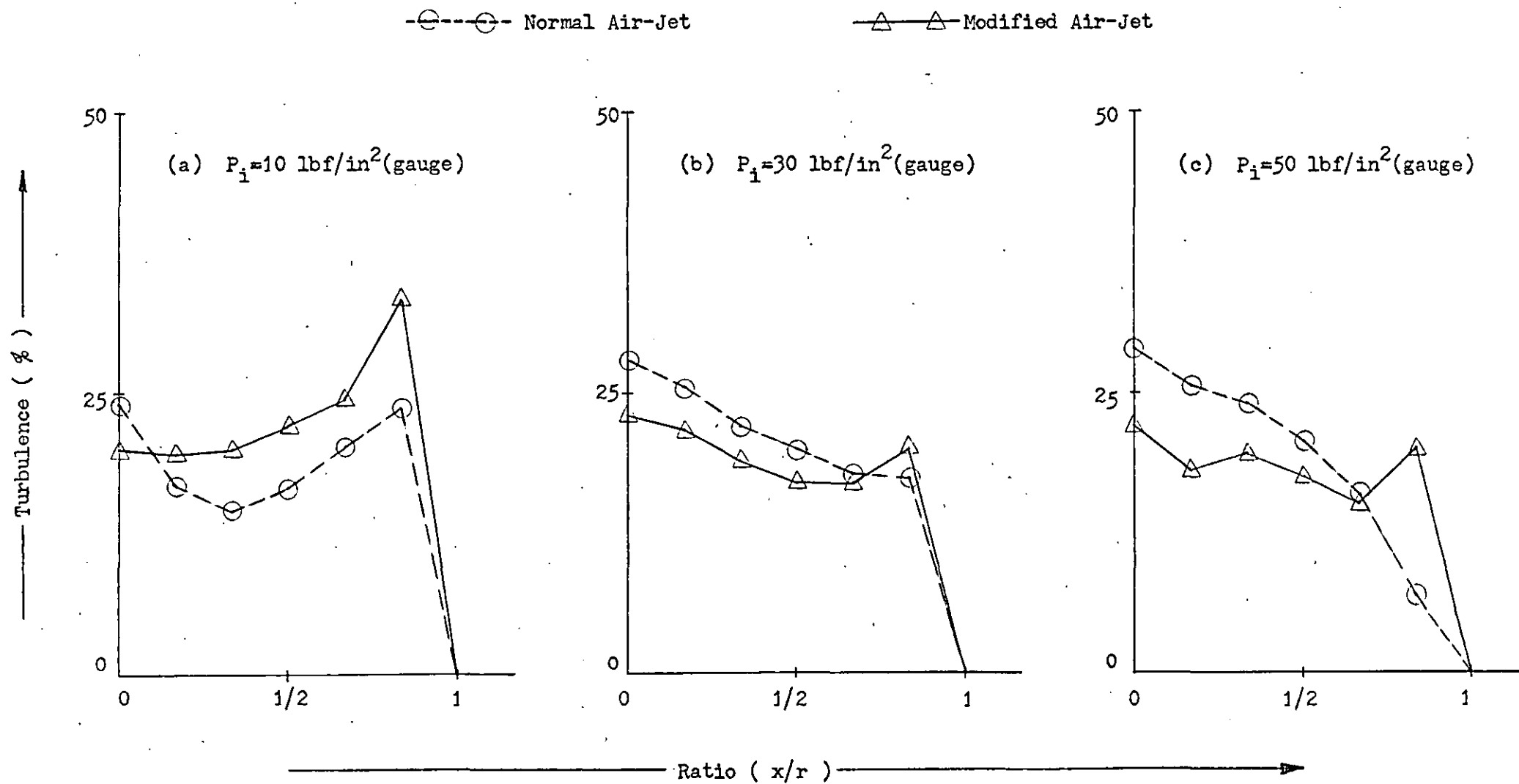


Fig. 3.30.2 Percentage Turbulence Distribution Along OC When $\alpha = 20^\circ$

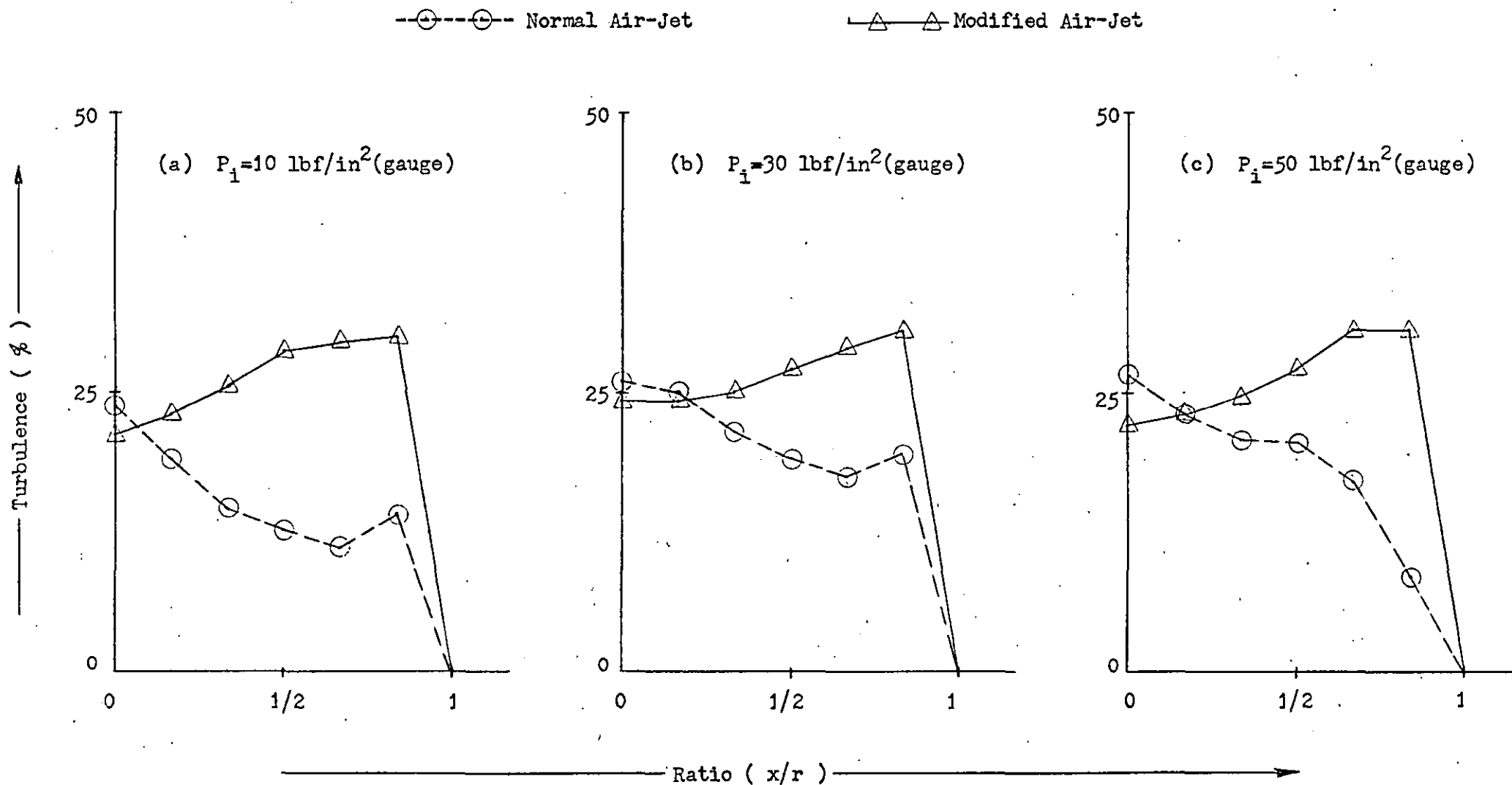


Fig. 3.30.3 Percentage Turbulence Distribution Along OC When $\alpha = 40^\circ$

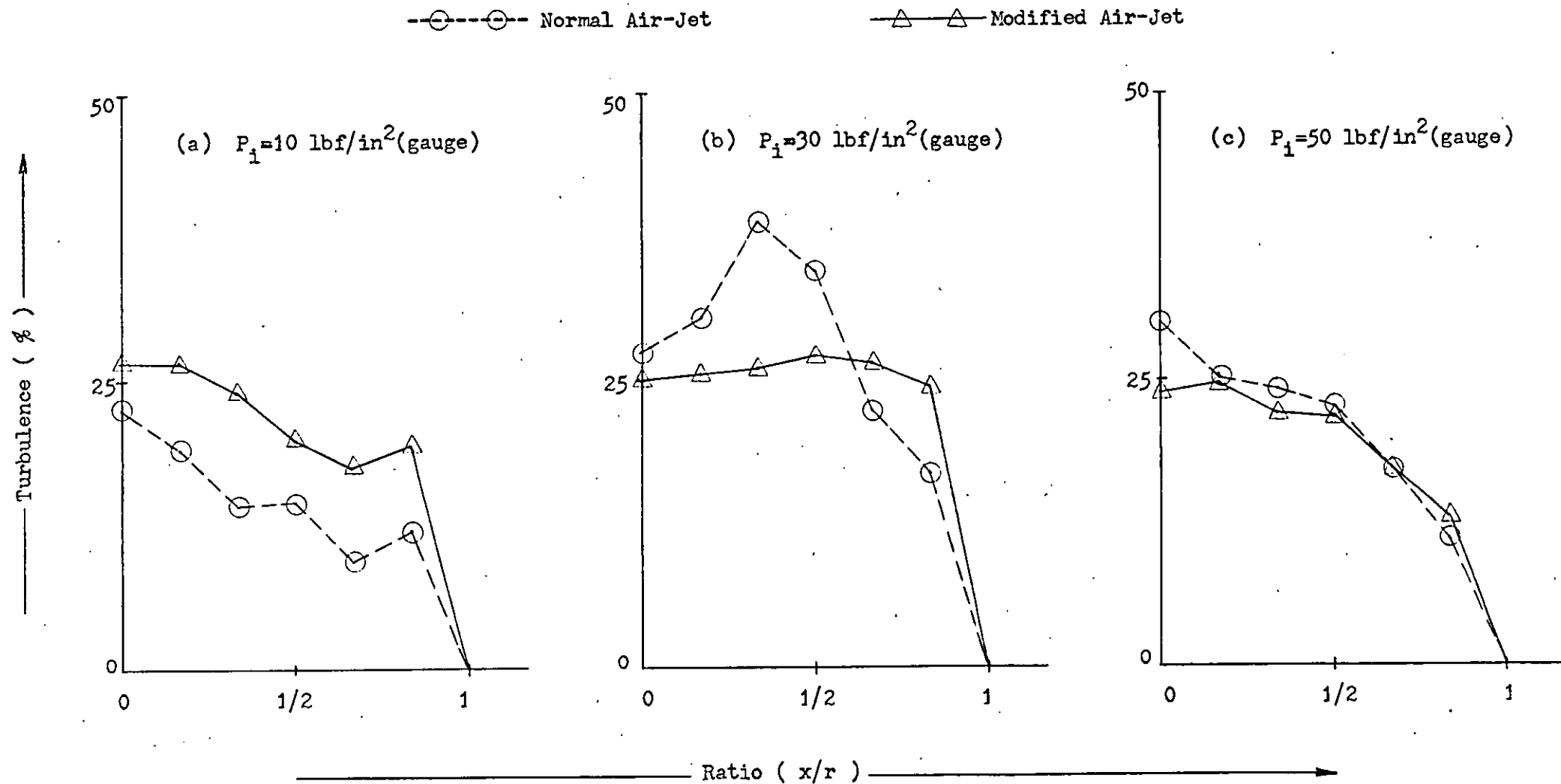


Fig. 3.30.4 Percentage Turbulence Distribution Along OC When $\alpha = 60^\circ$

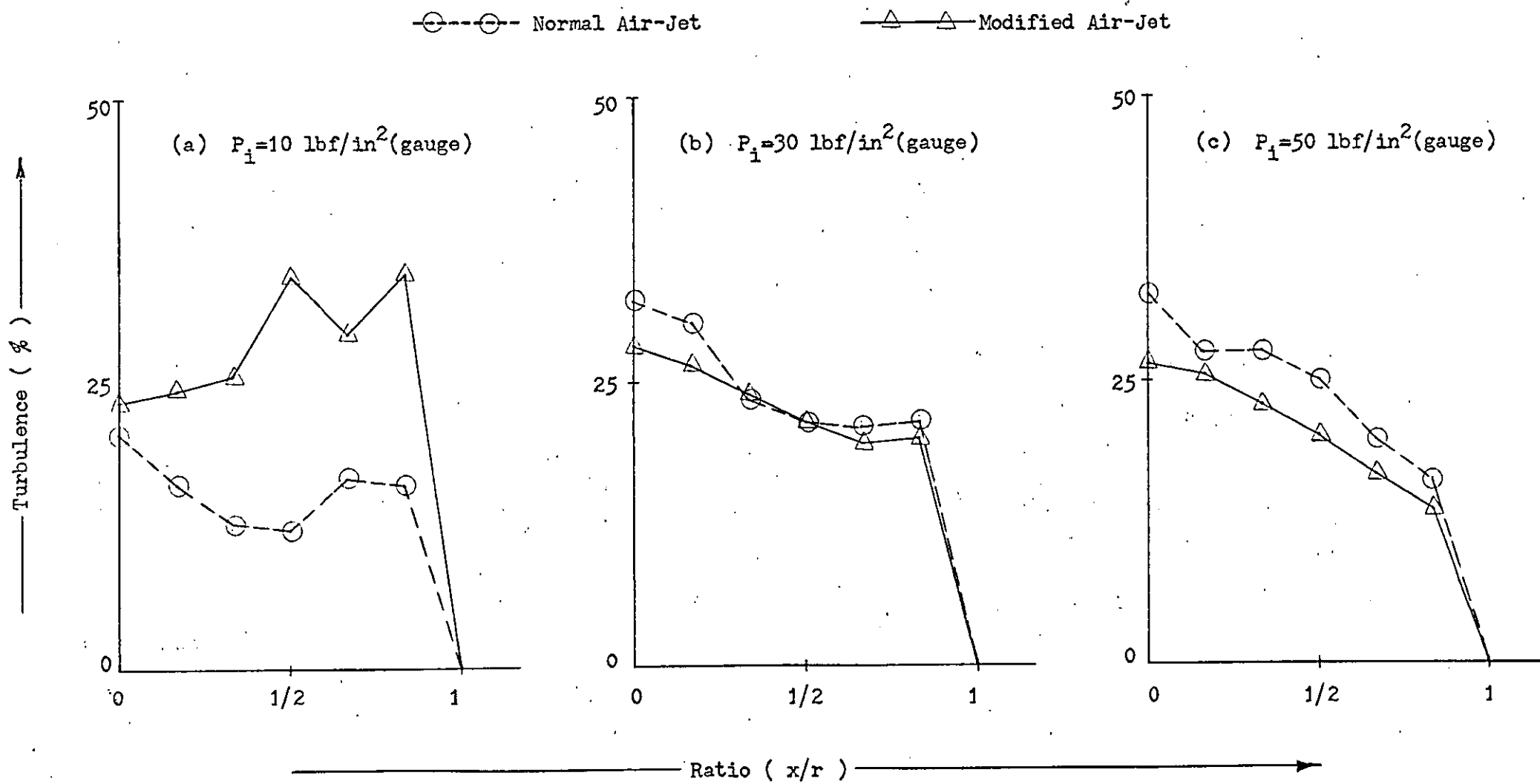


Fig. 3.30.5 Percentage Turbulence Distribution Along OC When $\alpha = 80^\circ$

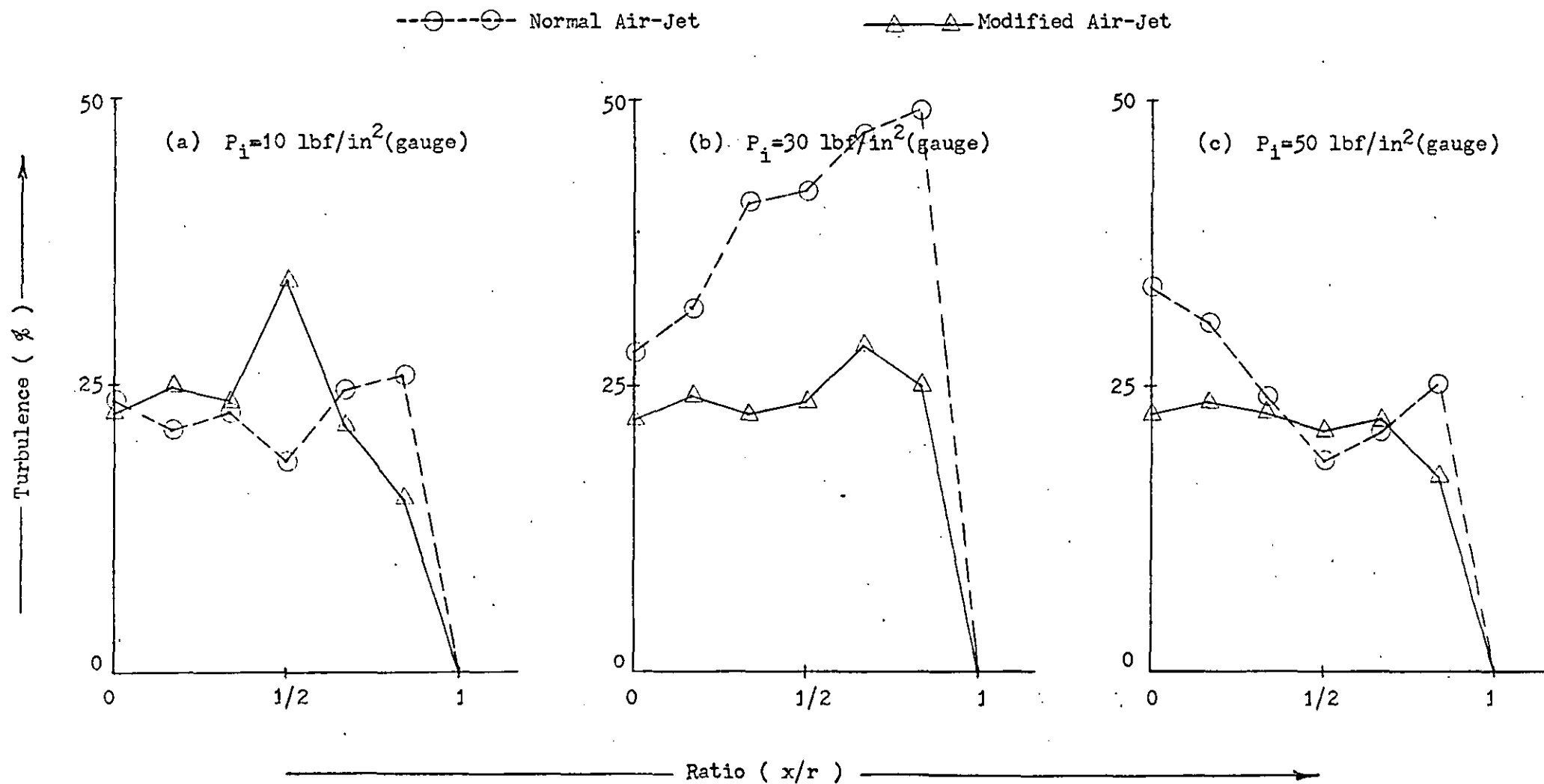


Fig. 3.31.1 Percentage Turbulence Distribution Along OD When $\alpha = 0^\circ$

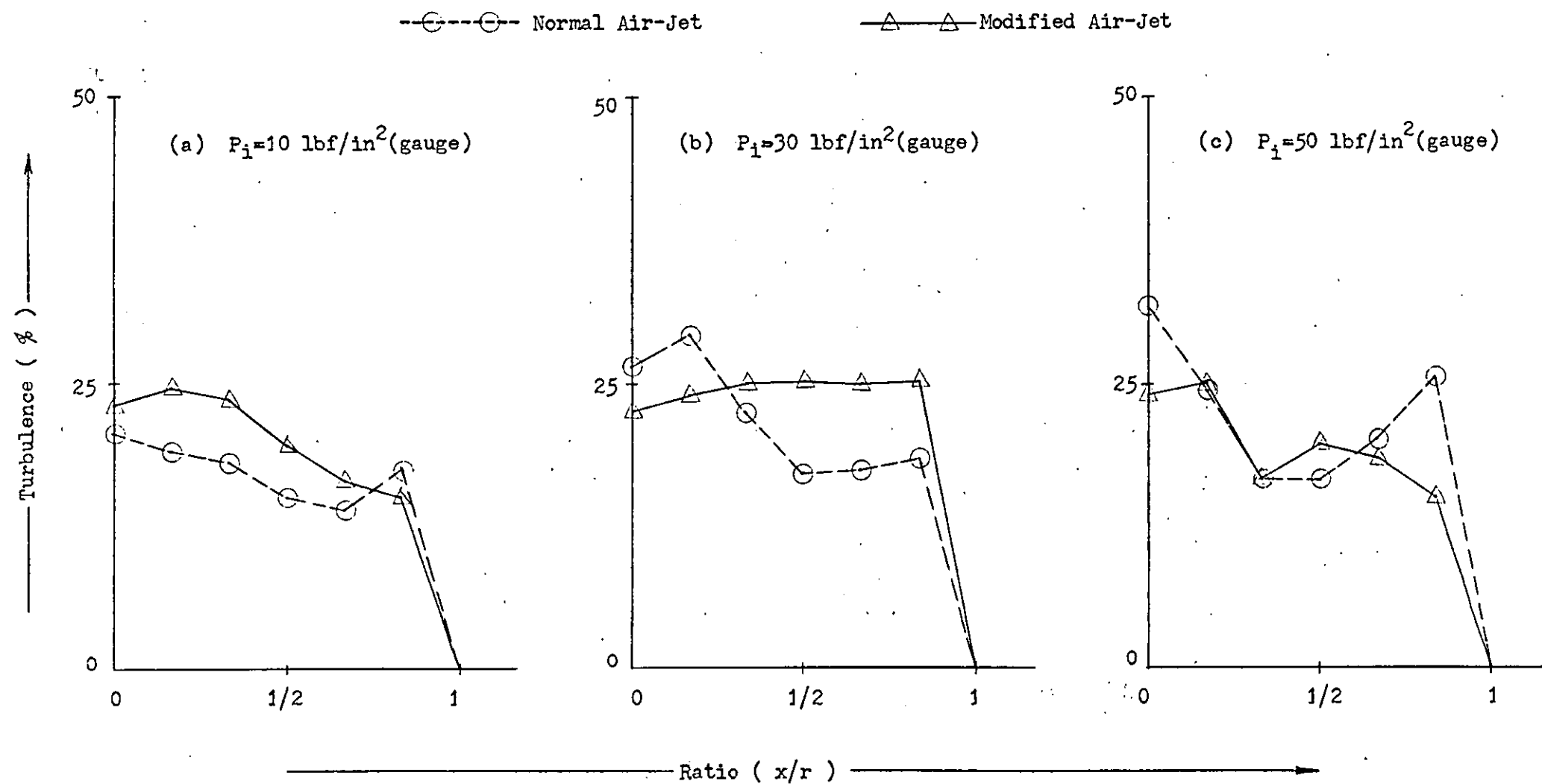


Fig. 3.31.2 Percentage Turbulence Distribution Along OD When $\alpha = 20^\circ$

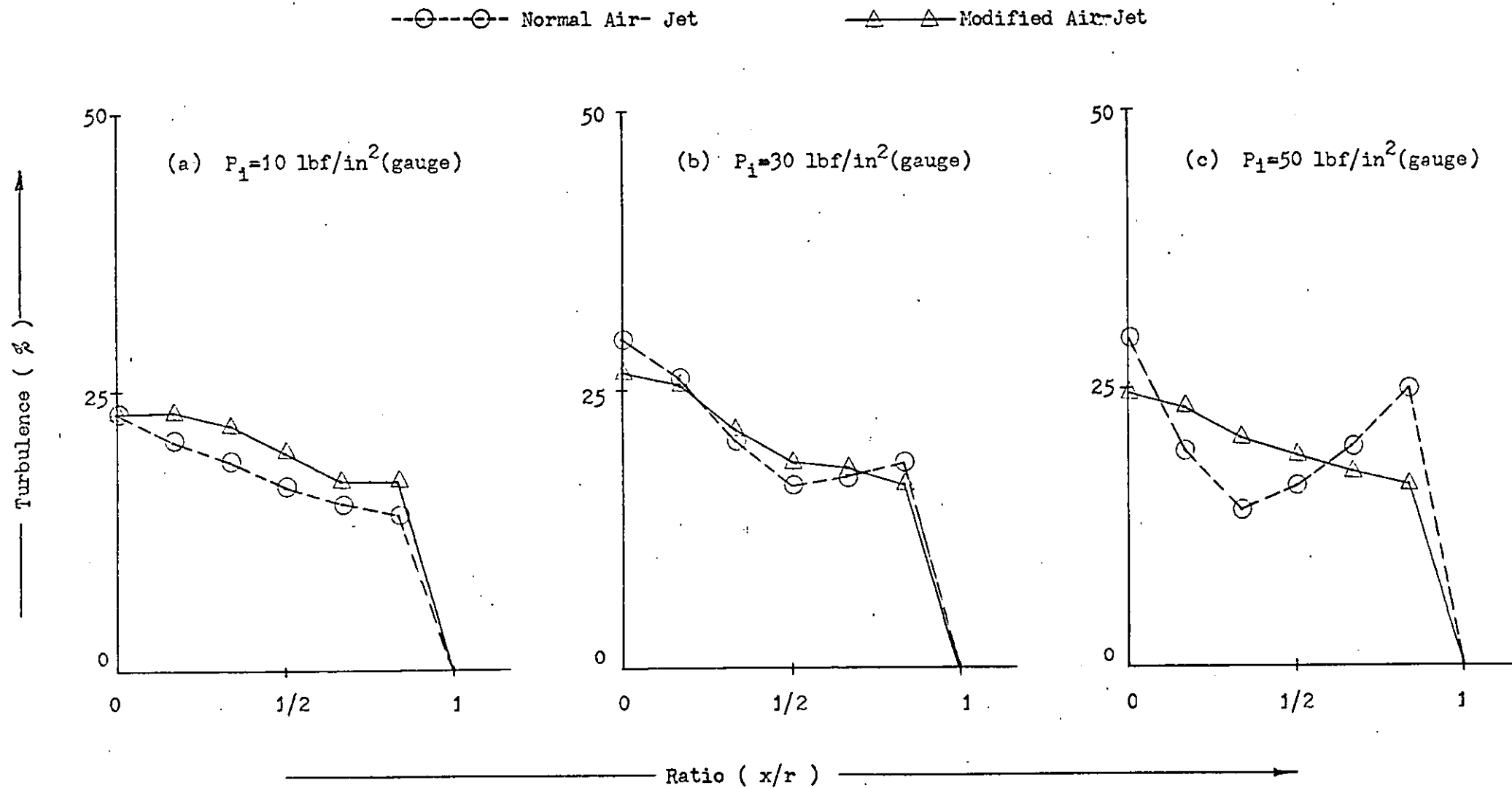


Fig. 3.31.3 Percentage Turbulence Distribution Along OD When $\alpha = 40^\circ$

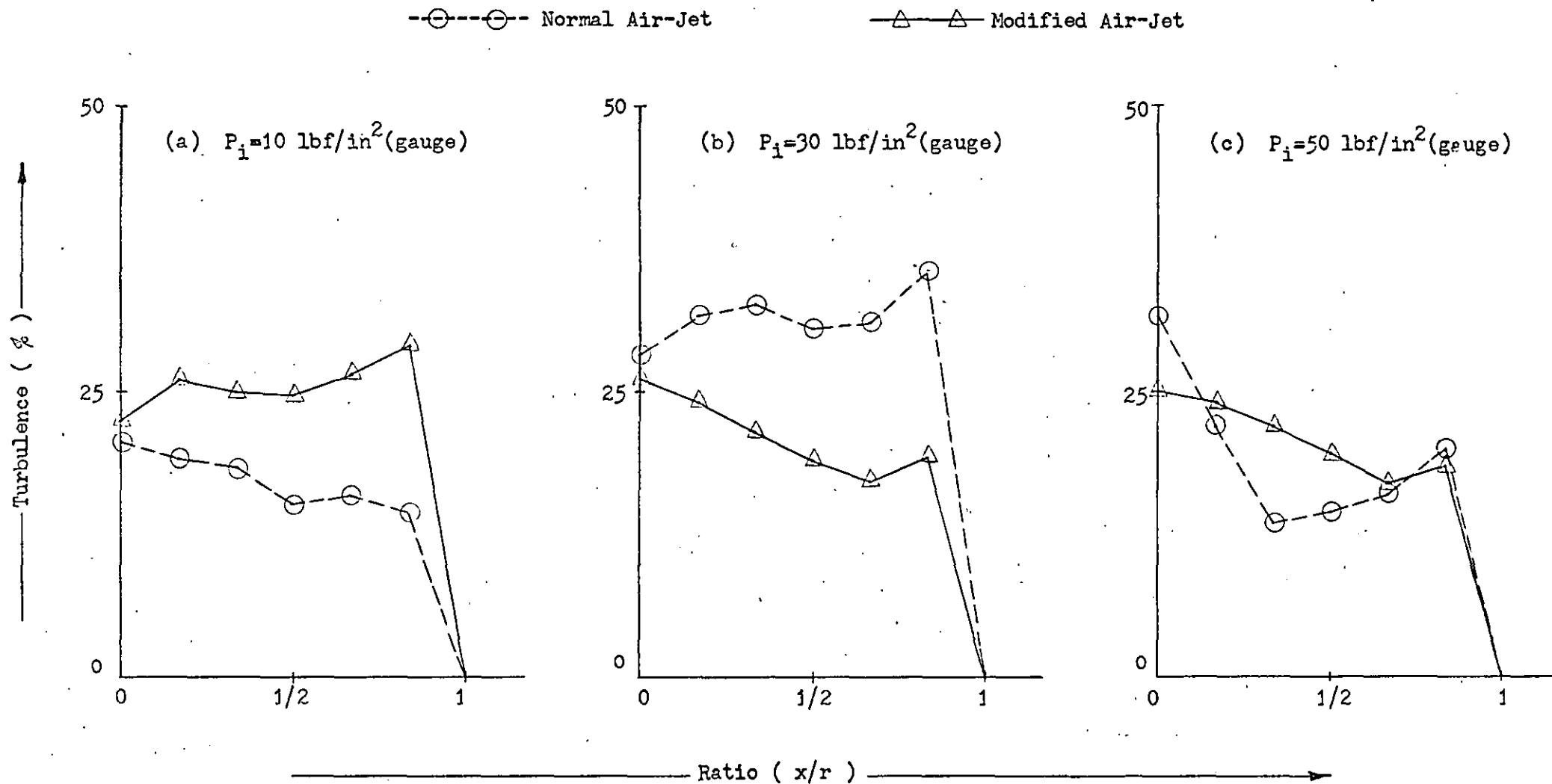


Fig. 3.31.4 Percentage Turbulence Distribution Along OD When $\alpha = 60^\circ$

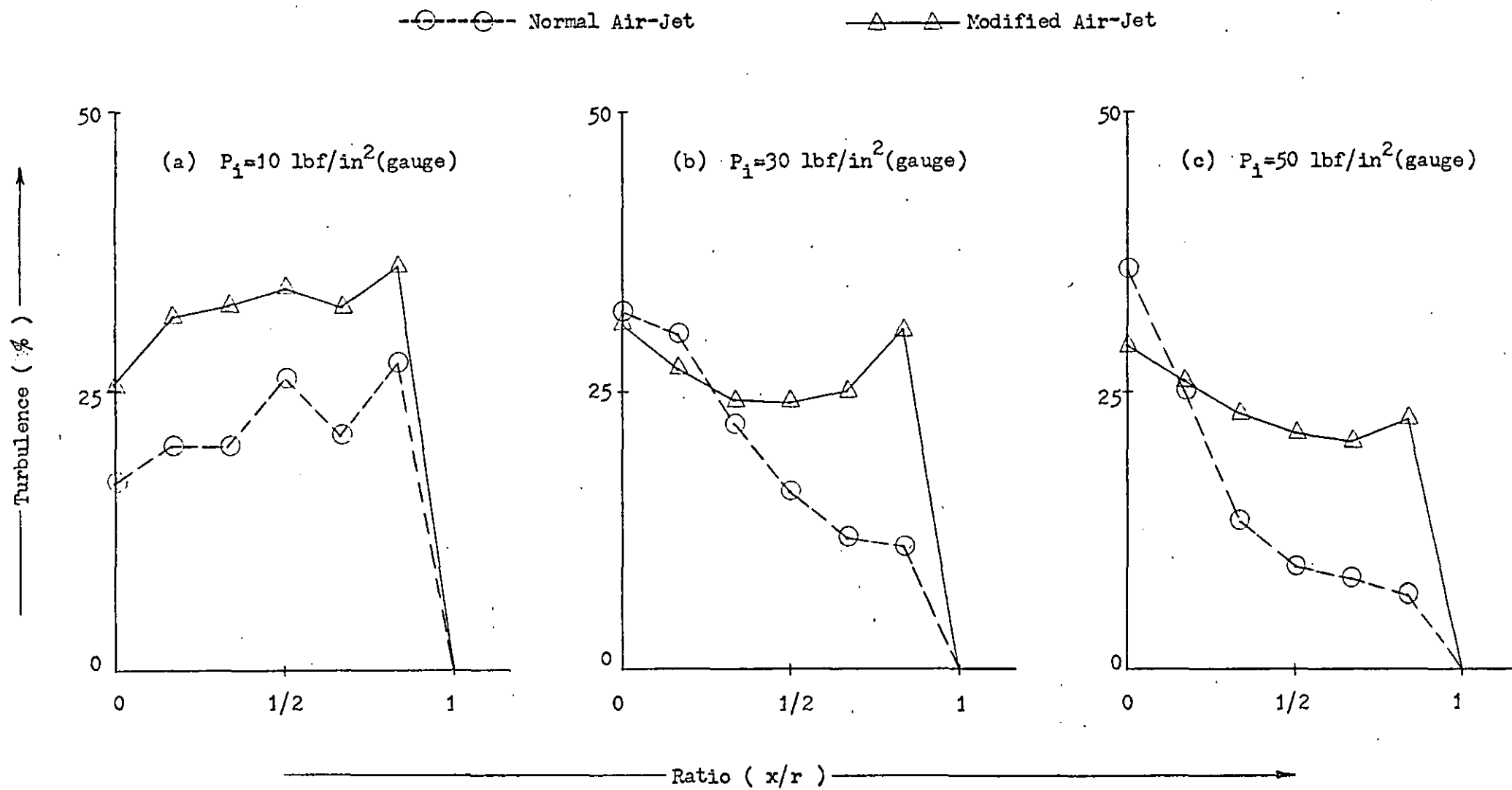


Fig. 3.31.5 Percentage Turbulence Distribution Along OD When $\alpha = 80^\circ$

CHAPTER 4

DISCUSSION OF PART (A) AND CONCLUSIONS

4.1 Summary of the Scaled-up Model Taslan Process

In the preceeding chapters the model study based on the scaling-up of the Taslan type 9 air-jet and of a 70 denier, 34 filaments, 15 turn/in (Z) twist parent yarn, has given a better understanding of the process and its mechanism. However the apparent simplicity of the model study must not lead one to the conclusion that experimental results obtained from the model are automatically equally applicable to similar experimental results for the prototype. For any comparison of the experimental results between the model and the prototype air-jet bulking processes to be valid, the sets of conditions associated with the scaling-up technique (see Chapter 2) must be satisfied, and yet a perfect similarity between the two processes is not easy to attain.

4.1.1 Application of Geometric Similarity

To satisfy geometric similarity conditions, the model air-jet and the model parent yarn must be perfect replicas of their prototypes. For instance, not only must the overall shapes of the models be geometrically similar to those of the prototypes, but also the roughness of the surfaces should be geometrically similar. If, for any reason, the scale factor is not the same throughout a distorted model results. Thus a critical discussion of the factors involved in this particular work is justified.

Although great care was taken during the measurement of the prototype air-jet (see Section 2.4), the possibility of human error during the visual measurement by travelling microscope was inevitable. Thus, as it is a fact that such measurement errors, however slight, will be magnified in scaling-up, then the "ideal" absolutely geometrically similar model is unattainable.

The extremely small size of the bore of the prototype air-jet prevents an accurate assessment of the inside surface roughness. However a visual inspection with the microscope suggests that efforts have been made to ensure as smooth a surface as practicable, and thus the model perspex air-jet was polished on the inside to give a good smooth surface finish. The model air-jet feed-needle was made from brass and again a good surface finish was given to simulate the smooth surface of the "hyperdermic" tubing needle used in the prototype.

For the scaled-up model parent yarn, it is reasonable to expect that the overall geometric similarity between it and the prototype parent yarn would be obtained simply by using the same number of filaments and the same twist angle, but this is an over simplification as manufacturing differences are also present. It was not possible to obtain a 30 denier monofilament nylon 6.6 and therefore the model parent yarn had to be constructed from 30 denier monofilament nylon 6. Thus, factors resulting from differences between a prototype multifilament nylon 6.6 yarn made by a commercially extrusion machine and drawn subsequently, and a nylon 6 model yarn separately assembled from previously drawn monofilaments (see Section 2.5.1) must obviously preclude any approach to an "ideal" scaling-up, and yet these factors are entirely beyond the author's control. Thus, the two yarns will inevitably differ from each other in some geometric features, such as the migration and packing of the filaments, due to their different methods of construction. The ratios of physical characteristics such as tensile properties, surface finish, etc. are also likely to be different from the desired scale-up ratio. Therefore, it is almost certain that in the model yarn, the individual monofilaments would not behave absolutely similar to those of the prototype parent yarn under dynamically similar operating conditions.

4.1.2 Application of Dynamic Similarity

The requirements for dynamic similarity between the model and prototype air-jets are discussed in Chapter 2. Ideally, it is desirable that both the model and the prototype air-jet bulking processes should be completely dynamically similar. Only then, can the possibilities leading to errors be eliminated. However for the reasons given in Section 3.3, and based on the analytic study of the compressed air flow through the air-jet at its normal operating conditions (see Section 3.1), a basic assumption was made that the elastic forces involved in this type of flow are more dominant than any other forces present. Therefore, the dynamic similarity between the model and the prototype air-jets was based on equating the Mach number in both systems. This means that the ratios of inertia force to elastic force in both systems are equal.

No doubt the above mentioned basic assumption, together with the geometric scaling considerations of Section 4.1.1, would give rise to questions regarding the validity of this model study and of the comparison of the experimental model results to those of the prototype air-jet. Nevertheless, operating the model air-jet under the conditions set by the equality of Mach number, and using the model parent yarn, produces bulked model yarn virtually undistinguishable in physical appearance to that of Taslan yarn produced under the normal prototype air-jet operating conditions. Therefore, it is reasonable to assume that a very near approximation to both geometric and dynamic similarities has been achieved between the model and the prototype air-jet bulking processes, and consequently that the results of the experimental investigations carried out on the model are equally applicable* to those of the prototype air-jet.

* That fibre stiffness increases as the cube of the scale factor whilst the forces applied to the fibre increase only as the square of the factor (see equation 2-1 on page 8) this requirement is not completely met. In practical terms however this is not important as air jet bulking equipment in commercial use normally deals with a fibre stiffness range of the order of 12 to 1.

4.2 Summary of the Experimental Investigations

The flow of compressed air through the normal and modified (partially blocked) model jets have been investigated analytically and experimentally in detail and the effect of the process variables on to the air flow have been studied in Chapter 3. The results of these investigations, which will be discussed separately later in this Section have provided new evidence on the mechanism of the process and the construction of bulked yarns of this type. The main outcome is that the du Pont type 9 Taslan air-jet, on which this model study has been based, is not ideally designed from the standpoints of efficiency, stability and ease of operation.

It is now verified experimentally that the main object of the air-jet is to false-untwist the pre twisted parent yarn so that the portion of yarn structure inside the jet is open, and the bulking action can easily take place at the jet exit. Previously, Wray⁽¹¹⁾ had suggested that this false-untwisting action of the air-jet was probably due to the shedding of vortices behind the cylindrical feed-needle. The modification⁽¹⁴⁾ of the Taslan jet was based on this supposition and it was designed to remove the suggested harmful secondary vortex stream by blocking off one side of the feed-needle. However, it is now shown in Section 3.8 that the Reynolds number based on air-jet throat diameter at the normal operating conditions is well above the range (i.e. $R \gg 100,000$) at which the periodic shedding of vortices in the wake of a cylindrical body could exist. Moreover, it is now clear from the photographic evidence obtained (see Section 3.5) that the actual bulking action occurs at the exit of the air-jet and the false-untwisting of the yarn is happening at the region immediately where the yarn leaves the air-jet exit. Therefore, the present author is of the opinion that the previously suggested false-untwisting vortex

mechanism of the normal and modified air-jets is invalid, although the overall principle of bulking by a temporary removal and reassertion of the twist is still applicable. An alternative explanation for the newly observed phenomenon will be given in Section 4.3.

4.2.1 Visualization of the Air-Jet Bulking Process

Examination of the high speed cine films of the model air-jet bulking process (see Section 3.5) clearly shows that the bulking action takes place at the exit of the air-jet. The portion of yarn inside the jet, (i.e. the part between the feed-needle and the exit) continuously rotates although apparently not at constant speed. This false-untwisting type yarn rotation removes the already present twist in the parent yarn and therefore the whole yarn structure inside the jet is completely open. The overfed and open yarn bundle is thrown upwards intermittently from the jet, the bulking action taking place at the jet exit, and finally the resultant bulked yarn is drawn away at a right angle to the jet axis.

As the whole portion of the yarn inside the jet is completely open during the bulking process, the false-untwisting effect must take place in the region immediately where the yarn leaves the air-jet exit. This region corresponds to the twist peg in the conventional false-twist tube.

The portion of yarn between the air-jet exit and the take-up guide roller also rotates and forms several balloons depending on the distance adjustment between the jet exit and the guide roller. This portion of yarn is in twisted form and its structure is compact although in the bulked state.

An attempt has been made to measure the actual yarn rotation inside the jet, but for the reason given in Section 3.6 it was not successful. As the time available for this particular experiment was limited, this method of yarn rotation measurement was not developed further.

4.2.2 Visualization of the Flow in the Air-Jet

The visual examination of the schlieren photographs shown in Section 3.7 suggests that the air-jet without its feed-needle behaves as a convergent-divergent nozzle and the flow through it follows the same pattern as discussed in Section 3.1. For the values of inlet pressure below the critical pressure ratio - i.e. when $P_i < 27.8 \text{ lbf/in}^2$ (absolute) the flow in the air-jet throughout is subsonic (see Figs. 3.10, a, b and c). However, when the inlet pressure is increased above the critical pressure ratio, a normal shock exists inside the jet; that part of the flow between the throat and the normal shock is supersonic, and from the normal shock a subsonic flow follows. For the reasons given in Section 3.7, it was not possible to observe this phenomena inside the jet. However in Figs. 3.10 (d) to 3.10 (m), the compression waves are clearly observed at the exit of the jet, and a study of the photographs reveals that these waves tend to move inside the air-jet as the inlet pressure decreases.

At the normal air-jet operational conditions, (i.e. with the feed-needle present and set in a particular position, and the inlet pressure $P_i = 50 \text{ lbf/in}^2$, gauge), the normal shock is inside the jet, and at the exit of the jet the flow is subsonic. If the inlet pressure is increased to $P_i = 60 \text{ lbf/in}^2$ (gauge), then for low values of α (i.e. $\alpha < 60^\circ$) this condition persists (see Fig. 3.11, a, b and c). However, for the values of $\alpha \geq 60^\circ$ the flow at the exit of the jet (see Fig. 3.11, d, e and f) has compression waves which are clearly observable - i.e. the flow is then very similar to that shown in Fig. 3.10, e, f and g, where the feed-needle is not present at all.

With the modified air-jet it is found that, even at high values of inlet pressure (i.e. $P_i = 60 \text{ lbf/in}^2$, gauge) and at any value of feed-needle setting, the normal shock never reaches the exit of the air-jet and the flow at the exit remains subsonic throughout.

4.2.3 Measurement of Flow Rate and Calculation of Reynolds Number

The rates of air flow through the normal and modified model air-jets are determined by using an orifice plate, and the Reynolds numbers based on the air-jet throat diameter are calculated in Section 3.8 for varying air-jet operating conditions.

Figs. 3.14 and 3.15 show the flow rate for the normal and modified air-jets with varying values of α for given values of P_i and a fixed value of L . It is clear from these graphs that the values of $\alpha > 40^\circ$ are critical, and that any small variation in values of α at this range alters the rate of flow considerably in both the normal and modified air-jets, although this variation in flow rates is more significant in the normal air-jet case.

Figs. 3.16 and 3.17 show the flow rate for the normal and modified model air-jets with varying values of L for given values of P_i and for fixed values of $\alpha = 40^\circ$ and $\alpha = 80^\circ$ respectively. Variations in values of L correspond to linear positioning of the half cylindrical portion of the feed-needle in the air-jet throat (see Fig. 3.7). In Figs. 3.16.1 and 3.17.1 when $\alpha = 40^\circ$ a critical value is reached at $L = 0.950 \text{ in.}$ (this critical value of L corresponds to a point at which the value of the flow rate starts to alter). However, Figs. 3.16.2 and 3.17.2 show that when $\alpha = 80^\circ$ the critical value of L is reached at $L = 0.862 \text{ in.}$ Thus, the importance of the longitudinal feed-needle setting is more noticeable with high values of feed-needle angular setting.

Obviously, the two effects must interact, since their independent adjustments influence the air flow in similar fashions by constricting the jet throat.

The calculated Reynolds numbers (based on air-jet throat diameter) for the normal model air-jet are tabulated in (i) Tables 3.2 with varying values of P_i and α when the longitudinal feed-needle setting is fixed at a value of $L = 1.050$ in, and (ii) in Tables 3.4.1 and 3.4.2 with varying values of P_i and L when the angular feed-needle settings are at fixed values of $\alpha = 40^\circ$ and $\alpha = 80^\circ$ respectively.

For the values of inlet pressure $10 \leq P_i \leq 60$ lbf/in² (gauge) and with the feed-needle in any position, the calculated Reynolds numbers are between $100,000 < R < 400,000$. This range of Reynolds numbers is in the critical Reynolds number region at which the drag coefficient for cylinders decreases considerably (see Fig. 3.6), and at which all traces of periodic pattern of the vortices in the wake of a cylinder are diminished (see Fig. 3.5). It is therefore clear that Wray's suggested false-untwisting mechanism⁽¹¹⁾ and the principle of the Wray and Entwistle modification⁽¹⁴⁾ to the air-jet are not entirely justified according to this new evidence. An alternative explanation is suggested in Section 4.3.

4.2.4 Measurement of Mean Flow Velocities

A constant temperature hot-film anemometer was used to measure the mean flow velocities along the radii OA, OB, OC and OD (as defined in Fig. 3.7) at the exits of the normal and modified air-jets with varying inlet pressure P_i and varying feed-needle angular setting α (see Section 3.9). The actual values of the mean flow velocities were obtained from the calibration curves for the type of hot-film probe used during the experiments (see Section 3.9.2 and 3.9.3). The results are tabulated in Tables 3.7 and 3.10, and selected values from these tables are also shown graphically in Figs. 3.24 to 3.27.

Figs. 3.24.1 to 3.24.5 show the velocity profiles along OA for the normal and modified air-jets. The normal air-jet velocity profiles have similar overall shapes at low values of P_i (i.e. $P_i = 10 \text{ lbf/in}^2$, gauge) for all values of α . At higher values of P_i the profiles are different from those obtained at low values of P_i , and at a fixed high value of P_i (i.e. $P_i = 30$ or 50 lbf/in^2 , gauge) the variation in values of α becomes critical and the shape of the velocity profiles changes considerably. For the modified air-jet, at low values of P_i there is a noticeable change in the shape of the velocity profiles at the values of $\alpha \geq 60^\circ$, the mean velocity decreasing towards the air-jet wall whereas previously it was increasing. At higher values of P_i the shape of the profiles are also different from those obtained at low values of P_i , and again at a fixed high value of P_i a change occurs at $\alpha \geq 60^\circ$ and the mean velocity decreases towards the air-jet wall.

Figs. 3.25.1 to 3.25.5 show the velocity profiles along OB. For the normal air-jet at low values of P_i and with varying values of α the shape of the profiles follow a similar pattern to that along OA, but the actual values of mean velocities are different. At $P_i = 30 \text{ lbf/in}^2$ (gauge) the value of α is critical, but at $P_i = 50 \text{ lbf/in}^2$ (gauge) the importance of the angular feed-needle setting is less critical and the velocity profiles follow a general pattern. For the modified air-jet, at low values of P_i no important change occurs until $\alpha \geq 80^\circ$. However, at $P_i = 30 \text{ lbf/in}^2$ (gauge), variations in α are again critical and yet at $P_i = 50 \text{ lbf/in}^2$ (gauge) the importance of the angular setting shows itself only when $\alpha \geq 60^\circ$.

Figs. 3.26.1 to 3.26.5 show the velocity profiles along OC. In this case, for the normal air-jet at low values of P_i , the shapes of the velocity profiles are different from those previously discussed and there is a small change in the general pattern at $\alpha \geq 80^\circ$.

At high values of P_i (i.e. $P_i = 30$ or 50 lbf/in², gauge) the feed-needle angular setting is important and the velocity profiles greatly depend on this setting. For the modified air-jet, at any value of P_i and at values of $\alpha \leq 40^\circ$ the velocity profiles follow the same overall pattern to those previously discussed above for the radii OA and OB. However, at values of $\alpha > 40^\circ$ there is a noticeable change and the mean flow velocity increases near the air-jet wall with the exception of the profile for $P_i = 10$ lbf/in² (gauge) (see Fig. 3.26.5).

Finally, Figs. 3.27.1 to 3.27.5 show the mean flow velocity profiles along OD. For the normal air-jet at low values of P_i the overall pattern of the profiles is different from all those previously discussed, but there is a slight similarity of shape among these profiles themselves for varying values of α . Also some similarity can be observed at high values of P_i , (i.e. $P_i = 30$ or 50 lbf/in², gauge), with the exceptions of the profiles shown in Fig. 3.27.1 ($P_i = 30$ lbf/in², gauge) and in Fig. 3.27.5 ($P_i = 50$ lbf/in², gauge). For the modified air-jet at values of $P_i = 10$ or 30 lbf/in² (gauge) and $\alpha \leq 60^\circ$ the profiles are similar in pattern but above these values of α the mean flow velocity starts to decrease towards the air-jet wall. At $P_i = 50$ lbf/in² (gauge) there is little similarity in profile patterns for any values of α .

The detailed examination of these velocity profiles has shown that the Taslan type 9 jet system is extremely sensitive to both the feed-needle settings and the operating pressures. This is undoubtedly due to the fact that the tilting of the stepped feed-needle, which is partially semi-cylindrical and partially cylindrical in shape at its position within the jet throat, produces extremely complex flow conditions which are themselves greatly influenced by any slight

experimental errors in feed-needle settings and in the positioning of the hot-film probe; these sources of errors are unavoidable due to the very small dimensions involved, and hence it is difficult to give detailed explanations for all the variations observed between the various profiles. In general, however, the experimental results reveal that for the normal air-jet a complete mixing of the turbulent flow in the wake of the feed-needle is not completed at the jet exit. The experimental results also make it apparent that the feed-needle settings are less critical for the modified air-jet. A possible reason for this fact will be given in Section 4.3.

4.2.5 Measurement of Turbulence

Turbulences (i.e. variations in the mean flow velocities) were measured by using the same constant temperature hot-film anemometry as used for the mean flow velocity measurements. The actual calculations of the percentage turbulences were made from the experimental results (see Section 3.9.6) and they have been tabulated in Tables 3.7 to 3.10 together with the mean flow velocity results. Some selected values from these tables are also shown graphically in Figs. 3.28 to 3.31.

Figs. 3.28.1 to 3.28.5 show the percentage turbulence distributions along OA. For the normal air-jet, the distribution shapes at the values of $P_i = 10$ or 30 lbf/in^2 (gauge), indicate that they are sensitive to variations in the feed-needle angular setting, but at $P_i = 50 \text{ lbf/in}^2$ (gauge) a slight similarity in distribution shapes can be observed for all feed-needle settings. For the modified air-jet at all P_i values with $\alpha \leq 60^\circ$ there is a distinct similarity in shapes. However, at $\alpha = 80^\circ$ the percentage turbulence distribution shapes differ from those previously obtained.

Figs. 3.29.1 to 3.29.5 show the plots of the percentage turbulences along OB. For the normal air-jet, at any values of P_i there is some similarity between the turbulence distribution shapes, but they depend on the angular feed-needle setting. For the modified air-jet, the graphical representations of the distributions follow a very near similarity in shapes at any values of P_i and with an exception at $\alpha = 60^\circ$ where the feed-needle angle appears to be critical (see Fig. 3.29.4).

Figs. 3.30.1 to 3.30.5 show the percentage turbulence distributions along OC. For the normal air-jet at $P_i = 10$ or 30 lbf/in^2 (gauge) the shape of the distributions are greatly dependent on the angular setting, but at $P_i = 50 \text{ lbf/in}^2$ (gauge) they follow a very close pattern for all values of α . For the modified air-jet for all values of P_i and for values of $\alpha \leq 20^\circ$ a distinct similarity exists, but for values of $\alpha > 20^\circ$ no such similarity in the distribution shapes can be discerned.

Finally, Figs. 3.31.1 to 3.31.5 show the percentage turbulence distributions along OD. In this case, for both normal and modified air-jets the inlet pressure and angular setting become important and at each combination of settings a different type of percentage turbulence distributions is obtained.

The above analysis of the experimental results is admittedly inadequate for the reasons given in the ultimate paragraph of Section 4.2.4. Nevertheless, it shows that the variations in mean flow velocities are large for any variations in the operational settings of both the normal and the modified air-jets. However, by comparison with the modified jet results, the effects of these settings are more noticeable in the normal air-jet operation. The reason for this fact can also be explained in the same way as for the mean flow velocity measurements (see Section 4.3).

4.3 The Flow Natures and Bulking Mechanisms of the Normal and Modified Air-Jets

In Section 4.2 experimental investigations undertaken with the models of the normal and modified air-jets were discussed. In the light of these experimental results, together with the simplified analysis made in Section 3.1, it is now possible to describe the nature of the air flow through the normal and modified air-jets, this leading to a clearer understanding of their bulking mechanisms.

Initially considering the case of the normal jet when the feed-needle angular setting $\alpha = 0^\circ$ then, for the values of $P_i \geq 27.8 \text{ lbf/in}^2$ (absolute), the critical pressure ratio is reached at the position where the smallest cross-sectional area exists i.e. the two areas between the wall of the air-jet and both sides of the feed-needle (see Fig. 1.1). The static pressure decreases and the velocity increases along the air-jet axis in the convergent part upstream of the needle and at the throat the air flow is divided into two channels as it passes through the two separate narrow passages on each side of the feed-needle. Due to the semi-cylindrical shape of the feed-needle at the throat, the cross-sectional areas in these passages between the air-jet wall and the feed-needle are also convergent. Therefore a further reduction in pressure occurs and the flow reaches the speed of sound ($M = 1$) in the minimum cross-sectional areas at each side of the feed-needle. From these positions onwards there is a sudden increase in cross-sectional area, and the flow separates from the feed-needle and in its wake the two flow channels join together. The resultant effects are a further decrease in pressure and an increase in velocity. When the decrease in static pressure reaches its limiting value set by the ratio $\frac{\text{inlet pressure}}{\text{atmospheric pressure}}$, a normal shock and a sudden increase in pressure occurs. After the normal shock a subsonic turbulent flow exists in the wake of the feed-needle (i.e. in the divergent part of the air-jet).

Now consider the feed-needle being tilted with increasing values of α about its own longitudinal axis. The minimum cross-sectional area, - i.e. on the side of the feed-needle which is opposite to the side to which it is tilted, stays the same as before but the flow separation point moves upwards on the back of the feed-needle - i.e. slightly towards the exit of the jet. However, in the other channel, - i.e. on the side to which the feed-needle is tilted, the minimum cross-sectional area increases with the increasing values of α , and its position together with the point of flow separation moves upstream - i.e. slightly away from the jet exit. As the values of α increase the immediate wake behind the feed-needle narrows, the flow rate increases, and the position of normal shock moves towards the air-jet exit.

In the case of the modified air-jet, - i.e. with one side of the feed-needle blocked and operated at low values of inlet pressure, the compressed air can only pass on one side of the feed-needle. The experimental results show that the effect of the feed-needle settings is less critical, thus confirming the previous findings⁽¹⁴⁾, and the flow rate is reduced considerably. But at such low values of inlet pressures (i.e. $P_i = 10 \text{ lbf/in}^2$, gauge) the flow never reaches the sonic condition and the values of the mean flow velocities are very much smaller than those previously obtained with the normal air-jet operated at high inlet pressures (i.e. $P_i = 50 \text{ lbf/in}^2$, gauge). Therefore the flow nature in the modified air-jet is completely different from that of normal air-jet.

On the other hand, with the normal air-jet two different types of air flow exist at each of the two channels on either side of the feed-needle, and when these are combined in the wake of the feed-needle the complete turbulent mixing is not finalized on leaving

the jet exit. However, with the modified air-jet, the flow is restricted to one type only through a single channel and thus the possibility of complete turbulent mixing before the jet exit is increased. Such a flow type would obviously not be as adversely affected by variations in feed-needle settings and this is probably an explanation of the previous findings with the modified jet⁽¹⁴⁾.

The actual bulking of the yarn takes place at the exit of the air-jet due to the false-untwisting of the yarn about this position, but the high speed photography (Section 3.5) has shown this effect to be of an irregular nature, rather than continuous as Wray⁽¹¹⁾ implied.

The author believes that the mechanism of this untwisting effect can be explained as follows. The highly turbulent air flow blows the overfed parent yarn out of the jet, and this causes the portion of yarn immediately following it (i.e. that just entering the jet) to be in high tension. As the variation in mean flow velocities is high this occurrence continues intermittently (see reference to the high speed cine films of the bulking process, Section 3.5). Thus there is an intermittent fluctuation of tension in the overfed yarn entering the jet. At the exit of the jet the yarn changes its path abruptly as it is withdrawn from the jet at a right angle to the jet axis. Due to the momentum of the blown out yarn, the end of yarn being withdrawn from the jet exit is subjected to an alternating force at right angle to its axis (i.e. an alternating torque). As a result of this a false-twisting effect is created such that it untwists the portion of the parent yarn inside the jet and thus its structure is opened. Then when the opened overfed yarn is blown out of the jet the extra available filament lengths snarl into a looped and entangled state at the jet exit under the extremely violent (turbulent) nature of the flow.

The maximum bulking speed attainable (i.e. the maximum yarn speed through the jet) depends on the speed of the air flow through the jet. The relative velocity between the flow and the yarn is an important factor in determining the degree of bulkiness the yarn receives during its small time duration in the jet. The maximum commercially acceptable speed of the du Pont type 9 Taslan jet is believed to be 450 ft/min.

The basic bulking mechanism of the modified air-jet⁽¹⁴⁾ is the same as the normal air-jet. The only difference is that by blocking off one side of the feed-needle and operating the jet at low inlet pressures reduces the flow rate, and thus the flow velocity and the intensity of turbulence decrease. Therefore, the author believes that although it is possible to impart an acceptable bulkiness to the yarn at fairly low values of bulking speed (Wray and Entwistle⁽¹⁴⁾ operated their modified air-jet at 150 ft/min. bulking speed), the modified air-jet would not operate satisfactorily at much higher bulking speeds (e.g. 450 ft/min) when using such a low inlet pressure (e.g. $P_1 = 10 \text{ lbf/in}^2$, gauge).

4.4 Production and Costs of a Typical Taslan Mill

Precise details regarding the break down of production costs in commercial processes are always difficult to obtain and this is particularly true in the case of bulked yarn processes which are usually manufactured under licence. However during a recent (1969) private communication with the management of one of the major Taslan producing mills in the country, some very general information was kindly provided. The production details and costs are for a 75 denier/36 filament Terylene yarn with 15 turns/in. parent yarn twist and 10% overfeed, based on a production of 8000 lb/week.

- (i) Parent yarn price = 12s. 1d. per lb.
- (ii) Selling Price of Taslan yarn = 19s. Od. per lb.,
(including royalty).
- (iii) Royalty (6% of basic yarn cost) = 8.7 d. per lb.

Although insufficient information has been provided to give an accurate breakdown of processing costs, the following plant and machinery information is useful as a general guide:

- (iv) Type of air jet used : Du Pont type 9.
- (v) Number of jets : 528
- (vi) Cost of bulking machinery : approx. £50 per jet unit.
- (vii) Production speed : 450 ft/min.
- (viii) Operative work load : 96 jet units per operative.
- (ix) Details of compressors (2) :
 - (a) One 220 H.P. two-stage water cooled centrifugal compressor, 1000 ft³/min capacity (at atmospheric pressure),
 - and (b) One 180 H.P. two-stage water cooled centrifugal compressor, 750 ft³/min capacity (at atmospheric pressure).
- (x) Price of compressors : £4000 for the two compressors.
- (xi) Expected life of compressors : 8 to 10 years giving approximately £500 p.a. depreciation.
- (xii) Operating jet inlet pressure : 50 lbf/in² (gauge).
- (xiii) Approximate cost of air in producing the above mentioned yarn : 5d. per lb.

Although these approximate costs are recorded here since they relate to air-jet bulking, the costs of air and the production rates are more usefully discussed by comparison with the savings which could accrue from the use of the mechanical bulking method which is the subject of Part B of this work (see Section 7.3).

4.5 Suggestions for Further Work

(i) The actual yarn rotation in the air-jet could be measured using the method described in Section 3.6, providing that a suitable large mono-filament was available.

(ii) At certain low values of R , the Strouhal number for cylinders stays constant. A technique based on measuring the frequency of the shedding of vortices from a cylinder in a flow region could then be used to measure the flow velocities. It is suggested that if a fine denier mono-filament yarn is continuously fed into the wake of a cylinder in a flow region, it would follow a path of moving from one vortex stream to another. The frequency of this movement could then be determined using the method described in Section 3.6. The calibration of this technique could be done by comparing the results obtained with the accurately measured frequencies of the shedded vortices using for instance the anemometry method described in Section 3.9. Work has already started in the Department on this topic as a final year undergraduate project.

(iii) In the previous sections, the importance of the feed-needle settings are discussed and it is shown that any small variation in these settings alters the flow characteristics and the performance of the jet. This is obviously a detrement in the commercial production of Taslan. As the size of the jet is small and no provision is made to calibrate or mark the jet, it is difficult to set the needle in order to obtain an optimum bulking condition and thus to maintain a good quality control.

Another disadvantage of the feed-needle is that as it is permanently inclined at an angle of 45° to the air-jet axis (i.e. to the flow direction), and thus the parent yarn changes its direction abruptly in the jet throat as it emerges from the sharp edged step at the open end of the feed-needle. The frictional force

exerted by the running yarn on this edge is sufficiently high to wear away this part after a relatively short time and therefore it is necessary to change the feed-needle frequently. Thus if an improved air-jet could be designed in order to eliminate the present yarn feeding means, i.e. the feed-needle in the type 9 du Pont jet, the new air-jet produced would probably be easier to set and more efficient to operate. Hence future work on air-jet bulking could profitably be made with newly designed air-jets incorporating the findings of this investigation.

Since the completion of this work, a type 10 Taslan air-jet, which is of a more recent du Pont design, has come into the author's possession and Fig. 4.1 shows its essential parts. Although this indicates that many of the faults inherent in the inclined stepped feed-needle used in the type 9 jet are eliminated by feeding the parent yarn along the jet axis, the new feeding mechanism is still adjustable and therefore its accurate setting still requires considerable skill. The author suggests that further modification could be done to the type 10 jet by permanently fixing the position of the feeding mechanism and controlling the flow rate of the compressed air from a position further upstream.

The performance of the jet could also be improved if the design of the flow contour was made according to the equations (3-9) and (3-16) so that the highest possible flow velocities are attained at the exit of the jet where the actual bulking occurs.

(iv) No work has yet been published on investigations into the manufacture of core-and-effect yarns, and similar methods of multi-end bulking (see Section 1.3). This type of bulking is unique in the field of bulked yarns and in the author's opinion it is capable of greater exploitation than it has so far had. The large scale modelling technique could be extended to obtain information which would enable the optimum conditions for multi-end bulking to be ascertained.

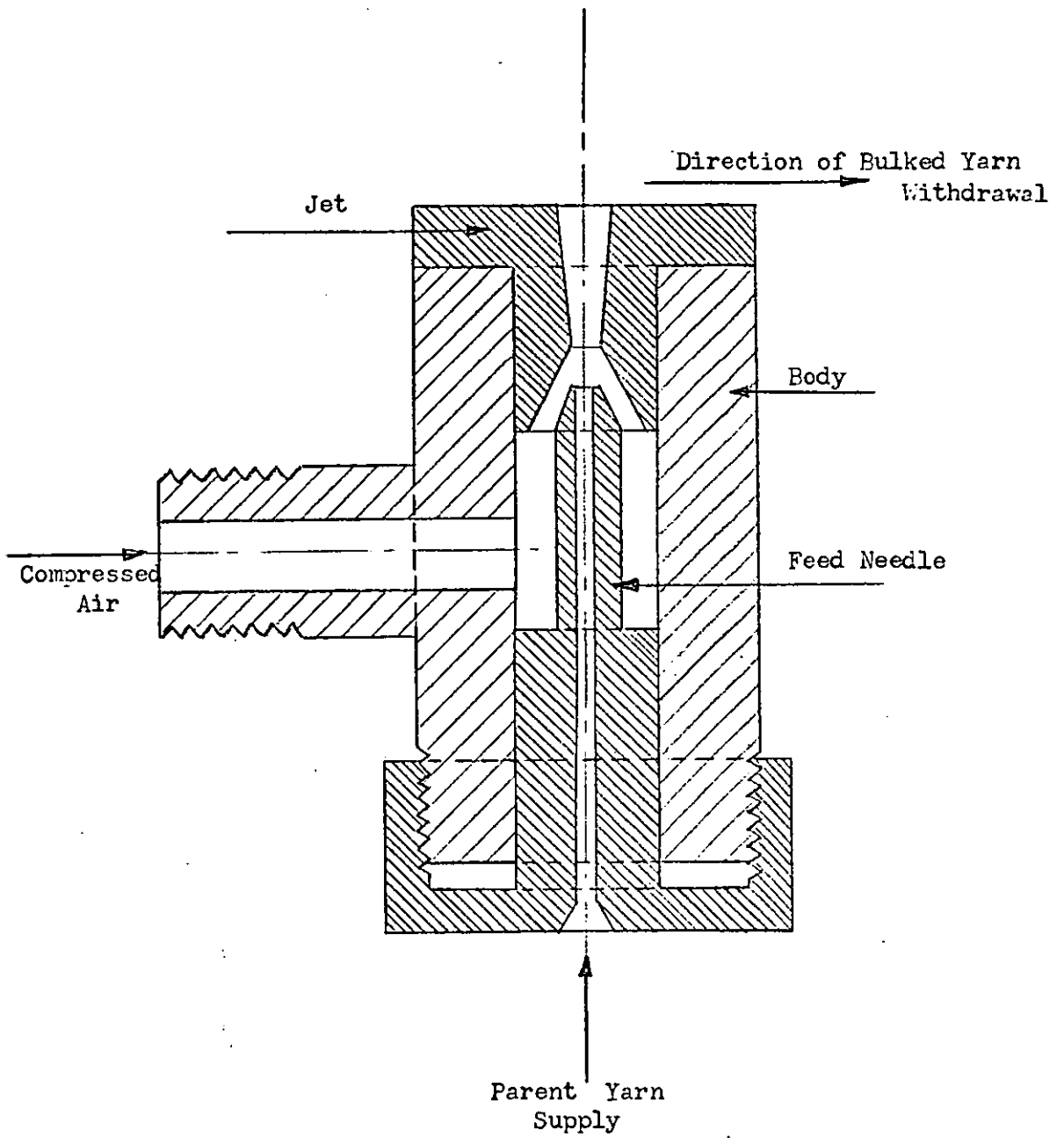


Fig. 4.1 Taslan Type 10 Air-Jet

P A R T B

THE MECHANICAL SIMULATION OF
AIR-JET BULKING

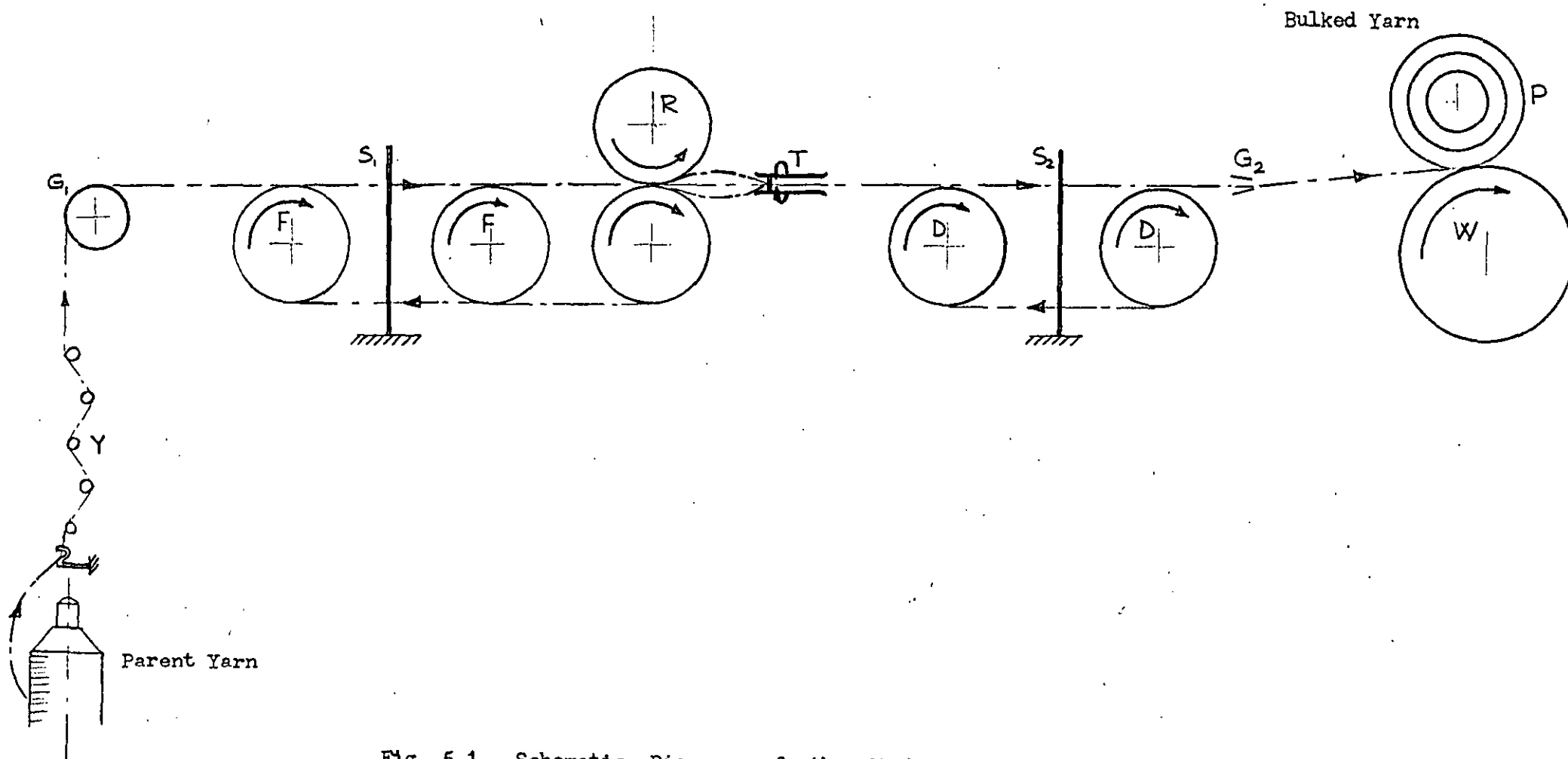
CHAPTER 5

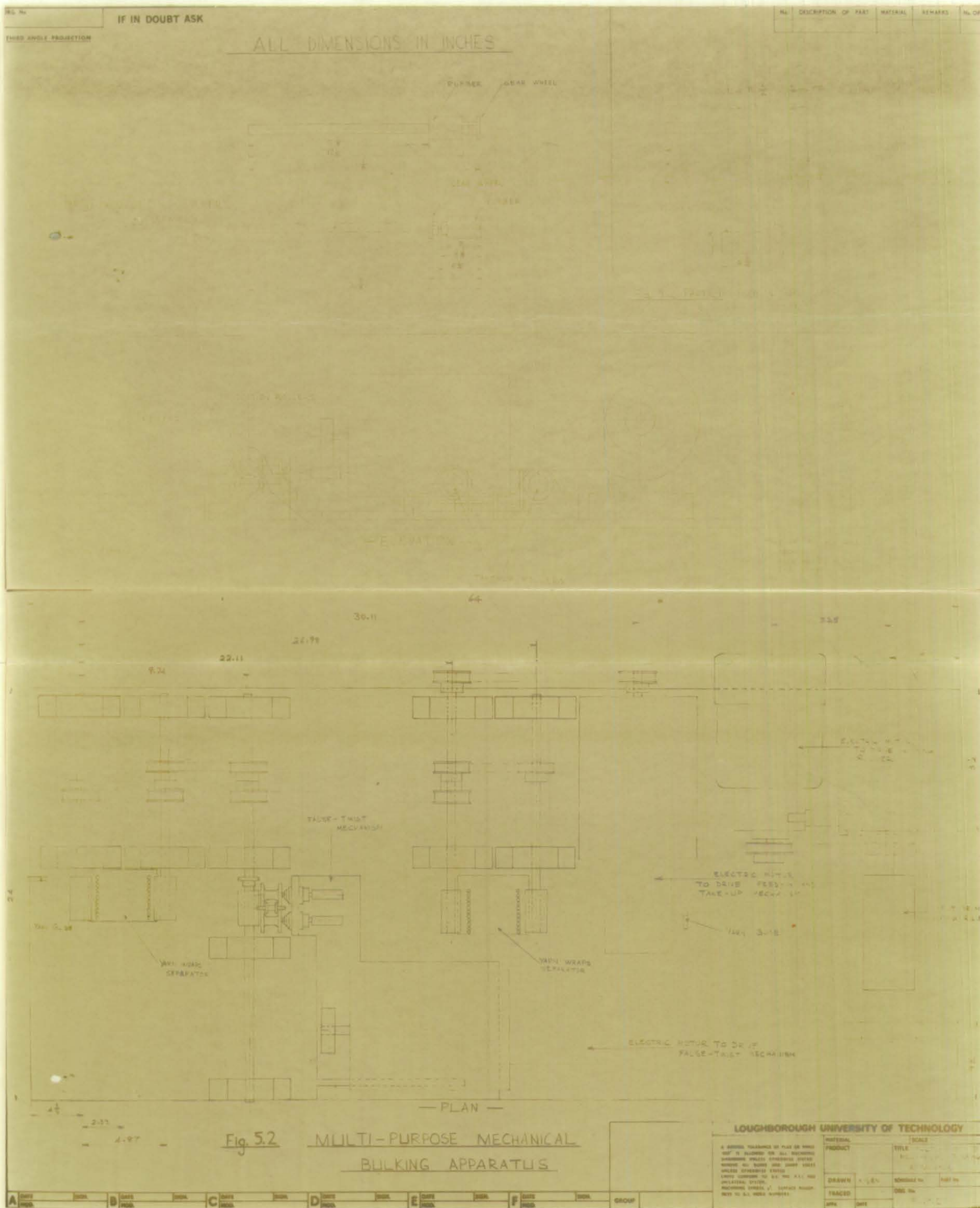
THE MANUFACTURE OF YARNS OF THE AIR-JET
BULKED TYPE WITHOUT THE USE OF AIR

5.1 Preliminary Work

Taking into account the suggested theory of the mechanism of bulking put forward by Wray⁽¹²⁾, an experimental mechanical apparatus simulating the air-jet action has been designed. The initial idea behind this design was to continuously untwist a short length of the parent yarn temporarily to the zero twist state, and then to cause some entanglement of the nearly parallel and twist-free filaments by blowing air across them. In order to have the required extra length of yarn for bulking, the parent yarn was overfed into the region where the yarn possesses no twist.

As Wray's experimental air-jet bulking machine⁽¹¹⁾ was available, the preliminary design was made to suit this existing machine, so that the yarn feeding and yarn winding mechanisms provided could be used with little modification. A separate false-twist unit was built to untwist the parent yarn temporarily, and this was arranged so that the yarn could by-pass the air-jet. A Klinger Mattingley false-twist spindle was readily available, and was adapted for the purpose. This is a friction-drum, free-field magnetic-suspension type false-twist spindle, but as it was specifically designed for use in the false-twist method of bulking it was found to be not ideally suitable for the new purpose. The inside bore of the spindle tube was too narrow to allow the looped and entangled yarn to pass through it and around the twist peg which provides the necessary grip for yarn rotation. Consequently, the bore had to be enlarged, and as a result of this, the weight of the spindle tube was reduced and hence the magnetic couple, which holds the tube in the yarn path, was weakened. Moreover, although great care was taken during the enlarging of the bores, the presence of a small amount of unbalanced weight was found to be unavoidable. These two factors prevented the apparatus from being operated at the designed speeds. Nevertheless the initial experiments





Dwg. No.		IF IN DOUBT ASK		THIRD ANGLE PROJECTION		No.		DESCRIPTION OF PART		MATERIAL		REMARKS		No. OF	
DATE	NO.	DATE	NO.	DATE	NO.	DATE	NO.	DATE	NO.	DATE	NO.	DATE	NO.	DATE	NO.
A	DATE	B	DATE	C	DATE	D	DATE	E	DATE	F	DATE	DATE	DATE	DATE	DATE
NO.	NO.	NO.	NO.	NO.	NO.	NO.	NO.	NO.	NO.	NO.	NO.	NO.	NO.	NO.	NO.
<p>Fig. 2.2</p>															

LOUGHBOROUGH UNIVERSITY OF TECHNOLOGY

PROJECT: _____

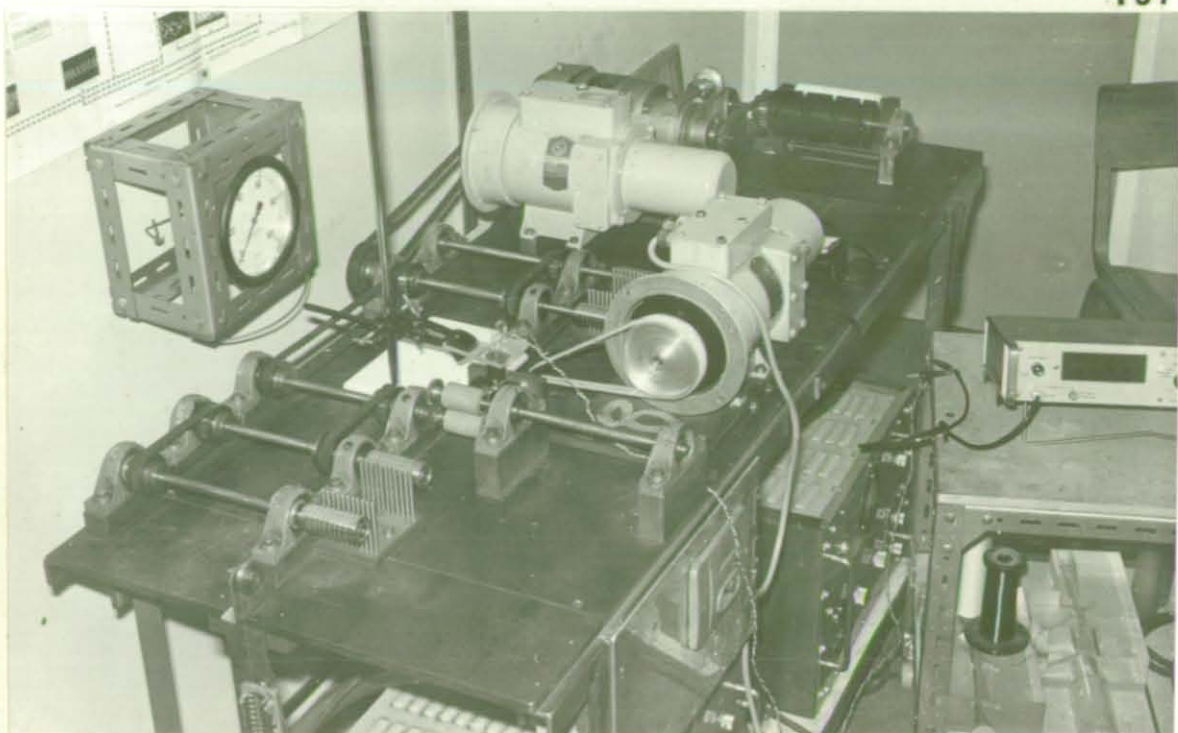
DATE: _____

BY: _____

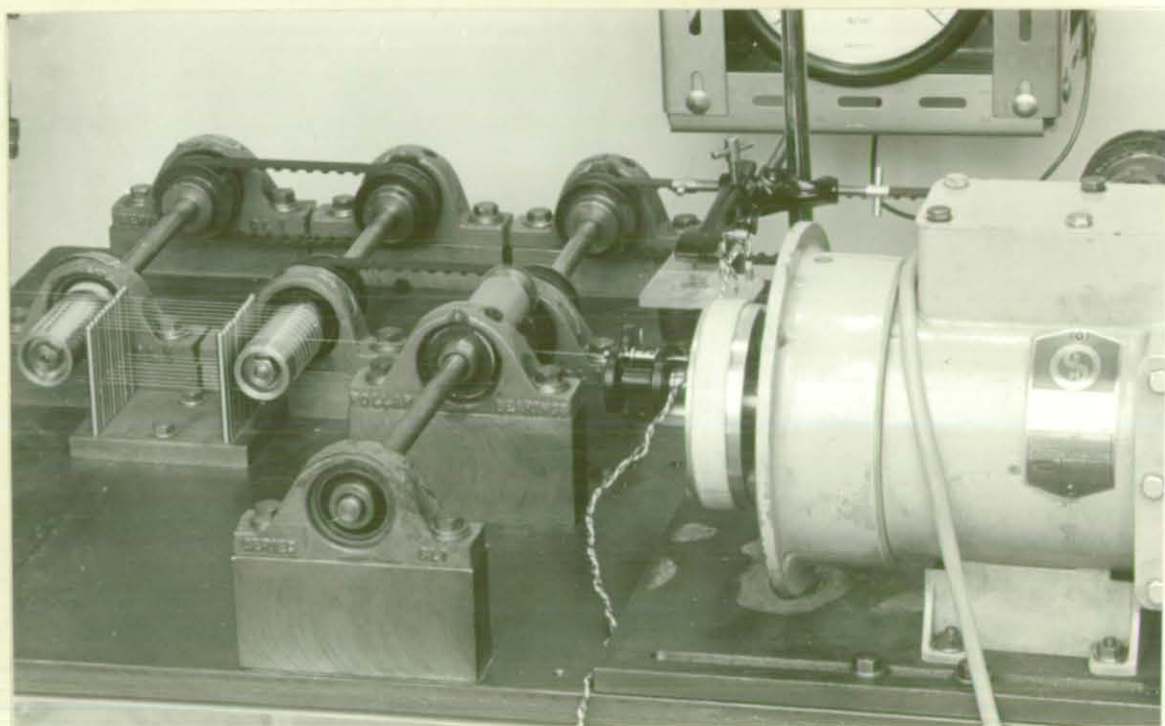
CHECKED BY: _____

DATE: _____

NO. OF: _____



a



b

Fig. 5.3 Mechanical Bulking Apparatus

(a) General View

(b) Bulking Zone

proved that production of air-jet type bulked yarn was possible with this new technique, and for the preliminary comparison of bulked yarns produced by using the new "mechanical bulking" method with those made by the conventional air-jet method, a series of essential tests was undertaken on bulked yarns produced from 100 denier/34 filaments, 15 turns/in, nylon 6.6 parent yarns. The results were sufficiently encouraging to merit further development of the technique, but they are not given in this work since they were merely of a preliminary nature. (See also Section 6.1).

5.2 Multi-Purpose Bulking Apparatus

As was stated in the previous Section, the prototype experimental mechanical bulking apparatus was a conversion of the existing air-jet bulking machine made by Wray for his research⁽¹¹⁾ and was modified without so greatly altering it as to prevent the manufacture of conventional air-jet bulked yarns. Although a simulation of the air-jet method of bulking was successful with this initial experimental apparatus, serious research in this field could only be carried out if an advanced "mechanical bulking" apparatus was available. Thus, a new design was made incorporating three variable speed drives, and having all the essential components assembled in the horizontal for ease of observation. It was also designed to allow for the use of the enlarged model jet with the same drives (see Section 2.6) and was thus a multi-purpose bulking apparatus. A schematic diagram of the apparatus is shown in Fig. 5.1, and details are illustrated in Figs. 5.2 and 5.3.

5.2.1 Yarn Feed-in Mechanism

The purpose of the feed-in mechanism was to project the parent yarn at a regular rate towards the false-twist spindle, and this comprised a pair of hollow rollers *F F* made of stainless steel, and a pair of nip rollers *R R* covered with rubber (see Fig. 5.1),

all four rollers having equal outside diameters. Both nip rollers were driven and the gap between them was adjustable to suit different deniers of yarn. A thread separator S_1 was provided between the feed-in rollers to separate the yarn as it passed several times around them for effective grip and regular feeding.

5.2.2 Yarn Take-up and Winding Mechanism

A pair of hollow stainless steel rollers D D were used to take-up the bulked yarn at a constant rate. The diameter of these rollers was made less than that of the feed-in rollers to give an over-feeding of the yarn. Eight pairs of rollers were made to various diameters, so as to be interchangeable and to give a range of overfeed from 0 to 20%, (see Fig. 5.2, Part 2). Again the yarn was separated by means of a separator S_2 between the rollers. The drives for the feed-in, nip and take-up rollers are all driven by the same Semlec MC.47 electric motor⁽³⁵⁾ capable of controlling the bulking speed from 0 to 1000 ft/min by means of a servo mechanism system.

A split drum type winding roller was used to wind the bulked yarn on to a package. A separate control system was necessary in order that the winding mechanism should give sufficient tension for the bulked yarn to achieve the desirable stability (see Section 6.8). A Kopp variable speed electric motor was therefore used to drive the split drum, and timing belts were employed throughout the apparatus to eliminate any independent variation in the speeds of the different parts. An accurate hand tachometer made by Hasler of Bern was used to measure the surface speeds of all rollers.

5.2.3 False-Twist Mechanism

Instead of the Klinger Mattingley spindle being used for inserting the false-twist (see Section 5.1), a FAG ML 1 magnetic spindle, made in Germany was used. The false-twist tube is again held in

position by a permanent magnet, but it is larger in diameter than the Mattingley spindle tube, thus making it better suited for enlarging the bore without too much loss of weight and the consequent weakening of the magnetic couple. The tube is driven by friction from a pair of rollers with a 10/1 drive ratio, the rollers themselves being driven on this machine by means of a cotton belt from a pulley with a 8/1 drive ratio. This pulley is mounted on the drive shaft of a further Semlec MC47 electric motor⁽³⁵⁾ and the speed is again controlled by means of a servomechanism. For accurate measurements of the spindle tube speed a simple method was to be devised, involving placing a pick-up coil just above the tube-end at the twist peg position. During the rotation of the tube, the magnetic field was changed due to the presence of the two gaps in the tube-end adjacent to the twist peg, and thus the pulses generated were fed into a counter. In order to nullify the reverse pulses a diode was placed between the terminals of the counter, and consequently for each rotation of the spindle-tube two pulses were recorded.

5.3 The Operation of the Apparatus

With reference to Fig. 5.1 the pre-twisted yarn passes through a tensioner Y and over a guide roller G_1 before passing several times around a pair of feed-in rollers F F so as to provide for an even tensioning and regular feeding of the yarn. The yarn is separated by means of a separator S_1 between the two feed-in rollers. From here the yarn is projected into the bulking zone through the nip rollers R R which have the same diameter as the feed-in rollers. After leaving the bulking zone, the yarn passes through the false-twist tube T which revolves in a direction such as would temporarily remove the yarn twist. Then it passes over a pair of take-up rollers D D the diameters of these being less than that of the feed-in rollers, to give an over-feeding of the yarn into the bulking zone. Again the yarn passes

several times around the take-up rollers to provide for a regular take-up speed and the yarn is separated by means of a separator S_2 between the rollers. Finally the bulked yarn is led through a guide G_2 to the winding drive roller W to be wound onto a yarn package P .

5.4 Variables likely to affect the Process

The major yarn and process variables likely to affect the resultant properties of the bulked yarns made by this new method are discussed below, and they are experimentally investigated in Chapter 6.

5.4.1 Initial Twist in the Parent Yarn

Parent yarn twist is a very important factor likely to affect the loop size, loop frequency and stability of the mechanically bulked yarns as it is with air-bulked yarns⁽¹⁵⁾. The helical configuration of the twisted parent yarn filaments is the prime cause of loop formation, and due to the migration of filaments in a twisted continuous filament yarn the frequency of individual filaments appearing on the surface of the twisted yarn and forming loops will also increase with the increase in twist. As the yarn twist should lock the already formed loops in position after the yarn leaving the false-twist spindle, higher amounts of parent yarn twist would more adequately secure the bulky structure in position, and this would give a greater stability to the bulked yarn.

Considering an idealised twisted continuous filament yarn and assuming that the yarn twist is temporarily removed, then the length of a filament available to form loops would be

$$= \sqrt{\left(\frac{1}{T}\right)^2 + \pi D^2} \quad \text{----- (5-1)}$$

where T is parent yarn twist (turns/in) and

D is parent yarn diameter (in).

It can be seen from the equation (5.1) that the loop size depends on the parent yarn twist and the parent yarn diameter (i.e. parent yarn denier), and it follows that with an increase in parent yarn twist the loop size decreases and the loop frequency increases.

5.4.2 Total Yarn Denier and Denier per Filament

For a different denier of parent yarn, the gap between the nip rollers R R should be adjusted to suit the new yarn diameter to avoid distorting its structure. The inside bore of the false-twist tube should also be larger for higher denier yarns to allow the looped and entangled high denier bulked yarn to pass through the tube and around the twist peg. Considering equation (5-1), since the parent yarn outside diameter is a function of yarn denier, then it is clear that with increasing yarn denier the loop size increases.

Individual filaments snarl into a looped state because of the torsional energy stored in them. If one assumes that a filament in its helical configuration closely resembles a helical spring, then, considering simple spring theory⁽³⁶⁾, the torsional strain energy of a helical filament will be a function of yarn denier, denier per filament, twist helix angle, modulus of rigidity, and the applied yarn tension. Thus any variations in yarn denier or filament denier would be expected to affect the resultant characteristics of the bulked yarn.

5.4.3 Total Number of Filaments in the Yarn

Once again, if the construction of a filament yarn is idealised, then it can be said that the number of outside filaments in the yarn construction increases with an increase in the total number of filaments, and thus the probability of a loop forming at any particular yarn section would be increased.

5.4.4 Percentage Overfeeding

The percentage overfeeding is the most important single factor likely to affect the resultant bulked yarn characteristics, since it provides the extra filament length for forming the loops.

$$\text{By definition, the overfeed \%} = a = \frac{V_1 - V_2}{V_2} \times 100\%$$

where, V_1 and V_2 are the feed-in and take-up speeds respectively.

The amount of percentage overfeeding could be altered by interchanging the take-up rollers which were made to different diameters (see Section 5.2.2).

During the early part of the investigation it was found that for high values of percentage overfeeding continuity of the bulking process could not be maintained owing to the breakage of the yarn. Reasons for this difficulty and ideas for improvement will be given later.

5.4.5 False-twist Spindle Speed

It is essential that the false twist spindle should temporarily remove all the twist from the portion of the yarn in the "bulking zone". Therefore, the speed of the spindle should be correctly adjusted to suit the initial twist in the parent yarn and the input and output speeds. However, in practice it was found that extra untwisting of the yarn was necessary, since untwisting to the zero twist state was insufficient for bulking to occur. For instance if the parent yarn twist was T turns/in(2), then it was found experimentally that the spindle speed needed to be adjusted such that about $0.3T$ turns/in(S) twist was present in the yarn portion within the bulking zone. The reasons for this requirement are considered in Section 5.6.1.

5.4.6 Yarn Tension during Bulking

Yarn tensioning, before and after the bulking zone, was found to be a very important factor affecting the resultant

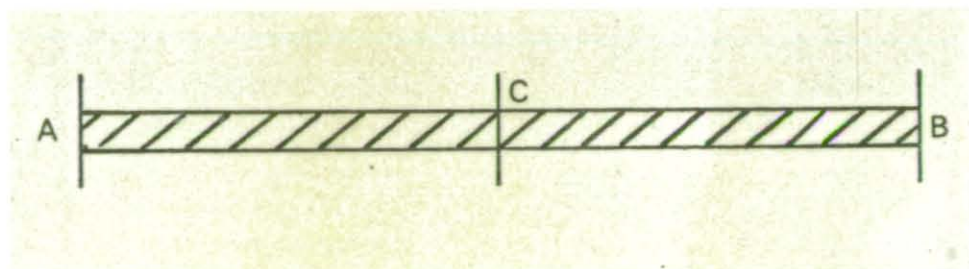
characteristics of the bulked yarn. Satisfactory tensioning of the entering parent yarn and clearance of any kinks from the yarn is essential in order to achieve a regular feeding to the bulking zone. Any irregularity in feed-in tension would give irregularities to the bulked yarn. Moreover, if such irregularity is not accompanied by a corresponding increase or decrease in spindle speed, then yarn breakage could occur and a continuous process would be impossible. An adequate yarn tension after the bulking zone is necessary for imparting the desired stability of the bulked yarn.

During the experimental investigations, the yarn tension was measured by using a WIRA yarn tension meter with 0-25 grams range; a 0.075 gram per denier tension (based on the parent yarn denier) was used for both the input and output tensioning since this was found to give satisfactory processing conditions.

5.4.7 Bulking Speed

A Leesona split-drum type winding roller was available for use as a winding mechanism. Although speeds as high as 250 yards/min presented no difficulties in actually producing a bulked yarn from the bulking unit itself, the package wind-up using this arrangement was unsatisfactory at these speeds. Thus a lower bulking speed of 67.5 yards/min was used for the main experiments in order that a good quality regularly wound bulked yarn package could be obtained for the physical bulk tests which are based on the measurement of the wound package density^(11,15).

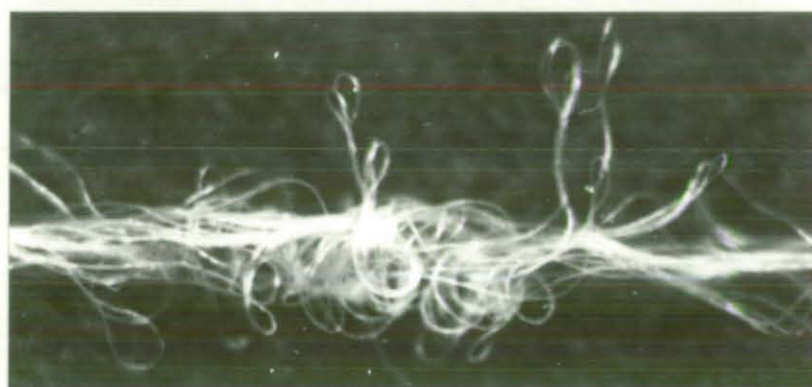
As this experimental apparatus was initially designed to simulate the air-jet method yarn bulking process rather than to be a prototype machine for a completely new process, then in order to study the effect of the variation of the process variables, three separate drive units were used so that an independent variation in speed of



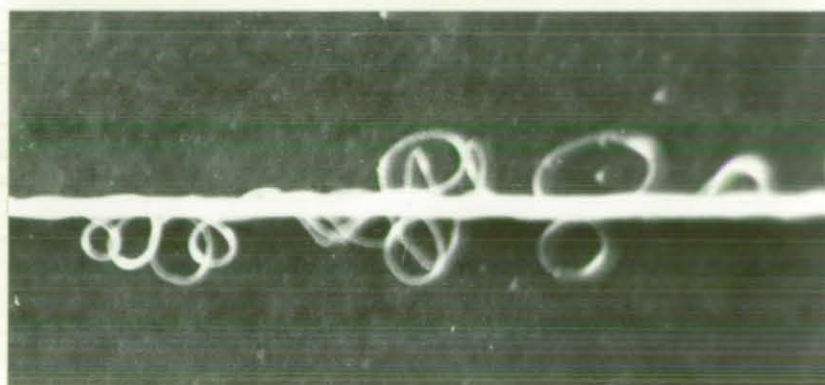
(a)



(b)



(c)



(d)

Fig. 5.4 The Principle of Mechanical Bulking

any one part could be made. Therefore, in order to start up the bulking process a manual synchronization of the three separate drive accelerations had to be made, since otherwise an increase in the length of unbulked yarn in the bulking zone would cause breakage. Although at the low speeds of bulking used for the experimental processing, starting up of the process was easy, at high speeds it demanded considerable acquired skill.

5.5 Hypothesis of the Bulking Mechanism as Applied to the Mechanical Bulking Method

As the mechanical method of bulking was initially devised to simulate the air-jet bulking mechanism, Wray's suggested explanation of this mechanism^(11,13) as applied to the air-jet should also apply to a certain extent to this new method of bulking. Continuous pre-twisted heat-set multi-filament yarn is projected through the nip rollers towards the false-twist spindle which temporarily untwists the portion of yarn contained in the bulking zone at any instant. The pre-twisted yarn structure consists of a helical configuration of continuous filaments. Under the action of the false-twist spindle, this configuration is distorted and filaments are not only untwisted but also are slightly twisted in the opposite direction because of the extra false-twist which needs to be provided (see Sections 5.4.5 and 5.6.1). Also, due to the overfeeding, the filaments are continuously being slackened, and the individual filaments would tend to resume their initial helical configuration with the help of the torsional energy stored in the filaments. However, as a result of the rotation of the yarn, the individual filaments are also caused to oscillate and are thrown outwards under the effect of centrifugal forces. The total result of these actions is that individual filaments are distorted, entangled and looped. After the yarn passes through the false-twist tube the initial yarn twist runs back and locks the already formed looped structure in position.

The principles embodied in the above hypothesis may be demonstrated by considering a small length of pre-twisted heat-set multi-filament yarn held between two points A and B under slight tension as represented in Fig. 5.4(a). If the yarn is gripped at a central position C by the finger tips and simply untwisted while allowing the gripped position of the fingers to move towards B to maintain a slight tension in the portion AC, then Fig. 5.4(b) shows the structure of the yarn in this portion. Now, if the tension in AC is relaxed by moving the still-gripped point C towards A, and at the same time slightly twisting the open yarn in the opposite direction to that in which it was previously twisted, then the yarn structure in portion AC will be looped similar to that shown in Fig. 5.4(c). Finally, if the grip applied by the fingers is removed, then twist will run from the highly twisted portion BC into the portion AC thereby "locking" the looped structure into position as shown in Fig. 5.4(d). This resultant structure appears to be similar to that of air-jet bulked yarns.

5.6 Experimental Observations

Two unexpected happenings were observed during the early part of this work when using the modified air-jet bulking apparatus described in Section 5.1. These were:

- (i) an untwisting of the yarn for a greater amount than that theoretically necessary for bringing it to the zero twist state i.e. the yarn had to be twisted by a few turns in a direction opposite to that of the original twist, (see Section 5.4.5), and
- (ii) a periodic bulking of the yarn. At first it was thought that, since the earlier experimental apparatus was not very accurately built, variations in process variables could be the cause of these effects. However, the above mentioned happenings still occurred with the more advanced bulking apparatus described in Section 5.2. Suggested explanations are offered below.

5.6.1 The Necessity for extra Untwisting of the Yarn

The need for extra untwisting has been mentioned in Section 5.4.5. However, the reasons for providing the extra twist could be two-fold in that (a) the filaments, instead of reverting to a helical configuration, are provided with extra impetus to enable them to snarl into a looped and entangled state, or (b) as the untwisted filaments snarl into loops there could be an apparent loss in twist which must be compensated for in order that the following portion of yarn should be freed of twist. This is similar to the argument offered by Denton⁽³⁷⁾ for the apparent loss of twist in false-twist stretch-type bulked yarns. It is possible that both of these arguments for extra untwisting to be applied are true, and in practice it is found that approximately 30% to 40% extra untwisting needs to be provided for satisfactory bulking to occur.

5.6.2 Periodic Bulking

Examinations of the bulked yarns under a microscope showed that a periodic bulking of the yarn was occurring and this would obviously be most undesirable if the yarn was to be used commercially.

The reasons for periodic bulking could be connected with the optimum adjustment of the bulking zone length (see Sections 5.7 and 5.8) and/or with the instantaneous twist present in the section of yarn in the bulking zone. This could be affected by either variations in the yarn properties, i.e. in the initial yarn twist, or variation in the process variables, i.e. in through-put speed, or in false-twist spindle speed.

To maintain a regular quality of bulking during the continuous production of the mechanically bulked yarn, the amount of pre-calculated twist in the portion of yarn contained within the bulking zone should be maintained constant, together with a regular

overfeeding of the yarn. The constant overfeeding is achieved by driving the feed-in and take-up rollers from the same motor and using timing belts (see Section 5.2.2). However the other possibility of a variation in the yarn twist in the bulking zone remains and hence is analytically investigated below.

Fig. 5.5 shows the bulking zone, where:

T = Initial twist in supply yarn (15 turns/in)

V_1 = Feed-in speed (60 in/sec)

L = Bulking zone length (1 inch)

N = Spindle speed (1125 revs/sec)

V_2 = Take-up speed (54.5 in/sec)

a = Overfeed % = $\frac{V_1 - V_2}{V_2} \times 100\%$ (10%)

(Note: Typical practical values are given in brackets)

Considering a small time δt , then:

Turns gained through feed-in rollers = $TV_1 \cdot \delta t$

Turns lost by yarn passing through spindle = $xV_2 \cdot \delta t$

Turns lost due to rotation of spindle = $N \cdot \delta t$

(where x is the twist in the yarn present in the bulking zone after time t from the start)

Total turns of twist in the bulking zone

$$= L(x + \delta x) = Lx + TV_1 \cdot \delta t - xV_2 \cdot \delta t$$

$$L \cdot \delta x = (TV_1 - N - xV_2) \cdot \delta t$$

Integrating:

$$\int \frac{dx}{(TV_1 - N - xV_2)} = \int \frac{dt}{L}$$

$$-\frac{1}{V_2} \log_e (TV_1 - N - xV_2) = \frac{t}{L} + C$$

when $T = 0$, $x = T$

$$C = -\frac{1}{V_2} \log_e (TV_1 - N - TV_2)$$

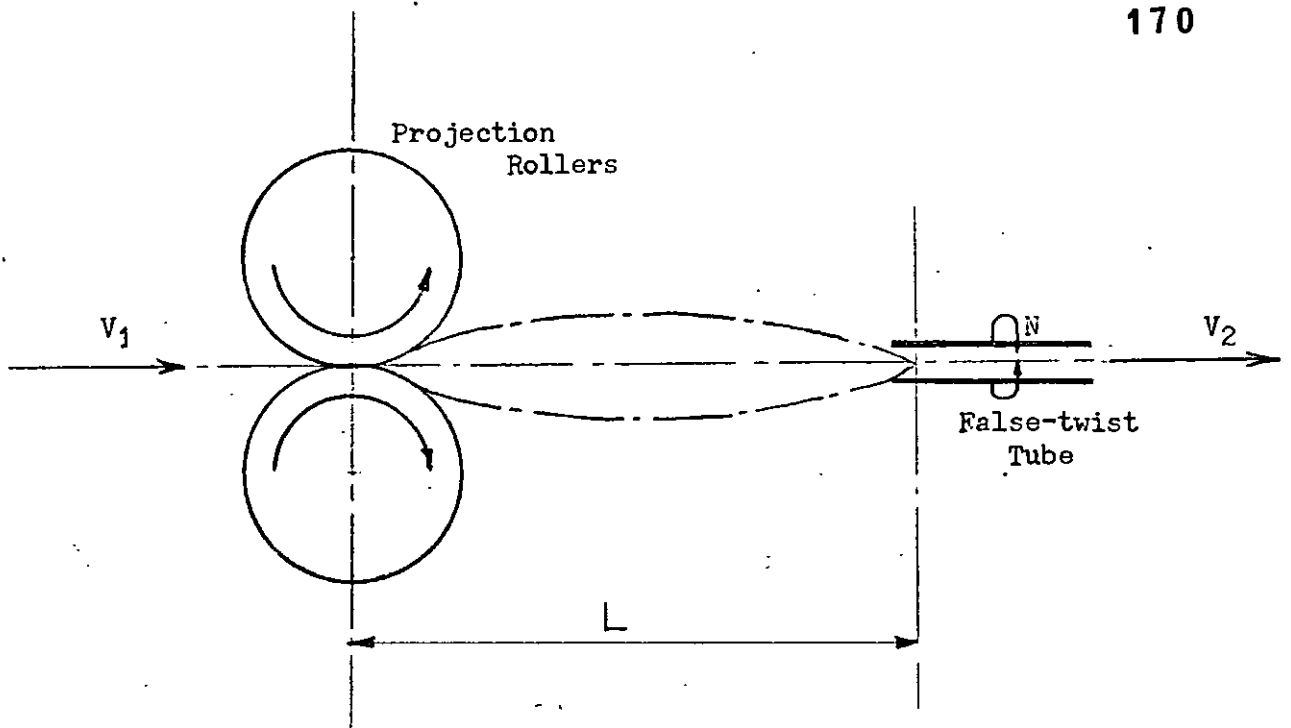


Fig. 5.5 Bulking Zone

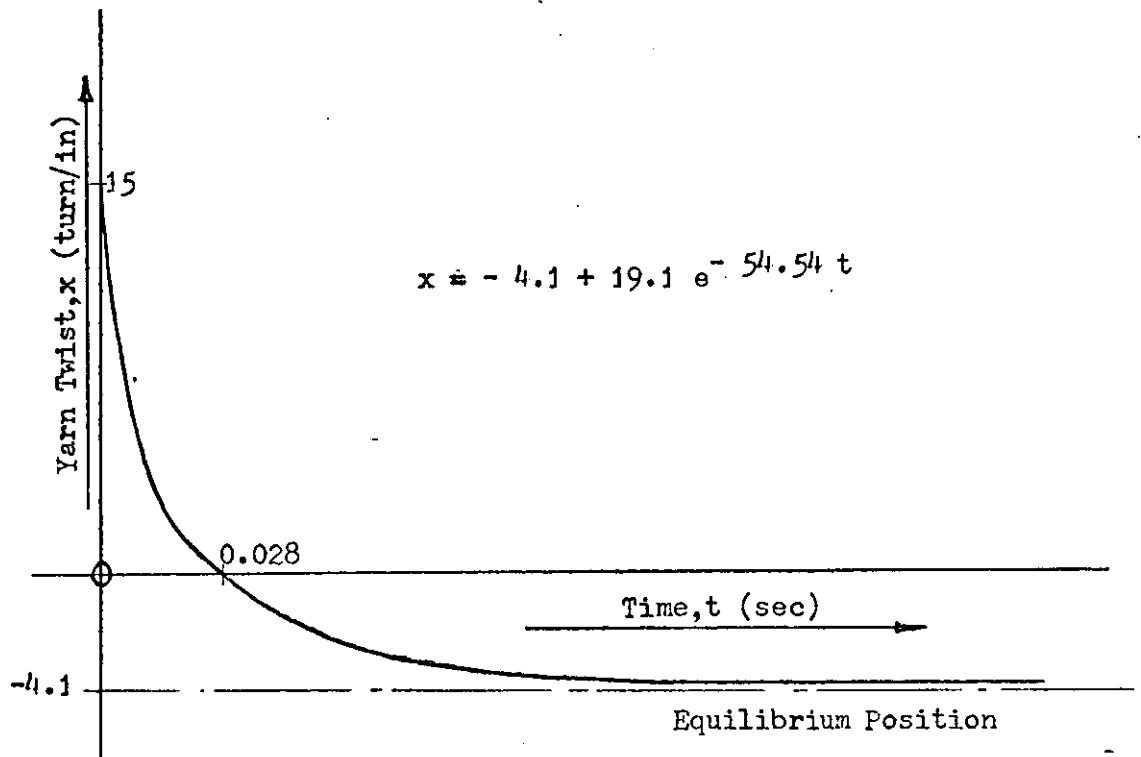


Fig. 5.6 Yarn Twist in the Bulking Zone versus Time

$$\therefore -\frac{1}{V_2} \log_e (TV_1 - N - xV_2) = \frac{t}{L} - \frac{1}{V_2} \log_e (TV_1 - N - TV_2)$$

$$\therefore -\frac{V_2 t}{L} = \log_e \frac{TV_1 - N - xV_2}{TV_1 - N - TV_2}$$

$$\therefore \frac{TV_1 - N - xV_2}{TV_1 - N - TV_2} = e^{-\frac{V_2 t}{L}}$$

$$xV_2 = TV_1 - N - (TV_1 - N - TV_2) \cdot e^{-\frac{V_2 t}{L}}$$

$$x = \frac{TV_1 - N}{V_2} - \left(\frac{TV_1 - N - TV_2}{V_2} \right) \cdot e^{-\frac{V_2 t}{L}} \quad \text{---(5-2)}$$

Fig. 5.6 is a plot of this relationship between x and t for the typical values given above.

At the equilibrium position:

$$X = \frac{TV_1 - N}{V_2}$$

By definition, the required extra untwisting is

$$-\frac{\alpha}{100} \cdot T \quad \text{(noting that the final twist direction is opposite to the initial yarn twist)}$$

$$\frac{TV_1 - N}{V_2} = -\frac{\alpha T}{100} \quad \text{---(5-3)}$$

$$\therefore N = TV_1 + \frac{\alpha}{100} T V_2 \quad \text{---(5-4)}$$

From the equation (5-4), the required spindle speed could be calculated for a given set of process variables to give the necessary percentage extra untwisting.

Now considering small changes in the process variables after the equilibrium position is reached, it is possible to find the variation of the yarn twist in the bulking zone from the equation (5-3). The typical values given above are again used during the calculations.

For a small change ΔT in the supply yarn twist,

$$X + \Delta X_1 = \frac{(T + \Delta T) V_1 - N}{V_2}$$

where ΔX_1 is the corresponding change in the yarn twist.

$$\Delta X_1 = \Delta T \frac{V_1}{V_2}$$

but,

$$a = \frac{V_1 - V_2}{V_2} \times 100$$

giving

$$\frac{V_1}{V_2} = \left(1 + \frac{a}{100}\right)$$

$$\therefore \Delta X_1 = \Delta T \left(1 + \frac{a}{100}\right) \text{ ---- (5-5)}$$

Hence for a variation of say 2.5% in the yarn twist,

$$\begin{aligned} \Delta X_1 &= 15 \times 0.025 \times (1 + 0.1) \\ &= 0.4 \text{ (turns/in)} \end{aligned}$$

For a small variation ΔV_1 in the feeding speed,

$$X + \Delta X_2 = \frac{T(V_1 + \Delta V_1) - N}{V_2 + \Delta V_2}$$

where ΔX_2 is the corresponding change of the yarn twist in the bulking zone.

$$\begin{aligned} \text{But, } V_2 &= \frac{V_1}{\left(1 + \frac{a}{100}\right)} \\ \therefore \Delta X_2 &= \frac{N \cdot \Delta V_1 \left(1 + \frac{a}{100}\right)}{V_1 (V_1 + \Delta V_1)} \text{ ---- (5-6)} \end{aligned}$$

Hence for a variation of say 2.5% in the feeding speed,

$$\Delta x_2 = \frac{1125 \times 60 \times 0.025 (1+0.1)}{60 (60 + 60 \times 0.025)}$$

$$= \underline{0.5} \text{ (turns/in)}$$

Once again, for a small change ΔN in the false twist spindle speed,

$$x + \Delta x_3 = \frac{TV_1 (N + \Delta N)}{V_2}$$

where Δx_3 is the corresponding change of yarn twist in the bulking zone.

$$\therefore \Delta x_3 = - \frac{\Delta N}{V_2} = - \frac{\Delta N (1 + \frac{2}{100})}{V_1} \quad \text{--- (5-7)}$$

Hence for a variation of say 2.5% in the spindle speed,

$$\Delta x_3 = \frac{1125 \times 0.025 (1+0.1)}{60}$$

$$= \underline{0.5} \text{ (turns/in)}$$

The above mathematical analysis has shown that appreciable variation in either parent yarn twist (equation 5-5) bulking speed (equation 5-6) or spindle speed (equation 5-7) could play a considerable part in altering the pre-calculated bulking zone yarn twist, and this in turn will vary the degree of bulkiness produced in the yarn. Therefore, a careful control of each of these variables should be maintained.

5.7 High-Speed Cine-Photography of the Process

Various parts of the bulking zone were filmed using high speed cine-photography to provide detailed information regarding the actual bulking process. These films are available within the Department for inspection purposes. During the filming, processing variables were maintained constant as follows:

Parent Yarn	= 205 denier nylon 6.6/34 filaments/15 turns per in
Overfeed	= 8.1%
Bulking speed (i.e. Feed-in Speed)	= 200 ft/min
False twist spindle speed	= 62,400 rev/min
Bulking Zone Length	= $1\frac{3}{4}$ in and $\frac{3}{4}$ in

The film speed was approximately 6000 frames/sec.

A close examination of the films taken with the bulking zone fixed at $1\frac{3}{4}$ in shows that opening of the pre-twisted filament bundle starts while the yarn is leaving the nip rollers. As soon as they are sufficiently opened the twist-free filaments are thrown outwards to form a balloon. This balloon rotates and travels linearly from the projection rollers towards the spindle. However, during this time the portions of yarn immediately before and after this balloon are under tension, and therefore a complete opening of the twist free filaments is difficult to achieve. During the rotation of this open filament bundle, individual filaments are entangled to form a looped configuration. As soon as this open filament bundle passes through the spindle, the yarn in the bulking zone becomes slack and opening of filaments in that portion of yarn then leaving the projection rollers starts again. This phenomena continues in a quite regular periodic pattern of bulked to unbulk portions of yarn.

Since the yarn is travelling at a regular linear speed through the bulking zone, one would expect that reducing the extent of this zone would also decrease the length of the unbulk portions of yarn. Consequently, a more regularly bulked yarn should be produced if the optimum bulking zone length could be found. Keeping all the yarn and processing variables constant, but reducing the length of the bulking zone from $1\frac{3}{4}$ in to $\frac{3}{4}$ in, other high speed films were taken.

Examination of these later films showed that the twist-free filament bundle is completely open in the bulking zone the whole of the time. Although this prevented the occurrence of periodic bulking, such a small bulking zone length was insufficient to form a large balloon. A better entanglement of looped filaments ought to be possible if the rotating open balloon formed by the untwisting filaments was arranged to be as large as possible and consistently maintained, and the films had indicated that there must be an optimum length at which this is achievable for any given set of processing conditions.

5.8 Mathematical Analysis of the Ballooning Phenomenon

As an aid to finding the optimum bulking zone length, for any combination of processing and yarn variables, a mathematical analysis of the ballooning of the yarn in the bulking zone was attempted. This could be expected to lead to a better understanding of the factors affecting the bulking mechanism and would, therefore, indicate ways of improving the yarn quality.

For complete opening of the yarn structure in the bulking zone, the distance between the projection rollers and the spindle should be adjusted such that while the open yarn bundle is forming a balloon in the bulking zone (rotating about the axis of spindle) the adjacent nodes of this balloon should be at the point of exit on the projection rollers and point of entry to the spindle.

Fig. 5.7 shows a filament of the yarn being rotated in ballooning form at a speed of w rad/sec. Applying ballooning yarn theory⁽³⁸⁾ to the rotating filaments in the bulking zone, and assuming air-drag and coriolis forces are negligible, then considering an element δs of yarn and letting the mass/unit length of this element be q .

For a narrow balloon the deflection of yarn from the spindle

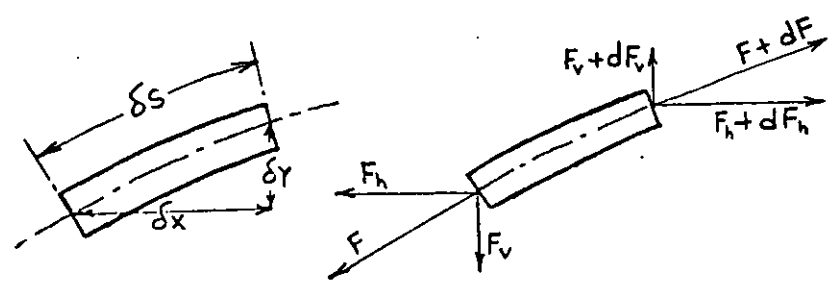
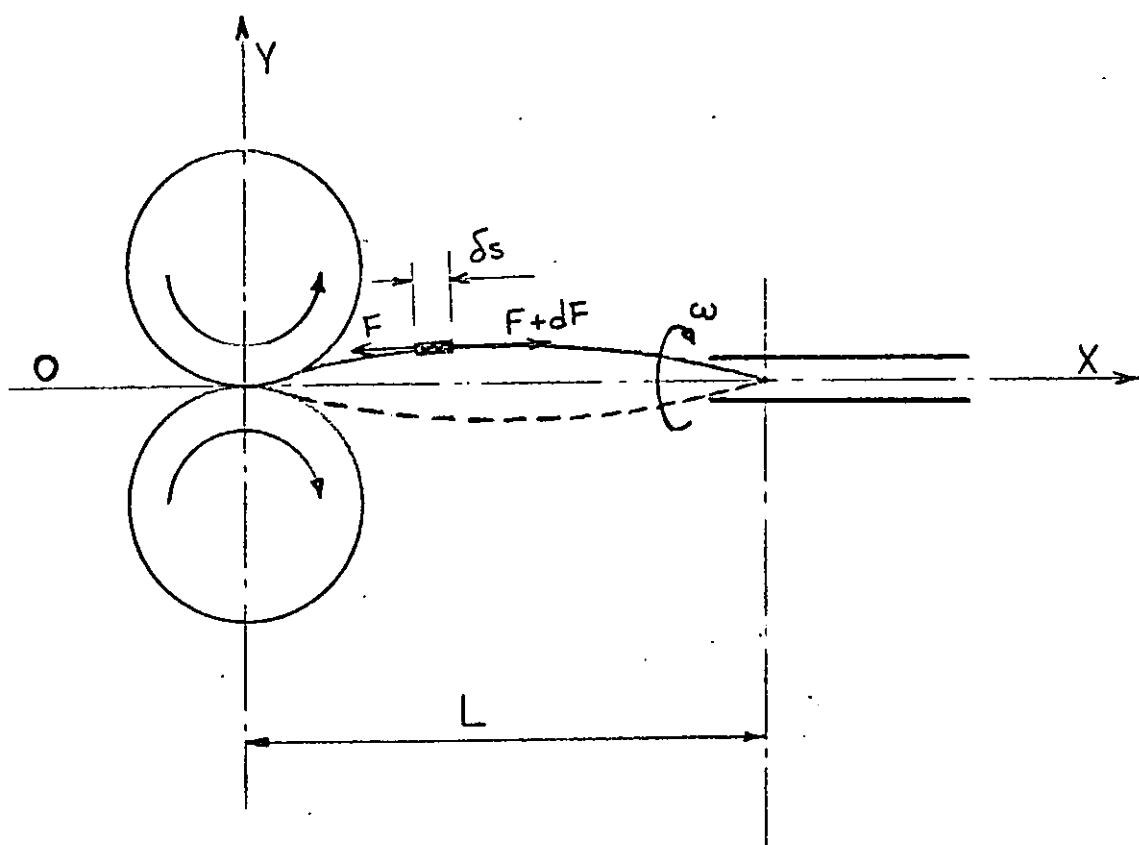


Fig. 5.7 Forces Acting on a Rotating Filament

axis (ox) is small and therefore the mass of this element can be expressed as $q \cdot dx$ instead of $q \cdot \delta s$ thus the integration is very much simpler. Let F be the tensile force (tension) in the yarn and F_h and F_v be its horizontal and vertical components.

Resolving horizontally:

$$F_h + dF_h - F_h = 0$$

$$dF_h = 0$$

$$F_h = \text{constant} \quad \text{--- (5-8)}$$

Resolving vertically:

$$F_v + dF_v - F_v + q \cdot dx \cdot \omega^2 \cdot y = 0$$

$$dF_v = -q \cdot dx \cdot \omega^2 \cdot y \quad \text{--- (5-9)}$$

Also

$$\frac{dy}{dx} = \frac{F_v}{F_h} \quad \text{--- (5-10)}$$

From (5-8) and (5-10):

$$dF_v = F_h \left(\frac{d^2y}{dx^2} \right) dx \quad \text{--- (5-11)}$$

From (5-9) and (5-11):

$$F_h \left(\frac{d^2y}{dx^2} \right) dx = -q \cdot dx \cdot \omega^2 \cdot y$$

$$\frac{d^2y}{dx^2} + \frac{q \cdot \omega^2 \cdot y}{F_h} = 0$$

$$\therefore y = C_1 \cdot \cos \left(\sqrt{\frac{q \cdot \omega^2}{F_h}} \cdot x \right) + C_2 \sin \left(\sqrt{\frac{q \cdot \omega^2}{F_h}} \cdot x \right)$$

$$\text{at } x = 0, y = 0$$

$$\therefore C_1 = 0$$

$$\therefore y = C_2 \sin \left(\sqrt{\frac{q \cdot \omega^2}{F_h}} \cdot x \right) \quad \text{--- (5-12)}$$

at $x = L$, $y = 0$

$$\text{from (5-12)} \quad 0 = C_2 \cdot \sin \left(\sqrt{\frac{q \cdot \omega^2}{F_h}} \cdot L \right)$$

$$\therefore \sqrt{\frac{q \cdot \omega^2}{F_h}} \cdot L = \pi$$

$$L = \frac{\pi}{\omega} \sqrt{\frac{F_h}{q}} \quad \text{-----} \quad (5-13)$$

If N is the spindle speed in rev/sec., then $\omega = 2\pi N$ and

$$L = \frac{1}{2N} \sqrt{\frac{F_h}{q}} \quad \text{-----} \quad (5-13-2)$$

The value of F_h can be measured. Hence formula (5-13) or (5-13-2) can be used to determine the bulking zone length for satisfactory ballooning and consequently optimum bulking.

5.9 Improvements to the Design of the False-Twist Unit

During the operation of the mechanical bulking apparatus the experience gained and observation made brought about two important improvements to the process. These are discussed below.

5.9.1 False-Twist Tube

As the false-twist tube used was actually made for the conventional false-twist method of bulking, it was not entirely satisfactory for this new method of bulking. Due to the overfeeding of the yarn and to the bulking action occurring before the yarn enters the spindle, the bulked yarn could not easily pass through the spindle and around its twist peg. Sometimes the slackened yarn wound around the spindle end adjacent to the twist peg, and thus a continuous bulking process was very difficult to maintain. It was during one of these frequent yarn breakages and the preparation of the apparatus for the next operation that it was unintentionally omitted to wind the yarn around the twist peg. It was then noticed that, whereas previously

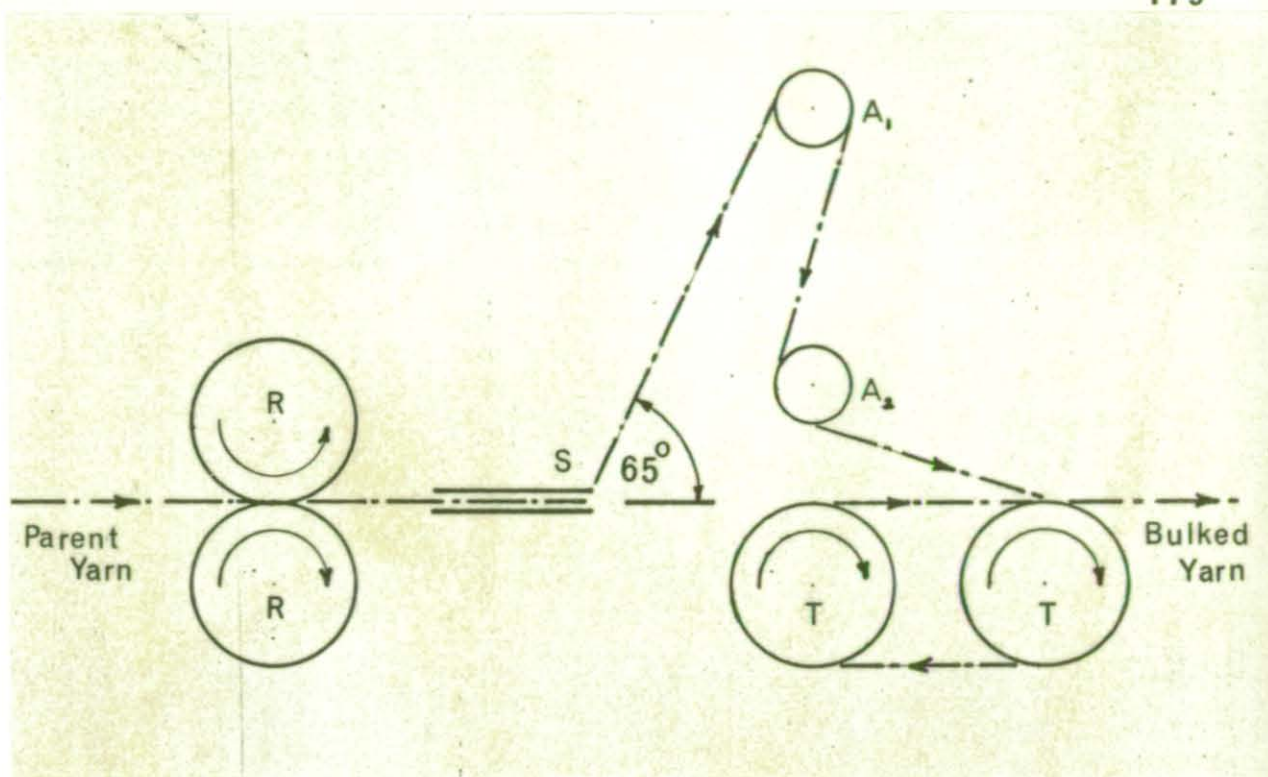


Fig. 5.8 Yarn Path with the Modified False Twist Tube

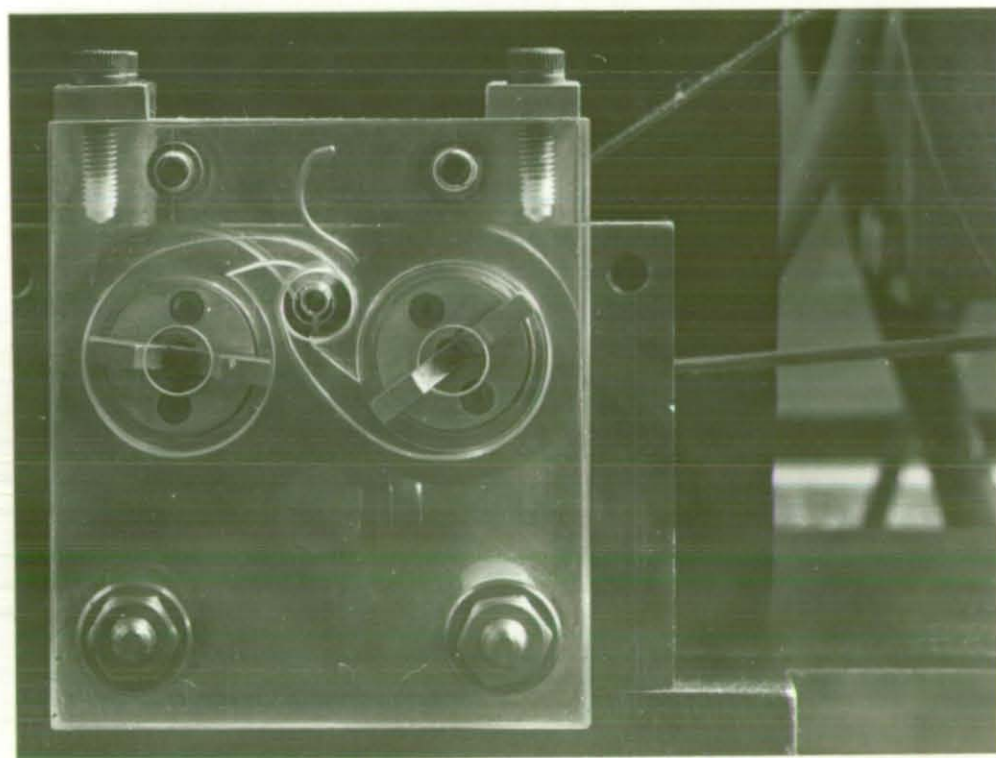


Fig. 5.9 Impellers and Localised Turbulent Region

continuous runs could not be maintained for more than a few minutes at a time, the accidentally "misprepared" operation ran without yarn breakage occurring. It was then realised that the cross-peg is not really necessary for this method of bulking, as due to the centrifugal forces the slackened yarn is thrown outwards and the frictional forces between the open filaments and the inside wall of the spindle are sufficient to grip the yarn for false-untwisting purposes. In the light of this discovery a new design of the twist tube was made without a cross peg, and this was used during the making of all the bulked yarns required for testing (see Chapter 6). However, to assist in starting up the process with this type of twist tube, the withdrawal path of the yarn from the tube is offset by an angle of 65° to the spindle axis. This is achieved using two assisting rollers (A_1 and A_2 in Fig. 5.8) before the yarn is drawn off by the take-up rollers D D.

5.9.2 Addition of Localised Turbulent Region to the Bulking Zone

In order to improve the entanglement of the open bundle of filaments and the quality of the bulked yarn produced, a localised turbulent region was created by a mechanical means. This was done by fixing two small impellers to the rollers which frictionally drive the false twist tube (see Fig. 5.9). The impellers revolve inside a housing machined in a perspex block, and air is forced into the region inside the perspex block at which the ballooning yarn is passing prior to entering the twist tube. Thus a vortex is created which revolves in the opposite direction to that of the rotating yarn and this gives a greater entanglement to the filaments. The product shows improvement from the visual viewpoint and, therefore, this simple modification was incorporated for producing all the bulked yarns for test purposes.

5.10 The Adaptation of the Mechanical Bulking Process to the Production of Novelty Effect Yarns

In the air-jet method of bulking, effect yarns can be produced by blending two or more similar or dissimilar yarns together, thereby producing a yarn that will have a combination of their individual properties (see Section 1.3). This process may be used in two different ways. Firstly, several yarns may be blended together simply by feeding the yarns together into the air-jet, and this is called "multi-end bulking". Secondly, two or more yarns may be fed into the air-jet in such a way that one yarn provides the core for the effect yarns. This is accomplished by feeding the effect yarns to the air-jet at a higher overfeed than that of the core yarn, and is called "core bulking". A slub-type variation of this can be obtained by an intermittent feed to the effect yarn or yarns.

Unlike the air-jet method of bulking, it is not possible to produce a blended novelty effect yarn by feeding two or more yarns into the mechanical bulking apparatus. This is because the two yarns would have to be fed into the one spindle tube and untwisted simultaneously; the result of this would be that the two yarns would be twisted together rather than individually opened. It was, therefore, considered that one way to produce a novelty effect yarn, by this apparatus, would be to have a core yarn which would undergo the untwisting/re-twisting bulking process and to feed the effect "yarn" in the form of loosely presented natural or man-made staple fibres. It was envisaged that such fibres could be introduced into the open structure of the core yarn while it was temporarily untwisted and its individual filaments were forming the rotating open balloon.

5.10.1 Method of Introducing the Fibres into the Core Yarn Structure

On considering the action of the impellers which were

a later improvement to the mechanical bulking process (see Section 5.9.2), these take in air through the holes at the centre of their housing, thus acting as centrifugal fans which accelerate the air radially outwards into a chamber through which the open core yarn is passing. It was, therefore, considered possible to inject fibres into this chamber by feeding the fibres into the impeller housing through the centre hole and thus allowing them to be blown into the ballooning filaments of the core yarn.

The problem of feeding the separated fibres at a regular rate into the air flow proved to be difficult and needed specially designed equipment. However, it was decided that hand feeding of the fibres for this experimental investigation would be satisfactory to demonstrate the feasibility of the idea.

When cotton-type staple-length fibres were injected into the bulking zone, it was found that most of the fibres were thrown out and could not mix with the core yarn. Although a few of the fibres were caught up by the yarn, on careful examination it was found that they were only wrapped around it having failed to become entangled with it. However, when $\frac{1}{4}$ cm staple length fibres were tried (these being cut from coloured acetate filaments), some degree of positive penetration of the fibres into the core yarn structure was obtained. The distribution of these fibres was at random due to the method of hand feeding.

The process of making effect yarns by this type of apparatus would obviously require further development before it could be considered as a practical proposition. Reasons for its not being effective to date with longer staples are discussed in Chapter 7, together with suggestions for further development of the technique.

CHAPTER 6

YARN TESTS AND RESULTS

6.1 Preliminary Testing

For a preliminary comparison of the "mechanically" bulked yarns with conventional air-jet bulked yarns, a series of essential tests had to be carried out. The geographical difficulties of having small quantities of the early parent yarns made at Manchester University, and consequently being forced to rely on their kind and generous co-operation in providing such labour as could be spared from other duties, precluded the possibility of also undertaking these tests at Manchester. Because no specialised textile testing equipment existed at Loughborough University of Technology, the initial tests were carried out by using extremely rudimentary methods. Although the test results were encouraging, they could not be considered sufficiently reliable, and, therefore, they have not been recorded here.

An alternative way had to be found to overcome these difficulties in order to make a detailed study of the bulked yarn characteristics; hence several textile research organisations in the Loughborough area were requested to kindly co-operate in the preparation of sufficient quantities of a wider range of parent yarn samples, and also to arrange for the use of their specialised textile testing equipment.

6.2 Preparation of Parent Yarns

All the parent yarns to be processed for the test purposes were prepared from various nylon 6.6 multi-filament yarns which were kindly supplied by I.C.I. Fibres Ltd., Pontypool. The small amount of producer twist present was ignored for the purpose of their being twisted in the Z direction to the various theoretical twist levels desired. This was kindly undertaken by the Courtaulds Textile Research Laboratory at Spondon, Derby.

TABLE 6.1 Twist in the Parent Yarn after Steam Setting

Parent Yarn before Preparation (Denier / No. of Filaments)	Theoretical Twist Inserted (turns/in)	Actual Twist after Steaming (turns/in)
100 / 34	10.0	11.00
100 / 34	12.5	13.75
100 / 34	15.0	16.49
100 / 34	17.5	19.25
100 / 34	20.0	22.00
100 / 34	22.5	24.75
100 / 34	25.0	27.50
30 / 26	15.0	16.50
70 / 34	15.0	16.50
150 / 50	15.0	16.50
205 / 34	15.0	16.50

TABLE 6.2 Parent Yarn Denier after Twisting and Steaming

Parent Yarn before Steaming (No. of Fils. / Theoretical Twist)	Parent Yarn Denier before Twisting	Actual Parent Yarn Denier after Twisting and Steaming
34 / 10.0	100	105.02
34 / 12.5	100	106.04
34 / 15.0	100	107.02
34 / 17.5	100	107.80
34 / 20.0	100	108.57
34 / 22.5	100	108.94
34 / 25.0	100	109.06
26 / 15.0	30	31.99
34 / 15.0	70	74.93
50 / 15.0	150	164.75
34 / 15.0	205	227.00

As it is the common practice to steam-set the twisted yarns intended for the air-jet method of bulking, the prepared parent yarns for mechanical bulking were also steam-set under the conditions of 190°F and 45 minutes duration. The theoretical twist inserted by the upwister was calculated from the gearing, but the steamed parent yarn contracts and therefore the actual yarn twist, together with the final denier after steaming, had to be measured. The results are shown in Table 6.1 and 6.2.

A simple nomenclature was used to designate the various parent yarn samples,

i.e. parent yarn denier/no. of filaments/parent yarn twist (turns/in)
(after twisting (after steaming)
and steaming)

and any parameters which changed during the tests were underlined.

For example, the parent yarns shown in say Table 6.6 are all made from 107 denier, 34 filament yarn, and the twist is being systematically varied.

6.3 Processing the Parent Yarns

As it was intended to study the effect of the major yarn and process variables on the resultant bulked yarn characteristics, all these variables (see Section 5.4) were changed systematically, and sample bulked yarn packages were made. The empty bobbins for these packages were specially made from a hard plastic tubing with a smooth and constant outside diameter so that the physical bulk-test (based on a package density method as described in Section 6.5) could be accurately undertaken.

The parent yarn input tension and the bulked yarn winding tension were both maintained constant at 0.075 g/den (based on parent yarn denier). A constant bulking speed of 67.5 yards/min was maintained throughout the preparation of the bulked yarn samples.

Again a simple nomenclature was used to designate the various processing conditions,

i.e. overfeeding/false twist tube speed/extra untwisting/bulking zone length
 (%) (rev/sec) (%) (in)

The quantity being varied was again underlined in each case.

6.4 Percentage Denier Increase

The purpose of this experiment was to ascertain how the bulked yarn denier varied with the processing variables. The deniers of the bulked yarns were determined by weighing 450 m lengths wound on a metre wrapreel at a tension of approximately 0.075 g/den.

The same method was also used for the calculation of the parent yarn denier and in both cases an average of two readings was taken. Then, the percentage denier increase is simply given by:

$$\frac{\text{Bulked Yarn Denier} - \text{Parent Yarn Denier}}{\text{Parent Yarn Denier}} \times 100\%$$

Since it was not anticipated that denier would be greatly influenced except by the overfeed, it might be reasonably expected that a given overfeed would produce a similar increase in denier after bulking. Thus the adjustment of yarn tension is based on this assumption.

6.4.1 Results

Table 6.2 shows the parent deniers after twisting and steaming. These values were used to calculate the percentage denier increases and they are tabulated in Tables 6.3 to 6.7 and are shown graphically in Figs. 6.1 to 6.6.

TABLE 6.3 Percentage Denier Increase at Varying Overfeed

Parent Yarn	Processing Conditions	Bulked Yarn Denier	% Denier Increase
107 / 3 $\frac{1}{2}$ / 16.5	<u>2.56</u> / 910 / 36.2 / 1.0	111.52	4.20
107 / 3 $\frac{1}{2}$ / 16.5	<u>5.26</u> / 910 / 36.2 / 1.0	112.89	5.48
107 / 3 $\frac{1}{2}$ / 16.5	<u>8.10</u> / 910 / 36.2 / 1.0	113.67	6.21
107 / 3 $\frac{1}{2}$ / 16.5	<u>11.10</u> / 910 / 36.2 / 1.0	116.02	8.41
107 / 3 $\frac{1}{2}$ / 16.5	<u>14.30</u> / 910 / 36.2 / 1.0	117.39	9.69
107 / 3 $\frac{1}{2}$ / 16.5	<u>17.65</u> / 910 / 36.2 / 1.0	119.74	11.88

TABLE 6.4 Percentage Denier Increase at Varying Bulking Zone Length

Parent Yarn	Processing Conditions	Bulked Yarn Denier	% Denier Increase
107 / 3 $\frac{1}{2}$ / 16.5	11.1 / 910 / 36.2 / <u>0.6</u>	113.08	5.66
107 / 3 $\frac{1}{2}$ / 16.5	11.1 / 910 / 36.2 / <u>0.7</u>	112.89	5.48
107 / 3 $\frac{1}{2}$ / 16.5	11.1 / 910 / 36.2 / <u>0.8</u>	113.48	6.03
107 / 3 $\frac{1}{2}$ / 16.5	11.1 / 910 / 36.2 / <u>0.9</u>	112.89	5.48
107 / 3 $\frac{1}{2}$ / 16.5	11.1 / 910 / 36.2 / <u>1.0</u>	116.02	8.41
107 / 3 $\frac{1}{2}$ / 16.5	11.1 / 910 / 36.2 / <u>1.1</u>	115.82	8.22
107 / 3 $\frac{1}{2}$ / 16.5	11.1 / 910 / 36.2 / <u>1.2</u>	115.43	7.85
107 / 3 $\frac{1}{2}$ / 16.5	11.1 / 910 / 36.2 / <u>1.3</u>	118.10	10.40
107 / 3 $\frac{1}{2}$ / 16.5	11.1 / 910 / 36.2 / <u>1.4</u>	117.70	10.00

TABLE 6.5 Percentage Denier Increase at Varying % Extra Untwisting

Parent Yarn	Processing Conditions	Bulked Yarn Denier	% Denier Increase
107 / 3 $\frac{1}{2}$ / 16.5	11.1 / <u>803</u> / <u>20.2</u> / 1.0	117.20	10.10
107 / 3 $\frac{1}{2}$ / 16.5	11.1 / <u>825</u> / <u>23.5</u> / 1.0	116.60	9.00
107 / 3 $\frac{1}{2}$ / 16.5	11.1 / <u>850</u> / <u>27.2</u> / 1.0	115.10	7.60
107 / 3 $\frac{1}{2}$ / 16.5	11.1 / <u>885</u> / <u>32.5</u> / 1.0	115.56	8.00
107 / 3 $\frac{1}{2}$ / 16.5	11.1 / <u>910</u> / <u>36.2</u> / 1.0	116.00	8.40
107 / 3 $\frac{1}{2}$ / 16.5	11.1 / <u>931</u> / <u>39.4</u> / 1.0	113.53	6.10
107 / 3 $\frac{1}{2}$ / 16.5	11.1 / <u>950</u> / <u>42.2</u> / 1.0	116.41	8.80
107 / 3 $\frac{1}{2}$ / 16.5	11.1 / <u>997</u> / <u>46.3</u> / 1.0	114.70	7.20
107 / 3 $\frac{1}{2}$ / 16.5	11.1 / <u>1007</u> / <u>50.7</u> / 1.0	116.74	9.10

TABLE 6.6 Percentage Denier Increase at Varying Parent Yarn Twist

Parent Yarn	Processing Conditions	Bulked Yarn Denier	% Denier Increase
107 / 3 $\frac{1}{2}$ / <u>11.0</u>	11.1 / <u>607</u> / 36.2 / 1.0	115.56	8.00
107 / 3 $\frac{1}{2}$ / <u>13.7</u>	11.1 / <u>758</u> / 36.2 / 1.0	118.13	10.40
107 / 3 $\frac{1}{2}$ / <u>16.5</u>	11.1 / <u>910</u> / 36.2 / 1.0	116.02	8.40
107 / 3 $\frac{1}{2}$ / <u>19.2</u>	11.1 / <u>1062</u> / 36.2 / 1.0	119.00	11.20
107 / 3 $\frac{1}{2}$ / <u>22.0</u>	11.1 / <u>1213</u> / 36.2 / 1.0	117.60	9.90
107 / 3 $\frac{1}{2}$ / <u>24.7</u>	11.1 / <u>1362</u> / 36.2 / 1.0	117.27	9.60
107 / 3 $\frac{1}{2}$ / <u>27.5</u>	11.1 / <u>1517</u> / 36.2 / 1.0	117.86	10.15

TABLE 6.7 Percentage Denier Increase at Varying Parent Yarn Denier and Number of Filaments

Parent Yarn	Processing Conditions	Bulked Yarn Denier	% Denier Increase
<u>32</u> / <u>26</u> / 16.5	11.1 / 910 / 36.2 / 1.0	33.59	4.97
<u>75</u> / <u>34</u> / 16.5	11.1 / 910 / 36.2 / 1.0	80.50	7.35
<u>107</u> / <u>34</u> / 16.5	11.1 / 910 / 36.2 / 1.0	116.02	8.41
<u>165</u> / <u>50</u> / 16.5	11.1 / 910 / 36.2 / 1.0	179.41	8.90
<u>227</u> / <u>34</u> / 16.5	11.1 / 910 / 36.2 / 1.0	250.04	10.15

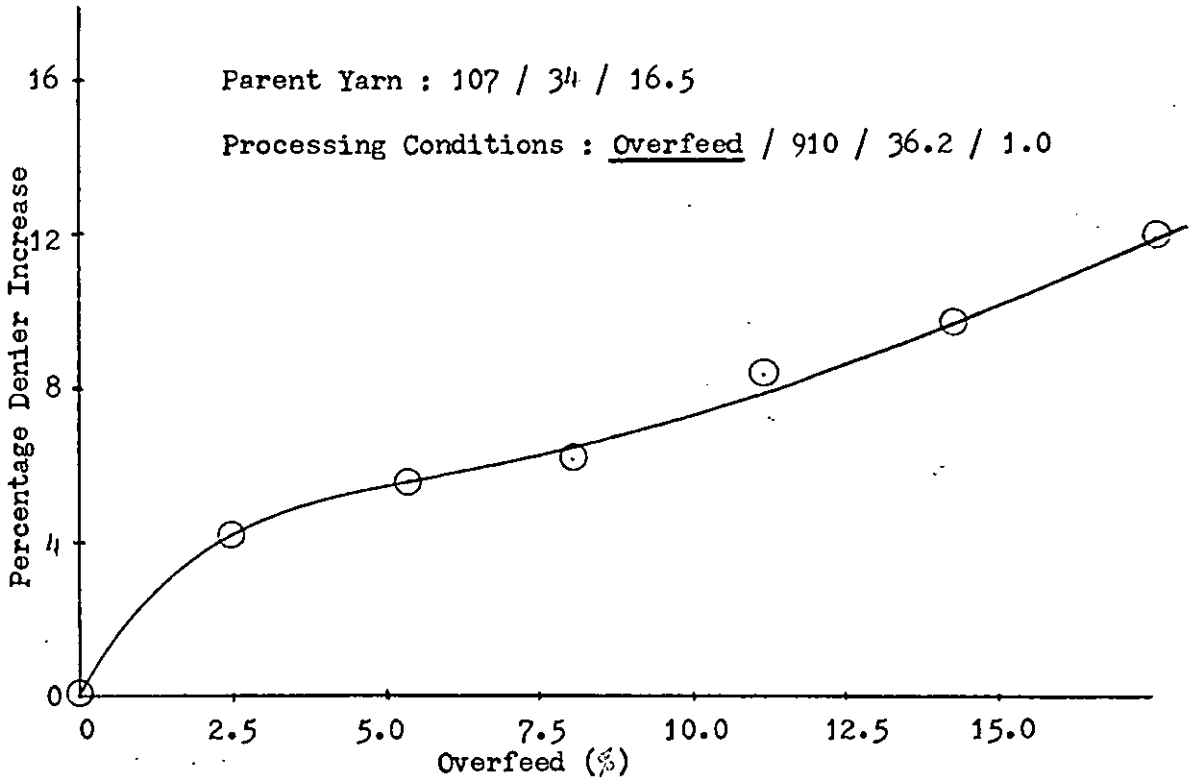


Fig. 6.1 Percentage Denier Increase versus Percentage Overfeed

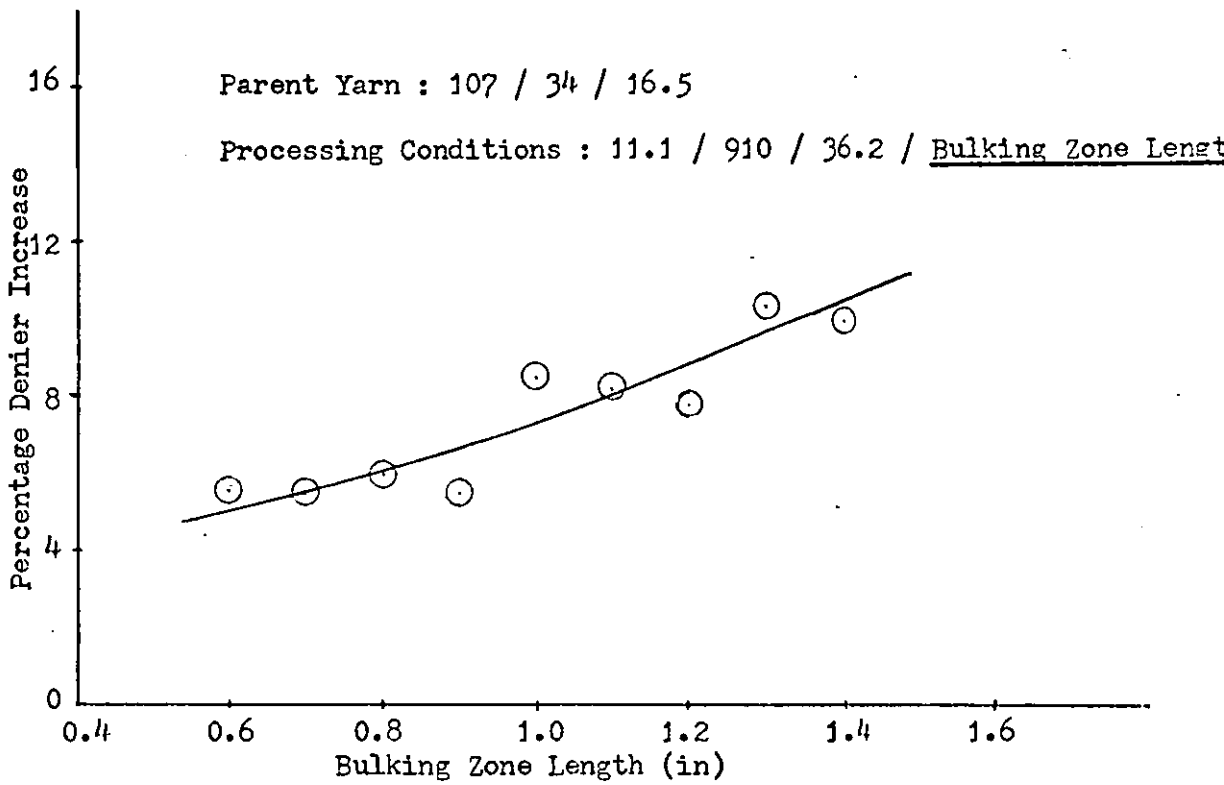


Fig. 6.2 Percentage Denier Increase versus Bulking Zone Length

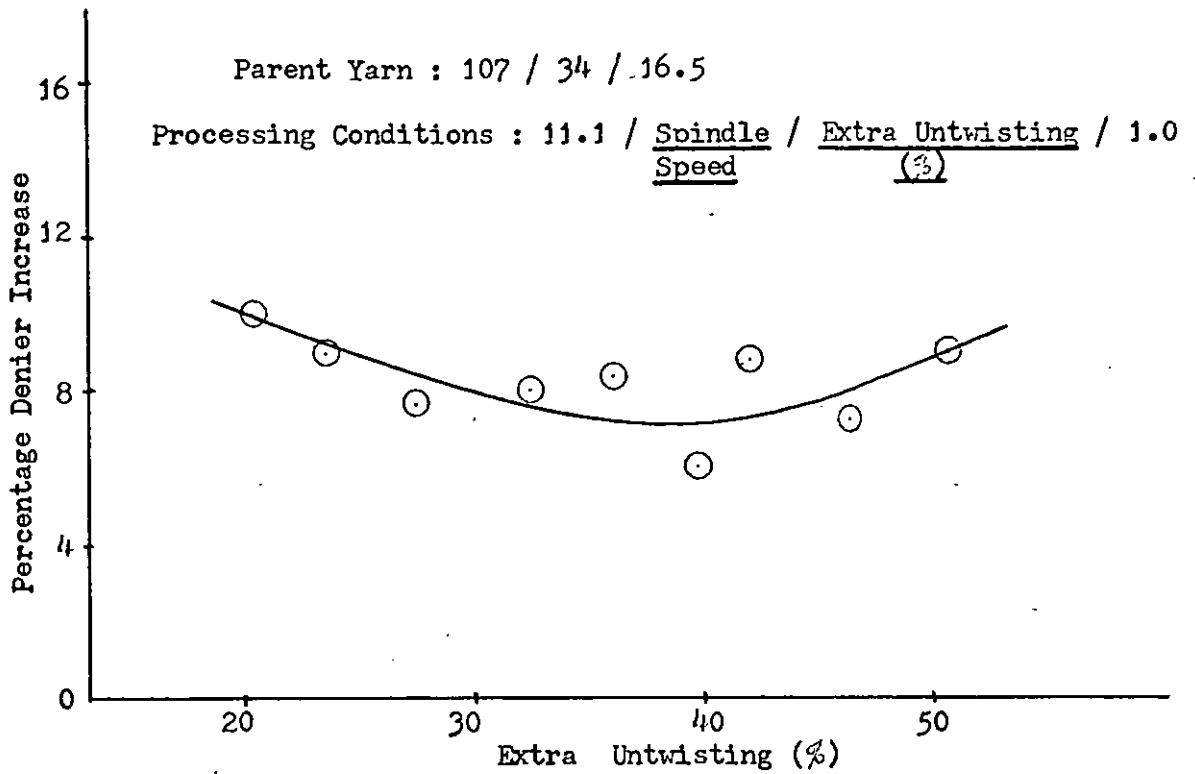


Fig. 6.3 Percentage Denier Increase versus Extra Untwisting (%)

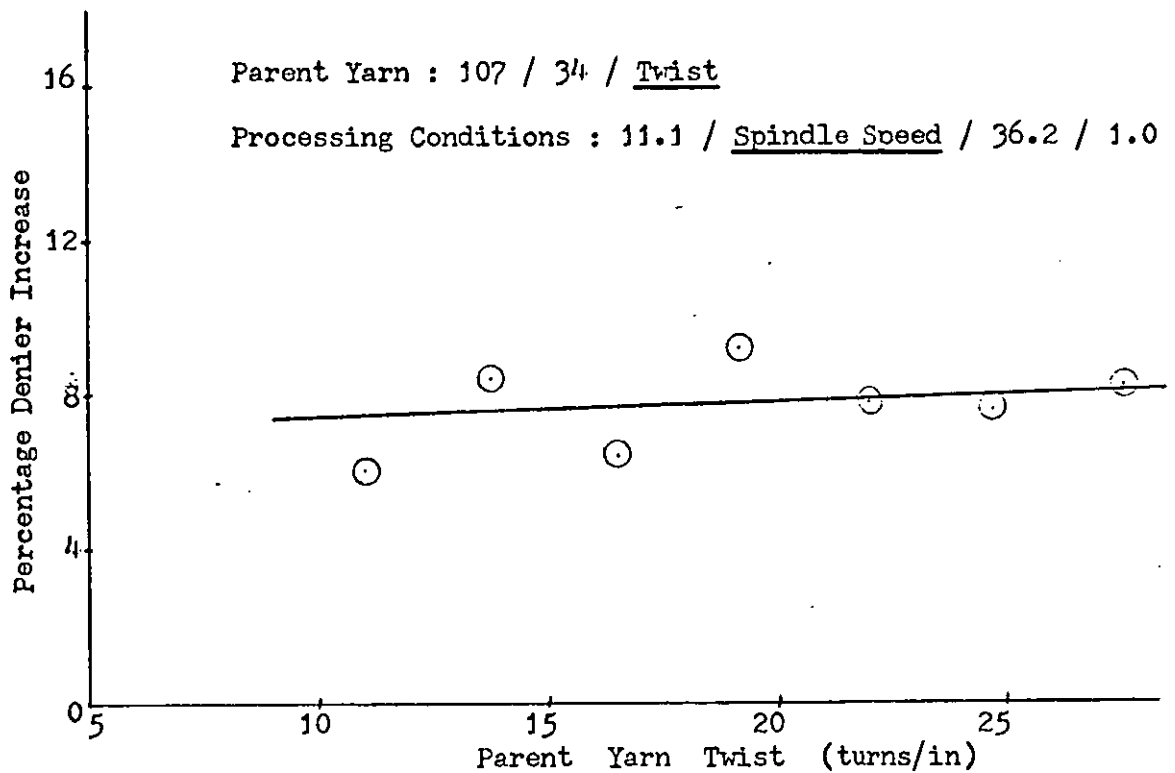


Fig. 6.4 Percentage Denier Increase versus Parent Yarn Twist

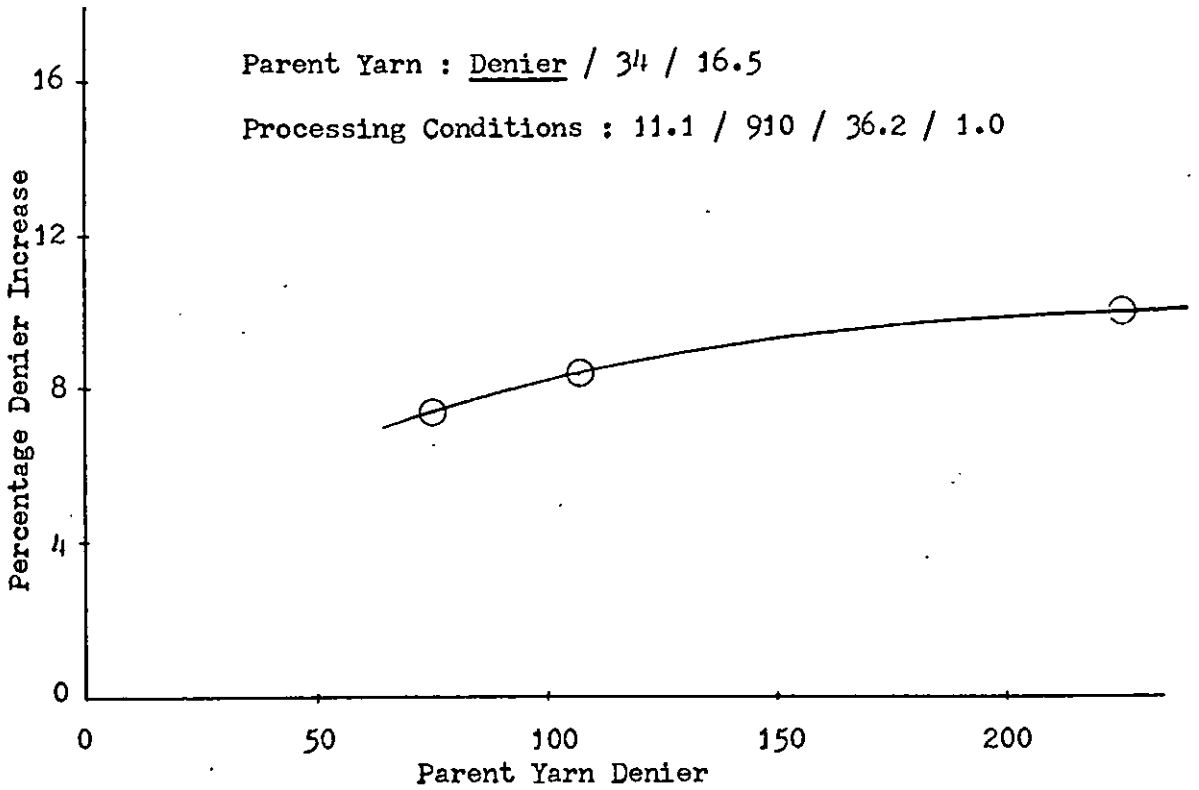


Fig. 6.5 Percentage Denier Increase versus Parent Yarn Denier

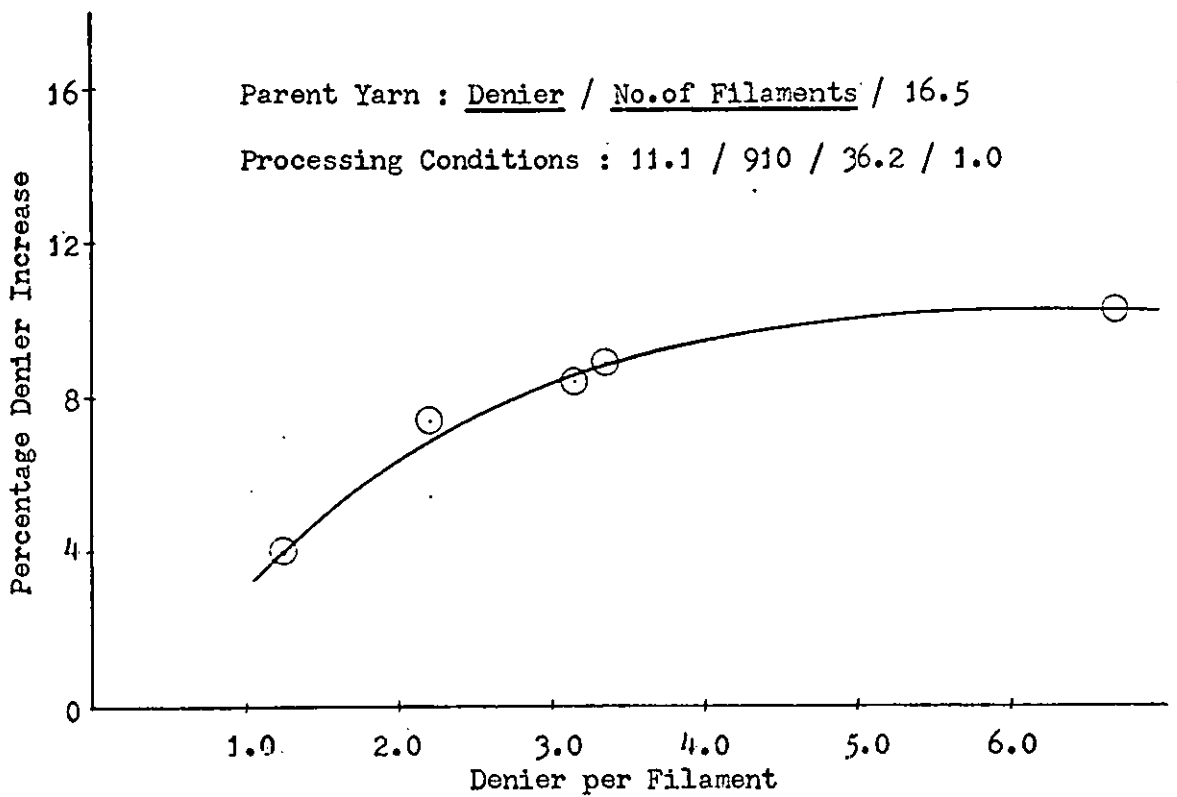


Fig. 6.6 Percentage Denier Increase versus Parent Yarn Denier per Filament

6.5 Physical Bulk Test Based on Package Density Method

This test gives some indication of the amount of bulking which a parent yarn has received during the process. The object of the standard test for determining the physical bulk of Taslan yarn is described by du Pont^(11,15) and compares the weight per unit volume of the yarn before and after bulking. This method was used here, the procedure being summarised as follows:

- a) An empty package is weighed, and its outside diameter is measured.
- b) A certain amount of yarn is then wound on the package under constant winding tension.
- c) Finally the package is weighed again and its outside diameter is measured.

The same method was used for both parent and bulked yarn packages and their respective weights per unit volume were calculated from the following equation:

$$\frac{W}{V} = \frac{W_f - W_i}{\frac{\pi}{4} L (D_f^2 - D_i^2)} \quad \text{--- (6-1)}$$

where,

- W = Weight of yarn wound on the package (g)
- V = Volume of yarn wound on the package (in³)
- W_f = Weight of final package with yarn (g)
- W_i = Weight of empty package (g)
- L = Length of wound package (in)
- D_f = Outside diameter of final package (in)
- D_i = Outside diameter of empty package (in).

$$\begin{aligned}
 \text{Then, Physical Bulk \%} &= \left(\frac{W}{V} \right)_p \times \left(\frac{V}{W} \right)_b \times 100 \\
 &= \frac{W_p}{(D_f^2 - D_i^2)_p} \times \frac{(D_f^2 - D_i^2)_b}{W_b} \times 100 \quad \text{-----(6-2)}
 \end{aligned}$$

where, the suffices p and b indicate the parent and bulked yarns respectively.

6.5.1 Results

The calculated physical bulk percentages are tabulated in Tables 6.8 to 6.12 and are shown graphically in Figs. 6.7 to 6.12. Table 6.13 shows the values of the parameters $(D_f^2 - D_i^2)_p$ and $(W_f - W_i)_p$ for the parent yarn packages which were necessary to calculate the physical bulk values for the Tables 6.8 to 6.12.

TABLE 6.8 Physical Bulk Percentage at Varying Overfeed

Parent Yarn	Processing Conditions	$(D_f^2 - D_i^2)_b$ (in ²)	$(W_f - W_i)_b$ (g)	Physical Bulk (%)
107 / 34 / 16.5	<u>2.56</u> / 910 / 36.2 / 1.0	0.6748	32.05	105.18
107 / 34 / 16.5	<u>5.26</u> / 910 / 36.2 / 1.0	0.6618	27.82	118.84
107 / 34 / 16.5	<u>8.10</u> / 910 / 36.2 / 1.0	0.6396	25.47	125.80
107 / 34 / 16.5	<u>11.10</u> / 910 / 36.2 / 1.0	0.6567	22.24	148.50
107 / 34 / 16.5	<u>14.30</u> / 910 / 36.2 / 1.0	0.6688	22.67	150.63
107 / 34 / 16.5	<u>17.65</u> / 910 / 36.2 / 1.0	0.5097	16.43	155.60

TABLE 6.9 Physical Bulk Percentage at Varying Bulking Zone Length

Parent Yarn	Processing Conditions	$(D_f^2 - D_i^2)_b$ (in ²)	$(W_f - W_i)_b$ (g)	Physical Bulk (%)
107 / 34 / 16.5	11.1 / 910 / 36.2 / <u>0.6</u>	0.4644	15.34	150.60
107 / 34 / 16.5	11.1 / 910 / 36.2 / <u>0.7</u>	0.4581	16.08	141.96
107 / 34 / 16.5	11.1 / 910 / 36.2 / <u>0.8</u>	0.6515	20.65	158.15
107 / 34 / 16.5	11.1 / 910 / 36.2 / <u>0.9</u>	0.6143	21.40	144.38
107 / 34 / 16.5	11.1 / 910 / 36.2 / <u>1.0</u>	0.6567	22.24	148.50
107 / 34 / 16.5	11.1 / 910 / 36.2 / <u>1.1</u>	0.6863	22.37	154.30
107 / 34 / 16.5	11.1 / 910 / 36.2 / <u>1.2</u>	0.7720	26.02	149.20
107 / 34 / 16.5	11.1 / 910 / 36.2 / <u>1.3</u>	0.8237	27.44	151.70
107 / 34 / 16.5	11.1 / 910 / 36.2 / <u>1.4</u>	0.6667	22.43	150.50

TABLE 6.10 Physical Bulk Percentage at Varying % Extra Untwisting

Parent Yarn	Processing Conditions	$(D_f^2 - D_i^2)_b$ (in ²)	$(W_f - W_i)_b$ (g)	Physical Bulk (%)
107 / 34 / 16.5	11.1 / <u>803</u> / <u>20.2</u> / 1.0	0.7039	24.88	141.58
107 / 34 / 16.5	11.1 / <u>825</u> / <u>23.5</u> / 1.0	0.6877	24.15	143.22
107 / 34 / 16.5	11.1 / <u>850</u> / <u>27.2</u> / 1.0	0.6430	22.06	145.60
107 / 34 / 16.5	11.1 / <u>885</u> / <u>32.5</u> / 1.0	0.6320	22.12	143.00
107 / 34 / 16.5	11.1 / <u>910</u> / <u>36.2</u> / 1.0	0.6567	22.24	148.50
107 / 34 / 16.5	11.1 / <u>931</u> / <u>39.4</u> / 1.0	0.5838	21.28	137.70
107 / 34 / 16.5	11.1 / <u>950</u> / <u>42.2</u> / 1.0	0.6540	22.50	145.20
107 / 34 / 16.5	11.1 / <u>977</u> / <u>46.3</u> / 1.0	0.7142	25.97	139.48
107 / 34 / 16.5	11.1 / <u>1007</u> / <u>50.7</u> / 1.0	0.7920	27.85	145.32

TABLE 6.11 Physical Bulk Percentage at Varying Parent Yarn Twist

Parent Yarn	Processing Conditions	$(D_f^2 - D_i^2)_b$ (in ²)	$(W_f - W_i)_b$ (g)	Physical Bulk (%)
107 / 34 / <u>11.0</u>	11.1 / <u>607</u> / 36.2 / 1.0	0.6319	23.13	138.00
107 / 34 / <u>13.7</u>	11.1 / <u>758</u> / 36.2 / 1.0	0.6193	21.98	142.27
107 / 34 / <u>16.5</u>	11.1 / <u>910</u> / 36.2 / 1.0	0.6567	22.24	148.50
107 / 34 / <u>19.2</u>	11.1 / <u>1062</u> / 36.2 / 1.0	0.7510	24.31	139.27
107 / 34 / <u>22.0</u>	11.1 / <u>1213</u> / 36.2 / 1.0	0.6643	22.67	137.10
107 / 34 / <u>24.7</u>	11.1 / <u>1362</u> / 36.2 / 1.0	0.6992	22.35	133.20
107 / 34 / <u>27.5</u>	11.1 / <u>1517</u> / 36.2 / 1.0	0.6720	22.10	129.27

TABLE 6.12 Physical Bulk Percentage at Varying Parent Yarn Denier and Number of Filaments

Parent Yarn	Processing Conditions	$(D_f^2 - D_i^2)_b$ (in ²)	$(W_f - W_i)_b$ (g)	Physical Bulk (%)
<u>32</u> / <u>26</u> / 16.5	11.1 / 910 / 36.2 / 1.0	0.3300	15.17	109.6
<u>75</u> / <u>34</u> / 16.5	11.1 / 910 / 36.2 / 1.0	0.6035	20.43	138.7
<u>107</u> / <u>34</u> / 16.5	11.1 / 910 / 36.2 / 1.0	0.6567	22.24	148.5
<u>165</u> / <u>50</u> / 16.5	11.1 / 910 / 36.2 / 1.0	0.8010	27.84	144.2
<u>227</u> / <u>34</u> / 16.5	11.1 / 910 / 36.2 / 1.0	0.9540	34.21	152.0

TABLE 6.13 Values of Parameters $(D_f^2 - D_i^2)_p$ and $(W_f - W_i)_p$ for Parent Yarn Packages

Parent Yarn	$(D_f^2 - D_i^2)_p$ (in ²)	$(W_f - W_i)_p$ (g)
107 / 34 / <u>11.0</u>	0.5409	27.32
107 / 34 / <u>13.7</u>	0.4830	24.39
107 / 34 / <u>16.5</u>	0.6902	34.48
107 / 34 / <u>19.2</u>	0.5673	25.57
107 / 34 / <u>22.0</u>	0.5239	24.50
107 / 34 / <u>24.7</u>	0.5620	26.30
107 / 34 / <u>27.5</u>	0.5323	22.63
<u>32</u> / <u>26</u> / 16.5	0.3970	20.01
<u>75</u> / <u>34</u> / 16.5	0.4500	21.14
<u>165</u> / <u>50</u> / 16.5	0.6594	32.76
<u>227</u> / <u>34</u> / 16.5	0.7760	42.30

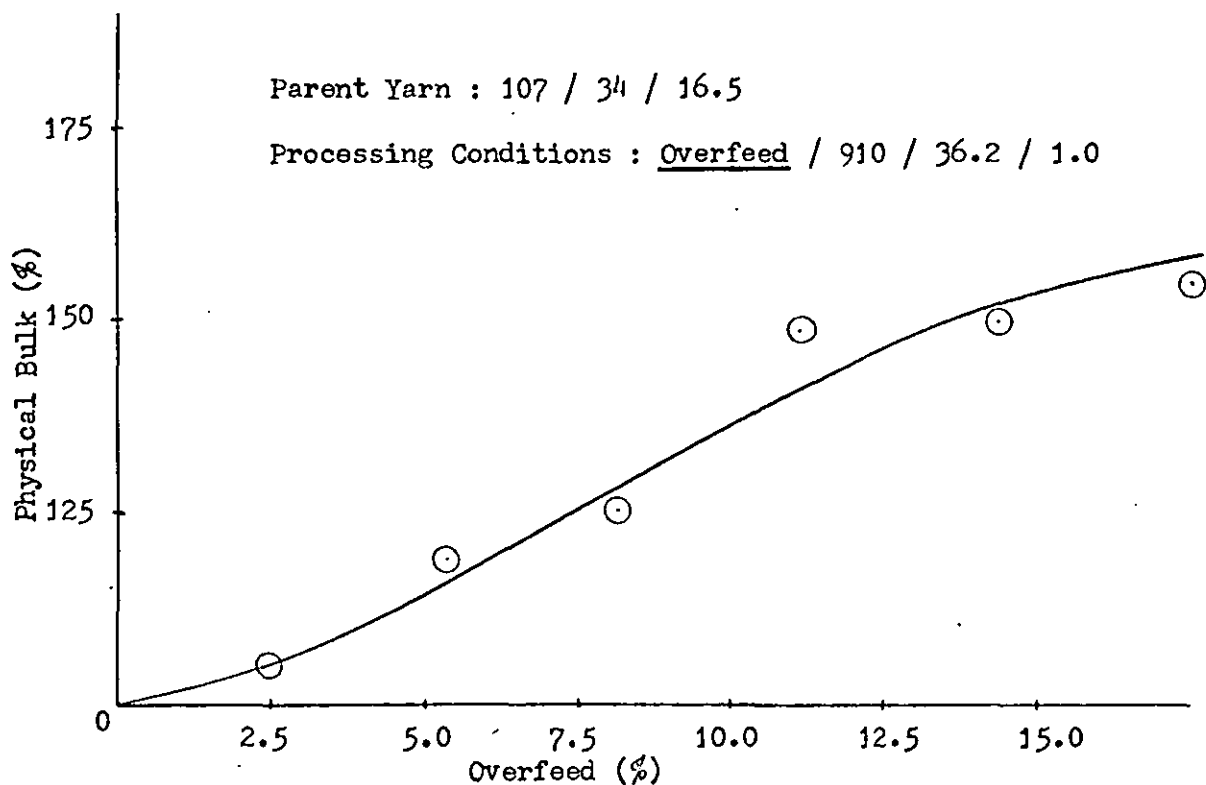


Fig. 6.7 Percentage Physical Bulk versus Percentage Overfeed

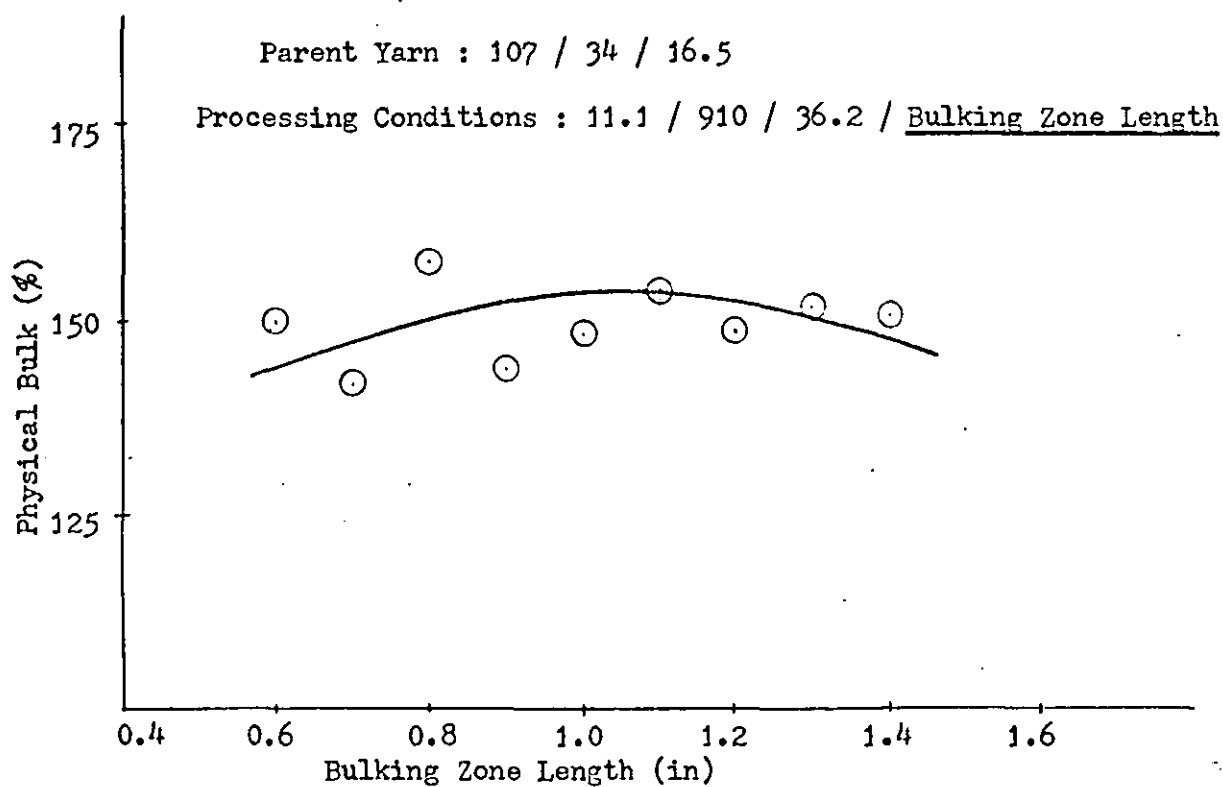


Fig. 6.8 Percentage Physical Bulk versus Bulking Zone Length

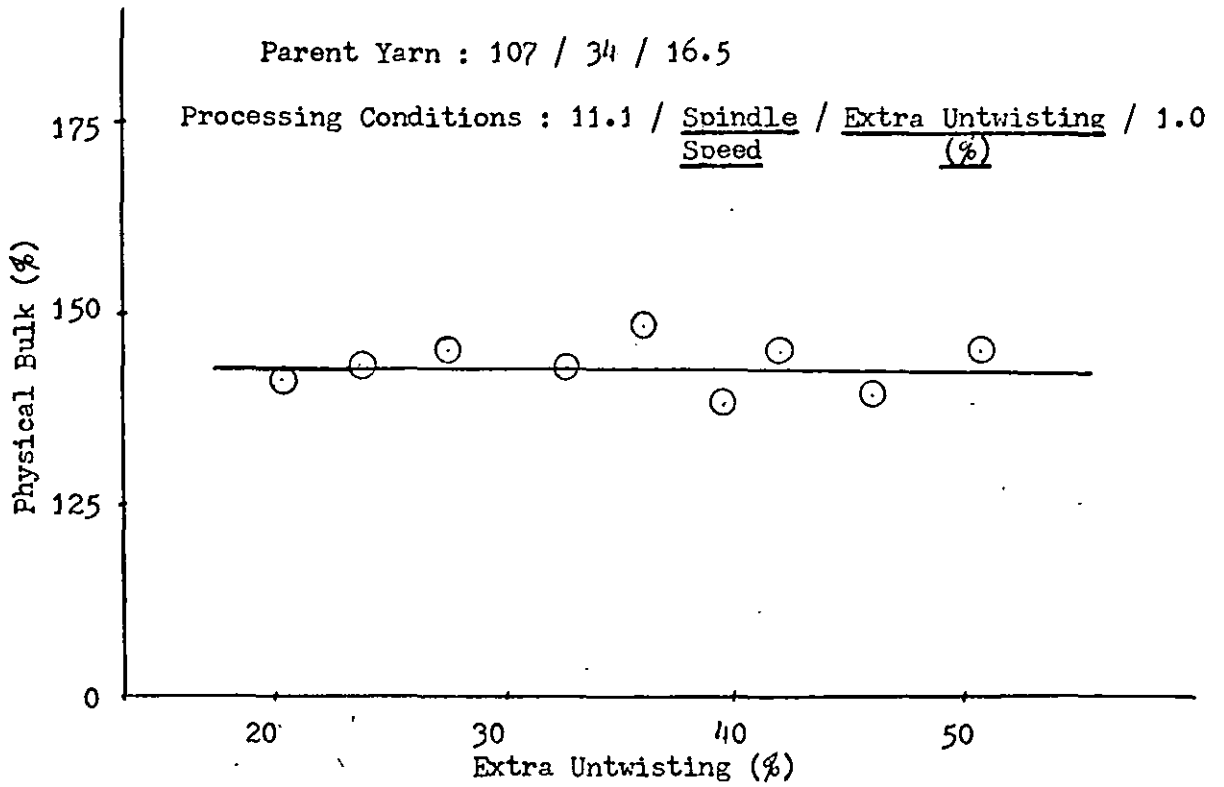


Fig. 6.9 Percentage Physical Bulk versus Extra Untwisting (%)

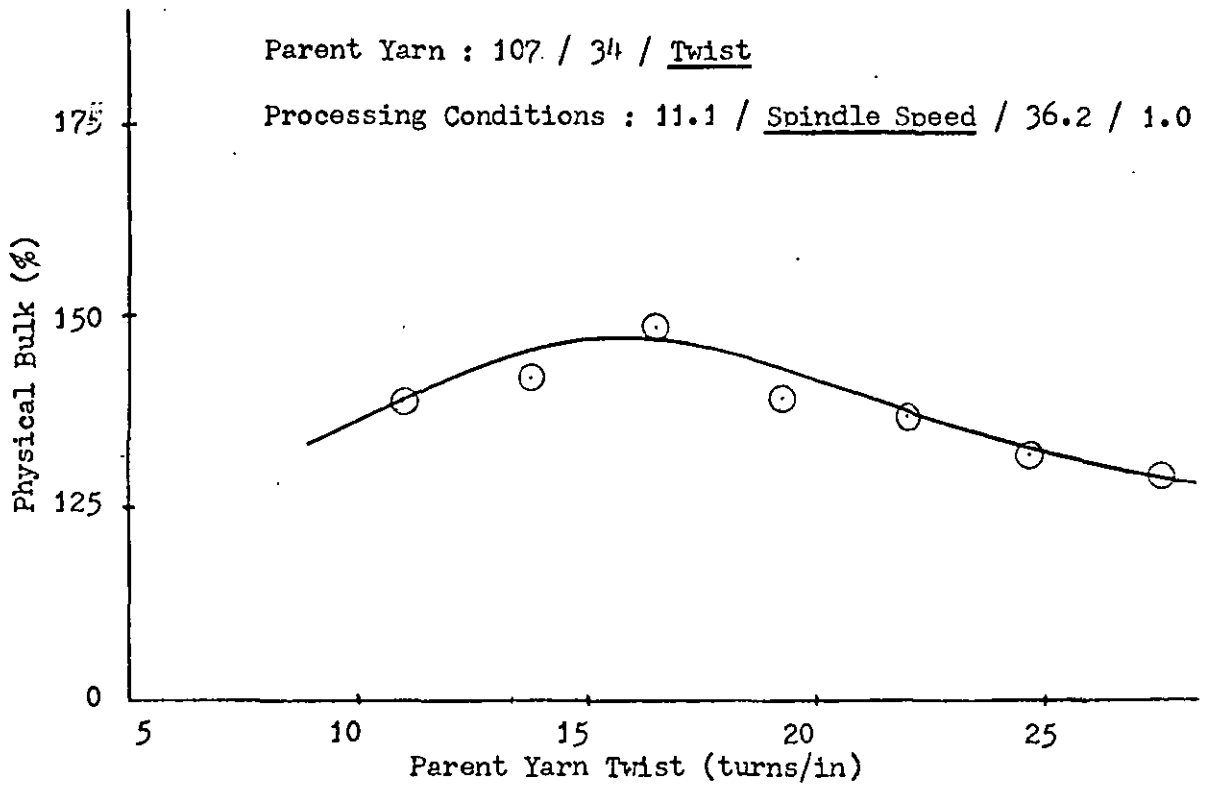


Fig. 6.10 Percentage Physical Bulk versus Parent Yarn Twist

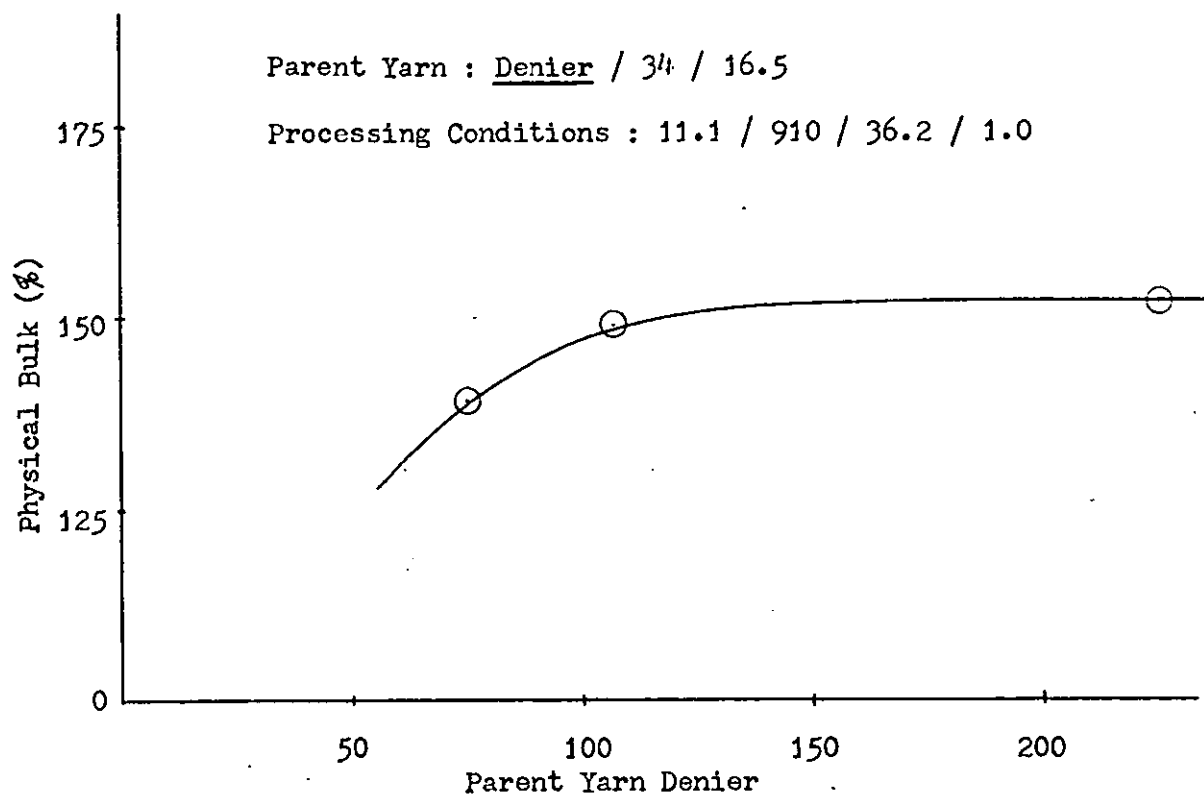


Fig. 6.11 Percentage Physical Bulk versus Parent Yarn Denier

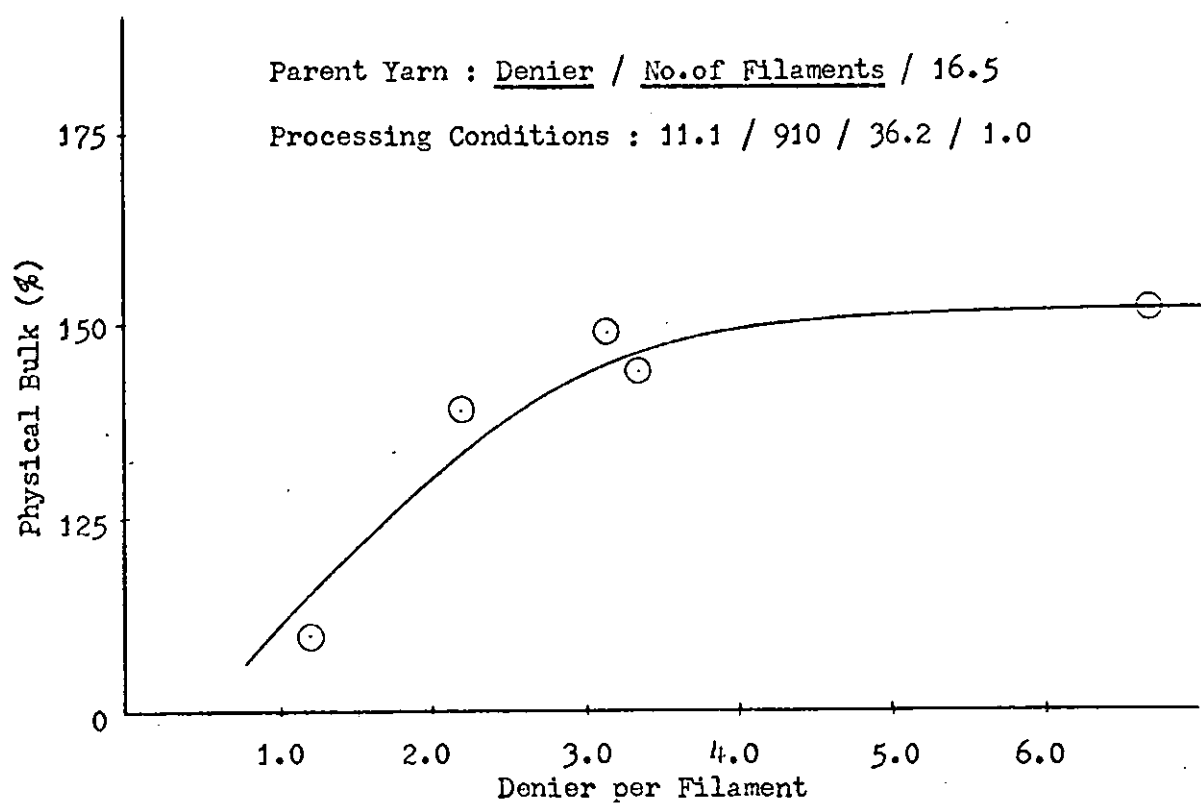


Fig. 6.12 Percentage Physical Bulk versus Parent Yarn Denier per Filament

6.6 Water Absorption Test

The difficulty in maintaining a constant winding tension during the manufacture of bulked yarn packages for the physical bulk test suggested that some alternative method of assessing the bulk should be found. Thus a method was devised for the purpose (see Fig. 6.13).

Briefly the method consists of passing the yarn under constant tension and speed through a water bath, so that water is absorbed by the looped filament yarn structure and is carried away with the running yarn. The procedure for this method is described as follows:

- a) The water bath is weighed when it is filled with water.
- b) 400 yards of yarn is allowed to pass through the bath at a speed of 40 yards/min, under a 0.1 g/den tension (measured at the output).
- c) The water bath again is weighed to ascertain the amount of water absorbed by the yarn. The same method was used for both parent and bulked yarns and the following equation was used:

$$\text{Increase in water absorption \%} = \frac{W_b - W_p}{W_p} \times 100$$

where, W_b = weight of water absorbed by the bulked yarn (g) and

W_p = weight of water absorbed by the parent yarn (g).

6.6.1 Results

The calculated increase in water absorption percentages are tabulated in Tables 6.14 to 6.18 and are shown graphically in Figs. 6.14 to 6.19. Table 6.19 shows the parent yarns water absorption, W_p which were used to calculate the increase in water absorption percentage values.

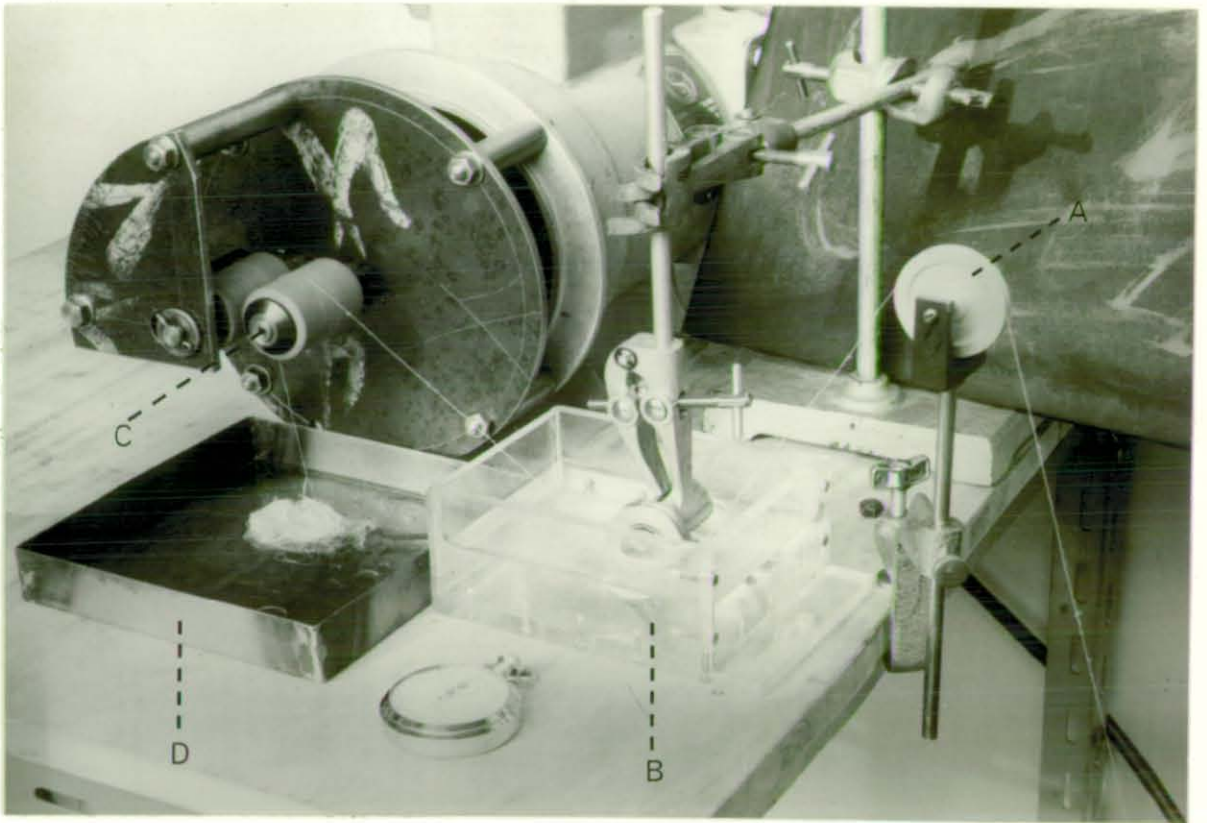


Fig. 6.13 Water Absorption Test Apparatus

A- Yarn Guide Roller

B- Water Bath

C- Yarn Take-up Mechanism

D- Yarn Collection Bin

TABLE 6.14 Percentage Water Absorption Test at Varying Overfeed

Parent Yarn	Processing Conditions	W_b (g)	Increase in Water Abs. (%)
107 / 34 / 16.5	<u>2.56</u> / 910 / 36.2 / 1.0	3.850	226
107 / 34 / 16.5	<u>5.26</u> / 910 / 36.2 / 1.0	9.000	662
107 / 34 / 16.5	<u>8.10</u> / 910 / 36.2 / 1.0	12.800	985
107 / 34 / 16.5	<u>11.10</u> / 910 / 36.2 / 1.0	17.800	1408
107 / 34 / 16.5	<u>14.30</u> / 910 / 36.2 / 1.0	23.550	1896
107 / 34 / 16.5	<u>17.65</u> / 910 / 36.2 / 1.0	27.300	2214

TABLE 6.15 Percentage Water Absorption Test at Varying Bulking Zone Length

Parent Yarn	Processing Conditions	W_b (g)	Increase in Water Abs. (%)
107 / 34 / 16.5	11.1 / 910 / 36.2 / <u>0.6</u>	13.800	1069
107 / 34 / 16.5	11.1 / 910 / 36.2 / <u>0.7</u>	13.600	1053
107 / 34 / 16.5	11.1 / 910 / 36.2 / <u>0.8</u>	17.100	1349
107 / 34 / 16.5	11.1 / 910 / 36.2 / <u>0.9</u>	17.600	1392
107 / 34 / 16.5	11.1 / 910 / 36.2 / <u>1.0</u>	17.800	1408
107 / 34 / 16.5	11.1 / 910 / 36.2 / <u>1.1</u>	19.700	1569
107 / 34 / 16.5	11.1 / 910 / 36.2 / <u>1.2</u>	19.150	1523
107 / 34 / 16.5	11.1 / 910 / 36.2 / <u>1.3</u>	18.850	1497
107 / 34 / 16.5	11.1 / 910 / 36.2 / <u>1.4</u>	16.730	1318

TABLE 6.16 Percentage Water Absorption Test at Varying % Extra Untwisting

Parent Yarn	Processing Conditions	W_b (g)	Increase in Water Abs. (%)
107 / 34 / 16.5	11.1 / <u>803</u> / <u>20.2</u> / 1.0	20.920	1673
107 / 34 / 16.5	11.1 / <u>825</u> / <u>23.5</u> / 1.0	20.000	1595
107 / 34 / 16.5	11.1 / <u>850</u> / <u>27.2</u> / 1.0	17.620	1393
107 / 34 / 16.5	11.1 / <u>885</u> / <u>32.5</u> / 1.0	16.900	1332
107 / 34 / 16.5	11.1 / <u>910</u> / <u>36.2</u> / 1.0	17.800	1408
107 / 34 / 16.5	11.1 / <u>931</u> / <u>39.4</u> / 1.0	14.200	1103
107 / 34 / 16.5	11.1 / <u>950</u> / <u>42.2</u> / 1.0	18.220	1444
107 / 34 / 16.5	11.1 / <u>977</u> / <u>46.3</u> / 1.0	14.620	1139
107 / 34 / 16.5	11.1 / <u>1007</u> / <u>50.7</u> / 1.0	14.650	1142

TABLE 6.17 Percentage Water Absorption Test at Varying Parent Yarn Twist

Parent Yarn	Processing Conditions	W_b (g)	Increase in Water Abs. (%)
107 / 34 / <u>11.0</u>	11.1 / <u>607</u> / 36.2 / 1.0	21.080	1687
107 / 34 / <u>13.7</u>	11.1 / <u>758</u> / 36.2 / 1.0	20.250	1616
107 / 34 / <u>16.5</u>	11.1 / <u>910</u> / 36.2 / 1.0	17.800	1408
107 / 34 / <u>19.2</u>	11.1 / <u>1062</u> / 36.2 / 1.0	18.720	1486
107 / 34 / <u>22.0</u>	11.1 / <u>1213</u> / 36.2 / 1.0	15.610	1223
107 / 34 / <u>24.7</u>	11.1 / <u>1362</u> / 36.2 / 1.0	14.070	1093
107 / 34 / <u>27.5</u>	11.1 / <u>1517</u> / 36.2 / 1.0	13.000	1002

TABLE 6.18 Percentage Water Absorption Test at Varying Parent Yarn Denier and No.of Filaments

Parent Yarn	Processing Conditions	W_b (g)	Increase in Water Abs. (%)
<u>32</u> / <u>26</u> / 16.5	11.1 / 910 / 36.2 / 1.0	1.720	102
<u>75</u> / <u>34</u> / 16.5	11.1 / 910 / 36.2 / 1.0	11.250	1003
<u>107</u> / <u>34</u> / 16.5	11.1 / 910 / 36.2 / 1.0	17.800	1408
<u>165</u> / <u>50</u> / 16.5	11.1 / 910 / 36.2 / 1.0	32.850	1953
<u>227</u> / <u>34</u> / 16.5	11.1 / 910 / 36.2 / 1.0	51.950	2230

TABLE 6.19 Water Absorption of Parent Yarn

Parent Yarn	W_p (g)
107 / 34 / <u>11.0</u>	1.180
107 / 34 / <u>13.7</u>	1.180
107 / 34 / <u>16.5</u>	1.180
107 / 34 / <u>19.2</u>	1.180
107 / 34 / <u>22.0</u>	1.180
107 / 34 / <u>24.7</u>	1.180
107 / 34 / <u>27.5</u>	1.180
<u>32</u> / <u>26</u> / 16.5	0.850
<u>75</u> / <u>34</u> / 16.5	1.020
<u>165</u> / <u>50</u> / 16.5	1.600
<u>227</u> / <u>34</u> / 16.5	2.230

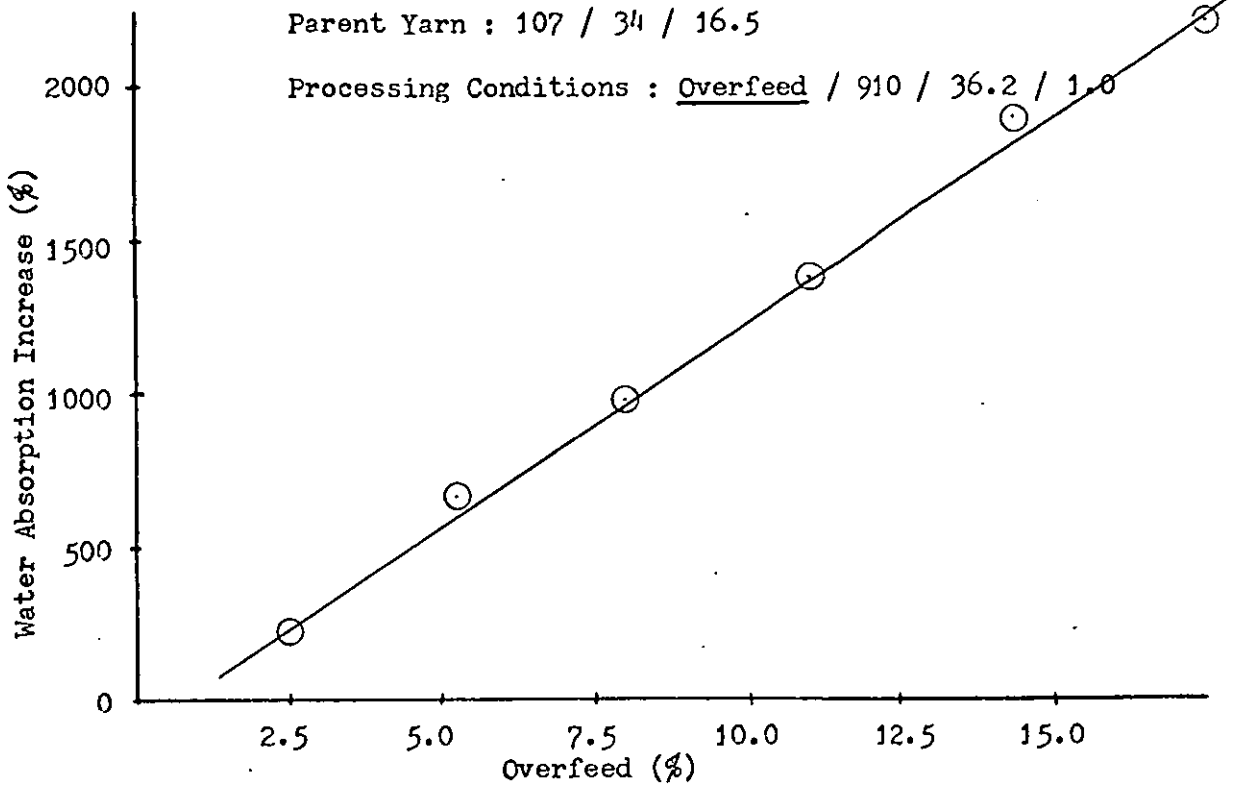


Fig. 6.14 Percentage Water Absorption Increase versus Percentage Overfeed

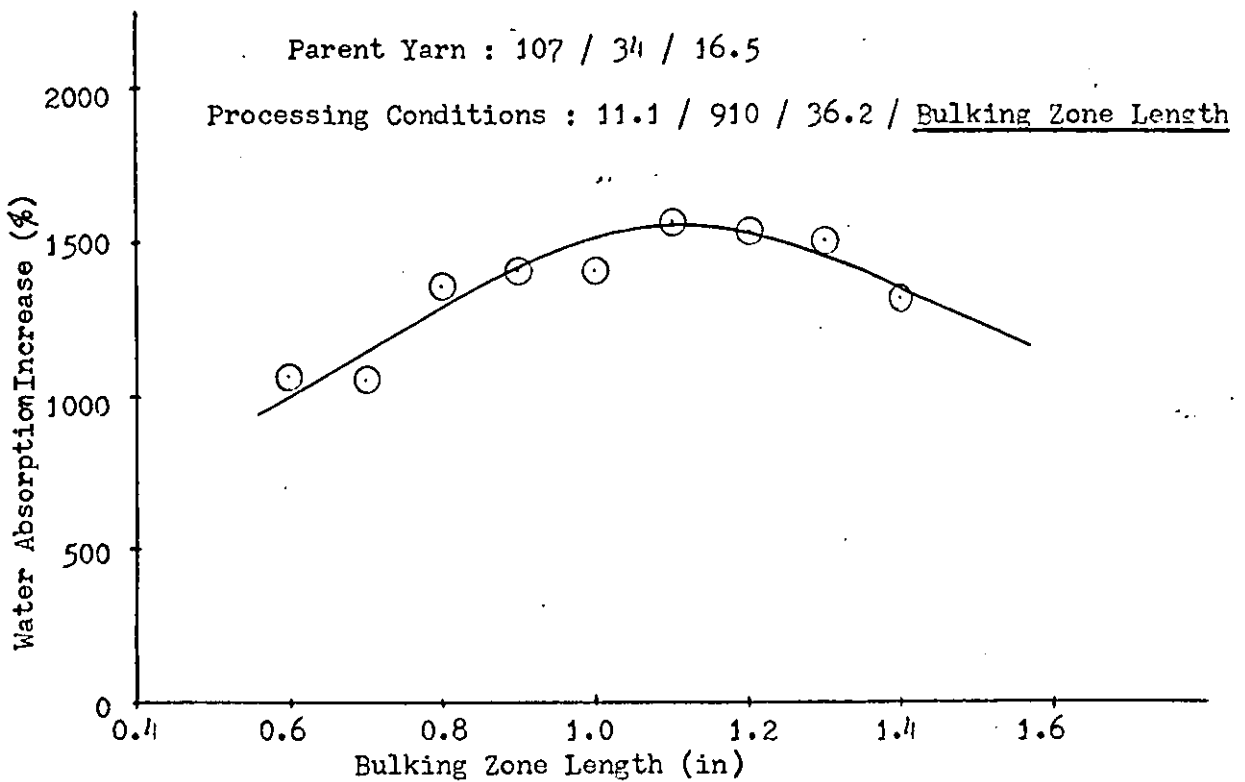


Fig. 6.15 Percentage Water Absorption Increase versus Bulking Zone Length

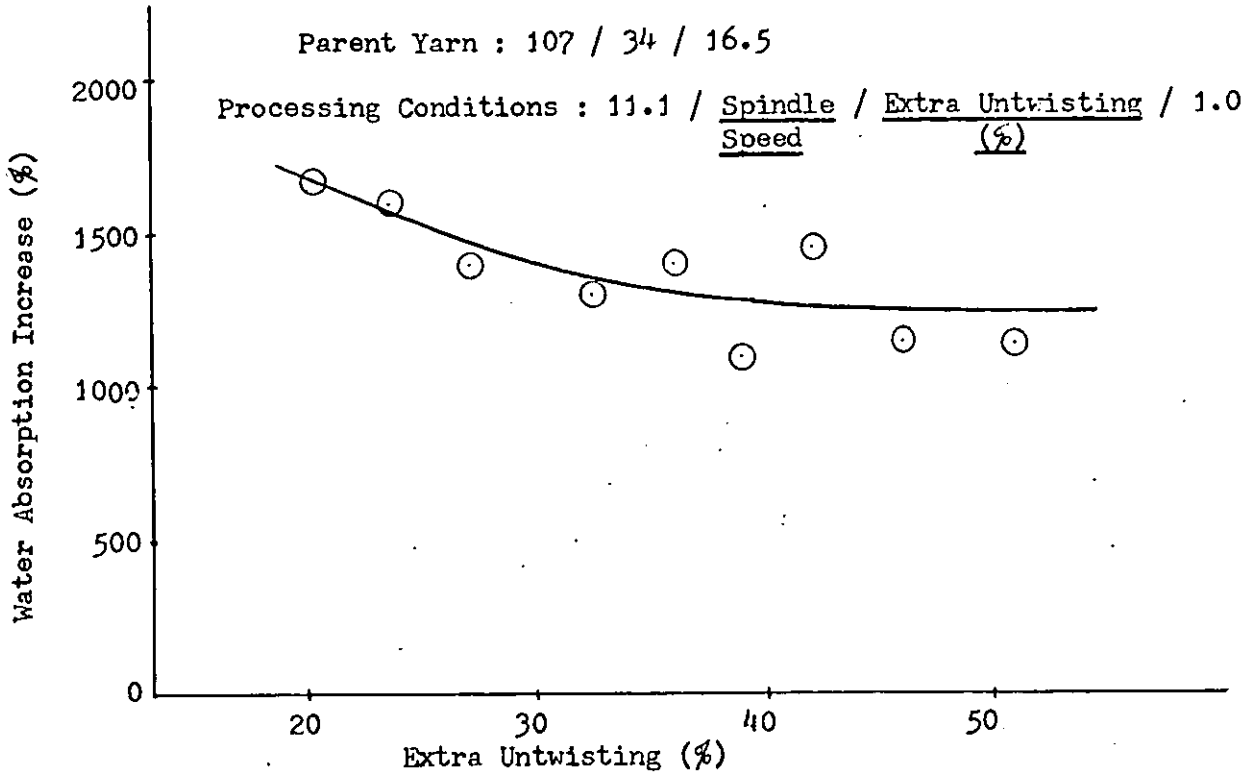


Fig. 6.16 Percentage Water Absorption Increase versus Extra Untwisting (%)

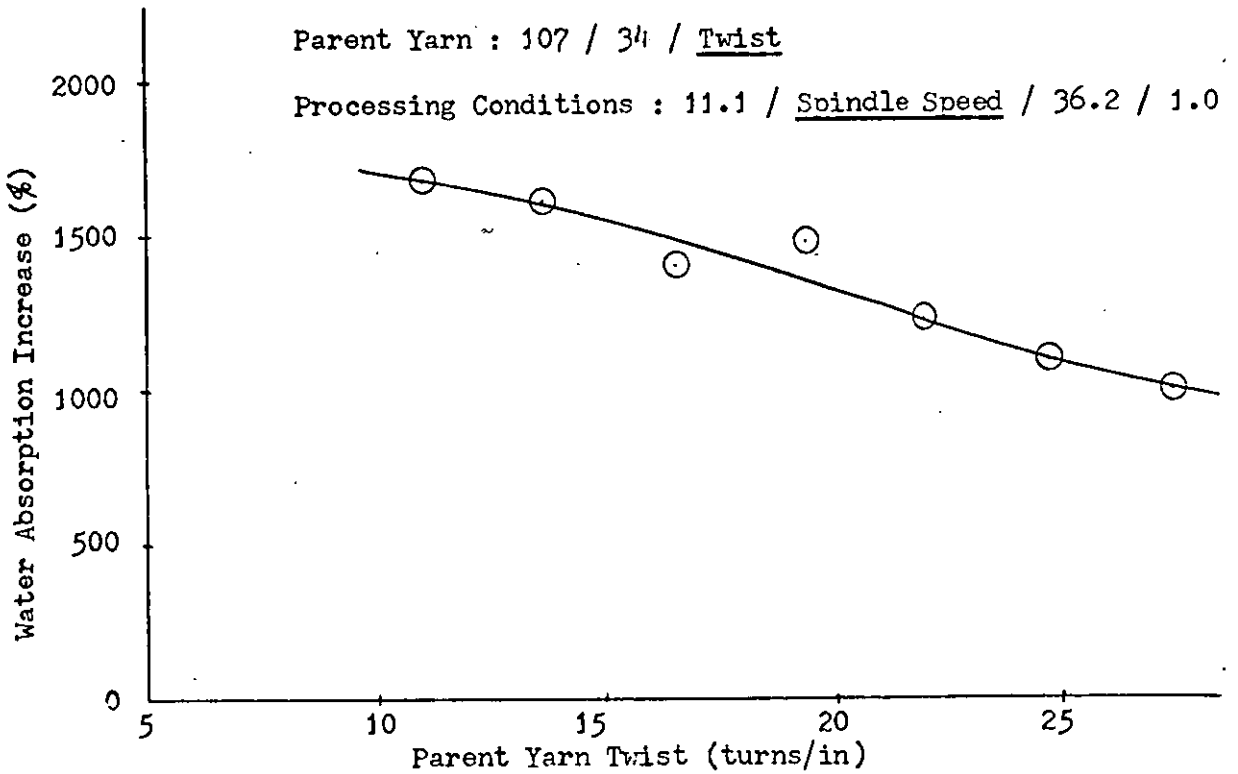


Fig. 6.17 Percentage Water Absorption Increase versus Parent Yarn Twist

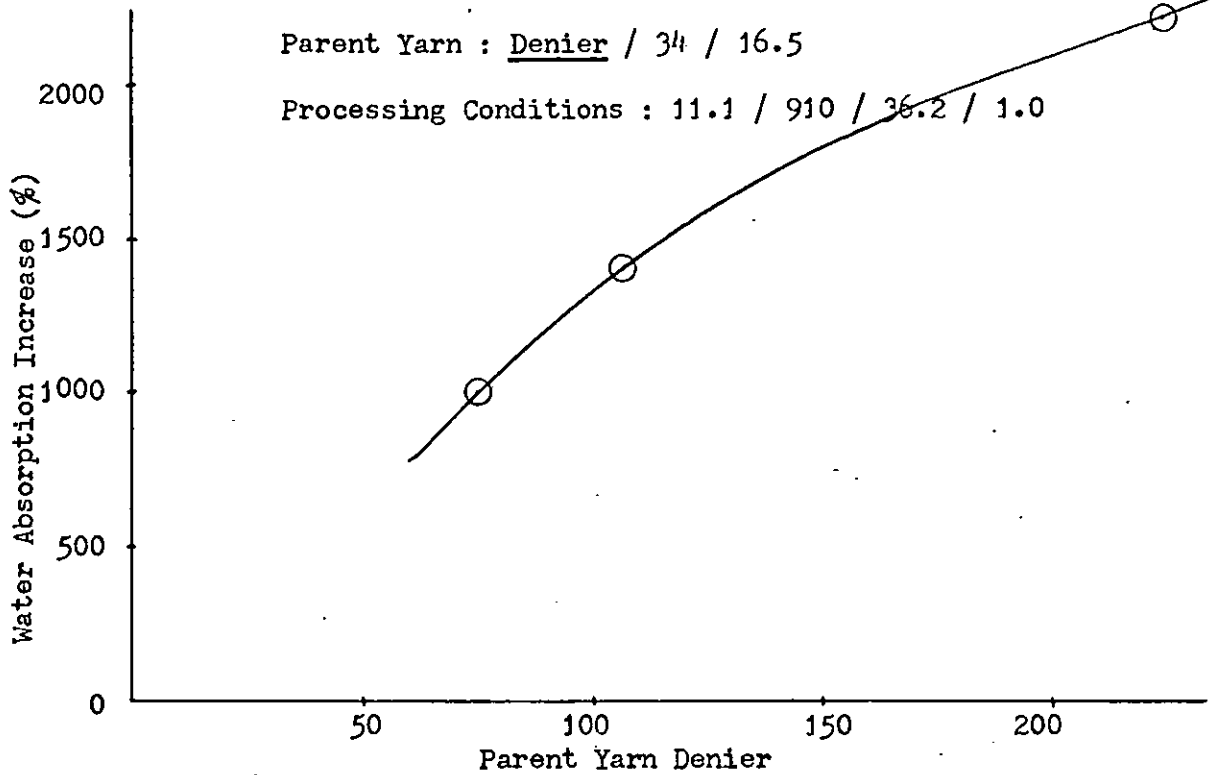


Fig. 6.18 Percentage Water Absorption Increase versus Parent Yarn Denier

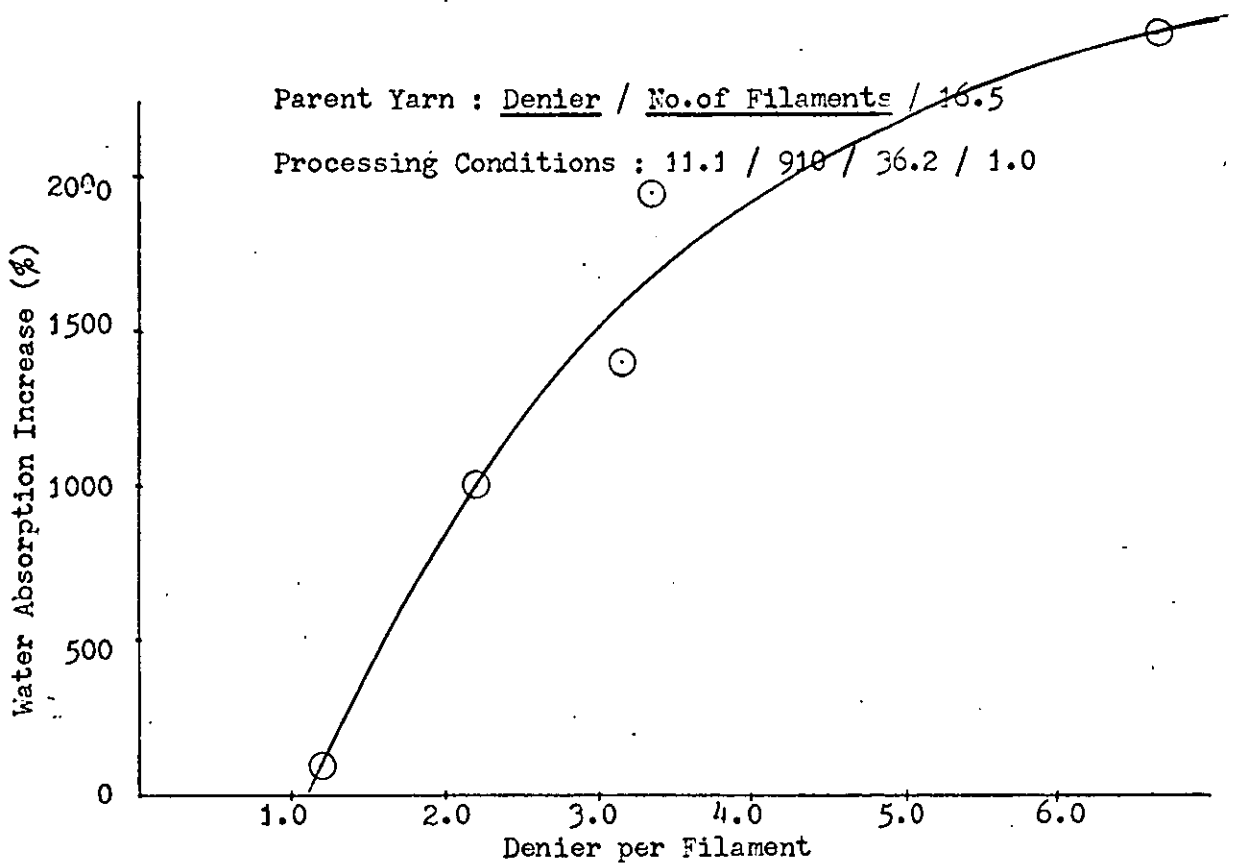


Fig. 6.19 Percentage Water Absorption Increase versus Parent Yarn Denier per Filament

6.7 Tensile Testing

Monsanto Textiles Ltd., Leicester, kindly allowed the author to use an Instron tensile testing instrument to obtain the breaking load-elongation curves. This instrument has several interchangeable load cells containing strain gauges. The load cell is located centrally in the fixed upper cross head, and the sample yarn to be tested is mounted between this fixed load cell and the traversing lower cross head, the rate of extension of the sample being controlled by the speed of the traversing cross head. The load cell output is fed to the control cabinet which houses the various electronic circuits and the pen recording equipment. The effect of extending the sample is to cause the pen to move across a chart a distance proportional to the tensile force applied to the sample, the chart also moving simultaneously to allow a load-elongation curve to be traced by the pen.

Ten graphs were obtained for each variable; a typical curve is shown in Fig. 6.20.

The tests were carried out under constant conditions as follows:

Room temperature	=	66°F
Humidity	=	64%
Traversing cross head speed	=	10 in/min
Chart Speed	=	10 in/min
Gauge length	=	10 in
Full scale load	=	1000 g

6.7.1 Results

From a careful assessment of the curves obtained, the breaking load, tenacity (specific strength) and breaking extension of each yarn type was calculated. These results are given in Tables 6.20 to 6.23 and are shown in Figs. 6.21 to 6.28. Table 6.24 shows the tensile properties of the parent yarns.

TABLE 6.20 Tensile Properties at Varying Overfeed

Parent Yarn	Processing Conditions	Breaking Load (g)	Tenacity (g/den.)	Breaking Extention (%)
107 / 34 / 16.5	<u>2.56</u> / 910 / 36.2 / 1.0	453.7	4.07	30.4
107 / 34 / 16.5	<u>5.26</u> / 910 / 36.2 / 1.0	355.3	3.15	18.6
107 / 34 / 16.5	<u>8.10</u> / 910 / 36.2 / 1.0	317.5	2.79	16.2
107 / 34 / 16.5	<u>11.10</u> / 910 / 36.2 / 1.0	304.3	2.62	18.2
107 / 34 / 16.5	<u>14.30</u> / 910 / 36.2 / 1.0	270.4	2.30	16.6
107 / 34 / 16.5	<u>17.65</u> / 910 / 36.2 / 1.0	254.2	2.12	18.7

TABLE 6.21 Tensile Properties at Varying Bulking Zone Length

Parent Yarn	Processing Conditions	Breaking Load (g)	Tenacity (g/den.)	Breaking Extention (%)
107 / 34 / 16.5	11.1 / 910 / 36.2 / <u>0.6</u>	295.3	2.61	16.3
107 / 34 / 16.5	11.1 / 910 / 36.2 / <u>0.7</u>	271.1	2.40	16.4
107 / 34 / 16.5	11.1 / 910 / 36.2 / <u>0.8</u>	259.3	2.28	14.8
107 / 34 / 16.5	11.1 / 910 / 36.2 / <u>0.9</u>	265.7	2.35	14.8
107 / 34 / 16.5	11.1 / 910 / 36.2 / <u>1.0</u>	304.3	2.62	18.2
107 / 34 / 16.5	11.1 / 910 / 36.2 / <u>1.1</u>	289.9	2.50	17.2
107 / 34 / 16.5	11.1 / 910 / 36.2 / <u>1.2</u>	274.6	2.37	16.9
107 / 34 / 16.5	11.1 / 910 / 36.2 / <u>1.3</u>	297.3	2.52	16.5
107 / 34 / 16.5	11.1 / 910 / 36.2 / <u>1.4</u>	278.4	2.37	16.6

TABLE 6.22 Tensile Properties at Varying % Extra Untwisting

Parent Yarn	Processing Conditions	Breaking Load (g)	Tenacity (g/den.)	Breaking Extention (%)
107 / 34 / 16.5	11.1 / <u>803</u> / <u>20.2</u> / 1.0	286.2	2.44	16.4
107 / 34 / 16.5	11.1 / <u>825</u> / <u>23.5</u> / 1.0	271.3	2.33	17.5
107 / 34 / 16.5	11.1 / <u>850</u> / <u>27.2</u> / 1.0	313.4	2.72	18.9
107 / 34 / 16.5	11.1 / <u>885</u> / <u>32.5</u> / 1.0	280.3	2.43	18.0
107 / 34 / 16.5	11.1 / <u>910</u> / <u>36.2</u> / 1.0	304.3	2.62	18.2
107 / 34 / 16.5	11.1 / <u>931</u> / <u>39.4</u> / 1.0	278.6	2.45	17.3
107 / 34 / 16.5	11.1 / <u>950</u> / <u>42.2</u> / 1.0	278.8	2.40	16.3
107 / 34 / 16.5	11.1 / <u>977</u> / <u>46.3</u> / 1.0	260.9	2.27	15.0
107 / 34 / 16.5	11.1 / <u>1007</u> / <u>50.7</u> / 1.0	287.8	2.47	16.5

TABLE 6.23 Tensile Properties at Varying Parent Yarn Twist

Parent Yarn	Processing Conditions	Breaking Load (g)	Tenacity (g/den.)	Breaking Extention (%)
107 / 34 / <u>11.0</u>	11.1 / <u>607</u> / 36.2 / 1.0	305.0	2.64	21.2
107 / 34 / <u>13.7</u>	11.1 / <u>758</u> / 36.2 / 1.0	283.6	2.40	18.8
107 / 34 / <u>16.5</u>	11.1 / <u>910</u> / 36.2 / 1.0	304.3	2.62	18.2
107 / 34 / <u>19.2</u>	11.1 / <u>1067</u> / 36.2 / 1.0	285.0	2.39	16.2
107 / 34 / <u>22.0</u>	11.1 / <u>1213</u> / 36.2 / 1.0	266.5	2.27	14.2
107 / 34 / <u>24.7</u>	11.1 / <u>1362</u> / 36.2 / 1.0	250.2	2.13	14.1
107 / 34 / <u>27.5</u>	11.1 / <u>1517</u> / 36.2 / 1.0	247.2	2.10	13.9

TABLE 6.24 Tensile Properties of the Parent Yarns at Varying Parent Yarn Twist

Parent Yarn	Breaking Load (g)	Tenacity (g/den.)	Breaking Extention (%)
107 / 34 / <u>11.0</u>	544.3	5.10	38.2
107 / 34 / <u>13.7</u>	528.7	4.94	40.2
107 / 34 / <u>16.5</u>	541.2	5.06	40.5
107 / 34 / <u>19.2</u>	542.6	5.07	43.6
107 / 34 / <u>22.0</u>	536.8	5.02	44.7
107 / 34 / <u>24.7</u>	527.3	4.93	46.1
107 / 34 / <u>27.5</u>	528.8	4.94	43.7

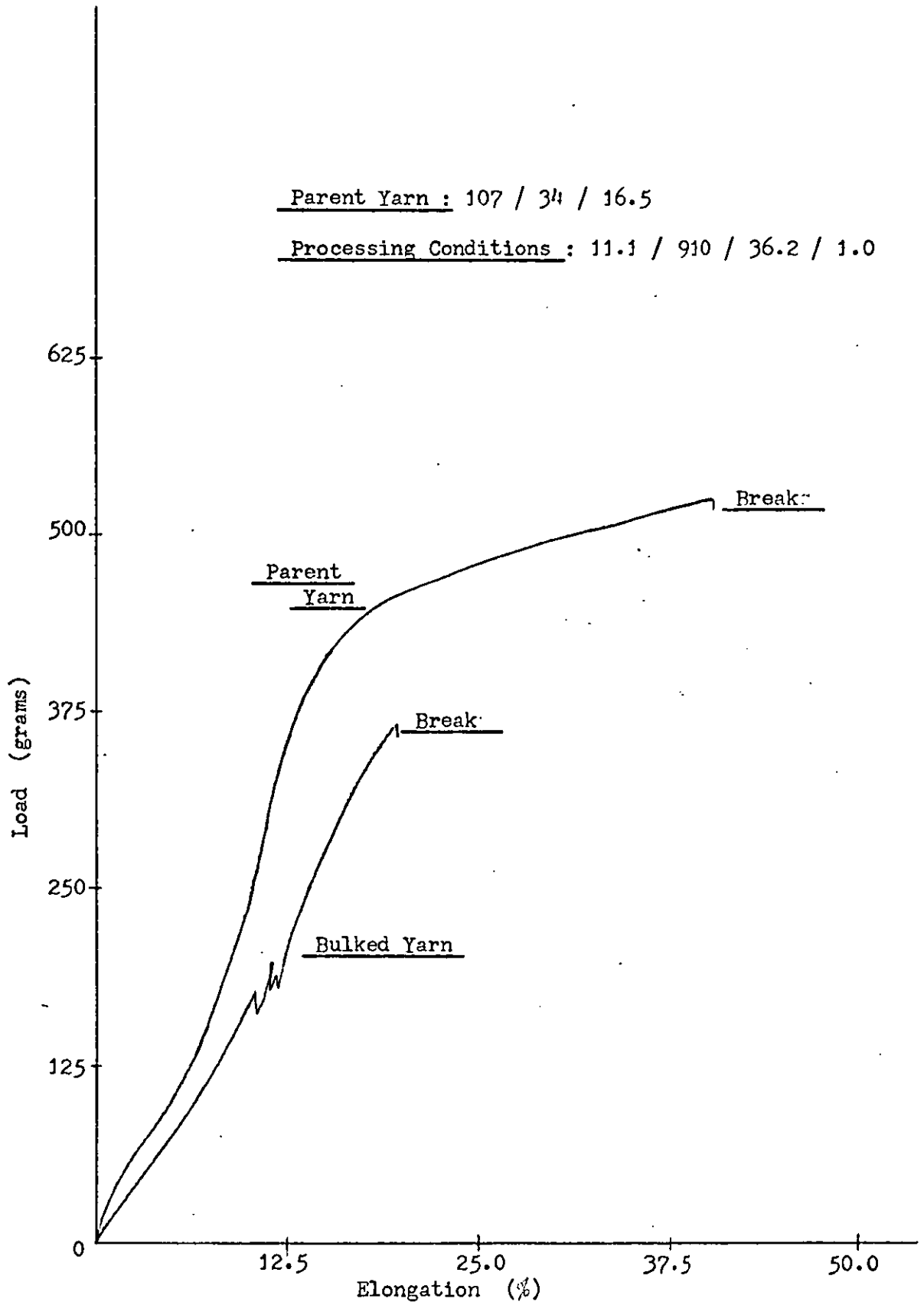


Fig. 6.20 Typical Load versus Elongation Curve for Mechanically Bulked Yarns

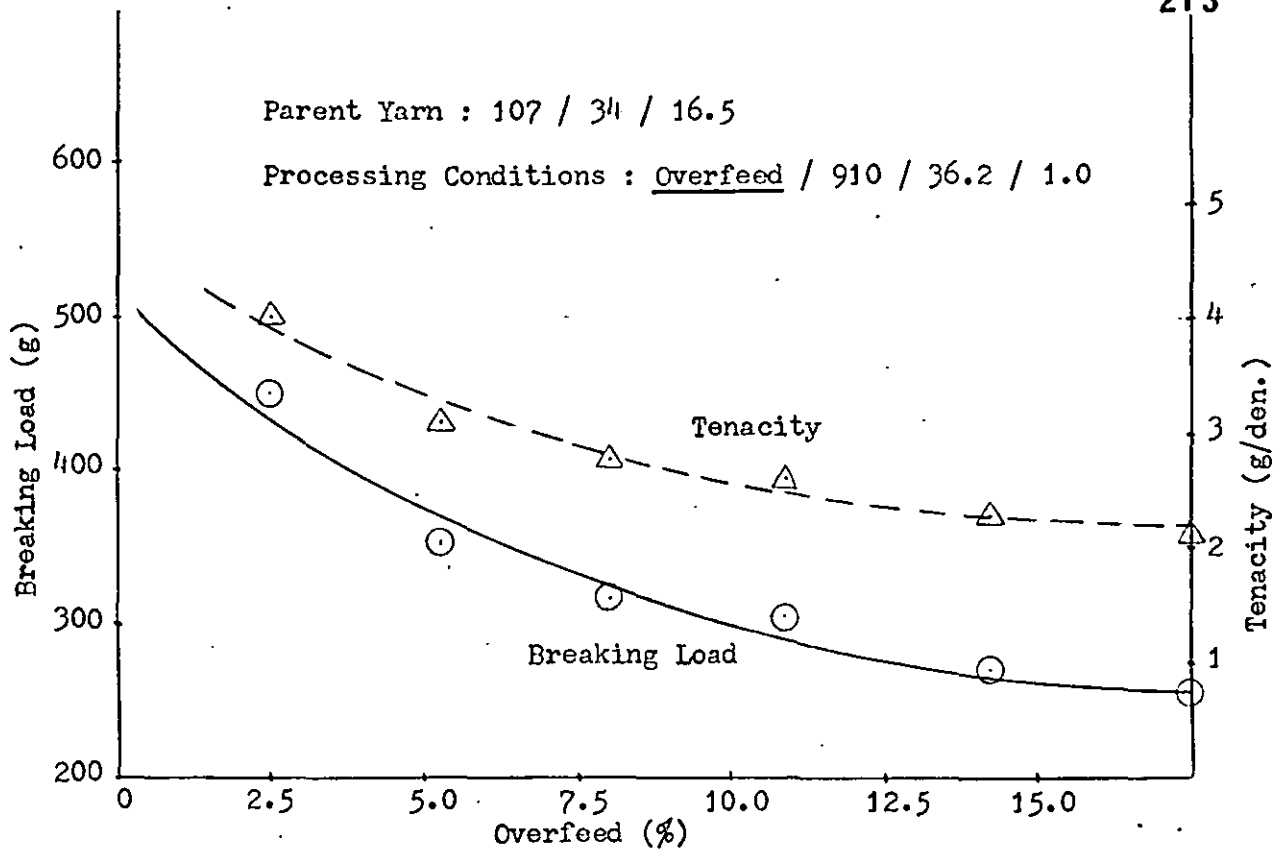


Fig. 6.6.21 Breaking Load and Tenacity versus Percentage Overfeed

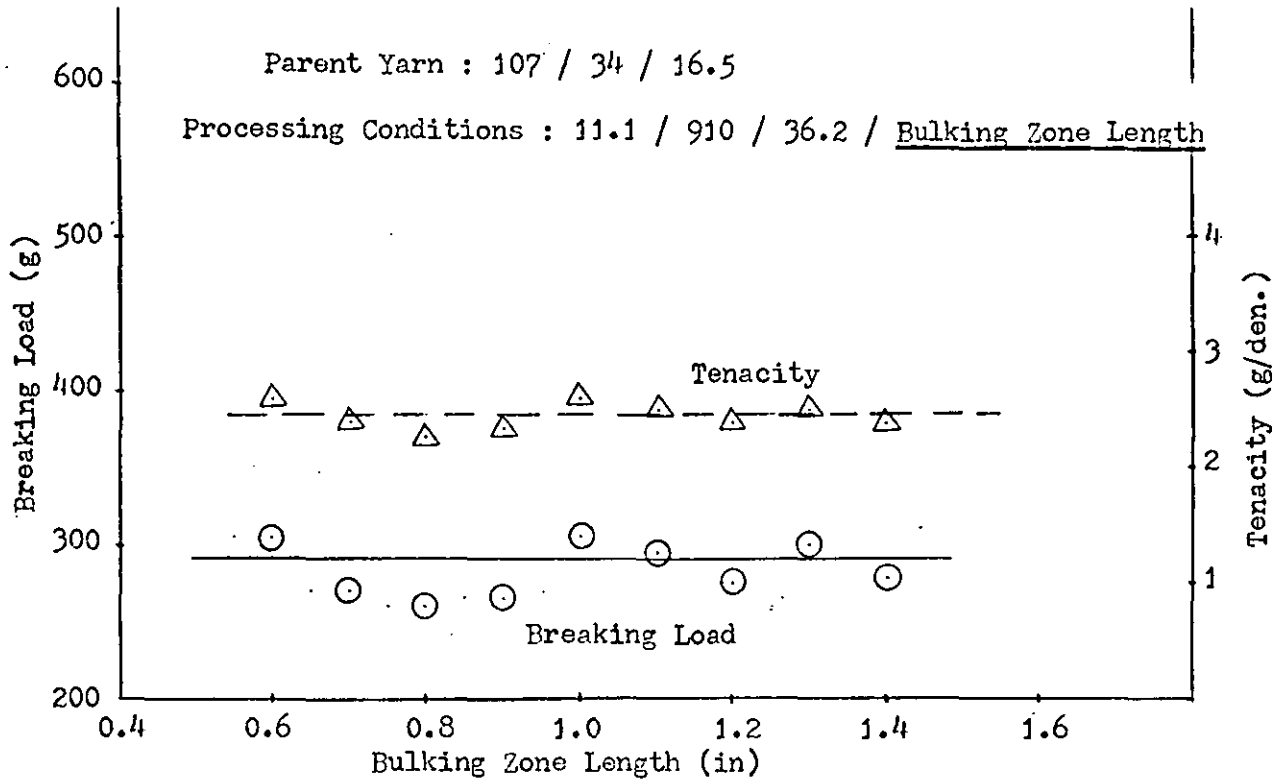


Fig. 6.22 Breaking Load and Tenacity versus Bulking Zone Length

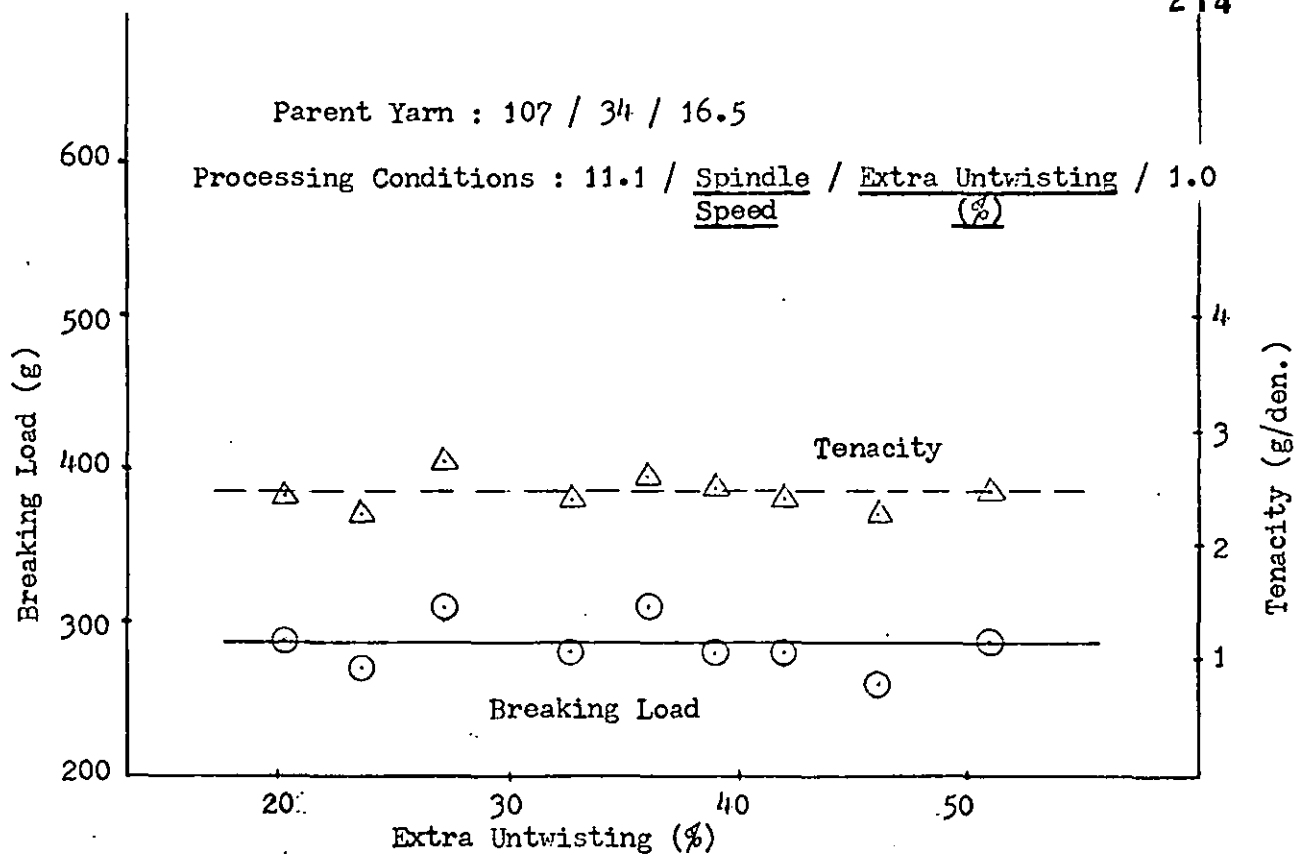


Fig. 6.23 Breaking Load and Tenacity versus Extra Untwisting (%)

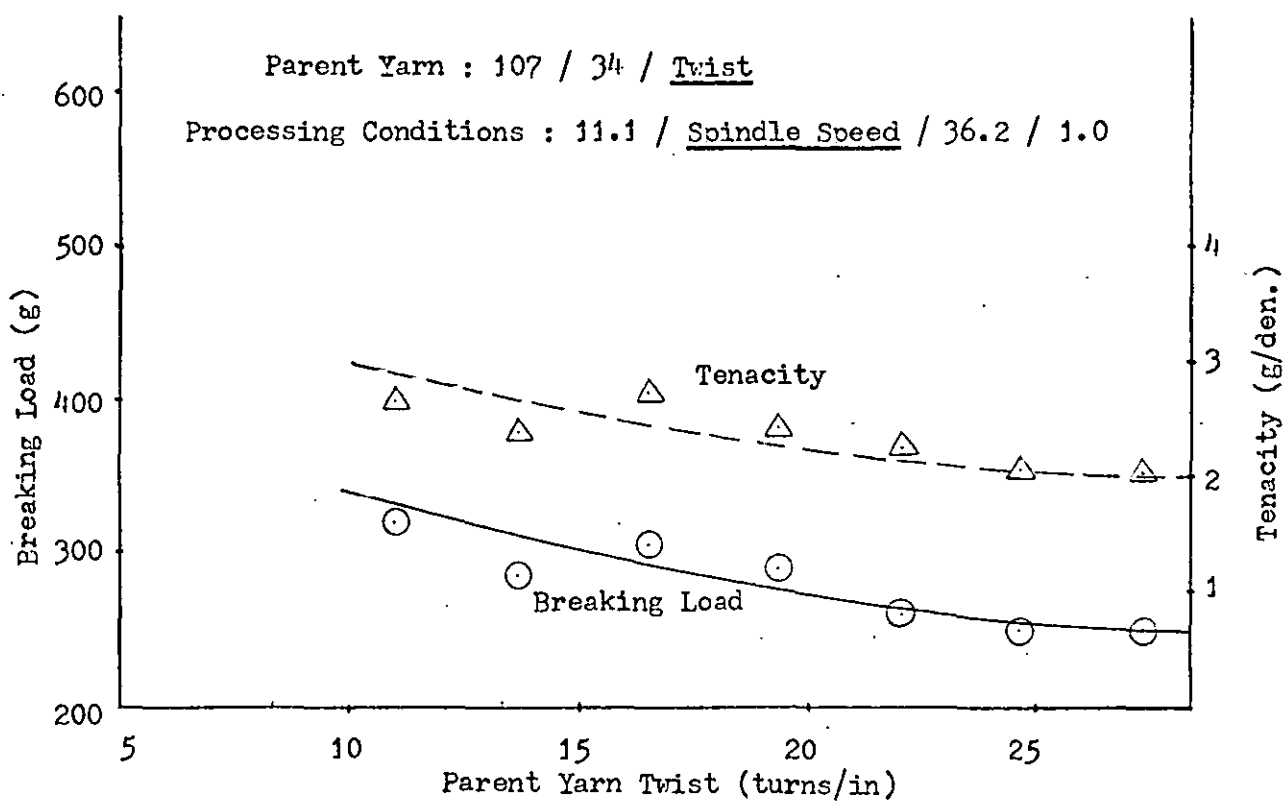


Fig. 6.24 Breaking Load and Tenacity versus Parent Yarn Twist

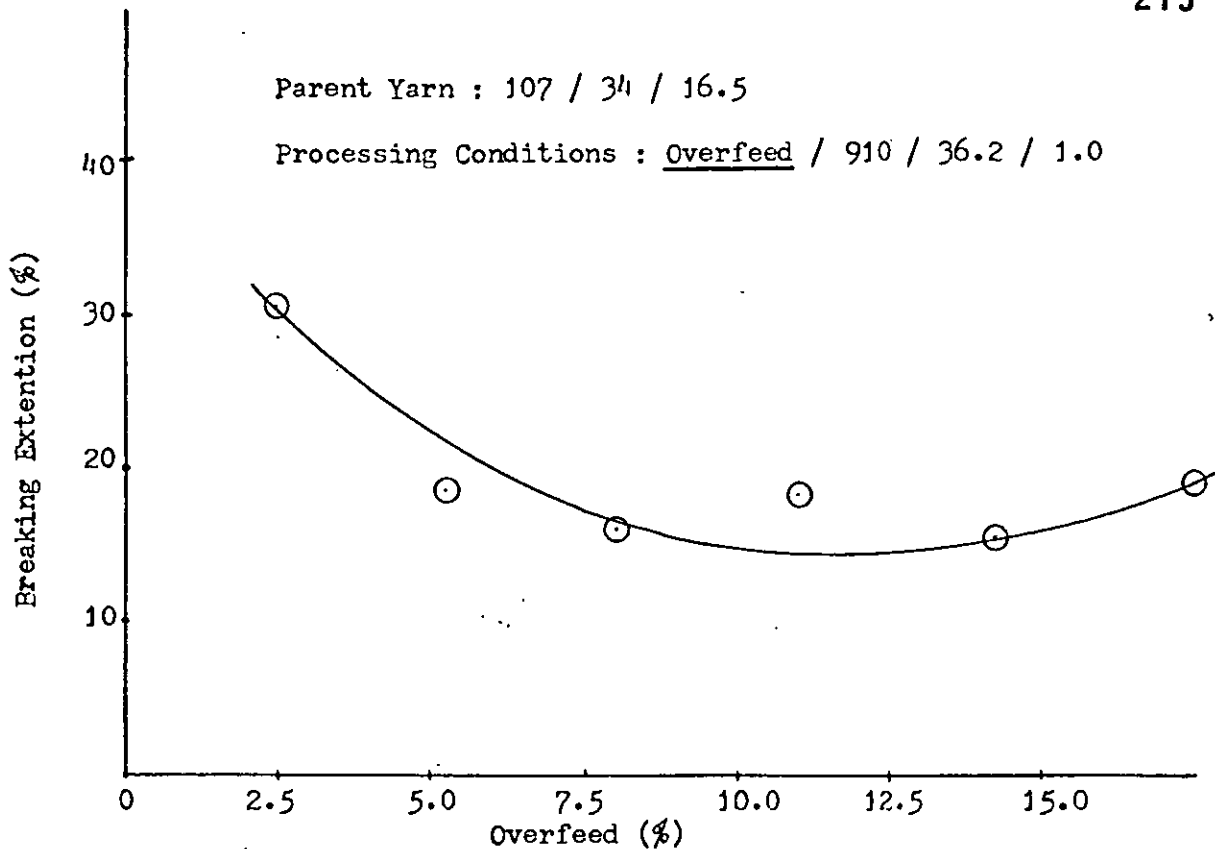


Fig. 6.25 Percentage Breaking Extension versus Percentage Overfeed

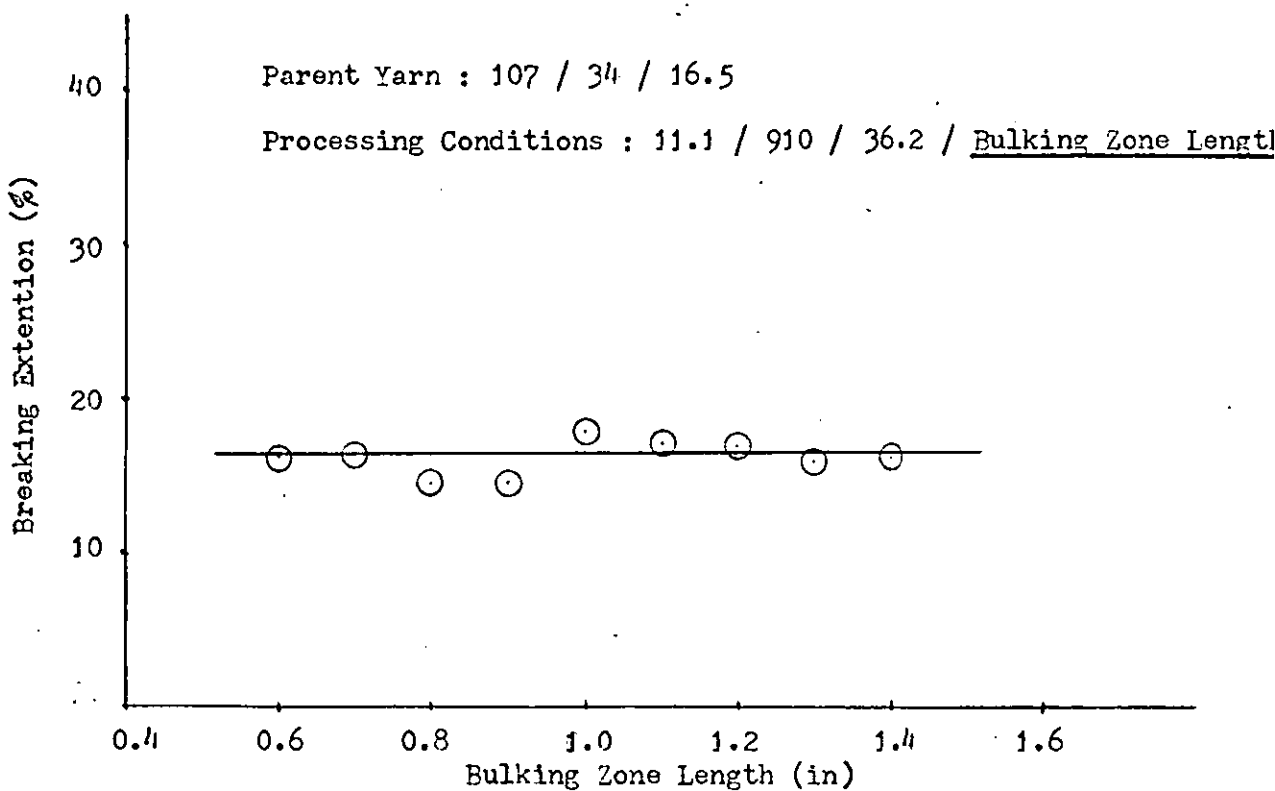


Fig. 6.26 Percentage Breaking Extension versus Bulking Zone Length

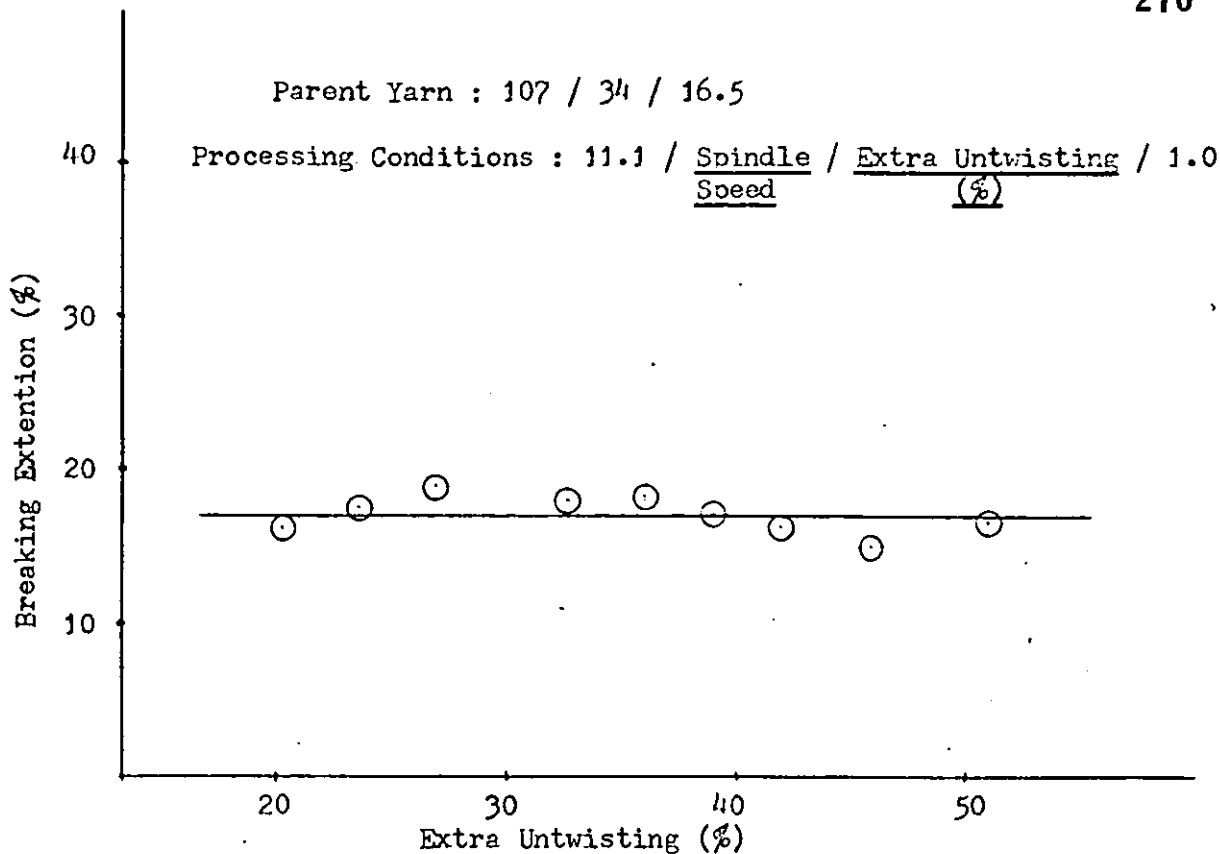


Fig. 6.27 Percentage Breaking Extension versus Extra Untwisting (%)

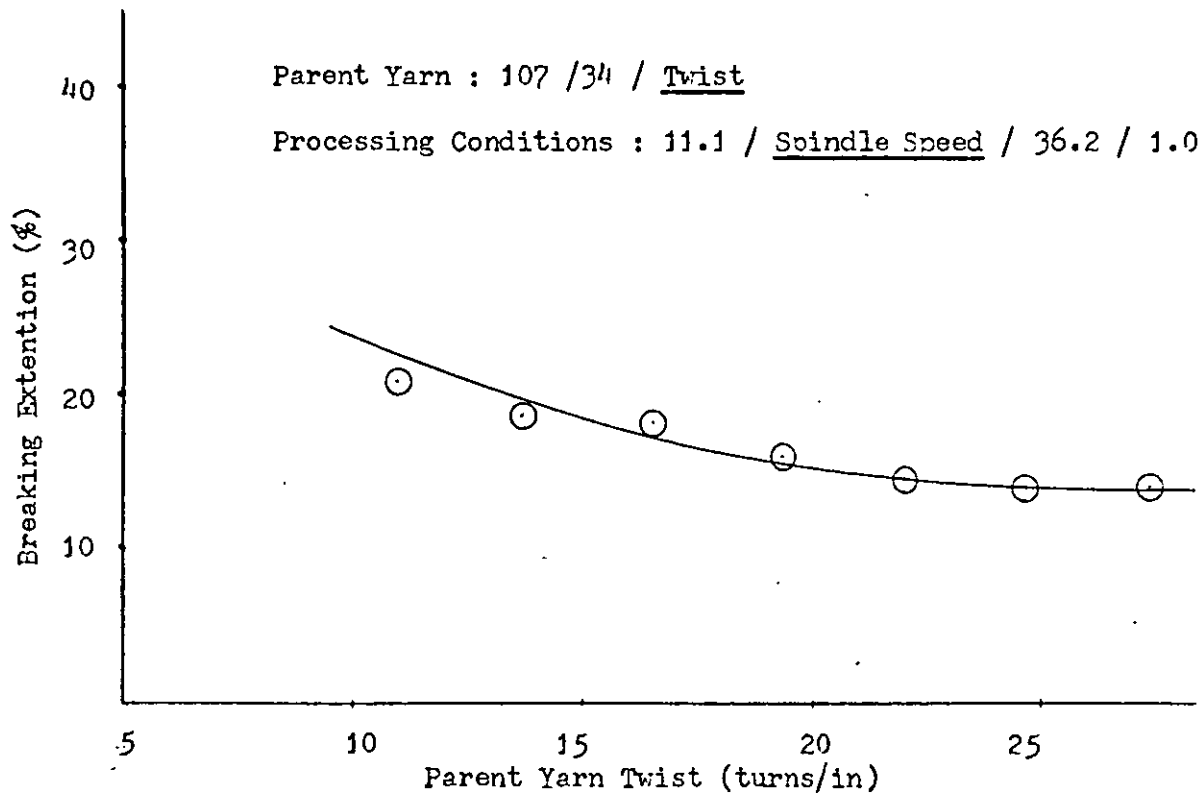


Fig. 6.28 Percentage Breaking Extension versus Parent Yarn Twist

6.8 Instability Test

A test for instability has been described by du Pont, and this has been referred to by Wray^(11,15). Its purpose is to determine the permanent increase in length of a bulked yarn under a load, and the method involves the use of a simple stability tester having a vertical board with a yarn clamp at the top. At a distance of 100 cm below this clamp is a marking notch, and below this is a small centimetre scale for the purpose of measuring the increase in length when weights are attached to the sample to be tested by means of a hook and weight holder. Wray tried to use this method in his earlier work and reported that the yarn tended to untwist under the effect of the loading and he observed that the extension of the yarn was not merely the removal of loops but also the removal of some twist from the yarn. Any attempt to impose a constraint on the yarn to prevent its untwisting, say by using a retort clamp against a flat portion of the hanging weight, would be interfering with the testing because of frictional contact. To overcome this inaccuracy in testing he adopted an alternative method by using the Instron tensile testing instrument in which the yarn is positively gripped at each end. This method was also used here and the procedure for it can be described as follows:

- a) Ten load-elongation curves were obtained for all the bulked yarn samples and the corresponding parent yarns.
- b) The extension of a particular yarn at a load corresponding to $\frac{1}{3}$ g/den (based on bulked yarn denier) was found, and an average of ten tests was taken in each case.
- c) If the extension percentage of the parent yarn and bulked yarn at $\frac{1}{3}$ g/den load are given by x_p and x_b respectively, then

$$\% \text{ Instability} = \frac{x_b - x_p}{100} \times (100 \text{ mm})\%$$

During the testing the conditions were maintained as follows:

Room temperature = 60°F
Humidity = 64%
Gauge length = 10 in
Cross head speed = 10 in/min
Chart speed = 10 in/min
Full scale load = 100 g.

Because the part of the curve nearest to the origin is the part to be used for the measurement of yarn instability, this portion of the curve was magnified in the load direction as provided for on the Instron machine.

6.8.1 Results

The calculated percentage instability results are tabulated in Tables 6.25 to 6.29 and are shown graphically in Fig. 6.29 to 6.34. Table 6.30 shows the percentage extension of the parent yarns and these values are used to calculate the percentage instability values.

TABLE 6.25 Percentage Instability at Varying Overfeed

Parent Yarn	Processing Conditions	\bar{x}_b (%)	Instability (%)
107 / 3 ⁴ / 16.5	<u>2.56</u> / 910 / 36.2 / 1.0	1.60	0.10
107 / 3 ⁴ / 16.5	<u>5.26</u> / 910 / 36.2 / 1.0	1.88	0.38
107 / 3 ⁴ / 16.5	<u>8.10</u> / 910 / 36.2 / 1.0	2.33	0.83
107 / 3 ⁴ / 16.5	<u>11.10</u> / 910 / 36.2 / 1.0	2.75	1.25
107 / 3 ⁴ / 16.5	<u>14.30</u> / 910 / 36.2 / 1.0	3.05	1.55
107 / 3 ⁴ / 16.5	<u>17.65</u> / 910 / 36.2 / 1.0	3.35	1.85

TABLE 6.26 Percentage Instability at Varying Bulking Zone Length

Parent Yarn	Processing Conditions	x_b (%)	Instability (%)
107 / 3 ⁴ / 16.5	11.1 / 910 / 36.2 / <u>0.6</u>	2.65	1.15
107 / 3 ⁴ / 16.5	11.1 / 910 / 36.2 / <u>0.7</u>	2.95	1.45
107 / 3 ⁴ / 16.5	11.1 / 910 / 36.2 / <u>0.8</u>	2.65	1.15
107 / 3 ⁴ / 16.5	11.1 / 910 / 36.2 / <u>0.9</u>	2.70	1.20
107 / 3 ⁴ / 16.5	11.1 / 910 / 36.2 / <u>1.0</u>	2.75	1.25
107 / 3 ⁴ / 16.5	11.1 / 910 / 36.2 / <u>1.1</u>	2.80	1.30
107 / 3 ⁴ / 16.5	11.1 / 910 / 36.2 / <u>1.2</u>	2.70	1.20
107 / 3 ⁴ / 16.5	11.1 / 910 / 36.2 / <u>1.3</u>	2.85	1.35
107 / 3 ⁴ / 16.5	11.1 / 910 / 36.2 / <u>1.4</u>	2.85	1.35

TABLE 6.27 Percentage Instability at Varying % Extra Untwisting

Parent Yarn	Processing Conditions	x_b (%)	Instability (%)
107 / 34 / 16.5	11.1 / <u>803</u> / <u>20.2</u> / 1.0	2.60	1.10
107 / 34 / 16.5	11.1 / <u>825</u> / <u>23.5</u> / 1.0	2.60	1.10
107 / 34 / 16.5	11.1 / <u>850</u> / <u>27.2</u> / 1.0	2.65	1.15
107 / 34 / 16.5	11.1 / <u>885</u> / <u>32.5</u> / 1.0	2.65	1.15
107 / 34 / 16.5	11.1 / <u>910</u> / <u>36.2</u> / 1.0	2.75	1.25
107 / 34 / 16.5	11.1 / <u>931</u> / <u>39.4</u> / 1.0	2.85	1.35
107 / 34 / 16.5	11.1 / <u>950</u> / <u>42.2</u> / 1.0	2.78	1.28
107 / 34 / 16.5	11.1 / <u>977</u> / <u>46.3</u> / 1.0	3.10	1.60
107 / 34 / 16.5	11.1 / <u>1007</u> / <u>50.7</u> / 1.0	3.05	1.55

TABLE 6.28 Percentage Instability at Varying Parent Yarn Twist

Parent Yarn	Processing Conditions	x_b (%)	Instability (%)
107 / 34 / <u>11.0</u>	11.1 / <u>607</u> / 36.2 / 1.0	2.72	1.72
107 / 34 / <u>13.7</u>	11.1 / <u>758</u> / 36.2 / 1.0	3.00	1.75
107 / 34 / <u>16.5</u>	11.1 / <u>910</u> / 36.2 / 1.0	2.75	1.25
107 / 34 / <u>19.2</u>	11.1 / <u>1062</u> / 36.2 / 1.0	2.50	0.90
107 / 34 / <u>22.0</u>	11.1 / <u>1213</u> / 36.2 / 1.0	2.75	1.12
107 / 34 / <u>24.7</u>	11.1 / <u>1362</u> / 36.2 / 1.0	2.65	0.95
107 / 34 / <u>27.5</u>	11.1 / <u>1517</u> / 36.2 / 1.0	2.80	1.05

TABLE 6.29 Percentage Instability at Varying at Varying Parent Yarn Denier and No.of Filaments

Parent Yarn	Processing Conditions	x_b (%)	Instability (%)
<u>32</u> / <u>26</u> / 16.5	11.1 / 910 / 36.2 / 1.0	1.55	0.30
<u>75</u> / <u>34</u> / 16.5	11.1 / 910 / 36.2 / 1.0	2.35	0.95
<u>107</u> / <u>34</u> / 16.5	11.1 / 910 / 36.2 / 1.0	2.75	1.25
<u>165</u> / <u>50</u> / 16.5	11.1 / 910 / 36.2 / 1.0	2.58	0.98
<u>227</u> / <u>34</u> / 16.5	11.1 / 910 / 36.2 / 1.0	2.82	1.20

TABLE 6.30 Percentage Extention of the Parent Yarns

Parent Yarn	x_p (%)
107 / 34 / <u>11.0</u>	1.00
107 / 34 / <u>13.7</u>	1.25
107 / 34 / <u>16.5</u>	1.50
107 / 34 / <u>19.2</u>	1.60
107 / 34 / <u>22.0</u>	1.63
107 / 34 / <u>24.7</u>	1.70
107 / 34 / <u>27.5</u>	1.75
<u>32</u> / <u>26</u> / 16.5	1.25
<u>75</u> / <u>34</u> / 16.5	1.40
<u>165</u> / <u>50</u> / 16.5	1.60
<u>227</u> / <u>34</u> / 16.5	1.62

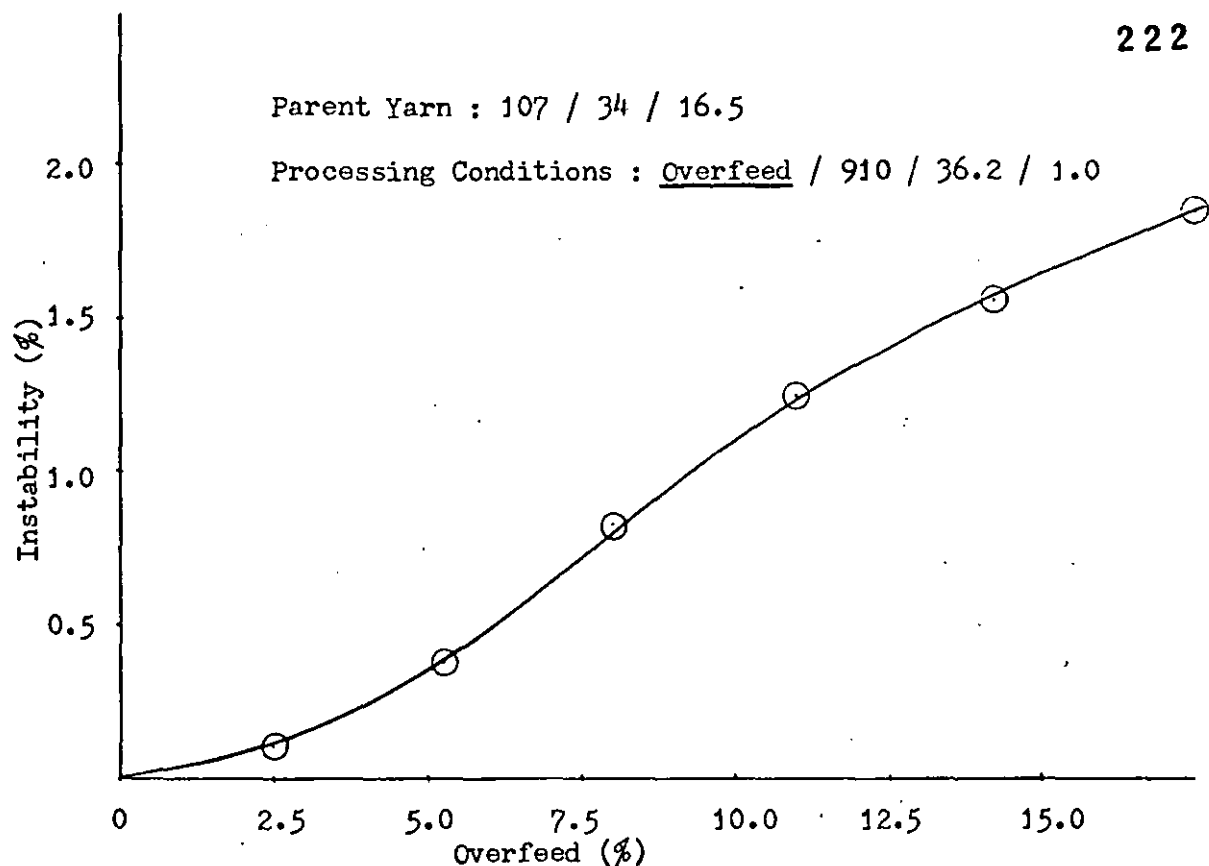


Fig. 6.29 Percentage Instability versus Percentage Overfeed

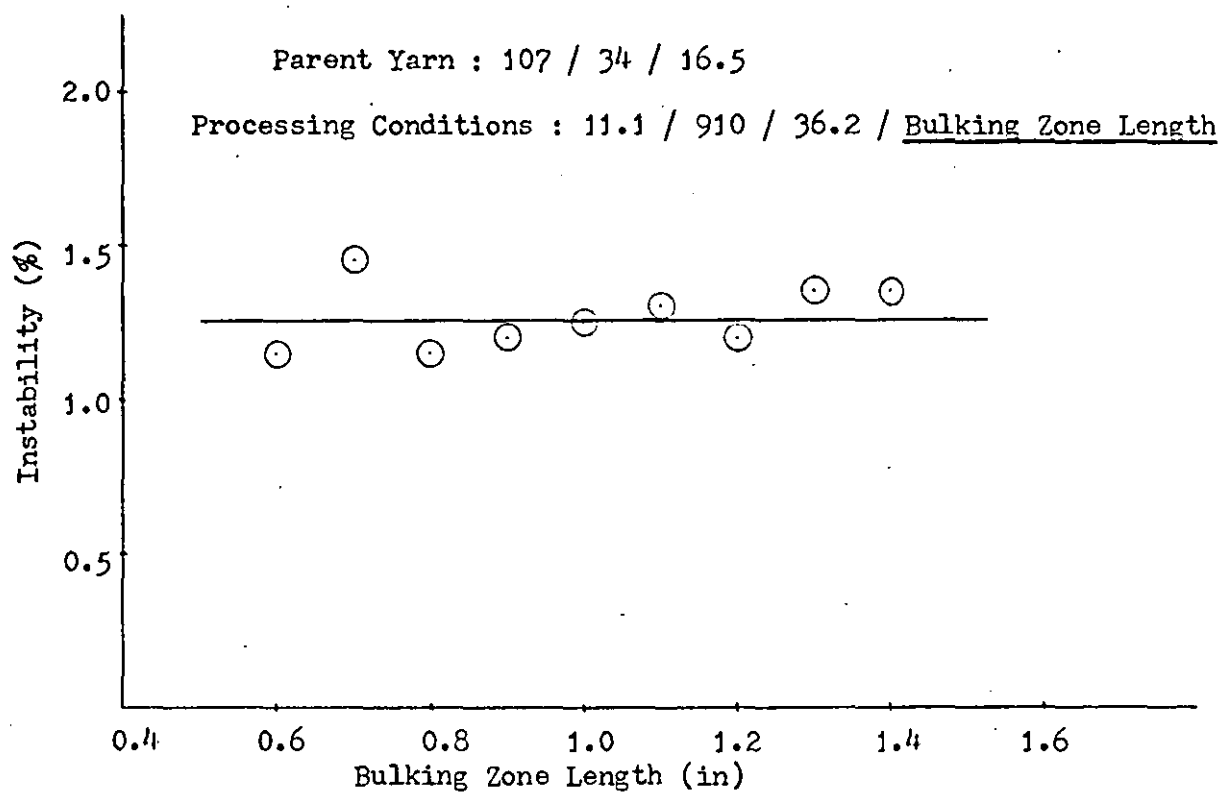


Fig. 6.30 Percentage Instability versus Bulking Zone Length

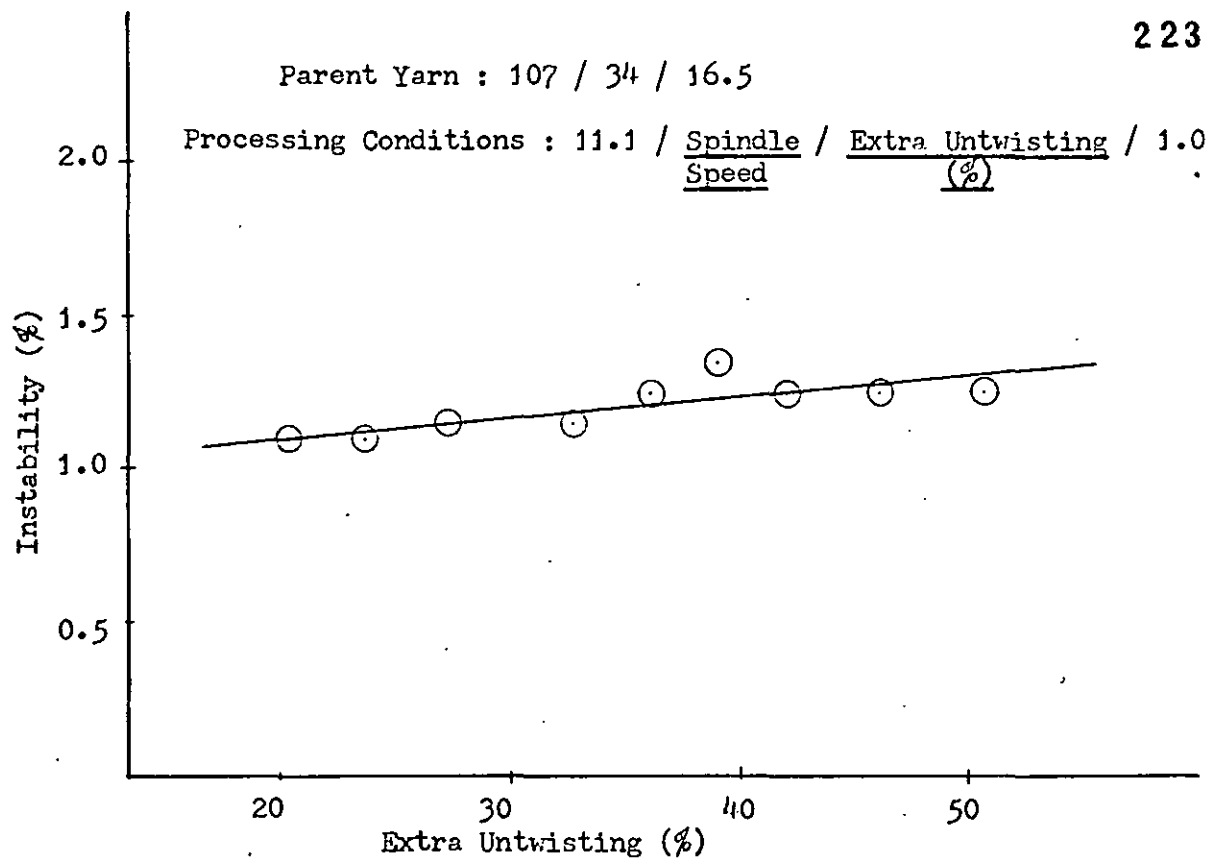


Fig. 6.31 Percentage Instability versus Extra Untwisting (%)

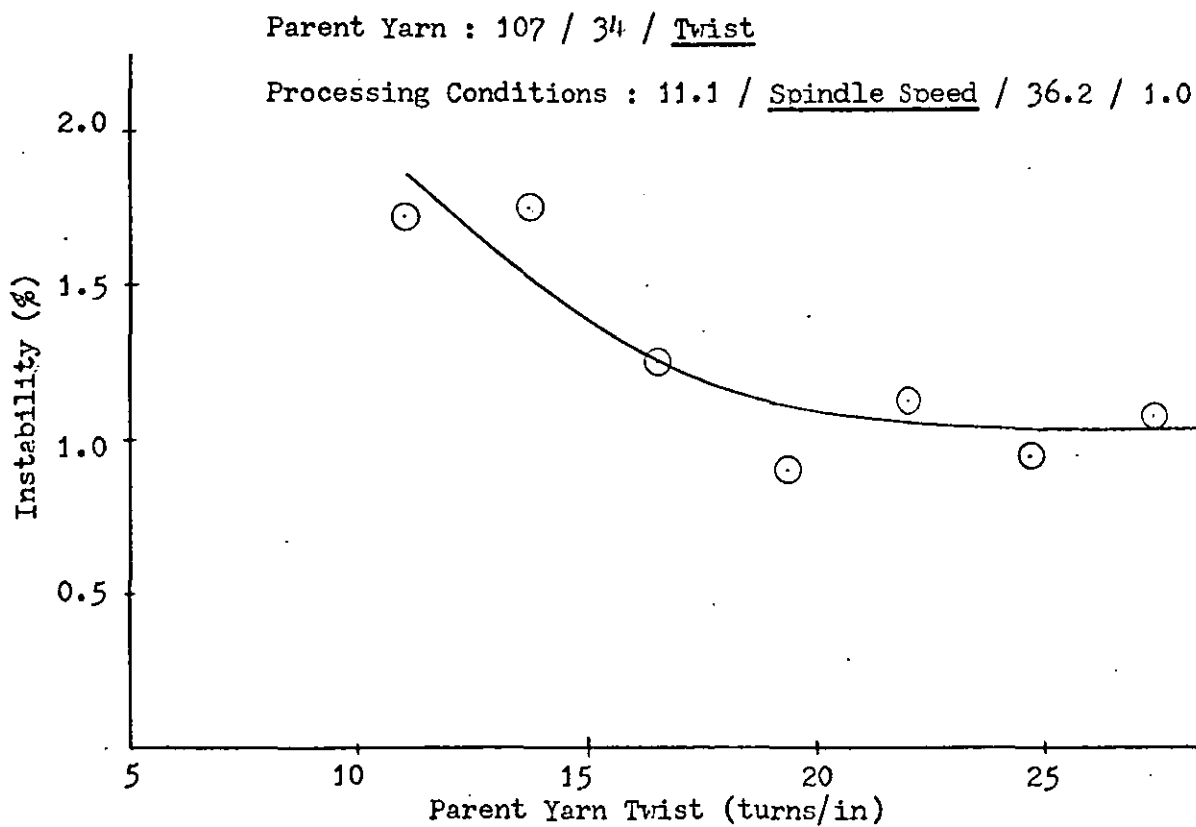


Fig. 6.32 Percentage Instability versus Parent Yarn Twist

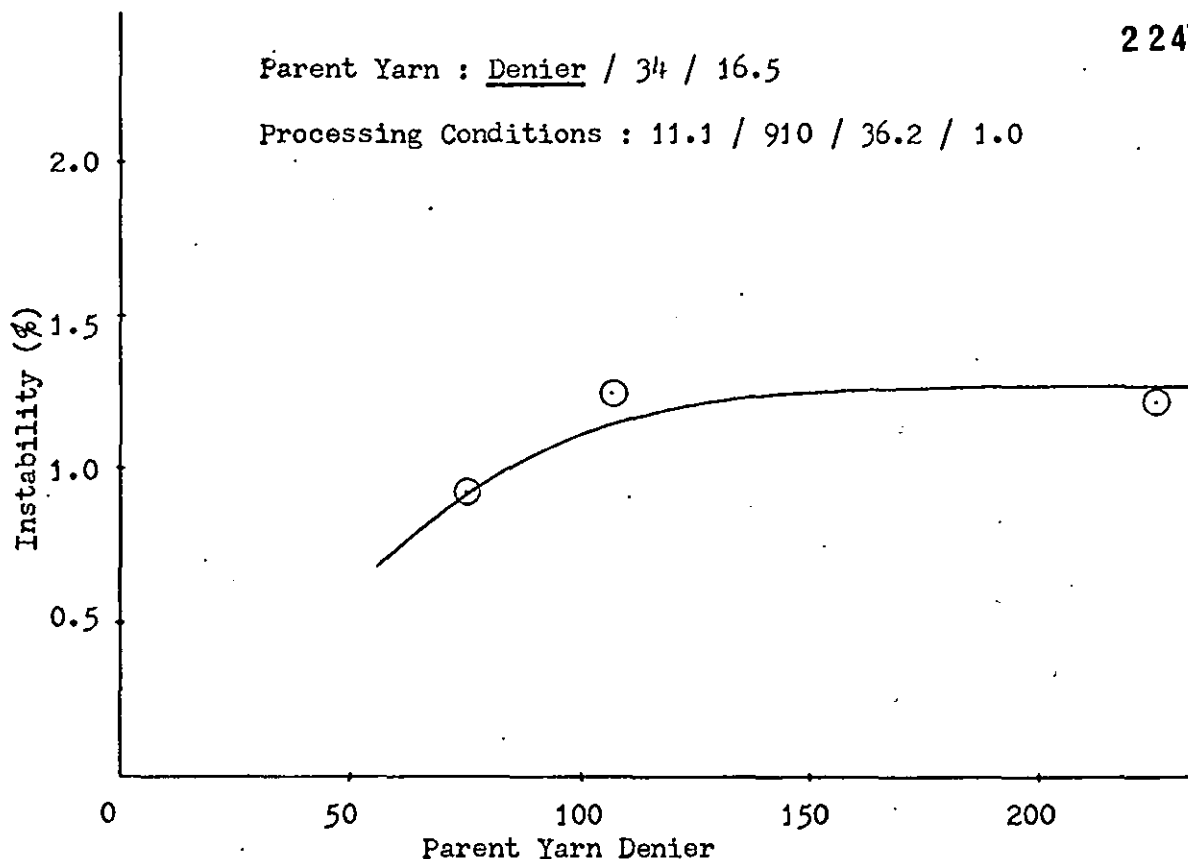


Fig. 6.33 Percentage Instability versus Parent Yarn Denier

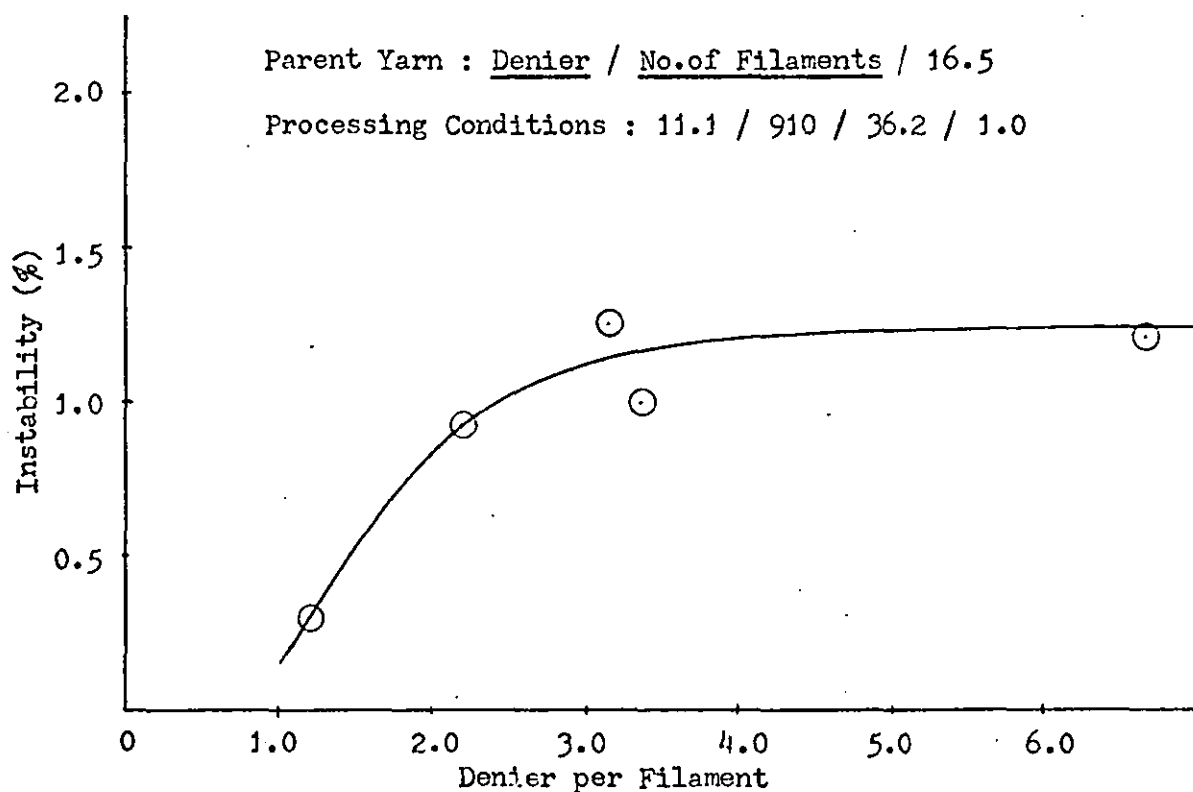


Fig. 6.34 Percentage Instability versus Parent Yarn Denier per Filament

CHAPTER 7

DISCUSSION OF PART (B) AND CONCLUSIONS

7.1 Summary of the Experimental Results

The factors (i.e. percentage overfeed, bulking zone length, percentage extra untwisting, parent yarn twist, parent yarn denier and denier per filament) affecting the bulked yarn characteristics processed by the mechanical method of bulking have been experimentally investigated in Chapter 6 and the results are now discussed in the following Sections.

7.1.1 Percentage Denier Increase

The graphs for the percentage denier increase versus percentage overfeeding, bulking zone length, percentage extra untwisting, parent yarn twist, parent yarn denier and denier per filament are plotted in Figs. 6.1 to 6.6 respectively. Obviously one would expect to obtain exactly the same amount of percentage denier increase with the percentage overfeed. However, Fig. 6.1 shows for instance that a 15% overfeed corresponds to approximately 10.5% percentage denier increase. As the tension used during the wrapping of the bulked yarn at the wrap reel was equal to the machine winding tension during bulking, and every care was taken during the weighing of the sample, it would not be expected that any experimental error in denier measurement would result in any significant error. Thus, the main error most probably comes from an inaccurate calculation of the percentage overfeed. The calculation for this is based on the accurate assessment of the yarn feed-in and take-up speeds and the assumption that the yarn feed-in and take-up tensions are both equal.

As explained in Section 5.2 both pairs of feed-in and projection rollers are made with constant outside diameters. The take-up rollers are interchangeable, being accurately turned to pre-calculated smaller outside diameters than the feed-in rollers. All three roller systems are driven by the same electric motor and thus no independent speed variation is possible. As the yarn is wound

several times around both the feed-in and take-up roller systems to give positive advancement, it is reasonable to expect that the assessment of yarn feed-in and take-up speeds is accurate in both cases.

However, the possibility of a difference between the parent yarn feed-in and bulked yarn take-up tensions still remains. Thus as the bulked yarn tension in the region between the spindle exit and the take-up rollers becomes considerably less than the parent yarn feed-in tension, the actual value of the percentage overfeed is also likely to be considerably less than the pre-set desired value. The bulked yarn, after leaving the false twist tube, rotates at the same speed as the tube and forms a number of rotating balloons depending on the distance between the spindle exit and the take-up guide roller. From the theoretical analysis of the rotating yarn balloon (see Section 5.8) it has been shown that the yarn tension would depend on the process variables and the parent yarn particulars. Therefore, the effects of such tension changes are probably being particularly observed in Figs. 6.2 and 6.6 which show the important roles which the bulking zone length adjustment and the denier per filament of the parent yarn play in determining the percentage denier increase.

7.1.2 Percentage Physical Bulk

The percentage physical bulk tests based on package density suggest that the percentage overfeed, the parent yarn denier and the denier per filament are the most important factors affecting the physical bulk. The minimum requirement of 150% physical bulk⁽¹⁵⁾ suggested by du Pont as a quality standard for Taslan yarns can only be obtained with the mechanical bulking apparatus for values of overfeeds above 12.5% (see Fig. 6.7). The importances of parent yarn total denier and the denier per filament were discussed in

Section 5.4.2, and there is a fair measure of agreement between the experimental findings and the arguments put forward in that Section. Figs. 6.11 and 6.12 show that the percentage physical bulk increases both with increasing parent yarn denier and with increasing denier per filament. Figs. 6.8, 6.9 and 6.10 show the graphical representations of percentage physical bulk versus bulking zone length, percentage extra untwisting and parent yarn twist respectively. In all cases there is an optimum processing condition at which a maximum percentage physical bulk can be achieved.

Although one test of this type is suggested by du Pont as acceptable for characterising Taslan yarn⁽¹¹⁾, it obviously cannot be sufficiently accurate for research purposes as, during the measurements of dimensions and weight, errors are almost certain to occur. Due to the limited quantities of twisted and set parent yarns available however, an adequate supply of wound packages for a more accurate assessment was unobtainable. This difficulty suggested that some alternative method of assessing the bulk should be found as this is considered in the next Section.

7.1.3 Water Absorption Test

The principle of the water absorption test which the author devised was based on the assumption that when a Taslan type bulked yarn was passed through a water bath, the looped filaments on the surface of the yarn would be filled with water. Thus such test results could also be used to assess the yarn bulk, but they would obviously be exaggerated compared with the package density test results, as the new physical bulk is a measure of the water absorption capacity of the yarn.

The graphical representation of the results (see Figs. 6.14 to 6.19) show that the assessment of the yarn bulk by this method is more reliable than the physical bulk test based on

the package density method (Figs. 6.7 to 6.12). The results show that increasing percentage overfeed (Fig. 6.14) and increasing denier per filament (Fig. 6.19) are the two most important factors affecting increased water absorption capacity. The experimental results also verify the importance of the bulking zone length, percentage extra untwisting, parent yarn twist and the yarn denier more effectively than did the results for the package density tests; the water absorption capacity continually decreases with increasing percentage extra untwisting and increasing parent yarn twist (see Figs. 6.16 and 6.17), whereas the physical bulk tests based on the package density method showed that there was an optimum value in both cases (see Section 7.2.2). These conflicting results may be associated with the fact that, at low values of the parent yarn twist and percentage extra untwisting, the average loop size is larger than that at higher values of these variables. Thus for a bulked yarn with a larger average loop size the water absorption capacity is expected to be more than that of a yarn with smaller average loop size.

7.1.4 Tensile Tests

As no textile testing equipment was available at Loughborough University, the tensile testing of the yarns had to be done at the Monsanto Textiles research centre in Leicester. Consequently being forced to rely on their generous co-operation, the tests had to be carried out in the limited time when the instrument could be spared from other duties. While gratefully acknowledging their kindness, it is unfortunate that insufficient continuous time was available for such testing and thus only ten graphs were obtained for each yarn sample. The breaking load, yarn tenacity and the percentage breaking extension were determined by averaging these ten values for each sample yarn.

Fig. 6.20 shows a typical load versus elongation curve for a mechanically bulked yarn. The general pattern of the curve is similar to that for the Taslan type of yarn as obtained by Wray⁽¹¹⁾.

The most important factors affecting the breaking load, tenacity and percentage breaking extension are the percentage overfeed and the parent yarn twist. Figs. 6.21 and 6.24 show that with increasing values of percentage overfeed and parent yarn twist, both the breaking load and tenacity decrease. These results are in agreement with those obtained by Wray⁽¹¹⁾ for Taslan type of bulked yarns.

Fig. 6.25 indicates that the percentage breaking extension decreases with increasing percentage overfeed up to a value of approximately 11% and then it starts to increase with further increasing values of percentage overfeed. However, the percentage breaking extension continuously decreases with increasing values of parent yarn twist (see Fig. 6.28). Both the bulking zone length and the percentage extra untwisting have negligible effects on the breaking loads and tenacities (see Figs. 6.22 and 6.23) and percentage breaking extension (see Figs. 6.26 and 6.27).

In conclusion, it can be said that mechanically bulked yarns produced with higher percentage overfeeds and parent yarn twists are weaker and less extensible than those produced at lower percentage overfeeds and parent yarn twists. This is because as argued by Wray⁽¹⁵⁾ at higher parent yarn twists the frequency of loops increases, and at higher percentage overfeeds the size of loops increases, therefore the number of straight filaments in the yarn cross section decreases causing the yarn to become weaker and less extensible.

7.1.5 Instability Test

The main factors influencing yarn stability are the percentage overfeed, parent yarn twist, parent yarn denier and denier

per filament. The influence of bulking zone length and percentage extra untwisting is negligible. Fig. 6.29 shows that the most important single factor is percentage overfeed and the graph indicates that with increasing percentage overfeed the percentage instability increases. This is because at higher percentage overfeed, more yarn is available for loop formation and thus under low loads the large loops will be easily removed. Increasing the parent yarn twist decreases the percentage instability (see Fig. 6.32). At low twists the bulked yarn structure is loose and extensible, but at high twists the structure becomes compact and the loops are tightly secured into yarn core, thus causing the extensibility at low loads to be less. Figs. 6.33 and 6.34 show the graphs of percentage instability versus parent yarn denier and denier per filament respectively and they indicate that the percentage instability increases with increasing values of these variables. This is because as shown in Figs. 6.11, 6.12 and Figs. 6.18, 6.19 the actual bulking (and therefore entanglement) of filaments increases with increasing values of parent yarn denier and denier per filament. Thus, as the yarn becomes bulkier, its extension under low loads increases.

7.1.6 Conclusion

This investigation has shown that the bulking action of the newly developed "mechanical" bulking method is a consequence of the combination of two basic effects namely (i) that due to the helical configuration of the filaments arising from the parent yarn twist, (ii) that due to the entanglement of rotating filaments in the bulking zone which results from their temporarily twist free and overfed condition. The detailed examination of the experimental results has shown that the major factors influencing these two basic effects, and therefore influencing the bulked yarn characteristics, are the

percentage overfeed, the initial parent yarn twist and the denier per filament of parent yarn; the minor influencing factors are the bulking zone length, percentage extra untwisting and parent yarn denier.

7.2 The Possibility of Commercial Exploitation of the Technique

In view of the fact that the mechanical simulation of the air-jet bulking had led to the manufacture of bulked yarns using a purely mechanical method, some comment is offered below regarding its commercial viability.

7.2.1 Patents

A provisional patent⁽³⁹⁾ was applied for after a search through the Abstract Sections of the Journal of the Textile Institute had revealed no similar British patent. However, a book⁽⁴⁾ reviewing all the important U.S. patents in yarn bulking was published soon after this application was made and this book revealed an abstract of an earlier American patent by Weiss et al⁽⁴⁰⁾ which contained substantially the same information. Nevertheless, it was decided that in view of the fact that the original intent of the mechanical simulation was to throw light on the air-jet bulking process, the main object of the work was not affected by this discovery, although the idea of using the mechanical method for yarn bulking appeared to be subject to a prior claim as regards commercial exploitation.

7.2.2 Bulking Speed

Chapter 5 reported that the multi-purpose mechanical bulking apparatus was satisfactorily operated at fairly low bulking speeds (67.5 yards/min) to investigate the basic factors involved in this new type of bulking process. However at higher bulking speeds (i.e. up to 250 yards/min) the manual synchronization of the three separate drive accelerations demanded considerable acquired skill (see Section 5.4.7).

Theoretically the throughput speed could be as high as the false-twist tube speed permitted. Taking into account a false-twist tube speed at 500,000 rev/min, which is quite feasible with modern false-twist units of the type used, and assuming a parent yarn twist of 15 turns/in, with 30% extra untwisting, then the theoretical throughput speed would be about 710 yards/min. This is nearly 5 times greater than typical commercial throughput speeds of the air-jet bulking process, as during a recent visit to a main Taslan producing mill in this country, it was observed that the commercial operating speed of the air-jet process was never above 150 yards/min (see Section 4.4).

The previous published works^(11,12,13,14,15) on the air-jet bulking process all related to experiments which were carried out at 50 yards/min because higher commercial bulking speeds were not generally known. As it was intended to compare the experimental results of the bulked yarns produced by the mechanical bulking process with those produced by the air-jet, and due to the mechanical drive limitations described in Section 5.4.7, the prototype mechanical bulking apparatus was also operated at low bulking speeds. A 250 yards/min bulking speed did not in itself present any fundamental problems in producing a mechanically bulked yarn from the present bulking unit, the only deficiencies arising from the use of a 3 motor drive system and an inadequate wind-up mechanism. However a commercial machine using this system as a bulking method would certainly operate from one common drive and could incorporate a better wind-up mechanism. This should obviate much of the operative skill needed for high-speed manufacture.

7.2.3 Cost Estimates

One of the obvious advantages of this method of bulking over the conventional air-jet method would be the higher speeds that could be achieved (Section 7.2.2). The most obvious other advantage

is that there is no need for a supply of compressed air; consequently this would represent a saving of capital and processing costs.

A Scragg CS 600 false-twist machine with 188 spindles costs £20,000 approximately. As a commercial mechanical bulking machine of the design envisaged would not require heater boxes and their associated control system, it is reasonable to expect that this type of machine if made would cost about £10,000 for the same number of spindles. This amount is about the same as the cost of an air-jet bulking machine of equivalent spindleage, (see Section 4.4).

Assuming a commercial mechanical bulking machine is built to run at 450 yards/min and its operating cost is the same as an air-jet bulking machine, and that no licensing fees are required, then the cost of producing 1 lb of mechanically bulked yarn would be approximately one-third that of producing Taslan yarns.

If the 75 denier Terylene yarn used in the air-jet bulking cost considerations (see Section 4.4), was also to be used as a typical basic yarn for the mechanical bulking, the estimated price of the bulked yarn produced would be equivalent to :

Selling price of Taslan (19s. Od.)	- compressed air cost (5d.)	- licensing fees (8d.)	- $\frac{2}{3}$ of the operating cost of Taslan machine (estimated at 4s. Od.)
--	-----------------------------------	------------------------------	--

This would work out to be roughly 15 shillings per pound of bulked yarn. Thus if it is compared with Taslan it is estimated that a 20 per cent reduction in selling price could be achieved if the mechanical bulking method was commercially employed.

7.3 Suggestions for Future Work

(i) At present the mechanical method of bulking can only be operated satisfactorily if a pre-twisted parent yarn is supplied. However the idea of bulking yarns possessing very small amounts of producer twist is attractive and commercially more profitable. Therefore in future work, a technique of modifying the present method might be found such that the bulking of yarns with little or no initial twist can be obtained. The present author suggests that this could possibly be achieved if the mechanism of the projection rollers R (see Fig. 5.1) was to be modified such that it could rotate as a unit about the same axis as that of the false-twist tube, while at the same time feeding the parent yarn into bulking zone. Only then could the overfed twist free parent yarn form a twist free rotating open balloon in the bulking zone such that the mechanical bulking action could occur.

(ii) In Section 5.10 an attempt was made to investigate the possibility of making effect yarns by blending short staple fibres into the open structure of the continuous filament yarn in the bulking zone. The outcome was only a very limited success, because the twist free rotating filaments formed a shield, thus making it difficult for the stationary fibres to penetrate the open but rotating structure. The author suggests that, if the stationary staple fibre introducing mechanism could also rotate around the balloon, then the relative velocity between the fibres and the rotating filaments would be small and the fibres would more easily enter the open filament structure.

REFERENCES

1. G. R. Wray (Editor), "Modern Yarn Production from Man-Made Fibres" Columbine Press, London and Manchester, 1960.
2. Monsanto Company, "Textured Yarn Technology" Vols. 1, 2, 3. Monsanto Textiles Division, Decatur, Alabama, U.S.A. 1967.
3. E. A. Hutton and W. J. Morris, "A Survey of the Literature and Patents Relating to Bulked Continuous Filament Yarns" Shirley Institute Pamphlet No. 81, July, 1963.
4. M. G. Harrison, "Textured and Novelty Yarn Process" Noyes Development Corporation, New Jersey, U.S.A., 1967.
5. B.P. 732, 929 Du Pont de Nemours, December 15, 1952.
6. B.P. 762, 630 Du Pont de Nemours, July 19, 1954.
7. B.P. 793, 044 British Celanese Limited, October 18, 1955.
8. B.P. 871, 797 British Celanese Limited, February 28, 1958.
9. (a) Du Pont Technical Information Bulletin X-32, "Taslan Textured Yarns" May, 1955.
(b) Du Pont Technical Information Bulletin X-154, "Characteristics of Taslan Textured Yarns" October, 1961.
10. Y. E. Chaudhari, "Air Bulking of Filament Yarn" M.Sc.Tech. Thesis, University of Manchester, May, 1963.
11. G. R. Wray, "The Construction and Resultant Properties of Air-Textured Filament Yarns" Ph.D. Thesis, University of Manchester, May, 1965.
12. "Bulk, Stretch and Texture", 1966, Baden-Baden (Conference) Papers of the 51st Annual Conference of the Textile Institute.
13. G. R. Wray and J. H. Entwistle, J.Text.Inst., 1968, 59, 122.
14. G. R. Wray and J. H. Entwistle, J.Text.Inst., 1969, 60, 411.
15. G. R. Wray, J.Text.Inst., 1969, 60, 102.
16. A. H. Shapiro, "The Dynamics and Thermodynamics of Compressible Fluid" Vol. I, The Ronald Press Company, New York, 1953.
17. H. W. Emmons (Editor), "Fundamentals of Gas Dynamics" Oxford University Press, London, 1958.

18. A. B. Cambel and B. H. Jennings, "Gas Dynamics"
McGraw-Hill Book Company, Inc., New York, Toronto, London, 1958.
19. R. H. F. Pao, "Fluid Mechanics"
John Wiley and Sons, Inc., New York and London, 1961.
20. A. Ferri, "Elements of Aerodynamics of Supersonic Flows"
The Macmillan Company, New York, 1949.
21. E. Carafoli, "High-Speed Aerodynamics"
Editura Tehnica, Bucharest, Roumania, 1956.
22. (a) A. Roshko, J. Fluid Mech. 1960, 10, 345.
(b) A. Roshko, N. A. C. A. Tech. Note no. 3169, 1954.
23. L. S. G. Kovasznay, Proc. Roy. Soc. A. 1949, 198, 174.
24. M. S. Bloor, J. Fluid Mech. 1964, 19, 290.
25. S. Goldstein (Editor) "Modern Developments in Fluid Dynamics"
Vol. II, Clarendon Press, Oxford, 1933.
26. Y. C. Fung, J. Aero Space Sci. 1960, 27, 801.
27. D. M. Sykes, J. Fluid Mech. 1962, 12, 367.
28. A. Acrivos, D. D. Snowdon, A. S. Grove and E. E. Petersen,
J. Fluid Mech. 1965, 21, 737.
29. B. S. I. 1042, "Methods for the Measurement of Fluid Flow in
Pipes" Part I, September, 1965.
30. H. J. Allen and W. G. Vincenti, N. A. C. A. Rep. 782, 1944.
31. J. O. Hinze, "Turbulence"
McGraw-Hill Book Company Inc., New York, 1959.
32. DISA Constant Temperature Anemometer Type 55AO1,
"Instruction Manual" Reg. No. 9150AO213.
DISA, Herlev, Denmark, June, 1966.
33. DISA Probes for Hot-wire and Hot-film Anemometry
Leaflet No. 603/E. DISA, Herlev, Denmark, May, 1968.
34. DISA Calibration Equipment Type 55D41/42,
"Instruction Manual" DISA, Herlev, Denmark, May, 1966.
35. Servomex Precision Motor Controller Type MC.47
"Instruction Manual 8/60"
Servomex Controls Ltd., Crowborough, Sussex.
36. S. Timoshenko, "Strength of Materials" Part II,
D. Van Nostrand Company, New Jersey, U.S.A., 1956.
37. M. J. Denton, J. Text. Inst., 1966, 57, T265.

38. A. E. De Barr and H. Catling,
"Manual of Cotton Spinning" Vol. V, The Textile Institute,
Butterworths, Manchester and London, 1965.
39. B. P. Application No. 29973/67, G. R. Wray and H. Sen,
July 13, 1967.
40. U.S.P. 3, 053, 038. E. Weiss, et al, September, 11, 1962.

